Quantum correlations and non-equilibrium quantum transport

Michele Coppola

Université de Lorraine - École doctorale C2MP
LPCT - Université de Lorraine, F-54000 Nancy, France

Thèse
Présentée et soutenue publiquement le 17 novembre 2023
pour l'obtention du titre de
Docteur en Physique
par

MICHELE COPPOLA

QUANTUM CORRELATIONS AND NON-EQUILIBRIUM QUANTUM TRANSPORT

Membres du jury

Président du jury:	**HERVÉ MOHRBACH**	LPCT, Université de Lorraine
Rapporteurs:	**ANNA MINGUZZI**	LPMMC, Université Grenoble-Alpes
	ADOLFO DEL CAMPO	University of Luxembourg
Examinateurs:	**FRÉDÉRIC MILA**	École polytechnique fédérale de Lausanne (EPFL)
	MAURIZIO FAGOTTI	LPTMS - Université Paris-Saclay
Directeur de Thèse:	**MALTE HENKEL**	LPCT, Université de Lorraine
Co-Directeur de Thèse:	**DRAGI KAREVSKI**	LPCT, Université de Lorraine

Abstract

This thesis analyses some aspects of open one-dimensional quantum systems, driven out of equilibrium by the interaction with external baths or monitoring apparatus. To begin, we introduce the background and the theoretical tools used in this thesis, such as the entanglement entropy, the Lindblad dynamics, the Langevin equations and the phase-space formulation of quantum mechanics.

In the first part of this thesis, we consider the non-equilibrium dynamics induced by local projective measurements, with a particular focus on the entanglement entropy, a powerful theoretical probe for quantum correlations. For a chain of hopping fermions, the typical linear growth of the entanglement after quenching the Néel state is replaced by a logarithmic one. As main result, we find a transition from volume to area law for the stationary entanglement.

We also generalise the hydrodynamic picture for chains of free particles coupled to Lindblad baths. For inhomogeneous one-body gain-loss processes and dephasing, we derive the equation of motion of the Wigner function, describing transport and non-equilibrium behaviour in terms of classical non-interacting quasi-particles.

Next, a case study of the non-equilibrium dynamics of open quantum systems is presented for two models based on a single harmonic oscillator in an external field. The interaction with the environment is specified by the Langevin equations, containing a deterministic damping term ad two markovian noises, whose second moments are derived from a set of phenomenological requirements. After mapping the reduced dynamics into a Fokker-Plank equation for the Wigner function, we find out that the complete positivity, as well as the relaxation toward the equilibrium state, is not always guaranteed.

Finally, we focus on the conditional no-jump dynamics of free particles coupled to Lindblad baths. For Gaussian preserving dynamical maps, the non-equilibrium dynamics under missed detection is captured by a Riccati-type differential equation for the correlation matrix, which gives access to the no-jump probability and the waiting-time distributions.

Résumé

Cette thèse analyse certains aspects des systèmes quantiques unidimensionnels ouverts, chassés de l'équilibre par l'interaction avec des bains externes ou des appareils de mesure. Pour commencer, nous introduisons le contexte et les outils théoriques nécessaires à cette étude, tels que l'entropie d'intrication, la dynamique de Lindblad, les équations de Langevin et la formulation en espace de phase de la mécanique quantique.

Dans un premier temps, nous considérons la dynamique non-équilibre induite par des mesures projectives locales, avec un accent particulier sur l'entropie d'intrication, une sonde théorique puissante pour les corrélations quantiques. Pour une chaîne de fermions sautants, la croissance linéaire typique de l'intrication pour l'état initial de Néel est remplacée par une croissance logarithmique. Comme résultat principal, nous avons trouvé une transition de la loi de volume à la loi de surface pour l'intrication stationnaire.

Après, nous généralisons l'hydrodynamique pour les chaînes de particules libres couplées aux bains de Lindblad. Pour les processus de gain-perte inhomogènes à un corps et le déphasage, nous dérivons la dynamique de la fonction de Wigner, décrivant le transport et le comportement hors-équilibre en termes de quasi-particules classiques sans interaction.

Ensuite, un cas d'étude de la dynamique hors équilibre des systèmes quantiques ouverts est présenté pour deux modèles basés sur un oscillateur harmonique unique dans un champ externe. L'interaction avec l'environnement est spécifiée par les équations de Langevin, contenant un terme de friction déterministe et deux bruits Markoviens, dont les seconds moments sont spécifiés à partir d'un ensemble d'exigences phénoménologiques. Après avoir exprimé la dynamique réduite avec une équation équivalente de Fokker-Plank pour la fonction de Wigner, nous constatons que la positivité complète, ainsi que la relaxation vers l'état d'équilibre, ne sont pas toujours garanties.

Enfin, nous nous intéressons à la dynamique conditionnelle sans saut des particules libres couplées aux bains de Lindblad. Pour les cartes dynamiques à préservation gaussienne, la dynamique de non-équilibre sous détection manquée est capturée par une équation différentielle de type Riccati pour la matrice de corrélation, qui donne accès à la probabilité de non-saut et aux distributions des temps d'attente.

Keywords: Open quantum systems, non-equilibrium dynamics, entanglement entropy, Lindblad equation, Langevin equations

Title: Quantum correlations and non-equilibrium quantum transport
Author: Michele Coppola
Supervisor: Malte Henkel
Co-supervisor: Dragi Karevski
Institution: LPCT, Université de Lorraine, F-54000 Nancy, France
Year: 2023

Acknowledgements

I would like to sincerely thank Malte and Dragi for having guided me during the development of this PhD thesis. Their supervision has been very fruitful for my growth as a physicist and I will always be grateful for that. I would also like to thank them for their countless advises, even outside scientific research.
A great thank goes also to my collaborators, Mario Collura, Gabriel Landi and Emanuele Tirrito, which undoubtedly contributed to make me a more eclectic scientist and improved my professional competencies. The research stays in Trieste and Rochester have been very important and prolific for my professional growth.
I am also thankful to Anna Minguzzi and Adolfo del Campo for their role of rapporteurs. I grateful to Hervé Mohrbach, Frédéric Mila and Maurizio Fagotti for having accepted to join the jury.
I would like to thank Jerôme Dubail for his advises, the nice scientific discussions together and having helped me to find a postdoc position. I am also grateful to Stefano Scopa, who gave me help several times like an older brother.
I would like to thank all the PhD students and postdocs of LPCT, with whom I shared the last three years of my life.
I thank the whole LPCT for having welcomed me so warmly.
Finally, I thank my family, my friends and colleagues in Lecce and Trieste who supported me during my PhD.

Contents

Introduction

The non-equilibrium quantum physics is a rich and prolific subject which, in its broadest interpretation, includes any quantum system driven out of equilibrium as a consequence of some external perturbations. A paradigmatic example is provided by the *quantum quenches*, where a quantum system is prepared in a steady state, e.g. the ground state, and one of the tunable parameters of the Hamiltonian operator is suddenly modified.

The popularity of out-of-equilibrium statistical physics goes hand-in-hand with a rising interest in transport phenomena, continuous measurement problems, stochastic processes, quantum relaxation and optimal control in modern quantum devices. However, non-equilibrium physics is still lacking a general theoretical framework and, therefore, particular problems require specific tools, whose development has been pushed and favoured by powerful numerical techniques, e.g. DMRG [1], Monte Carlo [C1], DMFT [2], tensor network [1, 3–6]. The above developments have led to important results, among which we quote the relaxation towards generalized Gibbs ensembles [7, 8], the generalized hydrodynamics [9, 10] and the novel results in quantum information [C2] and quantum thermodynamics [11].

In the last decades innovative experimental methods have allowed to test the theoretical predictions, which enhance the interest of the non-equilibrium quantum physics. We can mention the Nobel Prize in Physics 2012 in this regard, which was awarded jointly to Serge Haroche and David J. Wineland *for ground-breaking experimental methods that enable measuring and manipulation of individual quantum systems*. Their studies paved the way to a new era for quantum optics, making possible to measure and control fragile quantum states, which were previously thought inaccessible from direct observation [12, 13].

In this thesis, the focus is on quantum many-body systems, which are driven out of equilibrium by the interaction with an external environment, such as external baths or monitoring apparatus. This research study is framed into the wide subject of open quantum systems, whose dynamics and relaxation to equilibrium are still an on-going problem. The complexity of the system-bath(s) interactions and the difficulties connected to the extrapolation of the reduced dynamics have lead to the formulation of several theoretical approaches. In fact, along with the standard technique deriving the dynamics from first principles, other phenomenological approaches have been proposed, which have the advantage to circumvent some mathematical issues, but preserving the necessary physical requirements [14].

Our analysis deals with quantum chains of non-interacting particles, although part of the results achieved in this thesis could be generalised to higher dimensions. In recent years there has been a renewed interest in the physics of one-dimensional systems, due to the technological boom, the experimental manipulation of quantum platforms, such as quantum spin chains and cold atoms, and the subsequent realisation of quasi-1d geometries with the help of confining potentials. Moreover, free particle models still play a key role in the understanding of the many-body physics, where the acquired knowledge on the dynamics of closed systems is a springboard to generalise the same physical pictures for the open counterparts, such as quantum dots, boundary-driven chains or continuous monitored systems.

This thesis is organised in two main sections. The first part of the manuscript (Chapters 1, 2, 3) introduces the reader to the general background and the theoretical tools used in this work. Namely, the goal is to guide any reader, even non-expert, to the full understanding of the results.

Chapter 1 is devoted to quantum entanglement, which is undoubtedly one of the most celebrated phenomena of quantum mechanics and the landmark of quantum information theory. Since the early 1930s, quantum entanglement had triggered several long standing debates about the foundations of quantum mechanics. In this respect, the EPR paradox [15] was a thought experiment based on quantum entanglement, which had long been used to support the thesis that wave functions cannot provide a complete quantum-mechanical description of reality. The crucial part of the EPR paradox was the demonstration of non-locality, which apparently implies instantaneous information transfer and the violation of causality. The EPR paradox suggested the idea that any quantum object carries some hidden properties which are not currently included in quantum theory, usually referred to as *local hidden variables*. The solution to this paradox came from Bell's inequality [16, 17, C3], showing that any theory based on local hidden variables is not consistent with the results of quantum mechanics. Nevertheless, the experimental layout which Bell considered for his thought experiment is not practically reproducible. For this reason, a great effort has been made to prove experimentally the Bell's inequality, which earned Alain Aspect, John F. Clauser and Anton Zeilinger the Nobel Prize in Physics 2022 *for experiments with entangled photons, establishing the violation of Bell inequalities and pioneering quantum information science* [18–25].
At the beginning of Chapter 1, we use the Schmidt decomposition for an intu-

itive approach to quantum entanglement. Afterwards we formalise our statements by defining the entanglement entropy, which is one of the possible entanglement measures for pure states. Next, we analyse the good properties of the von Neumann entropy, which make it more attractive and physically relevant than other entanglement measures. The final part of this chapter is dedicated to the mathematical techniques to compute entanglement, with a particular focus on the Peschel's trick for Gaussian states and the generalized hydrodynamics for integrable models, where the spread of quantum correlations is described by non-interacting quasi-particles which are entangled in pairs.

In Chapter 2 we present two of the most celebrated models for open quantum systems, i.e. the Langevin and Lindblad dynamics, used in this thesis to characterise the system-bath(s) interactions. In the first part of this chapter, we introduce the Lindblad equation, which finds mathematical origin in the dynamical semigroup hypothesis. Furthermore, following a first principle approach, we show that the Lindblad dynamics, as well as the complete positivity, arises from the second order perturbation theory, the separability of the system-bath states, the Markov hypothesis and the rotating wave approximation. Next, we present the Langevin dynamics, arguing about the equivalence between the ab initio approach by Ford, Kac and Mazur and the axiomatic one by Araújo, Wald and Henkel. We show how the Langevin noises must be intrinsically non-markovian to satisfy all the good quantum-mechanical properties. However, even the Bedeaux-Mazur proposal deserves a special mention, where the authors derive the Langevin equations from a mesoscopic non-equilibrium thermodynamic scheme. This approach is a paradigmatic example of how markovian noises may generate a Langevin dynamics, but the quantum fluctuation-dissipation theorem is not verified.

Chapter 3 aims to be a pedagogical review of the Wigner function approach, which is an alternative formulation of quantum mechanics developed starting around 1932 [26]. We show how the Wigner formalism arises from the Weyl transform, which builds a one-to-one map between Hilbert operators and phase-space functions. Using a semiclassical expansion, we derive the equation of motion of the Wigner function, which is defined as the phase-space representation of the density operator. This phase space formalism really plays a key role in this thesis, being the starting point toward the generalized hydrodynamics for open systems (Chapter 5) and the instrument to access the quantum relaxation for dissipative models (Chapter 6).

The second part of this manuscript (Chapters 4, 5, 6, 7) is devoted to the study of specific problems. The analysis mostly follows the published papers during the last three years of thesis [A1–A4], presenting the original contribution of our research work.

Inspired by the last research works about measurement-induced entanglement phase transitions [27], in Chapter 4 we study a dynamical protocol where the unitary evolution of a chain of hopping fermions is perturbed by projective measurements of the local number operators. In this still unexplored scenario, any measurement projects the quantum state on the eigenvariety of the corresponding outcome. After sampling many quantum trajectories, the main focus is the entanglement entropy, a powerful theoretical probe to access the spread of quantum correlations. In particular, we show how and to what extent the dynamical and asymptotic behaviour of the entanglement entropy is affected by random interactions with local measuring apparatus. We find out that the linear time-growth of the entanglement characterising the unitary evolution is suddenly replaced by a logarithmic one. Concerning the asymptotic regime, we numerically show the existence of a single area-law phase for the entanglement entropy. Furthermore, we interpret the results with the help of the collapsed quasi-particle ansatz, extrapolating the area-law scaling of the stationary entanglement. Finally, we focus on the entanglement fluctuations, with the scaling behaviour for large and low measurement rates.

In Chapter 5, we study the markovian dynamics of non-interacting chains coupled to Lindblad baths. For one-body gain-loss processes and dephasing, we derive the equations of motion of the two-point functions in a closed form, which give us the physical insight to generalise the hydrodynamic approach for this class of open systems. We find the differential equation governing the dynamics of the Wigner function which, for weakly-entangled and highly excited initial states, is pictorially view as a distribution of classical non-interacting quasi-particles. The motion of each excitation in the phase-space is governed by the group velocity and the external potential, while inhomogeneous jump rates make the quasi-particle's time-of-flight finite and act as a source of new excitations. We also apply the theoretical results to some specific examples, describing the density evolution and the transport phenomena in terms of classical quasi-particles.

In Chapter 6, our study is framed in the general context of markovian open quantum systems. The dynamics of such systems is commonly specified either in terms of a master equation for the reduced density matrix or else through a Langevin equation for the local observables. The quantum harmonic oscillator has always been used as a paradigmatic model to explore such scenarios. Yet, we do encounter several surprises. Firstly, contrary to a widely held conviction, it has apparently passed unnoticed that the two most common formulations of a damped quantum harmonic oscillator, namely the *friction model* and the *cavity model* in Chapter 6, are not equivalent. Second, the form of the dynamical map $\mathcal{L}$ of friction model does not respect the generally admitted Lindblad form and is not completely positive. This last observation may appear shocking since the complete positivity is traditionally required to ensure that the extended map $\mathcal{L} \otimes \mathbb{1}_N$, emerging from the coupling with any N-level ancilla, still generates positive semi-definite density matrices. However, in the scientific literature, this requirement has been very intensely and controversially debated and, in Chapter 6, we provide a new and concrete example of how a quantum master equation may emerge from a set of phenomenological postulates, yet without being necessarily completely positive.

More formally, the friction and the cavity models are defined in terms of two different Langevin equations, bypassing any explicit discussion about the initial state and correlation system-bath. After obtaining the second moments of the noises by a well-defined set of phenomenological requirements, we move to the two-point functions, whose dynamics may equivalently be derived using two effective master equations for the reduced density operators. Despite the friction model does not map into a completely positive dynamics, its master equation preserves the simple positivity if either time is large enough or else if the initial states are not squeezed too much. The time evolution of the states is studied by the Wigner function formalism. Furthermore, we analyse the relaxation to the stationary state, which is identical for both models without an external field. Finally, we recast the friction and cavity models as mean-field approximations of a many-body interacting magnet, deriving the phase diagrams at zero temperature. While the friction model relaxes to a proper thermal state independently on the damping parameter γ, this is not true for the cavity model, whose stationary state is γ-dependent.

Chapter 7 is dedicated to the conditional no-jump dynamics of free particles coupled to Lindblad baths. Given that any quantum jump may be pictorially seen as the action of some detectors monitoring the exchange of particles between the system and the external environment, we assign to each dissipative channel a finite efficiency $\Lambda \in [0, 1]$, with $\Lambda = 1$ for perfect efficiency and $\Lambda = 0$ when the channel is not monitored at all. In a nutshell, some quantum jumps may not be detected due to the non-ideal efficiency of the monitoring apparatus. In this chapter, we focus on the no-jump evolution, where the dynamics of the states is constrained on no jumps being detected in $[0, t]$. This gives access to the no-jump probability, namely the probability of not detecting any jump in $[0, t]$, and the waiting-time distribution $W_k(t)$, which is the probability distribution of detecting the first quantum jump in the dissipative channel k at time t.

This chapter may be divided in two parts. In the first half, we obtain general results relating the no-jump probability and the waiting-time distributions to the conditional evolution of specific system observables. Afterwards we study some examples involving a single qubit, either incoherently or coherently driven. In the second part of Chapter 7, we move to many-body systems, analysing the no-jump dynamics for quantum chains of non-interacting particles. For linear jump operators in the creation/annihilation operators, the Gaussian ansatz solves the conditional no-jump dynamics. The no-jump evolution is provided by a Riccati-type differential equation for the correlation matrix. Finally, we compute the no-jump probability and the waiting-time distributions for boundary driven systems and tight binding chains with specific emission/absorption profiles.

At the beginning of Chapters 4, 5, 6, 7, we provide a brief introduction for a quick focus on the the main goals and achieved results.
In Chapters 2, 5, 6 we make use of the Wigner formalism and, in order to avoid confusion, we put the symbol $\wedge$ over Hilbert operators to distinguish them from phase-space variables.
Our main findings are summarised at the end of this manuscript, where we also draw some future perspectives.

Chapter 1

Entanglement and Gaussian states

Consider a pure normalized quantum state $|\Psi\rangle$, living in the Hilbert space $\mathscr{H} = \mathscr{H}_A \otimes \mathscr{H}_B$, where $\mathscr{H}_A$ and $\mathscr{H}_B$ are two partitions of $\mathscr{H}$ (see Fig. 1.1). In general, $|\Psi\rangle$ is written as

$$|\Psi\rangle = \sum_{i=1}^{d_A}\sum_{j=1}^{d_B} C_{ij} \left|\psi_i^A\right\rangle \otimes \left|\psi_j^B\right\rangle , \tag{1.1}$$

where $\left\{\left|\psi_A^i\right\rangle\right\}_{i\in\{1,\dots,d_A\}}$ and $\left\{\left|\psi_B^i\right\rangle\right\}_{i\in\{1,\dots,d_B\}}$ are the orthonormal sets spanning $\mathscr{H}_A$ and $\mathscr{H}_B$, with dimension d_A and d_B; $\mathbf{C}$ is a $d_A \times d_B$ complex matrix with elements C_{ij}, satisfying the normalization condition $\langle\Psi|\Psi\rangle = \mathrm{tr}\big(\mathbf{C}^\dagger\mathbf{C}\big) = 1$.

The *Schmidt decomposition* is an important mathematical theorem which generalises the eigendecomposition to any $d_A \times d_B$ matrix [28]. The coefficient matrix $\mathbf{C}$ can be factorized as

$$\mathbf{C} = \mathbf{U}\boldsymbol{\Lambda}\mathbf{V}^\dagger , \tag{1.2}$$

where $\mathbf{U}$ is a $d_A \times d_A$ complex unitary matrix, $\boldsymbol{\Lambda}$ is a $d_A \times d_B$ rectangular diagonal matrix with non-negative real values λ_i on the main diagonal, and $\mathbf{V}$ is a $d_B \times d_B$ complex unitary matrix. For instance, if $d_A < d_B$, $\boldsymbol{\Lambda} = (\boldsymbol{\lambda}|\mathbf{0})$, which is a rectangular matrix where $\boldsymbol{\lambda} = \mathrm{diag}(\lambda_1, \dots, \lambda_{d_A})$ is a square diagonal matrix $d_A \times d_A$ and $\mathbf{0}$ is a null matrix $d_A \times (d_B - d_A)$.

Performing a unitary rotation of the basis $\left\{\left|\psi_A^i\right\rangle\right\}_{i\in\{1,\dots,d_A\}}$ and $\left\{\left|\psi_B^i\right\rangle\right\}_{i\in\{1,\dots,d_B\}}$,

$$\left|\omega_A^i\right\rangle := \sum_{j=1}^{d_A} U_{ij} \left|\psi_A^j\right\rangle , \qquad \left|\omega_B^i\right\rangle := \sum_{j=1}^{d_B} V_{ij}^\dagger \left|\psi_B^j\right\rangle , \tag{1.3}$$

and rewriting the quantum state $|\Psi\rangle$ in terms of the complete orthonormal basis

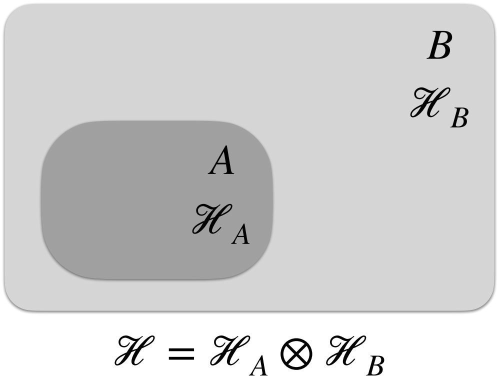

Figure 1.1: A quantum system S is divided into two complementary partitions A and B: $S = A \cup B$; the total Hilbert space $\mathscr{H}$ is given by the tensor product $\mathscr{H}_A \otimes \mathscr{H}_B$.

$\{|\omega_A^i\rangle\}_{i\in\{1,\dots,d_A\}}$ and $\{|\omega_B^i\rangle\}_{i\in\{1,\dots,d_B\}}$, we get

$$|\Psi\rangle = \sum_{i=1}^{d} \lambda_i \, |\omega_i^A\rangle \otimes |\omega_i^B\rangle \, , \tag{1.4}$$

where $d = \min(d_A, d_B)$ and the λ_i are non-negative coefficients satisfying the normalization condition $\sum_{i=1}^{d} \lambda_i^2 = 1$.

If there is exactly one $\lambda_i \neq 0$, Eq. (1.4) reduces to

$$|\Psi\rangle = |\omega^A\rangle \otimes |\omega^B\rangle \, , \tag{1.5}$$

and $|\Psi\rangle$ is a *product state* (or *separable state*). By definition, we state there is no entanglement between the partitions A and B. A system described by the product state (1.5) is uncorrelated and the probabilities of different outcomes under local measurements on A and B factorize; if there are many coefficients $\lambda_i \neq 0$, $|\Psi\rangle$ is *entangled*; finally, if $\lambda_i = d^{-1/2}$ $\forall i$, the entanglement between the partitions A and B is maximum and $|\Psi\rangle$ is a *maximally entangled state*. In the next section, we shall discuss general benchmark criteria for measuring entanglement and ordering states and partitions.

1.1 Measure of entanglement

So far, we have distinguished entangled from unentangled states. In order to find a more easy access to this kind of quantum correlations, we introduce a measure of the entanglement and an ordering between different states and bipartitions. This section will be mostly dedicated to the *entanglement entropy*, also known as *von Neumann entropy*, which is one of the possible measures of entanglement for pure states.

Let $\rho = |\Psi\rangle\langle\Psi|$ be the density matrix of the system. By definition, the reduced density matrix for the subsystem A is

$$\rho_A := \mathrm{tr}_B(\rho) = \sum_{i=1}^{d} p_i \left|\omega_A^i\right\rangle \left\langle\omega_A^i\right| , \tag{1.6}$$

where $p_i = \lambda_i^2$ and the label B indicates the trace over the degrees of freedom of the partition B. The von Neumann entropy [29] between A and B is

$$S_A[\rho] := -\mathrm{tr}_A(\rho_A \ln \rho_A) = -\sum_{i=1}^{d} p_i \ln(p_i), \tag{1.7}$$

which is invariant under any unitary transformation of the density matrix. Furthermore, thanks to the Schmidt decomposition, the von Neumann entropy verifies $S_A[\rho] = S_B[\rho]$. In the next paragraphs, we show that Def. (1.7) fulfils all the requirements to be considered a good measure of entanglement.

The entanglement entropy $S_A[\rho]$ is known to be an *entanglement monotone* (or *entanglement measure*) [29], which is a non-negative map from pure quantum states ρ and bipartitions (A, B) into real values, $S_A : \mathscr{H} \to \mathbb{R}^+$. The entanglement entropy $S_A[\rho]$ satisfies the properties

(i) $S_A[\rho] = 0 \quad \Longleftrightarrow \quad |\Psi\rangle = \left|\omega^A\right\rangle \otimes \left|\omega^B\right\rangle$;

(ii) $S_A[\rho]$ takes maximum value for maximally entangled states, which is $S_{\max} = \ln(d)$;

(iii) $S_A[\rho]$ is monotonically decreasing under local operations and classical communication (LOCC) .

The properties (i) and (ii) are easy to understand. The third one deserves more attention and finds a physical motivation in real settings involving quantum communication across distances [30, 31].

The statement (i) is immediately proved. Since for product states there is exactly one $p_i \neq 0$, using the definition (1.7), $S_A[\rho] = 0$ and then there is no entanglement between A and B.

To check the property (ii), we proceed by computing the extremum points of the von Neumann entropy (1.6). Due to the normalization constraint $\sum_{i=1}^{d} p_i = 1$, S_A is a function of $d-1$ variables,

$$S_A(p_1, \ldots, p_{d-1}) = -\sum_{i=1}^{d-1} p_i \ln(p_i) - \left(1 - \sum_{i=1}^{d-1} p_i\right) \ln\left(1 - \sum_{i=1}^{d-1} p_i\right) , \tag{1.8}$$

and then the gradient is

$$\nabla S_A(p_1, ..., p_{d-1}) = \left(\ln\left(\frac{1-\sum_{i=1}^{d-1} p_i}{p_1}\right), ..., \ln\left(\frac{1-\sum_{i=1}^{d-1} p_i}{p_{d-1}}\right)\right). \tag{1.9}$$

Setting each component to zero,

$$p_j = 1 - \sum_{i=1}^{d-1} p_i\,, \qquad \forall j \tag{1.10}$$

which is fulfilled only for $p_j = d^{-1}\ \forall j$. By definition, this is the condition for maximally entangled states, with $S_{\rm max} = \ln(d)$.

The property (iii) assures that quantum correlations cannot originate from classical communication channels (CC) and local operations (LO). The purpose of Sec. 1.2 is to go deeply into the physical motivation behind this statement, rather than checking (iii) for the von Neumann entropy (1.7). However, the interested reader can find a huge literature which demonstrates it is always possible to find a LOCC map which takes a maximally entangled state to any bipartite pure state [29].

In addition to (i,ii,iii), the von Neumann entropy satisfies other properties which make the definition (1.7) more attractive than others, e.g. the Rényi entropy. Given two spatial subsystems A_1 and A_2, not necessarily one the complement of the other, the von Neumann entropy verifies two important inequalities [32–34], namely subadditivity

$$S_{A_1\cup A_2} \leq S_{A_1} + S_{A_2}\,, \tag{1.11}$$

and strong subadditivity

$$S_{A_1\cup A_2} + S_{A_1\cap A_2} \leq S_{A_1} + S_{A_2}\,, \tag{1.12}$$

providing an ordering between partitions. From subadditivity follows concavity,

$$S_A\left[\sum_i p_i\,\rho_i\right] \geq \sum_i p_i\, S_A\left[\rho_i\right]\,, \qquad \forall p_i\ :\ \sum_i p_i = 1\,. \tag{1.13}$$

Without going into details, it is important to keep in mind that the bipartite entanglement entropy is a measure of the mutual connections between partitions and represents a powerful theoretical probe for quantum many-body systems. The scaling of entanglement can reveal the long-distance properties or be useful to construct new algorithms to simulate the quantum many-body dynamics.

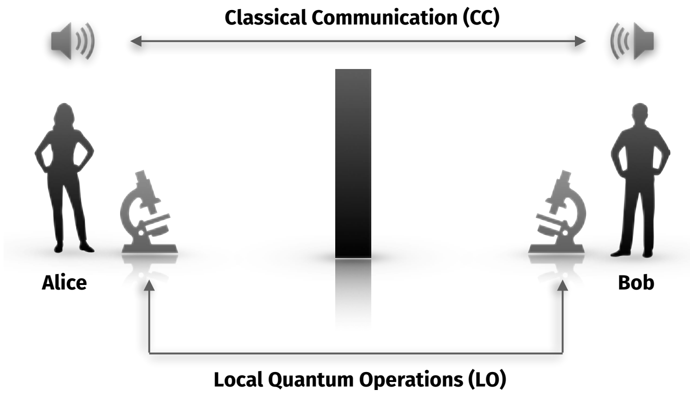

Figure 1.2: Typical quantum communication setting, where two experimentalists (Alice and Bob) can perform local measurements and communicate via classical telecom channels; the wall which separates Alice and Bob emphasises that no coherent exchange of particles is allowed.

1.2 Local operations and classical communication (LOCC)

LOCC protocols involve all the physical settings where two independent experimentalists have access only to one of the two partitions and can communicate over long distances via classical telecom technologies [29]. In this paragraph, we shall provide a simple example of state discrimination and quantum teleportation, which are meaningful tasks that can be achieved by LOCC protocols. For this purpose, we are going to make use of the experimental setup in Fig. 1.2, where two independent experimentalists, hereinafter Alice and Bob, may act via a local monitoring apparatus on a two-qubit system. Moreover, Alice and Bob can share information and communicate via classical channels.

The first example regards state discrimination, a quantum-informatics technique implemented to identify a specific quantum state by performing a finite, ideally small, number of local measurements. Let's assume Alice and Bob are given randomly two Bell states

$$|\phi\rangle = \frac{1}{\sqrt{2}}\left(|{\downarrow^A}\rangle \otimes |{\downarrow^B}\rangle + |{\uparrow^A}\rangle \otimes |{\uparrow^B}\rangle\right), \tag{1.14}$$

$$|\theta\rangle = \frac{1}{\sqrt{2}}\left(|{\uparrow^A}\rangle \otimes |{\downarrow^B}\rangle - |{\downarrow^A}\rangle \otimes |{\uparrow^B}\rangle\right), \tag{1.15}$$

which are maximally entangled states. Without communication, Alice and Bob can not distinguish the two states, since the measurement statistics is exactly the same. Indeed, there is the same probability 1/2 to get the outcomes ± 1 after monitoring the local observable σ_z^A. In order to discriminate the states, suppose Alice can communicate to Bob the measurement outcome via a classical channel. To give a practical example, assume Alice gets the outcome -1. Therefore, Bob can make a local measurement and use the information from the Alice's lab to distinguish the states. For instance, if Bob gets the outcome -1 after monitoring σ_z^B, according to the projection postulate, the post-measured state is $|\downarrow^A\rangle \otimes |\downarrow^B\rangle$ and he can conclude the initial state was $|\phi\rangle$. Via this simple example, we showed that LOCC protocols might be used to distinguish quantum states and, above all, cannot increase the entanglement since we get separable states.

The second example concerns quantum teleportation, which is a standard technique to transfer information between two distant laboratories which communicate via classical channels [35–39]. As before, we use the same scheme in Fig. 1.2. Suppose Alice has a qubit and wants to transfer it to Bob, who is placed at long distances. Of course, we implicitly assume that any coherent exchange of qubits is allowed. The qubit in Alice's lab is

$$|A\rangle = \alpha |\uparrow^A\rangle + \beta |\downarrow^A\rangle \,, \tag{1.16}$$

where $\alpha, \beta \in \mathbb{C}$ are complex coefficients which verify the normalization condition

$$|\alpha|^2 + |\beta|^2 = 1 \,. \tag{1.17}$$

We assume to prepare another entangled state, the Bell state $|\theta\rangle$ in Eq. (1.15), with the first qubit to Alice and the second one to Bob. Under these hypothesis, the full state $|\Psi\rangle = |A\rangle \otimes |\theta\rangle$ reads

$$\begin{aligned} |\Psi\rangle &= \frac{\alpha}{\sqrt{2}} \left(|\uparrow^A\rangle \otimes |\uparrow^A\rangle \otimes |\downarrow^B\rangle - |\uparrow^A\rangle \otimes |\downarrow^A\rangle \otimes |\uparrow^B\rangle \right) \\ &\quad + \frac{\beta}{\sqrt{2}} \left(|\downarrow^A\rangle \otimes |\uparrow^A\rangle \otimes |\downarrow^B\rangle - |\downarrow^A\rangle \otimes |\downarrow^A\rangle \otimes |\uparrow^B\rangle \right) . \end{aligned} \tag{1.18}$$

Now we introduce a Bell basis for the first and the second spin in Alice's lab,

$$|\phi_\pm^A\rangle = \frac{1}{\sqrt{2}} \left(|\uparrow^A\rangle \otimes |\uparrow^A\rangle \pm |\downarrow^A\rangle \otimes |\downarrow^A\rangle \right) , \tag{1.19}$$

$$|\theta_\pm^A\rangle = \frac{1}{\sqrt{2}} \left(|\uparrow^A\rangle \otimes |\downarrow^A\rangle \pm |\downarrow^A\rangle \otimes |\uparrow^A\rangle \right) , \tag{1.20}$$

and the state $|\Psi\rangle$ can be written as

$$\begin{aligned} |\Psi\rangle = \frac{1}{2} \Big[& |\phi_+^A\rangle \otimes \left(\alpha |\downarrow^B\rangle - \beta |\uparrow^B\rangle \right) + |\phi_-^A\rangle \otimes \left(\alpha |\downarrow^B\rangle + \beta |\uparrow^B\rangle \right) \\ & - |\theta_+^A\rangle \otimes \left(\alpha |\uparrow^B\rangle - \beta |\downarrow^B\rangle \right) - |\theta_-^A\rangle \otimes \left(\alpha |\uparrow^B\rangle + \beta |\downarrow^B\rangle \right) \Big] . \end{aligned} \tag{1.21}$$

Suppose Alice takes a joint measurement on her lab. According to the projection postulate and the decomposition (1.21), Alice can obtain as outcome one of the states of the Bell basis (1.19,1.20), with the same probability 1/4. After taking the local measurement, the wave function collapses and Alice uses the classical channels to communicate to Bob the corresponding outcome. The knowledge of the outcome is fundamental for Bob to reproduce the initial Alice's state. Indeed, depending on the Alice's outcome, the Bob's state is a particular linear combination of $|\uparrow^B\rangle$ and $|\downarrow^B\rangle$, with coefficients α and β. Therefore, Bob can perform a special local operation to reconstruct the initial Alice's qubit. For instance, if Alice projects on $|\theta_+^A\rangle$, Bob gets $|B\rangle = -\alpha\,|\uparrow^B\rangle + \beta\,|\downarrow^B\rangle$ and he needs to apply the local operator $-\sigma_z^B$: $-\sigma_z^B\,|B\rangle = \alpha\,|\uparrow^B\rangle + \beta\,|\downarrow^B\rangle$. In general, for each case, the transformation rules read

$$
\begin{aligned}
|\phi_+^A\rangle &\implies \mathrm{i}\sigma_y\left(\alpha\,|\downarrow^B\rangle - \beta\,|\uparrow^B\rangle\right) = \alpha\,|\uparrow^B\rangle + \beta\,|\downarrow^B\rangle\,, && (1.22)\\
|\phi_-^A\rangle &\implies \sigma_x\left(\alpha\,|\downarrow^B\rangle + \beta\,|\uparrow^B\rangle\right) = \alpha\,|\uparrow^B\rangle + \beta\,|\downarrow^B\rangle\,, && (1.23)\\
|\theta_+^A\rangle &\implies -\sigma_z\left(-\alpha\,|\uparrow^B\rangle + \beta\,|\downarrow^B\rangle\right) = \alpha\,|\uparrow^B\rangle + \beta\,|\downarrow^B\rangle\,, && (1.24)\\
|\theta_-^A\rangle &\implies -\mathbb{1}\left(-\alpha\,|\uparrow^B\rangle - \beta\,|\downarrow^B\rangle\right) = \alpha\,|\uparrow^B\rangle + \beta\,|\downarrow^B\rangle\,, && (1.25)
\end{aligned}
$$

and the initial state $|A\rangle$ is reconstructed. Quantum teleportation has been realised experimentally, where the polarization of a photon is transferred by performing a joint Bell-state measurement on the input photon and the member of the shared entangled photon pair [35]. It is important to remind that teleportation cannot be superluminal and any qubit cannot be reconstructed until the accompanying classical information arrives. This is another way to enunciate the *no-communication theorem*, which states the impossibility to transfer information between Alice and Bob by only making local measurements in each lab. This important theorem solves some apparent paradoxes in quantum mechanics, such as the EPR paradox [15].

1.3 Entanglement and mixed states

More generally, a quantum system is described by a mixed state, which takes the general form

$$\rho = \sum_i p_i\,|\psi_i\rangle\langle\psi_i|\,, \tag{1.26}$$

where $\{|\psi_i\rangle\}$ is a set of normalized states but not necessarily orthogonal, and $p_i \in [0,1]$ are probabilities that sum up to one: $\sum_i p_i = 1$.

For mixtures, the state ρ is a product state if $\rho = \rho_A \otimes \rho_B$. On the other hand, the state ρ is separable if

$$\rho = \sum_i p_i \, \rho_{i\,A} \otimes \rho_{i\,B} \,, \tag{1.27}$$

In all other cases, the state ρ is entangled.

If ρ is a product state, the system is uncorrelated. If ρ is separable (1.27), it can be produced only through LOCC protocols and shares classical correlations [30, 31]. Once again, entangled states clearly emerge as the most intriguing aspects of quantum mechanics, carrying correlations that cannot originate from classical procedures. We conclude that, for mixed states the entanglement entropy is no longer a good measure of entanglement since both quantum and classical correlations contribute. Note that, pure states can be either product states or entangled states.

For mixed states, it is necessary to introduce other measures of entanglement like the *negativity* or the *logarithmic negativity*. To explain the idea behind these measures, assume that Alice and Bob share a joint density matrix of two spins. Suppose to transpose the density matrix for that part of the system which corresponds to the Alice's lab. This partial transposition is equivalent to a time reversal transformation in Alice's lab. However, only unentangled states still reproduce physical density matrices under partial transposition. In any other case, entangled states are mapped into nonphysical operators with negative eigenvalues. The negativity and the logarithmic negativity quantify how much the eigenvalues of the partial transposed density matrix are negative and then how far the mixed state is from an unentangled state.

1.4 Entanglement and quantum phase transitions

In this section, we would like to emphasise the mutual connection between entanglement entropy and quantum phase transitions. While classical phase transitions occur at finite temperature, quantum phase transitions take place at zero temperature [40, C4] and are driven by quantum fluctuations. Let H_0 be the Hamiltonian of a closed quantum system and suppose $|\Psi\rangle$ is the ground state. Imagine to perturb the system with an operator gH_1 which does not commute with H_0, where g is a tunable parameter. After turning on the parameter g, the ground state $|\Psi(g)\rangle$ is modified until we reach a quantum critical point at which we observe a crossover between two different ground states, with a typical power law decay of the energy gap and the correlation length. A prototypical example is the Hamiltonian of the XY spin chain,

$$H = -\sum_i h\sigma_i^z + \left(\frac{1+\kappa}{2}\sigma_i^x\sigma_{i+1}^x + \frac{1-\kappa}{2}\sigma_i^y\sigma_{i+1}^y\right), \tag{1.28}$$

where σ^x, σ^y, σ^z are the Pauli matrices, κ is the anisotropy constant and h is the transverse field. It can be proved that the couple of parameters (κ, h) distinguish an oscillatory and non-oscillatory phase in the phase diagram [C4, 41, C5, 42].

The purpose of this section is not to discuss about quantum phase transitions, of which there is a huge literature about [40, C4]. On the other hand, we would like to recall and quote some known results for one-dimensional systems, which are the subject of study of this thesis. Assume the system is at the ground state and let l be the size of a partition embedded in a L-site quantum chain. It is possible to prove that the behaviour of the entanglement entropy changes whether the system is at the critical point or not [43, 44]. Indeed, at the critical point $g = g_c$ the entanglement entropy scales logarithmically with l, showing a sub-extensive behaviour. Otherwise, away from the critical point ($g \neq g_c$), the entanglement behaviour is governed by a correlation length ξ. In such a case, if $\xi \ll l$, the entropy is proportional to $\ln \xi$, with a manifest area-law behaviour. In other terms, this implies that only the chain sites close to the boundary between the two partitions contribute to quantum correlations.

$$S_l = \begin{cases} \ln l & g = g_c \\ \ln \xi & g \neq g_c \end{cases} \tag{1.29}$$

1.5 Entanglement entropy for Gaussian states

Computing the von Neumann entropy for many-body quantum systems has always been challenging and many theoretical and numerical techniques have been developed to address this problem, e.g. tensor network [1, 3–6], Replica approach [43, 45], charged moments approach [46]. However, computing entanglement turns to be very simple in same specific contexts. Here, we are going to illustrate the Peschel's trick [47–50], a famous approach to compute the entanglement entropy for Gaussian states and quadratic lattice Hamiltonian operators. In this section, we deal with fermionic systems but similar techniques may be implemented for bosons as well.

Let's consider a L-site chain of free fermions. Let $c, c^\dagger$ be the fermionic creation and annihilation operators,

$$\{c_i^\dagger, c_j\} = \delta_{ij}, \qquad \{c_i, c_j\} = 0. \tag{1.30}$$

Suppose $|\Psi\rangle$ verifies the Wick's theorem, which reads

$$\langle c^\dagger_{\alpha_1}...c^\dagger_{\alpha_n}c_{\beta_1}...c_{\beta_n}\rangle_\Psi = \sum_{j=1}^{n}(-1)^{n-j}\langle c^\dagger_{\alpha_1}c_{\beta_j}\rangle_\Psi\langle c^\dagger_{\alpha_2}...c^\dagger_{\alpha_n}c_{\beta_1}...c_{\beta_{j-1}}c_{\beta_{j+1}}...c_{\beta_n}\rangle_\Psi\,, \tag{1.31}$$

assuming that $\langle c_j c_i\rangle_\Psi = 0\ \forall i, j$. Thanks to the Wick's theorem, any many body quantity is provided by the two-point functions $C_{ij} = \langle c^\dagger_j c_i\rangle_\Psi$, which therefore fully characterise the state $|\Psi\rangle$. As an example, one may consider the Néel state or the ground state of the non-interacting Hamiltonian (1.30), which is a Slater determinant.

Let A be a subsystem with l contiguous sites. Let $\rho_A = \mathrm{tr}_B(|\Psi\rangle\langle\Psi|)$ be the reduced density matrix, where B is the complementary partition. If ρ verifies the Wick's theorem, ρ_A is fully characterised by the reduced correlation matrix $(\mathbf{C}_A)_{ij} = \langle c^\dagger_j c_i\rangle_\Psi,\ \forall i, j \in A$. In particular, ρ_A turns to be the Gaussian operator

$$\rho_A = \frac{e^{-\mathcal{H}_A}}{Z}\,, \qquad Z = \mathrm{tr}\big(e^{-\mathcal{H}_A}\big)\,, \tag{1.32}$$

where

$$\mathcal{H}_A = \sum_{ij\in A} M_{ij}c^\dagger_i c_j\,, \tag{1.33}$$

is a fictitious Hamiltonian called *entanglement Hamiltonian* and $\mathbf{M}$ a given coefficient matrix to be determined. In order to diagonalize $\mathcal{H}_A$, we perform the canonical transformation

$$c_i = \sum_{k=1}^{l} U_{ik}\eta_k\,, \tag{1.34}$$

where $\mathbf{U}$ is a unitary matrix and η_k are the eigenmodes of $\mathcal{H}_A$. In other terms, $\mathbf{U}^\dagger\mathbf{M}\mathbf{U}$ is a diagonal matrix with elements ϵ_k, and

$$\mathcal{H}_A = \sum_{k=1}^{l}\epsilon_k\eta^\dagger_k\eta_k\,, \qquad Z^{-1} = \prod_{k=1}^{l}\frac{e^{\epsilon_k}}{1+e^{\epsilon_k}}\,. \tag{1.35}$$

The correlation matrix becomes

$$\langle c^\dagger_j c_i\rangle_{\rho_A} = \mathrm{tr}_A(c^\dagger_j c_i\rho_A) = \sum_{k_1\,k_2} U^*_{j\,k_1}U_{i\,k_2}\langle\eta^\dagger_{k_1}\eta_{k_2}\rangle_{\rho_A}\,, \qquad \forall i, j\in A\,. \tag{1.36}$$

However, due to the Gaussian ansatz (1.32), the matrix with elements $\langle\eta^\dagger_{k_1}\eta_{k_2}\rangle_{\rho_A}$ is diagonal and $\langle\eta^\dagger_k\eta_k\rangle_{\rho_A} = f(\epsilon_k)$, where $f(\epsilon_k) = (1+e^{\epsilon_k})^{-1}$ is the Fermi-Dirac distribution. Eq. (1.36) relates the reduced correlation matrix $\mathbf{C}_A$ with the coefficient matrix $\mathbf{M}$,

$$\mathbf{C}_A = \frac{1}{\mathbb{1} + e^{\mathbf{M}}} . \tag{1.37}$$

At this point, the computation of the von Neumann entropy is quite simple. According to Def. (1.7),

$$\begin{aligned} S_A[\rho] &= -\langle \ln \rho_A \rangle_{\rho_A} , \\ &= \langle \mathcal{H}_A \rangle_{\rho_A} + \ln Z , \\ &= \sum_{k=1}^{l} \epsilon_k \left[f(\epsilon_k) - \ln\left(\frac{e^{\epsilon_k}}{1 + e^{\epsilon_k}} \right) \right] , \\ &= -\sum_{k=1}^{l} \left[\zeta_k \ln \zeta_k + (1 - \zeta_k) \ln(1 - \zeta_k) \right] , \end{aligned} \tag{1.38}$$

where ζ_k are the eigenvalues of the reduced density matrix $\mathbf{C}_A$. Eq. (1.38) is known as the *Peschel's trick* [47–50], which is a very powerful method to compute the entanglement entropy for Gaussian states. The Peschel's trick reduces the problem to the eigendecomposition of the matrix $\mathbf{C}_A$.

Eq. (1.38) is especially helpful to access the entanglement evolution under Gaussian preserving dynamical protocols. For instance, one may consider the unitary dynamics generated by a simple quadratic Hamiltonian of hopping fermions,

$$H = \sum_{ij} h_{ij} c_i^\dagger c_j , \tag{1.39}$$

where $\mathbf{h}$ is an Hermitian coefficient matrix. The time-evolved state $|\Psi(t)\rangle = e^{-\mathrm{i}Ht} |\Psi\rangle$ (here $\hbar = 1$) is still a Gaussian state and the equation of motion of the correlation matrix $\mathbf{C}(t)_{ij} = \langle \Psi(t)| c_j^\dagger c_i |\Psi(t)\rangle$ is

$$\frac{\mathrm{d}\mathbf{C}}{\mathrm{d}t} = -\mathrm{i}[\mathbf{h}, \mathbf{C}] . \tag{1.40}$$

The time evolution of the bipartite entanglement entropy comes from the solution of Eq. (1.40) and the subsequent truncation of the matrix $\mathbf{C}(t)$ to the subsystem A.

The previous results may be generalised for non-vanishing correlators $\langle c_i c_j \rangle_\Psi$. In such a case, we introduce the Majorana fermions

$$y_i^1 = c_i^\dagger + c_i , \qquad y_i^2 = \mathrm{i}(c_i^\dagger - c_i) , \tag{1.41}$$

which are Hermitian ($y_k^{1\dagger} = y_k^1$, $y_k^{2\dagger} = y_k^2$) and satisfy the Clifford algebra

$$\{y_k^1, y_\ell^1\} = 2\delta_{k\ell} , \qquad \{y_k^2, y_\ell^2\} = 2\delta_{k\ell} , \qquad \{y_k^1, y_\ell^2\} = 0 . \tag{1.42}$$

Hence the vector $\mathbf{Y} = (y_1^1, \dots, y_L^1, y_1^2, \dots, y_L^2)$ verifies the identity $\mathbf{Y}^\dagger \cdot \mathbf{Y} = 2L$. It can be shown that the reduced density matrix ρ_A satisfies the Gaussian ansatz (1.32) [51, 52], where

$$\mathcal{H}_A = -\frac{1}{4}\mathbf{Y}^\dagger \cdot \boldsymbol{\mathcal{M}} \cdot \mathbf{Y}, \qquad Z = \mathrm{tr}\left\{e^{\frac{1}{4}\mathbf{Y}^\dagger \cdot \boldsymbol{\mathcal{M}} \cdot \mathbf{Y}}\right\} = \sqrt{\det(\mathbb{1} + e^{\boldsymbol{\mathcal{M}}})}. \tag{1.43}$$

$\boldsymbol{\mathcal{M}}$ is a $2l \times 2l$ Hermitian ($\boldsymbol{\mathcal{M}}^\dagger = \boldsymbol{\mathcal{M}}$) and anti-symmetric ($\boldsymbol{\mathcal{M}}^\mathrm{T} = -\boldsymbol{\mathcal{M}}$) matrix. Furthermore,

$$\boldsymbol{\mathcal{M}} = \ln\left(\frac{\mathbb{1} - \boldsymbol{\Theta}_A}{\mathbb{1} + \boldsymbol{\Theta}_A}\right), \tag{1.44}$$

where

$$(\boldsymbol{\Theta}_A)_{ij} = \frac{1}{2}\,\mathrm{tr}\left\{[Y_i, Y_j]\rho(t)\right\} = \frac{1}{2}\langle [Y_i, Y_j]\rangle(t), \qquad \forall i, j \in A \tag{1.45}$$

is the reduced correlation matrix. The matrix $\boldsymbol{\Theta}_A$ is Hermitian ($\boldsymbol{\Theta}_A^\dagger = \boldsymbol{\Theta}_A$) and anti-symmetric ($\boldsymbol{\Theta}_A^\mathrm{T} = -\boldsymbol{\Theta}_A$) as well. Again, using Def. (1.7), Eqs. (1.43,1.44) and the anti-symmetry of $\boldsymbol{\mathcal{M}}$,

$$\begin{aligned} S_A[\rho] &= -\frac{1}{4}\sum_{i\,j=1}^{2l} \mathcal{M}_{ij}\langle Y_i Y_j\rangle_{\rho_A} + \frac{1}{2}\ln\left(\det(\mathbb{1} + e^{\boldsymbol{\mathcal{M}}})\right), \\ &= -\frac{1}{2}\,\mathrm{tr}\Big((\mathbb{1} + \boldsymbol{\Theta}_A)\ln(\mathbb{1} + \boldsymbol{\Theta}_A)\Big) + l\ln(2). \end{aligned} \tag{1.46}$$

Eq. (1.46) is not computationally expensive and allows us to access the entanglement entropy from the knowledge of the reduced correlation matrix $\boldsymbol{\Theta}_A$. The price we pay in presence of pairing terms $\langle c_i c_j\rangle$ is to deal with $2l \times 2l$ matrices.

As before, Eq. (1.46) is especially helpful for the entanglement evolution under Gaussian preserving dynamical protocols. For instance, one may consider a unitary dynamics generated by the quadratic Hamiltonian

$$H = \frac{1}{4}\mathbf{Y}^\dagger \cdot \boldsymbol{\mathcal{T}} \cdot \mathbf{Y}, \tag{1.47}$$

where $\boldsymbol{\mathcal{T}}$ is a $2L \times 2L$ anti-symmetric and Hermitian matrix. The time evolved state $|\Psi(t)\rangle = e^{-\mathrm{i}Ht}|\Psi\rangle$ is still Gaussian and the equation of motion of the correlation matrix $\boldsymbol{\Theta}(t)_{ij} = \frac{1}{2}\langle\Psi(t)|\,[Y_i, Y_j]\,|\Psi(t)\rangle$ reads

$$\frac{\mathrm{d}\boldsymbol{\Theta}}{\mathrm{d}t} = -\mathrm{i}[\boldsymbol{\mathcal{T}}, \boldsymbol{\Theta}]. \tag{1.48}$$

Again, from the solution of Eq. (1.48), we obtain the reduced matrix $\boldsymbol{\Theta}_A(t)$ and then the full evolution of the bipartite entanglement entropy.

As we shall see in Chapter 4, Peschel's trick is extremely useful to compute the entanglement dynamics under Gaussian preserving dynamical maps, where the unitary evolution is perturbed by continuous measurements of local observables.

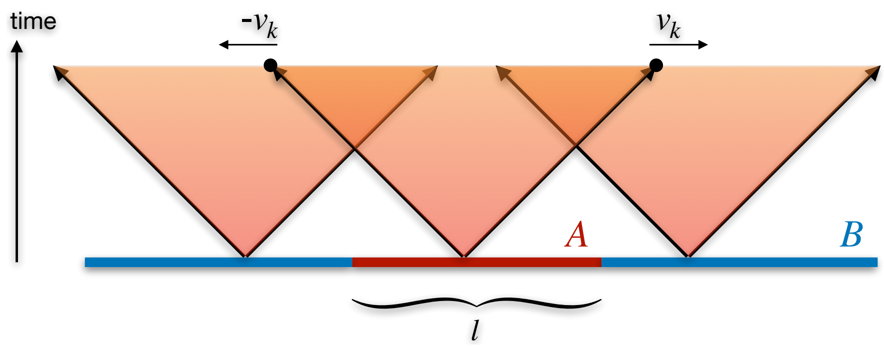

Figure 1.3: After quenching the state, pairs of entangled quasi-particles are emitted from every chain site with opposite momenta $\pm k$, taking values in the Brillouin zone $[-\pi, \pi]$. The entanglement at time t between the partitions A and B is proportional to the number of shared quasi-particle pairs.

1.6 Entanglement spreading and quasiparticle picture

The mechanisms behind the spread of correlations are often very complicated and not intuitive. However, much progress has been made by studying the relation between thermodynamics and entanglement in the framework of nonequilibrium dynamics of quantum correlations. Quantum quench dynamics are paradigmatic protocols where the system is prepared in a steady state, e.g. the ground state, and then a parameter in the Hamiltonian operator is suddenly modified. For integrable systems, the nonequilibrium dynamics and the von Neumann entropy are efficiently described by the quasi-particle picture [53–56]. Entanglement and correlations result to be generated by pairs of quasi-particles moving ballistically with opposite momenta. In this section, we shall introduce the quasi-particle picture, which inspired a couple of research works we present in this thesis (see Chapters 4, 5).

Let's consider a chain of non-interacting fermions with nearest neighbour interactions. The unitary dynamics is generated by the Hamiltonian (1.39), where

$$h_{ij} = -\frac{1}{2}(\delta_{i,j-1} + \delta_{i,j+1}), \tag{1.49}$$

which is diagonalized by the Fourier modes

$$\eta_k = \frac{1}{\sqrt{L}} \sum_{j=0}^{L-1} e^{-\mathrm{i}kj} c_j, \tag{1.50}$$

where L is the total number of chain sites and k is the particle momentum taking values in the Brillouin zone $\mathcal{B} = \{-\pi + 2\pi n/L \; n \in \{0, ..., L-1\}\}$. Therefore, Eq. (1.39) with the single-particle Hamiltonian (1.49) takes the form

$$H = \sum_{k\in\mathcal{B}} \epsilon_k\, \eta_k^\dagger \eta_k\,, \tag{1.51}$$

where the $\epsilon_k = -\cos(k)$ are the single particle eigenvalues.

The basic idea is that highly excited and low entangled states behave as reservoir of classical excitations. After the quench, quasiparticle pairs are emitted from every point in space and spread ballistically with opposite momenta $\pm k$ and group velocity $v_k := \partial_k \epsilon_k = \sin(k)$ (see Fig. 1.3). The maximum velocity is $v_m = 1$, which is limited by the Lieb-Robinson bound. Entanglement generation is strictly connected to the quasi-particles motion. In particular, those excitations generated at the same sites are entangled while those created far apart from each other are incoherent. During unitary evolution, these pairs propagate coherently and remain entangled, while no entanglement is generated between different pairs. Of course, as the excitations propagate, larger regions of the system get entangled.

Let $\mathcal{I} = [x_1, x_2]$ be the spatial interval which defines the subsystem A. Entanglement at time t originates from the quasi-particle pairs such that one partner is inside the interval $\mathcal{I}$ and the other is outside,

$$S_A[\rho(t)] = \int_{-\pi}^{\pi} \frac{\mathrm{d}k}{2\pi} \int_{\mathcal{Q}_{k,t}} dx\; s(x - v_k t, k, 0)\,, \tag{1.52}$$

where $\mathcal{Q}_{k,t} = \{x \in \mathcal{I} \mid x - 2v_k t \notin \mathcal{I}\}$ and $s(x,k,t) = s(x - v_k t, k, 0)$ is the entanglement entropy contribution for a quasi-particle pair at positions x and $x - 2v_k t$ with quasi-momenta k and $-k$, respectively. It is known that, at least for certain classes of quenches in integrable models, the function $s(x,k,t)$ can be conjectured from the equivalence between entanglement and thermodynamic entropy in the stationary state [53, 55–59]:

$$s(x,k,t) = s_{YY}[n(x,k,t)]\,, \tag{1.53}$$

where

$$s_{YY}[n] = -n\ln n - (1-n)\ln(1-n)\,, \tag{1.54}$$

is the Yang-Yang entropy and

$$n(x,k,t) = \sum_{j=0}^{L-1} e^{2\mathrm{i}kj} \langle c^\dagger_{x+j}(t) c_{x-j}(t)\rangle\,, \tag{1.55}$$

is the Wigner function. For spatially independent initial condition, e.g. the Néel state, $s = s(k)$ and the entanglement entropy reduces to

$$S_A[\rho(t)] = \int_{-\pi}^{\pi} \frac{\mathrm{d}k}{2\pi} \min(l, 2|v_k|t) s(k)\,, \tag{1.56}$$

where $l = x_2 - x_1$ is the length of the subsystem. For initial Néel states, $s(k) = \ln(2)$ and the entanglement entropy is characterised by a linear growth $S_A[\rho(t)] = 4\ln(2)t/\pi$ for $t < l/2$, until reaching the stationary value $S_A[\rho(t)] = \ln(2)l$ for $t \to \infty$.

Chapter 2

Open quantum systems

An open quantum system is a quantum-mechanical system $\mathcal{S}$ interacting with another quantum system $\mathcal{B}$, playing the role of the external environment. Hence the total Hilbert space is $\mathscr{H} = \mathscr{H}_\mathcal{S} \otimes \mathscr{H}_\mathcal{B}$, where $\mathscr{H}_\mathcal{S}$ and $\mathscr{H}_\mathcal{B}$ are the Hilbert subspaces of the system $\mathcal{S}$ and the environment $\mathcal{B}$. If $\rho \in \mathscr{H}$ is the total density matrix, then the evolution of $\rho_\mathcal{S} = \mathrm{tr}_\mathcal{B}(\rho) \in \mathscr{H}_\mathcal{S}$ is characterised by the internal dynamics plus the interactions with the surroundings.

To begin, we suppose that the total system $\mathcal{S}+\mathcal{B}$ is described the Hamiltonian

$$H(t) = H_S \otimes \mathbb{1}_B + \mathbb{1}_S \otimes H_B + H_I(t)\,, \tag{2.1}$$

where H_S and H_B determine the internal evolution of the two subsystems; $H_I(t)$ is the interaction Hamiltonian, which encodes all the couplings between the system and the environment. In general, the total quantum-mechanical system is closed but not isolated, as when it is subjected to external time-dependent fields. For simplicity, we assume that the interaction Hamiltonian $H_I(t)$ includes any possible time-dependent contribution to the total Hamiltonian $H(t)$.

The evolution of the full state ρ is governed by the the Liouville-von Neumann equation (we set $\hbar = 1$),

$$\frac{\mathrm{d}\rho}{\mathrm{d}t} = -\mathrm{i}[H(t), \rho]\,, \tag{2.2}$$

with solution

$$\rho(t) = U(t)\,\rho(0)\,U(t)^\dagger\,, \tag{2.3}$$

$$U(t) = \mathcal{T}_\leftarrow \exp\left\{-\mathrm{i}\int_0^t H(s)\,\mathrm{d}s\right\}, \tag{2.4}$$

where $\rho(0)$ is the initial condition at time $t = 0$ and $\mathcal{T}_\leftarrow$ is the Dyson time-ordering operator, which orders products of time-dependent Hamiltonians such that their time-arguments increase from right to left as indicated by the arrow. The reduced density operator is

$$\rho_S(t) = \mathrm{tr}_B \left\{ U(t)\, \rho(0)\, U(t)^\dagger \right\} , \tag{2.5}$$

and solves the differential equation

$$\frac{\mathrm{d}\rho_S}{\mathrm{d}t} = -\mathrm{i}\, \mathrm{tr}_B \left\{ [H(t), \rho] \right\} . \tag{2.6}$$

The main purpose of the theory of open quantum systems is to derive the equation of motion of $\rho_S(t)$ in the reduced space of the system's degrees of freedom. More formally, the goal is to find the *dynamical map* $V(t)$ from the Liouville space $\mathcal{S}(\mathscr{H}_S)$ of density operators onto itself, $V(t) \;:\; \mathcal{S}(\mathscr{H}_S) \to \mathcal{S}(\mathscr{H}_S)$, such that

$$\rho_S(t) := V(t)\rho_S(0) = \mathrm{tr}_B \left\{ U(t)\, \rho(0)\, U(t)^\dagger \right\} . \tag{2.7}$$

In fact, a complete mathematical description of the combined system-environment dynamics is often too much complicated. For instance, the environment could be a thermal bath with infinitely many degrees of freedom, and thus an exact treatment would require to handle an infinite number of coupled equations of motion. Beside this, we do not want to develop a fully detailed theory of bath but rather a simpler formalism in the reduced space of the system's degrees of freedom, where a few parameters like the bath temperature encode the influence of the external environment on the system.

Since any dynamical map $V(t)$ for $\rho_S = \mathrm{tr}_B(\rho)$ depends on the state $\rho(0)$, the choice of the initial conditions is still a matter of scientific debate. In this respect, the most simple assumption is that the initial state is a product state. Choosing initially uncorrelated partitions has always been considered a natural hypothesis and it is the starting point to generate completely positive trace-preserving (CPTP) dynamical maps, e.g. the markovian Lindblad evolution [60, 61, C6]. Complete positivity is a stronger condition than simple positivity. In fact, if simple positivity ensures that the dynamical map $V(t)$ always generates positive semi-definite density matrices $\rho_S(t)$, by definition complete positivity guarantees that any extended dynamical map $V(t) \otimes \mathbb{1}_N$ emerging from the coupling between the system $\mathcal{S}$ and any N-level ancilla, is still positive. Without going immediately into details which will be largely provided in this manuscript (see also Chapter 6), we can anticipate that the product state hypothesis, as well as the need of complete positivity as dynamical postulate, has been questioned a lot. For instance, in Ref. [60] it is argued that initial correlated states may not generate CPTP dynamical maps.

For the moment, let's assume the initial state is a product state $\rho(0) = \rho_S(0) \otimes \rho_B(0)$, where $\rho_S(0)$ is the reduced density matrix of the system $\mathcal{S}$ and $\rho_B(0)$ the reduced density operator of the environment $\mathcal{B}$. By hypothesis, $\rho_B(0)$ is a stationary state of H_B, e.g. any thermal equilibrium state, and the influence of the system dynamics on the reservoir is negligible, which means $\rho_B(t) \simeq \rho_B(0) = \rho_B$. Therefore, the evolution of the reduced density matrix $\rho_S(t)$ reads

$$\rho_S(t) := V(t)\rho_S(0) = \mathrm{tr}_B \left\{ U(t)(\rho_S(0) \otimes \rho_B)U(t)^\dagger \right\} . \tag{2.8}$$

In order to rewrite the abstract map (2.8) in a more useful form, we consider the spectral decomposition of ρ_B,

$$\rho_B = \sum_\alpha \lambda_\alpha \left|\varphi_\alpha\right\rangle \left\langle\varphi_\alpha\right| , \tag{2.9}$$

where $\{|\varphi_\alpha\rangle\}$ is an orthonormal complete set in $\mathscr{H}_B$, λ_α are positive real coefficients and $\sum_\alpha \lambda_\alpha = 1$ due to the normalization condition. Hence we get

$$\begin{aligned} V(t)\rho_S(0) &= \sum_{\alpha\beta} \lambda_\alpha \left\langle\varphi_\beta\right| U(t) \left(\rho_S(0) \otimes \left|\varphi_\alpha\right\rangle \left\langle\varphi_\alpha\right|\right) U(t)^\dagger \left|\varphi_\beta\right\rangle \\ &= \sum_{\alpha\beta} W_{\alpha\beta}(t)\rho_S(0)W_{\alpha\beta}(t)^\dagger , \end{aligned} \tag{2.10}$$

where

$$W_{\alpha\beta}(t) = \sqrt{\lambda_\beta} \left\langle\varphi_\alpha\right| U(t) \left|\varphi_\beta\right\rangle , \qquad \sum_{\alpha\beta} W_{\alpha\beta}(t)^\dagger W_{\alpha\beta}(t) = \mathbb{1}_S . \tag{2.11}$$

The operators into (2.11) are the so-called *Kraus operators* and make $V(t)$ a completely positive trace-preserving (CPTP) dynamical map [C6].

2.1 Markovian Lindblad generator

If we promote the variable t to a continuous variable, we get an one-parameter family $\{V(t),\ t > 0\}$ of dynamical maps, where $V(0) = \mathbb{1}$. Such a family describes the dynamics of open systems, which is often very complicated. However, if the characteristic time scales of the reservoir correlation functions are much smaller than the time scale of the reduced system dynamics, it is justified to neglect any memory effect and

$$V(t_1)V(t_2) = V(t_1 + t_2) \qquad \forall t_1, t_2 \geq 0 . \tag{2.12}$$

Eq. (2.12) is called Markov approximation and $\{V(t),\ t > 0\}$ is a *quantum dynamical semigroup*, that is a continuous, one-parameter family of dynamical maps which is closed under the standard product and satisfies the associative property. The most general form which verifies the semigroup property is $V(t) = e^{\mathcal{L}t}$. Eq. (2.12) implies

$$\frac{\mathrm{d}\rho_S}{\mathrm{d}t} = \mathcal{L}\,\rho_S\,, \tag{2.13}$$

which is a markovian quantum master equation. $\mathcal{L}$ is the generator of the open dynamics, and it is called Liouvillian super-operator.

In this section, we shall derive the general form of the Liouvillian $\mathcal{L}$ for a finite-dimensional Hilbert space $\mathscr{H}_S$: $\dim(\mathscr{H}_S) = N$. However, the prove could be generalised for infinite-dimensional spaces [C6], as is the case with harmonic oscillators (Chapter 6). The Liouville space has dimension N^2 and is equipped by the scalar product

$$(A, B) := \mathrm{tr}\big(A^\dagger B\big)\,, \tag{2.14}$$

where A and B are general Hilbert operators. Let $\{F_i\}$, $i \in \{1, \ldots, N^2\}$ be a complete basis of orthonormal operators,

$$(F_i, F_j) = \mathrm{tr}\{F_i^\dagger F_j\} = \delta_{ij}\,. \tag{2.15}$$

For simplicity, let's put $F_{N^2} = \mathbb{1}_S/\sqrt{N}$, such that the other basis operators are traceless. In fact, by definition,

$$(F_{N^2}, F_i) = \frac{1}{\sqrt{N}}\,\mathrm{tr}\{F_i\} = 0\,, \qquad \forall i \neq N^2\,. \tag{2.16}$$

Applying the completeness relation to the Kraus operator $W_{\alpha\beta}(t)$ (2.11), we obtain

$$W_{\alpha\beta}(t) = \sum_{i=1}^{N^2} F_i\,(F_i, W_{\alpha\beta}(t))\,. \tag{2.17}$$

Using Eq. (2.17) into Eq. (2.10), we get

$$V(t)\,\rho_S = \sum_{i\,j=1}^{N^2} c_{ij}(t)\,F_i \rho_S F_j^\dagger\,, \tag{2.18}$$

where

$$c_{ij}(t) = \sum_{\alpha\,\beta} (F_i, W_{\alpha\beta}(t))\,(F_j, W_{\alpha\beta}(t))^*\,. \tag{2.19}$$

The coefficient matrix $\mathbf{c}$, with elements into Eq. (2.19), is manifestly Hermitian. Since the matrix $\mathbf{c}$ also verifies the identity

$$\mathbf{v}^\dagger\,\mathbf{c}\,\mathbf{v} = \sum_{\alpha\,\beta} \left| \left(\sum_i v_i F_i, W_{\alpha\beta}(t) \right) \right|^2 \geq 0\,. \qquad \forall \mathbf{v}\,, \tag{2.20}$$

then **c** is positive semi-definite, which means **c** has real and positive eigenvalues. The Liouvillian super-operator $\mathcal{L}$ derives from the dynamical map (2.18),

$$\begin{aligned}
\mathcal{L}\rho_S = \frac{\mathrm{d}\rho_S}{\mathrm{d}t} &= \lim_{\epsilon\to 0}\frac{1}{\epsilon}\left(V(\epsilon)\rho_S - \rho_S\right) \\
&= \lim_{\epsilon\to 0}\frac{1}{\epsilon}\left(\sum_{i\,j=1}^{N^2} c_{ij}(\epsilon)\, F_i\rho_S F_j^\dagger - \rho_S\right) \\
&= \lim_{\epsilon\to 0}\frac{1}{\epsilon}\Bigg[\left(\frac{c_{N^2N^2}(\epsilon)}{N} - 1\right)\rho_S + \sum_{i\,j=1}^{N^2-1} c_{ij}(\epsilon)\, F_i\rho_S F_j^\dagger \\
&\quad + \frac{1}{\sqrt{N}}\sum_{i\,j=1}^{N^2-1}\left(c_{iN^2}(\epsilon)\, F_i\rho_S + c_{N^2i}(\epsilon)\,\rho_S F_i^\dagger\right)\Bigg]. \qquad (2.21)
\end{aligned}$$

Let **a** be a coefficient matrix with elements

$$a_{N^2N^2} := \frac{1}{\epsilon}\left(c_{N^2N^2}(\epsilon) - N\right), \qquad (2.22)$$

$$a_{iN^2} := c_{iN^2}/\epsilon, \qquad \forall i \in \{1, ..., N^2-1\} \qquad (2.23)$$

$$a_{N^2i} := c_{N^2i}/\epsilon, \qquad \forall i \in \{1, ..., N^2-1\} \qquad (2.24)$$

$$a_{ij} := c_{ij}/\epsilon. \qquad \forall i, j \in \{1, ..., N^2-1\} \qquad (2.25)$$

Using Eqs. (2.22,2.23,2.24,2.25) into Eq. (2.21),

$$\mathcal{L}\rho_S = -\mathrm{i}[H, \rho_S] + \{G, \rho_S\} + \sum_{i\,j=1}^{N^2-1} a_{ij}\, F_i\rho_S F_j^\dagger, \qquad (2.26)$$

where

$$\mathcal{F} := \frac{1}{\sqrt{N}}\sum_{i=1}^{N^2-1} a_{iN^2}F_i, \qquad (2.27)$$

$$H := \frac{1}{2\mathrm{i}}(\mathcal{F}^\dagger - \mathcal{F}), \qquad (2.28)$$

$$G := \frac{1}{2N}a_{N^2N^2}\mathbb{1}_S + \frac{1}{2}(\mathcal{F}^\dagger + \mathcal{F}). \qquad (2.29)$$

Since the dynamical map is trace preserving ($\mathrm{tr}\{\mathcal{L}\rho_S\} = 0$) and $\mathrm{tr}\,[H, \rho_S] = 0$, we require

$$\mathrm{tr}_S\left\{\left(2G + \sum_{i\,j=1}^{N^2-1} a_{ij}F_j^\dagger F_i\right)\rho_S\right\} \stackrel{!}{=} 0. \qquad (2.30)$$

Eq. (2.30) must hold for any operator ρ_S, and thus

$$G = -\frac{1}{2}\sum_{i\,j=1}^{N^2-1} a_{ij} F_j^{\dagger} F_i \,. \tag{2.31}$$

Eq. (2.31) relates the operators G and F_j. Using Eq. (2.31) into Eq. (2.26),

$$\mathcal{L}\rho_S = -\mathrm{i}[H, \rho_S] + \sum_{i\,j=1}^{N^2-1} a_{ij}\left(F_i \rho_S F_j^{\dagger} - \frac{1}{2}\{F_j^{\dagger} F_i, \rho_S\}\right), \tag{2.32}$$

which is not yet in the proper Lindblad form. However, the reduced $(N^2-1)\times(N^2-1)$ coefficient matrix $\mathbf{a}^r$ with elements $(\mathbf{a}^r)_{ij} = a_{ij}\,,\ \ \forall i, j \in \{1, ..., N^2-1\}$ is Hermitian and positive semi-definite [C6], and may be diagonalized with a unitary transformation $\boldsymbol{\mu}$,

$$\boldsymbol{\gamma} = \boldsymbol{\mu}^{\dagger}\,\mathbf{a}^r\,\boldsymbol{\mu} = \mathrm{diag}(\gamma_1, \gamma_2, ..., \gamma_{N^2-1})\,, \tag{2.33}$$

with non-negative eigenvalues γ_i. Thanks to a unitary rotation of the operators F_i, $L_i := \sum_j \mu_{ji} F_j$, we get

$$\mathcal{L}\rho_S = -\mathrm{i}[H, \rho_S] + \sum_{i=1}^{N^2-1} \gamma_i\left(L_i \rho_S L_i^{\dagger} - \frac{1}{2}\{L_i^{\dagger} L_i, \rho_S\}\right). \tag{2.34}$$

Eq. (2.34) is called *Lindblad equation* and provides the generator of the quantum dynamical semigroup, which verifies the Markov property. The first term $-\mathrm{i}[H, \rho_S]$ corresponds to the unitary part of the dynamics, while the operators L_i are usually referred to as *Lindblad operators* or *jump operators*. The Lindblad equation is a CPTP dynamical map and this statement is mathematically equivalent to the condition $\gamma_i \geq 0\ \forall i$, which is automatically verified because the coefficient matrix $\mathbf{a}^r$ is Hermitian and positive semi-definite [61].

One may notice that the non-negative eigenvalues γ_i have the dimension of a frequency, assuming that L_i are dimensionless. For this reason, γ_i are known as *jump rates*, in reference to the *quantum trajectory techniques* [62–66]. Quantum trajectory techniques represent a powerful tool to access the open dynamics (2.34) without solving directly the differential equation for the density operator. The Lindblad dynamics (2.34) can be rewritten as a stochastic average over individual trajectories evolving in time as pure states. Hence, the dynamics of each trajectory is generated by an effective non-Hermitian Hamiltonian and it is perturbed by quantum jumps appearing scholastically in time with characteristic rates γ_i.

Beside this, it is also important to remark that, in general, H cannot be strictly identified with the Hamiltonian of the reduced system $\mathcal{S}$, since H may contain additional terms due to the coupling with the environment, i.e. the Lamb shifts. Furthermore, the Liouvillian $\mathcal{L}$ does not fix uniquely the form of the Hamiltonian H and the Lindblad operators L_i. In fact, $\mathcal{L}$ is invariant under unitary transformations of the jump operators L_i and inhomogeneous transformations

$$L_i \to L_i + \alpha_i \,, \quad H \to H + \frac{1}{2\mathrm{i}} \sum_j \gamma_j (\alpha_j^* L_j - \alpha_j L_j^\dagger) + \beta \,, \quad \forall \alpha_i \in \mathbb{C}, \, \forall \beta \in \mathbb{R} \,. \tag{2.35}$$

Up to now, we have derived mathematically the generator of the dynamical semigroup. However, from a physical viewpoint, it is desirable to get the dynamical map starting from first principles. Below, we provide the microscopic derivation of the Lindblad equation, following Ref. [C6] as guideline.

In the interaction picture, the Liouville-von Neumann equation (2.2) reduces onto

$$\frac{\mathrm{d}\tilde{\rho}}{\mathrm{d}t} = -\mathrm{i}\big[\widetilde{H}_I(t), \tilde{\rho}\big] \,, \tag{2.36}$$

where the symbol $\sim$ is used to label operators in the interaction picture. More explicitly,

$$\begin{aligned} \tilde{\rho} &= e^{\mathrm{i}H_0 t} \, \rho \, e^{-\mathrm{i}H_0 t} \,, && (2.37) \\ \widetilde{H}_I(t) &= e^{\mathrm{i}H_0 t} \, H_I(t) \, e^{-\mathrm{i}H_0 t} \,, && (2.38) \end{aligned}$$

and $H_0 = H_S \otimes \mathbb{1}_B + \mathbb{1}_S \otimes H_B$. By integration of Eq. (2.36),

$$\frac{\mathrm{d}\tilde{\rho}}{\mathrm{d}t} = -\mathrm{i}\big[\widetilde{H}_I(t), \tilde{\rho}(0)\big] - \int_0^t \mathrm{d}s \, \big[\widetilde{H}_I(t), \big[\widetilde{H}_I(s), \tilde{\rho}(s)\big]\big] \,, \tag{2.39}$$

and tracing over the degrees of freedom of the bath,

$$\frac{\mathrm{d}\tilde{\rho}_S}{\mathrm{d}t} = -\mathrm{i} \, \mathrm{tr}_B \left(\big[\widetilde{H}_I(t), \tilde{\rho}(0)\big] \right) - \int_0^t \mathrm{d}s \, \mathrm{tr}_B \left(\big[\widetilde{H}_I(t), \big[\widetilde{H}_I(s), \tilde{\rho}(s)\big] \big] \right) . \tag{2.40}$$

Eq. (2.40) is not a closed time-evolution equation for $\tilde{\rho}_S$ because the time derivative still depends on the full density matrix $\tilde{\rho}$. To proceed, we need further assumptions and approximations. Firstly, we prepare the total system in the uncorrelated state

$$\rho(0) = \rho_S(0) \otimes \rho_B(0) \,, \tag{2.41}$$

at time $t = 0$, which is a strong but necessary hypothesis to build the CPTP Lindblad map. Second, we assume that $\rho_B(0)$ is a steady state of H_B, such as any thermal equilibrium state $\rho_B \propto e^{-H_B/T}$, where T is the bath temperature.

Third, we use the *Born approximation*, which applies in the weak coupling regime between the system and the bath, such that the correlations between the two are negligible,

$$\rho(t) \simeq \rho_S(t) \otimes \rho_B(0)\,. \tag{2.42}$$

Since the bath state $\rho_B(0)$ is a steady state of H_B and $\rho_B(0)$ is not affected by the dynamics of the system, we write $\rho_B = \rho_B(0)$ to simplify the notation.

Furthermore, we assume a time independent system-bath interaction

$$H_I = \sum_\alpha A_\alpha \otimes B_\alpha\,, \tag{2.43}$$

where A_α and B_α are Hilbert operators acting on the system and the environment, respectively. In the interaction picture,

$$\widetilde{H}_I(t) = \sum_\alpha \widetilde{A}_\alpha(t) \otimes \widetilde{B}_\alpha(t)\,, \tag{2.44}$$

where

$$\widetilde{A}_\alpha(t) = e^{\mathrm{i}H_S t} A_\alpha e^{-\mathrm{i}H_S t}\,, \tag{2.45}$$
$$\widetilde{B}_\alpha(t) = e^{\mathrm{i}H_B t} B_\alpha e^{-\mathrm{i}H_B t}\,. \tag{2.46}$$

From Eqs. (2.41,2.44,2.45,2.46), the first addendum of Eq. (2.40) reads

$$\begin{aligned} \mathrm{tr}_B\left(\left[\widetilde{H}_I(t), \tilde{\rho}(0)\right]\right) = & \sum_\alpha \Big[\widetilde{A}_\alpha(t)\rho_S(0) \otimes \mathrm{tr}_B(B_\alpha \rho_B(0)) \\ & -\rho_S(0)\widetilde{A}_\alpha(t) \otimes \mathrm{tr}_B(B_\alpha \rho_B(0))\Big]\,. \end{aligned} \tag{2.47}$$

Without loss of generality, Eq. (2.47) may be simplified if we assume $\mathrm{tr}_B(B_\alpha \rho_B(0)) = 0\ \forall \alpha$. Indeed, if this condition is not fulfilled, we can still rewrite the Hamiltonian as

$$\begin{aligned} H = & \left[H_S + \sum_\alpha \mathrm{tr}_B(B_\alpha \rho_B(0))\, A_\alpha\right] \otimes \mathbb{1}_B + \mathbb{1}_S \otimes H_B \\ & + \sum_\alpha A_\alpha \otimes \left[\, B_\alpha - \mathrm{tr}_B(B_\alpha \rho_B(0))\,\right]\,. \end{aligned} \tag{2.48}$$

Hence, Eq. (2.40) becomes

$$\frac{\mathrm{d}\tilde{\rho}_S}{\mathrm{d}t} = -\int_0^t \mathrm{d}s\, \mathrm{tr}_B\left(\left[\,\widetilde{H}_I(t), \left[\widetilde{H}_I(s), \tilde{\rho}(s)\right]\,\right]\right)\,. \tag{2.49}$$

Under these hypothesis, Eq. (2.49) reduces onto

$$\begin{aligned}\frac{\mathrm{d}\tilde{\rho}_S}{\mathrm{d}t} &= -\sum_{\alpha\beta}\int_0^t \mathrm{d}s\,\mathrm{tr}_B\left(\left[\widetilde{A}_\alpha(t)\otimes\widetilde{B}_\alpha(t),\left[\widetilde{A}_\beta(t)\otimes\widetilde{B}_\beta(t),\tilde{\rho}_S(t)\otimes\rho_B\right]\right]\right),\\ &= -\sum_{\alpha\beta}\int_0^t \mathrm{d}s\left(\mathcal{B}_{\alpha\beta}(s)\left[\widetilde{A}_\alpha(t),\widetilde{A}_\beta(t-s)\tilde{\rho}_S(t-s)\right]+\mathrm{h.c.}\right), \qquad (2.50)\end{aligned}$$

where

$$\mathcal{B}_{\alpha\beta}(s) := \mathrm{tr}_B\left(\widetilde{B}_\alpha(t)\widetilde{B}_\beta(t-s)\rho_B\right) = \mathrm{tr}_B\left(\widetilde{B}_\alpha(s)\widetilde{B}_\beta(0)\rho_B\right), \qquad (2.51)$$

and

$$\mathrm{tr}_B\left(\widetilde{B}_\beta(t-s)\widetilde{B}_\alpha(t)\rho_B\right) = \mathcal{B}_{\beta\alpha}(-s) = \mathcal{B}_{\alpha\beta}(s)^*. \qquad (2.52)$$

Unfortunately, Eq. (2.50) depends on the entire history of the system state, since the argument of $\tilde{\rho}_S(t-s)$ runs from 0 to t. Our goal is to get a time-local differential equation so that the evolution satisfies the semigroup property (2.12). According to the Markov approximation, the time scale τ_B of the reservoir correlation functions $\mathcal{B}_{\alpha\beta}(s)$ is much smaller than the time scale of the system dynamics. More explicitly, we assume

$$\left|\mathcal{B}_{\alpha\beta}(s)\right| \sim e^{-s/\tau_B}, \qquad (2.53)$$

where $\tau_B \ll 1$ and $t \gg \tau_B$. Therefore, since $\mathcal{B}_{\alpha\beta}(s) \simeq 0$ for $s \gg \tau_B$, we can replace $\tilde{\rho}_S(t-s)$ by $\tilde{\rho}_S(t)$,

$$\frac{\mathrm{d}\tilde{\rho}_S}{\mathrm{d}t} = -\sum_{\alpha\beta}\int_0^\infty \mathrm{d}s\left(\mathcal{B}_{\alpha\beta}(s)\left[\widetilde{A}_\alpha(t),\widetilde{A}_\beta(t-s)\tilde{\rho}_S(t)\right]+\mathrm{h.c.}\right), \qquad (2.54)$$

which is the *Redfield equation* [C6, C7]. The upper limit of the integral in Eq. (2.54) can be extended to infinity because $\mathcal{B}_{\alpha\beta}(s)$ rapidly approaches zero.

Let's define the Fourier representation,

$$\mathcal{A}_\alpha(\omega) = \sum_{\substack{a,b\\ \omega=\epsilon_b-\epsilon_a}} \langle\epsilon_a|A_\alpha|\epsilon_b\rangle\,|\epsilon_a\rangle\langle\epsilon_b|, \qquad (2.55)$$

where $|\epsilon_a\rangle\langle\epsilon_a|$ is the projection onto the eigenspace corresponding to the eigenvalue ϵ_a of $H_S = \sum_a \epsilon_a|\epsilon_a\rangle\langle\epsilon_a|$. Using $\mathcal{A}_\alpha(\omega) = \mathcal{A}_\alpha(-\omega)^\dagger$ and $\widetilde{A}_\alpha(t) = \sum_\omega \mathcal{A}_\alpha(\omega)e^{-\mathrm{i}\omega t}$,

$$\frac{\mathrm{d}\tilde{\rho}_S}{\mathrm{d}t} = -\sum_{\alpha\beta}\sum_{\omega_1\omega_2}\left(\Gamma_{\alpha\beta}(\omega_1)e^{\mathrm{i}(\omega_2-\omega_1)t}\left[\mathcal{A}_\alpha(\omega_2)^\dagger,\mathcal{A}_\beta(\omega_1)\tilde{\rho}_S(t)\right]+\mathrm{h.c.}\right), \qquad (2.56)$$

where

$$\Gamma_{\alpha\beta}(\omega) := \int_0^{+\infty} \mathrm{d}s\, e^{\mathrm{i}\omega s} \mathcal{B}_{\alpha\beta}(s) \,. \tag{2.57}$$

Eq. (2.56) is still not in the Lindblad form, due to the presence of the off-diagonal terms $\omega_1 \neq \omega_2$. The *rotating wave approximation* (or *secular approximation*) states that the off-diagonal terms are rapidly oscillating for $t > |\omega_1 - \omega_2|^{-1}$ and, for this reason, they average to zero. More formally,

$$\min_{\omega_1 \neq \omega_2} |\omega_1 - \omega_2| > \tau_B^{-1} \,, \tag{2.58}$$

and thus

$$\frac{\mathrm{d}\tilde{\rho}_S}{\mathrm{d}t} = -\sum_{\alpha\beta}\sum_{\omega} \left(\Gamma_{\alpha\beta}(\omega)\big[\mathcal{A}_\alpha(\omega)^\dagger, \mathcal{A}_\beta(\omega)\tilde{\rho}_S(t)\big] + \text{h.c.}\right) . \tag{2.59}$$

The complex coefficients $\Gamma_{\alpha\beta}(\omega)$ may be written as

$$\Gamma_{\alpha\beta}(\omega) := \frac{1}{2}\gamma_{\alpha\beta}(\omega) + \mathrm{i}S_{\alpha\beta}(\omega) \,, \tag{2.60}$$

where

$$\gamma_{\alpha\beta}(\omega) = \Gamma_{\alpha\beta}(\omega) + \Gamma_{\beta\alpha}(\omega)^* \,, \tag{2.61}$$

$$S_{\alpha\beta}(\omega) = \frac{1}{2\mathrm{i}}(\Gamma_{\alpha\beta}(\omega) - \Gamma_{\beta\alpha}(\omega)^*) \,, \tag{2.62}$$

are Hermitian coefficient matrices. Eq. (2.59) reduces into

$$\begin{aligned}\frac{\mathrm{d}\tilde{\rho}_S}{\mathrm{d}t} &= -\mathrm{i}[H_{\mathrm{LS}}, \tilde{\rho}_S] \\ &\quad + \sum_{\alpha\beta}\sum_{\omega} \gamma_{\alpha\beta}(\omega)\left(\mathcal{A}_\beta(\omega)\tilde{\rho}_S\mathcal{A}_\alpha(\omega)^\dagger - \frac{1}{2}\left\{\mathcal{A}_\alpha(\omega)^\dagger\mathcal{A}_\beta(\omega), \tilde{\rho}_S\right\}\right) ,\end{aligned} \tag{2.63}$$

where the operator

$$H_{\mathrm{LS}} := \sum_{\omega}\sum_{\alpha\beta} S_{\alpha\beta}(\omega)\mathcal{A}_\alpha(\omega)^\dagger\mathcal{A}_\beta(\omega) \,, \tag{2.64}$$

commutes with the Hamiltonian H_S ($[H_{\mathrm{LS}}, H_S] = 0$) and only produces a shift of the spectrum. For this reason, H_{LS} is usually referred to as Lamb shift. In the Schrödinger picture, Eq. (2.63) becomes

$$\begin{aligned}\frac{\mathrm{d}\rho_S}{\mathrm{d}t} &= -\mathrm{i}[H_S + H_{\mathrm{LS}}, \rho_S] \\ &\quad + \sum_{\alpha\beta}\sum_{\omega} \gamma_{\alpha\beta}(\omega)\left(\mathcal{A}_\beta(\omega)\rho_S\mathcal{A}_\alpha(\omega)^\dagger - \frac{1}{2}\left\{\mathcal{A}_\alpha(\omega)^\dagger\mathcal{A}_\beta(\omega), \rho_S\right\}\right) .\end{aligned} \tag{2.65}$$

Eq. (2.65) can be brought into the Lindblad form by diagonalizing the Hermitian matrix $\boldsymbol{\gamma}(\omega)$ with elements $\gamma_{\alpha\beta}(\omega)$. Indeed, using the spectral decomposition of the bath density operator $\rho_B = \sum_\mu \lambda_\mu |\mu\rangle\langle\mu|$, where $\lambda_\mu \geq 0\ \forall\mu$ and $\sum_\mu \lambda_\mu = 1$, it can be proved that

$$\mathbf{v}^\dagger\, \boldsymbol{\gamma}(\omega)\, \mathbf{v} = \lim_{T\to\infty} \frac{1}{T} \sum_\mu \lambda_\mu \left| \sum_\alpha \int_0^T \mathrm{d}s\, v_\alpha B_\alpha(s) e^{-\mathrm{i}\omega s} |\mu\rangle \right|^2 \geq 0\,, \quad \forall \mathbf{v}\,, \tag{2.66}$$

and then $\boldsymbol{\gamma}(\omega)$ is positive semi-definite. Finally, we get

$$\begin{aligned} \frac{\mathrm{d}\rho_S}{\mathrm{d}t} &= -\mathrm{i}[H_S + H_{\mathrm{LS}}, \rho_S] \\ &\quad + \sum_\alpha \sum_\omega \kappa_\alpha(\omega) \left(L_\alpha(\omega)\rho_S L_\alpha(\omega)^\dagger - \frac{1}{2}\left\{ L_\alpha(\omega)^\dagger L_\alpha(\omega), \rho_S \right\} \right), \end{aligned} \tag{2.67}$$

where $\kappa_\alpha(\omega) \geq 0\ \forall\alpha,\omega$ are the eigenvalues of $\boldsymbol{\gamma}(\omega)$ and $L_\alpha(\omega)$ are the Lindblad operators given by a unitary rotation of the operators $\mathcal{A}_\alpha(\omega)$. Eq. (2.67) is an important result and shows that the Lindblad dynamics naturally emerges from the initial product state hypothesis, the weak coupling limit, the Markov hypothesis and the secular approximation.

2.2 Quantum Langevin dynamics

In classical non-equilibrium statistical mechanics, the Langevin equations are a standard, successful and tested way to describe the dissipative dynamics towards its stationary (or equilibrium) state. However, the extension to quantum systems is not immediate and intuitive. In order to recall the difficulties connected to quantization, we consider the example of a single harmonic oscillator $H = \frac{g}{2}p^2 + \frac{\omega^2}{2g}x^2$, where g is the quantum coupling and ω is the angular frequency, see e.g. Ref. [C8]. If we write down the 'natural Langevin equations' (hereinafter we set $k_B = 1$), we get

$$\partial_t x = g p\,, \tag{2.68}$$

$$\partial_t p = -\frac{\omega^2}{g}x - \gamma p + \eta\,, \tag{2.69}$$

where the coupling with the external environment is described by the damping term $-\gamma p$ and the quantum noise η, which classically play the role of the friction and the random impulsive forces, respectively. If we assume η is a Gaussian white noise,

$$\langle \eta(t) \rangle = 0\,, \qquad \langle \eta(t)\eta(t') \rangle = \frac{2T\gamma}{g}\delta(t-t')\,. \tag{2.70}$$

Writing down the equation of motion of the equal time commutator $c(t) = \langle [x(t), p(t)] \rangle$, we get

$$\partial_t c(t) = -\gamma c(t) . \tag{2.71}$$

Solving for the boundary condition $c(0) = i\hbar$, we get $c(t) = i\hbar e^{-\gamma t}$, which is in contrast with the postulates of quantum mechanics.

The Bedeaux-Mazur proposal tried to address the harmonic oscillator problem starting from a mesoscopic non-equilibrium thermodynamic scheme [67, 68]. They built a new Liouvillian super-operator starting from the Gibbs' entropy postulate, a weak limit for the thermodynamic force, the conservation of probability and the Onsager relations. Therefore, they derived the Green's functions for position and momentum and they checked the consistency with the Heisenberg equations

$$\begin{aligned} \partial_t x &= g p + \eta^{(x)} , & (2.72)\\ \partial_t p &= -\frac{\omega^2}{g} x - \gamma p + \eta^{(p)} , & (2.73) \end{aligned}$$

and the noise correlators

$$\begin{aligned} \langle \eta^{(x)}(t)\, \eta^{(x)}(t') \rangle &= 0 , & (2.74)\\ \langle \eta^{(p)}(t)\, \eta^{(p)}(t') \rangle &= \frac{\hbar\gamma\omega}{g} \coth\left(\frac{\hbar\omega}{2T}\right) \delta(t-t') , & (2.75)\\ \langle \eta^{(x)}(t)\, \eta^{(p)}(t') \rangle &= -\langle \eta^{(p)}(t)\, \eta^{(x)}(t') \rangle = i\hbar \frac{\gamma}{2}\, \delta(t-t') . & (2.76) \end{aligned}$$

Differently from the classical formulation into Eqs. (2.68,2.69), one may observe the presence of an extra random velocity in Eq. (2.72). The set of Eqs. (2.74,2.75,2.76) satisfies the Markov property, as one can see from the Dirac deltas, and in the classical limit ($\hbar \to 0$) leads back to a classical brownian particle in a harmonic potential. Alongside this, we could mention that Eqs. (2.72,2.73) find also concrete and clear application in LRC circuits [14, 69–71], where the noises $(\eta^{(x)}, \eta^{(p)})$ are mapped into $(\eta^{(U)}, \eta^{(I)})$, for the voltage and current fluctuations.

Unfortunately, the Bedeaux-Mazur proposal (2.72,2.73) with the markovian correlators (2.74, 2.75, 2.76) does not verify the quantum fluctuation-dissipation theorem, a fundamental requirement for quantum equilibrium states and the second fundamental theorem of quantum thermodynamics. There are two different but equivalent ways to solve this problem. The first one is to follow the ab initio approach by Ford, Kac and Mazur, which considers a one-body system coupled to a large ensemble of harmonic oscillators through a bi-linear interaction Hamiltonian [72]. Solving the dynamics, Ford, Kac and Mazur found the explicit form of the noise correlators. Alternatively, one may use a phenomenological approach, following the proposal by Araújo, Wald and Henkel [14]. This method postulates the Heisenberg equations (2.72,2.73) and then the noise correlators are purpose-built to satisfy a set of desirable physical requirements,

(A) the canonical equal-time commutator $\langle [x(t), p(t)] \rangle = i\hbar$;

(B) the Kubo formula of linear response theory ;

(C) the virial theorem, both classical [C9–C11] and quantum-mechanical [14, 73], characterizing the stationary regime. For a quantum oscillator, it reads $\langle p^2 \rangle = \frac{\omega^2}{g^2} \langle x^2 \rangle$;

(D) the quantum fluctuation-dissipation theorem.

These are meant to guarantee that the stationary state will be a quantum equilibrium state. The conditions (A) and (B) fix the noise commutators, while the conditions (C) and (D) the noise anti-commutators. The microscopic derivation by Ford, Kac and Mazur and the axiomatic approach by Araújo, Wald and Henkel produce the same noises [14, 72]

$$\left\langle \left[\eta^{(x)}(t), \eta^{(p)}(t')\right] \right\rangle = i\hbar\gamma\delta(t-t') , \tag{2.77}$$

$$\left\langle \left\{\eta^{(x)}(t), \eta^{(p)}(t')\right\} \right\rangle = \gamma T \coth\left(\frac{\pi}{\hbar} T(t-t')\right) . \tag{2.78}$$

Eqs. (2.77,2.78) show that, in order to satisfy all the requirements (A-D), the noises must be explicitly non-markovian and the only physical parameters governing the dissipation are the damping constant γ and the bath temperature T, differently from Eq. (2.75). The interested reader can find a proof of the equivalence of the two approaches in Ref. [14].

Eqs. (2.72,2.73) with the correlators (2.77,2.78) represent the usual form of the *quantum Langevin equations*. As stressed in Ref. [14], the qualitative differences between the classical and quantum cases may be illustrated through the motion of a free one-dimensional Brownian particle. Indeed, the variance $\langle x(t)^2 \rangle$ scales linearly with time t at finite temperature, while $\langle x(t)^2 \rangle \propto \ln t$ at $T = 0$, showing that quantum diffusion is more weak than the classical analogous.

The axiomatic approach by Araújo, Wald and Henkel will be largely mentioned and used in this thesis, especially to characterise the noises of the *friction model* and *cavity model* into Chapter 6. In the last part of this chapter, we prefer to briefly introduce the microscopic derivation of the Langevin equations by Ford, Kac and Mazur, following Refs. [72, 74] as guideline. The knowledge of the ab-initio approach is also important to gain a overall view.

Suppose to couple a single oscillator to a large ensemble of harmonic oscillators, along with a bi-linear interaction Hamiltonian. The total system-bath

Hamiltonian reads

$$H = \frac{g}{2}p^2 + V(x) + \sum_i \frac{g_i}{2}p_i^2 + \frac{\omega_i^2}{2g_i}(x - q_i)^2\,, \tag{2.79}$$

where (x, p) and (q_i, p_i) are the system and bath variables, respectively. These quantum variables satisfy the commutation rules

$$[x, p] = \mathrm{i}\hbar\,, \qquad \left[q_i, p_j\right] = \mathrm{i}\hbar\delta_{ij}\,. \tag{2.80}$$

The interaction Hamiltonian is $H_I = -x \otimes \sum_i(\omega_i^2/g_i)q_i$, while $V(x)$ is any potential for which the spectrum of the system Hamiltonian

$$H_S = \frac{g}{2}p^2 + V(x)\,, \tag{2.81}$$

is lower bounded. The Heisenberg equations of motion read

$$\begin{aligned}
\partial_t x &= \frac{\mathrm{i}}{\hbar}[x, H] = gp\,, && (2.82)\\
\partial_t p &= \frac{\mathrm{i}}{\hbar}[p, H] = -\partial_x V(x) + \sum_j \frac{\omega_j^2}{g_j}(q_j - x)\,, && (2.83)\\
\partial_t q_j &= \frac{\mathrm{i}}{\hbar}\left[q_j, H\right] = g_j p_j\,, && (2.84)\\
\partial_t p_j &= \frac{\mathrm{i}}{\hbar}\left[p_j, H\right] = -\frac{\omega_j^2}{g_j}(q_j - x)\,, && (2.85)
\end{aligned}$$

Eliminating the momentum variables, we can rewrite the Heisenberg equations as

$$\begin{aligned}
\frac{1}{g}\partial_t^2 x + \partial_x V(x) &= \sum_j \frac{\omega_j^2}{g_j}(q_j - x)\,, && (2.86)\\
\partial_t^2 q_j + \omega_j^2 q_j &= \omega_j^2 x\,. && (2.87)
\end{aligned}$$

The solution of Eq. (2.87) may be written in terms of the homogeneous solution q_j^h of the differential equation

$$\partial_t^2 q_j^h + \omega_j^2 q_j^h = 0\,. \tag{2.88}$$

In particular, we get

$$q_j(t) = q_j^h(t) + x(t) - \int_{-\infty}^{t} \mathrm{d}s\, \cos[\omega_j(t - s)]\, \partial_s x(s)\,. \tag{2.89}$$

Eq. (2.89) deserves some more attention, because the retarded solution of the inhomogeneous equation breaks the time-reversal invariance of the original equations. The picture we have in mind is that at time $t = -\infty$ the particle is keeped fixed at $x = 0$, while the bath is at thermal equilibrium T. Next, the system is free to evolve with the Hamiltonian (2.79). If we use Eq. (2.89) into Eq. (2.86), we get

$$\frac{1}{g}\partial_t^2 x + \int_{-\infty}^{t} \mathrm{d}s\, \mu(t-s)\, \partial_s x(s) + \partial_x V(x) = F(t)\,, \tag{2.90}$$

where

$$\mu(t) = \sum_j \frac{\omega_j^2}{g_j} \cos\big(\omega_j t\big)\, \Theta(t)\,, \tag{2.91}$$

$$F(t) = \sum_j \frac{\omega_j^2}{g_j} q_j^h(t)\,, \tag{2.92}$$

and $\Theta(t)$ is the Heaviside step function. Here, $F(t)$ plays the role of the quantum noise. We remember that, in the distant past, the bath is at thermal equilibrium

$$\rho_B = \exp\{-H_B/T\}/\,\mathrm{tr}(\exp\{-H_B/T\})\,. \tag{2.93}$$

and the two-point functions read

$$\langle q_j q_k\rangle = \mathrm{tr}\big(q_j q_k \rho_B\big) = \frac{\hbar g_j}{2\omega_j} \coth\left(\frac{\hbar\omega_j}{2T}\right) \delta_{jk}\,, \tag{2.94}$$

$$\langle p_j p_k\rangle = \mathrm{tr}\big(p_j p_k \rho_B\big) = \frac{\hbar\omega_j}{2g_j} \coth\left(\frac{\hbar\omega_j}{2T}\right) \delta_{jk}\,, \tag{2.95}$$

$$\langle q_j p_k\rangle = -\langle p_j q_k\rangle = \frac{1}{2}\mathrm{i}\hbar\delta_{jk}\,. \tag{2.96}$$

Thanks to Eqs. (2.94,2.95,2.96), in the continuum limit we get

$$\frac{1}{2}\langle\{F(t),F(t')\}\rangle = \frac{\hbar}{\pi}\int_0^\infty \mathrm{d}\omega\ \Re\{\tilde{\mu}(\omega+\mathrm{i}0^+)\} \times \omega \coth\left(\frac{\hbar\omega}{2T}\right)\cos[\omega(t-t')]\,, \tag{2.97}$$

$$\frac{1}{2}\langle[F(t),F(t')]\rangle = -\frac{\mathrm{i}\hbar}{\pi}\int_0^\infty \mathrm{d}\omega\ \Re\{\tilde{\mu}(\omega+\mathrm{i}0^+)\}\,\omega\, \sin[\omega(t-t')]\,, \tag{2.98}$$

where

$$\tilde{\mu}(z) = \int_0^\infty \mathrm{d}t\ e^{\mathrm{i}zt}\mu(t) = \frac{\mathrm{i}}{2}\sum_j \frac{\omega_j^2}{g_j}\left[\frac{1}{z-\omega_j} + \frac{1}{z+\omega_j}\right], \qquad z\in\mathbb{C}\,. \tag{2.99}$$

Finally, if we assume $\Re\{\tilde{\mu}(\omega + \mathrm{i}0^+)\}$ to be independent on ω, we prove the equivalence with Eqs. (2.77,2.78), where $F = g\eta^{(p)} + \gamma\eta^{(x)} + \partial_t\eta^{(x)}$ [14].

Chapter 3

Phase-space formulation of quantum mechanics

The Wigner's phase-space picture is an alternative formulation of quantum mechanics where the position-momentum operators $(\hat{x}, \hat{p})$ and the quantum observables $\hat{O}(\hat{x}, \hat{p})$ are mapped onto classical variables (x, p) and real-valued functions $O(x, p)$ with domain in the phase-space. This facilitates connections to classical mechanics and semi-classical limits [75–77, C12, 78], where the quantum properties emerge as series expansion of $\hbar$. The phase-space formulation of quantum mechanics is of considerable practical use and has been used for a broad spectrum of applications. Although this approach has been originally formulated from the position-momentum operators $(\hat{x}, \hat{p})$, in quantum optics it is preferable to build a one-to-one map between bosonic creation/annihilation operators $(\hat{a}, \hat{a}^\dagger)$ and coherent state c-variables (α, α^*), which leads to the celebrated *characteristic function approach* and the *Q-P representations* [C12]. Recently, an analogous approach has been developed to treat open fermion systems, by mapping the Liouville-Fock space onto the Grassmann algebra. It represents a valid alternative to the third quantization method [79], thanks to the rich analytic and algebraic tools for functions in the Grassmann algebra.

In this chapter, we shall present the phase-space formalism, in its original formulation introduced by Wigner [26], from the single particle to the many-body case. Afterwhich, we shall show how the Wigner approach can be used in nonequilibrium physics, with some interesting applications in open systems.

3.1 Weyl transform

Quantum observables can be represented by Hermitian operators acting on the Hilbert space of system states, such that their eigenvalues coincide with the measurement outcomes. Quantisation establishes a map between classical variables and quantum operators, such that the canonical commutation relation $[\hat{x}, \hat{p}] = i\hbar$ between position $\hat{x}$ and momentum $\hat{p}$ holds, known as *Dirac correspondence rule*. However, non-linear classical observables in position and momentum generate ambiguities in the definition of the corresponding quantum counterpart. A typical example is the quantization of the classical observable $f(x, p) = xp$, where the standard commutative multiplication offers many possibilities,

$$f(x,p) = xp \qquad \longrightarrow \qquad \hat{f}(\hat{x}, \hat{p}) = \left\{ \hat{x}\hat{p},\ \hat{p}\hat{x},\ \frac{1}{2}(\hat{x}\hat{p} + \hat{p}\hat{x}),\ ... \right\}. \tag{3.1}$$

To solve this ambiguity, we introduce a one-to-one map $\Phi[\hat{f}] = f(x, p)$ between Hilbert space operators and phase-space functions. The existence of the inverse transform Φ^{-1} is guaranteed by the bijective correspondence. Since any classical observable is a combination of the position-momentum canonical variables, it is possible to introduce a new operation $\star$, which uniquely chatacterizes the product between two Hilbert operators $\hat{f}$, $\hat{g}$. In the phase-space formalism, it reads

$$\Phi^{-1}[f \star g] = \Phi^{-1}[f]\, \Phi^{-1}[g] = \hat{f}\hat{g}\,, \tag{3.2}$$

where the map Φ has to be consistent with the commutation relation $[\hat{x}, \hat{p}] = \mathrm{i}\hbar$. One may notice that the map Φ is not uniquely defined and different maps Φ imply different products $\star$, keeping in mind that $\star$ should reduce to the standard commutative product in the limit $\hbar \to 0$. The *Weyl quantisation* is one way to carry out this programme.

For any Hilbert operator $\hat{f}$, the *Weyl transform* is the functional [75, 80–83]

$$\Phi[\hat{f}] = f(x,p) = \int_{\mathbb{R}} e^{\frac{\mathrm{i}}{\hbar} p w} \left\langle x - w/2 \,\middle|\, \hat{f} \,\middle|\, x + w/2 \right\rangle \mathrm{d}w\,, \tag{3.3}$$

where $|x\rangle$ are the eigenstates of the position operator: $\hat{x}\,|x\rangle = x\,|x\rangle$. Eq. (3.3) may be rewritten in terms of the eigenstates $|p\rangle$ of the momentum operator $\hat{p}\,|p\rangle = p\,|p\rangle$, by using the completeness relation $\int \mathrm{d}p\,|p\rangle\langle p| = \mathbb{1}$ and the scalar product $\langle x|p\rangle = \frac{1}{\sqrt{2\pi\hbar}} e^{\frac{\mathrm{i}}{\hbar}xp}$,

$$\Phi[\hat{f}] = \int_{\mathbb{R}} e^{\frac{\mathrm{i}}{\hbar} x k} \left\langle p + k/2 \,\middle|\, \hat{f} \,\middle|\, p - k/2 \right\rangle \mathrm{d}k\,. \tag{3.4}$$

The Weyl transform is linear in $\hat{f}$, always well-defined and builds a unique phase-space representation for any quantum-mechanical operator.

For simple polynomials $\hat{Q}_n(\hat{x})$ or $\hat{Q}_n(\hat{p})$ of degree n, the Wigner representation coincides with the Dirac correspodence rule and

$$\Phi[\hat{Q}_n(\hat{x})] = Q_n(x)\,, \qquad \Phi[\hat{Q}_n(\hat{p})] = Q_n(p)\,. \tag{3.5}$$

The same observation holds for a fully symmetrized polynomial $\widehat{Q}_n(\hat{x},\widehat{p})$ of degree n, which may be expressed as

$$\widehat{Q}_n(\hat{x},\widehat{p}) = \hat{x}\widehat{Q}_{n-1}(\hat{x},\widehat{p}) + \widehat{Q}_{n-1}(\hat{x},\widehat{p})\hat{x}\,, \tag{3.6}$$

or as

$$\widehat{Q}_n(\hat{x},\widehat{p}) = \widehat{p}\widehat{Q}_{n-1}(\hat{x},\widehat{p}) + \widehat{Q}_{n-1}(\hat{x},\widehat{p})\widehat{p}\,, \tag{3.7}$$

where $\widehat{Q}_{n-1}(\hat{x},\widehat{p})$ is a polynomial of degree $n-1$ [80]. In other terms, the phase-space representation of a fully symmetrized polynomial $\widehat{Q}_n(\hat{x},\widehat{p})$ can be easily obtained with the substitution $\hat{x}\to x$ and $\widehat{p}\to p$, e.g. $\Phi[\hat{x}\widehat{p}+\widehat{p}\hat{x}] = 2xp$, $\Phi[\hat{x}^2\widehat{p}+2\hat{x}\widehat{p}\hat{x}+\widehat{p}\hat{x}^2] = 4x^2p$.

Apart from some particular cases, the Weyl transform of the standard product between Hilbert operators is not so simple. Let $f(x,p)$ and $g(x,p)$ be the phase-space representations of two operators $\widehat{f}$ and $\hat{g}$. Using Def. (3.3), the Weyl transform of the product $\widehat{f}\hat{g}$ is

$$\Phi[\widehat{f}\hat{g}] := f(x,p)\star g(x,p) = f(x,p)\exp\left(\frac{i\hbar}{2}\left(\overleftarrow{\partial}_x\overrightarrow{\partial}_p - \overleftarrow{\partial}_p\overrightarrow{\partial}_x\right)\right)g(x,p)\,, \tag{3.8}$$

where the exponential operator $\exp\left(\frac{i\hbar}{2}\left(\overleftarrow{\partial}_x\overrightarrow{\partial}_p - \overleftarrow{\partial}_p\overrightarrow{\partial}_x\right)\right)$ is called *Moyal product* [75]. The arrows indicate the direction for the differentiation; $\overrightarrow{\partial}$ acts on the right and $\overleftarrow{\partial}$ on the left. Notice that the Moyal product becomes the standard commutative product in the classical limit $\hbar\to 0$.

For the sake of completeness, the commutator $\left[\widehat{f},\hat{g}\right]$ and the anti-commutator $\{\widehat{f},\hat{g}\}$ are mapped into

$$\Phi\left(\left[\widehat{f},\hat{g}\right]\right) = 2if(x,p)\sin\left(\frac{\hbar}{2}\left(\overleftarrow{\partial}_x\overrightarrow{\partial}_p - \overleftarrow{\partial}_p\overrightarrow{\partial}_x\right)\right)g(x,p) \tag{3.9}$$

$$\Phi\left(\{\widehat{f},\hat{g}\}\right) = 2f(x,p)\cos\left(\frac{\hbar}{2}\left(\overleftarrow{\partial}_x\overrightarrow{\partial}_p - \overleftarrow{\partial}_p\overrightarrow{\partial}_x\right)\right)g(x,p)\,. \tag{3.10}$$

3.2 Definition of the Wigner function

The *Wigner function* is defined as [26, 75, 78, 80–83]

$$\mathcal{W}(x,p) := \int_{\mathbb{R}} e^{\frac{i}{\hbar}pw}\,\langle x-w/2\,|\,\hat{\rho}\,|\,x+w/2\rangle\,\mathrm{d}w \tag{3.11}$$

where $\hat{\rho}$ is the density operator of the system, which may be pure or mixed; $\hat{\rho}$ is assumed to be properly normalised ($\mathrm{tr}(\hat{\rho})=1$). The Wigner function $\mathcal{W}(x,p)$ is nothing but the Weyl transform of the density matrix and fully characterises the system. The Wigner function verifies the properties [78, 80]:

(i) $\mathcal{W}(x, p)$ is a real function but, in general, is not positive definite ;

(ii) by virtue of the Cauchy–Schwarz inequality, for a pure state, $\mathcal{W}(x, p)$ is constrained to

$$\left|\mathcal{W}(x, p)\right| \leq 2\,; \tag{3.12}$$

(iii) the marginals of the Wigner function coïncide with the probability densities in position and momentum space

$$\rho(x) := \langle x|\, \rho\, |x\rangle = \frac{1}{2\pi\hbar}\int \mathrm{d}p\, \mathcal{W}(x, p)\,, \tag{3.13}$$

$$\tilde{\rho}(p) := \langle p|\, \rho\, |p\rangle = \frac{1}{2\pi\hbar}\int \mathrm{d}x\, \mathcal{W}(x, p)\,; \tag{3.14}$$

(iv) If $O(x, p)$ is the Wigner representation of the observable $\widehat{O}$, the average value is

$$\langle\widehat{O}\rangle := \mathrm{tr}\big(\widehat{O}\hat{\rho}\big) = \frac{1}{2\pi\hbar}\iint \mathrm{d}x\, \mathrm{d}p\, O(x, p)\mathcal{W}(x, p)\,. \tag{3.15}$$

Since the Wigner function $\mathcal{W}(x, p)$ may take negative values, cannot strictly be interpreted as a joint probability distribution. However, as we shall see in Chapter 5, there are some special circumstances where the Wigner function may be pictorially viewed as a distribution of classical excitations. In general, $\mathcal{W}(x, p)$ is usually referred to as a *quasi-probability distribution*, in the sense that it may be used to compute any average quantity and probability, encoding all the features of quantum systems.

In this paragraph, we generalise the previous equations for many-body systems. In such a case, the position-momentum operators satisfy the commutation rules

$$[\hat{x}_j, \hat{x}_k] = 0\,, \quad [\widehat{p}_j, \widehat{p}_k] = 0\,, \quad [\hat{x}_j, \widehat{p}_k] = \mathrm{i}\hbar\delta_{jk}\,, \quad \forall j, k \in \{1, \dots, N\} \tag{3.16}$$

where N is the number of particles. The phase-space is $2N$-dimensional, generated by $(\boldsymbol{x}, \boldsymbol{p})$, where $\boldsymbol{x} = (x_1, \dots, x_N)$ and $\boldsymbol{p} = (p_1, \dots, p_N)$. It follows that any quantum operator $\widehat{f}(\hat{\boldsymbol{x}}, \widehat{\boldsymbol{p}})$ and its representation $f(\boldsymbol{x}, \boldsymbol{p})$ are a function of $2N$ variables. The Weyl transform for many-body systems is

$$\Phi[\widehat{f}] = \int \exp\left(\frac{\mathrm{i}}{\hbar}\boldsymbol{p}\cdot\boldsymbol{w}\right) \langle \boldsymbol{x} - \boldsymbol{w}/2 \,|\, \widehat{f} \,|\, \boldsymbol{x} + \boldsymbol{w}/2\rangle\, \mathrm{d}\boldsymbol{w}\,, \tag{3.17}$$

and the inverse transform is

$$\widehat{f} = \frac{1}{(2\pi\hbar)^{2N}} \iiiint f(\boldsymbol{k},\boldsymbol{h}) \exp\left(-\frac{\mathrm{i}}{\hbar}\Big[\boldsymbol{w}\cdot(\hat{\boldsymbol{x}}-\boldsymbol{k}) + \boldsymbol{z}\cdot(\widehat{\boldsymbol{p}}-\boldsymbol{h})\Big]\right) \mathrm{d}\boldsymbol{k}\,\mathrm{d}\boldsymbol{h}\,\mathrm{d}\boldsymbol{w}\,\mathrm{d}\boldsymbol{z}\,. \tag{3.18}$$

Thanks to Eq. (3.18), the many-body Moyal product becomes

$$f(\boldsymbol{x},\boldsymbol{p}) \star g(\boldsymbol{x},\boldsymbol{p}) = f(\boldsymbol{x},\boldsymbol{p}) \exp\left(\frac{\mathrm{i}\hbar}{2}\Big(\overleftarrow{\boldsymbol{\nabla}}_x\cdot\overrightarrow{\boldsymbol{\nabla}}_p - \overleftarrow{\boldsymbol{\nabla}}_p\cdot\overrightarrow{\boldsymbol{\nabla}}_x\Big)\right) g(\boldsymbol{x},\boldsymbol{p})\,, \tag{3.19}$$

where $\boldsymbol{\nabla}_x = (\partial/\partial x_1,\dots,\partial/\partial x_N)$, $\boldsymbol{\nabla}_p = (\partial/\partial p_1,\dots,\partial/\partial p_N)$ and $f(\boldsymbol{x},\boldsymbol{p})$, $g(\boldsymbol{x},\boldsymbol{p})$ are some analytic phase-space functions. The quantum state $\hat{\rho}$ is mapped into the Wigner function

$$\mathcal{W}(\boldsymbol{x},\boldsymbol{p}) = \int \exp\left(\frac{\mathrm{i}}{\hbar}\boldsymbol{p}\cdot\boldsymbol{w}\right) \langle \boldsymbol{x}-\boldsymbol{w}/2\,|\,\hat{\rho}\,|\,\boldsymbol{x}+\boldsymbol{w}/2\rangle\,\mathrm{d}\boldsymbol{w}\,, \tag{3.20}$$

where the features (i − iv) hold with obvious modifications. For many-body problems, it is also useful to define the reduced Wigner function, which reads

$$n(x,p) = N\int \mathcal{W}(x,x_2,\dots,x_N,p,p_2,\dots,p_N)\,\mathrm{d}x_2\dots\mathrm{d}x_N\mathrm{d}p_2\dots\mathrm{d}p_N\,. \tag{3.21}$$

The reduced Wigner function $n(x,p)$ is still a quasi-probability distribution function, but only gives a direct access to the single-particle quantities, e.g. the particle density in real space and average occupation in momentum space.

3.3 Evolution of the Wigner function

The goal of this section is to study the evolution of the Wigner function for both closed and open systems. In the first part, we shall focus on the unitary dynamics and then, following the same philosophy, we shall extend our picture to markovian Lindblad maps (see Sec.2.1). Hereinafter, we shall focus on one-dimensional systems, but all the results of this section may be easily generalised to many-body systems.

In this paragraph, we shall provide a pedagogical derivation of the Moyal equation [75, 84] for the evolution of the Wigner function. For closed quantum systems, the Liouville-von Neumann equation governs the time evolution of the density operator,

$$\frac{\mathrm{d}\hat{\rho}}{\mathrm{d}t} = -\frac{\mathrm{i}}{\hbar}[\widehat{H},\hat{\rho}], \tag{3.22}$$

where $\widehat{H}$ is the Hamiltonian operator. If $\widehat{H}$ is time-independent, the solution of Eq. (3.22) is

$$\hat{\rho}(t) = e^{-\frac{i}{\hbar}\widehat{H}t}\,\hat{\rho}(0)\,e^{\frac{i}{\hbar}\widehat{H}t}\,, \tag{3.23}$$

where $\hat{\rho}(0)$ is the initial state. Let $H(x,p)$ the phase-space representation of $\widehat{H}$. According to Eq. (3.9), the Weyl transform of the Liouville-von Neumann equation (3.22) is

$$\begin{aligned}
\partial_t \mathcal{W}(x,p,t) &= -\frac{i}{\hbar}\Phi\left(\left[\widehat{H},\hat{\rho}\right]\right)\,, \\
&= \frac{2}{\hbar}H(x,p)\sin\left(\frac{\hbar}{2}\left(\overleftarrow{\partial}_x\overrightarrow{\partial}_p - \overleftarrow{\partial}_p\overrightarrow{\partial}_x\right)\right)\mathcal{W}(x,p,t)\,,
\end{aligned} \tag{3.24}$$

Eq. (3.24) is the Moyal equation and provides the evolution of the Wigner function $\mathcal{W}(x,p,t)$. In series of $\hbar$, Eq. (3.24) becomes

$$\partial_t \mathcal{W}(x,p,t) = \{H(x,p), \mathcal{W}(x,p,t)\}_{\mathcal{PB}} + \mathcal{O}(\hbar^2)\,, \tag{3.25}$$

where $\{\mathcal{F},\mathcal{G}\}_{\mathcal{PB}} = \partial_x\mathcal{F}\partial_p\mathcal{G} - \partial_p\mathcal{F}\partial_x\mathcal{G}$ is the Poisson bracket which describes the classical dynamics. The semi-classical expansion (3.25) suggests that quantum corrections emerge at the second order in $\hbar$.

Below, we consider the Lindblad equation (see Sec. 2.1)

$$\frac{d\hat{\rho}}{dt} = -\frac{i}{\hbar}\left[\widehat{H},\hat{\rho}\right] + \sum_j \gamma_j\left(\hat{L}_j\hat{\rho}\hat{L}_j^\dagger - \frac{1}{2}\{\hat{L}_j^\dagger\hat{L}_j,\hat{\rho}\}\right)\,, \tag{3.26}$$

and we study the dynamics of $\hat{\rho}$ in the Wigner formalism. Let $L_j(x,p)$ be the phase-space representation of the jump operator $\hat{L}_j$. Thanks to the Moyal product (3.8) and Eqs. (3.9,3.10), the Weyl transform of Eq. (3.26) is

$$\begin{aligned}
\partial_t \mathcal{W}(x,p,t) &= -\frac{i}{\hbar}\Phi\left(\left[\widehat{H},\hat{\rho}\right]\right) + \sum_j\gamma_j\left[\Phi\left(\hat{L}_j\hat{\rho}\hat{L}_j^\dagger\right) - \frac{1}{2}\Phi\left(\{\hat{L}_j^\dagger\hat{L}_j,\hat{\rho}\}\right)\right] \\
&= \frac{2}{\hbar}H(x,p)\sin\left(\frac{\hbar}{2}\left(\overleftarrow{\partial}_x\overrightarrow{\partial}_p - \overleftarrow{\partial}_p\overrightarrow{\partial}_x\right)\right)\mathcal{W}(x,p,t) \\
&\quad -\sum_j\gamma_j\,\Phi\left(\hat{L}_j^\dagger\hat{L}_j\right)\cos\left(\frac{\hbar}{2}\left(\overleftarrow{\partial}_x\overrightarrow{\partial}_p - \overleftarrow{\partial}_p\overrightarrow{\partial}_x\right)\right)\mathcal{W}(x,p,t) \\
&\quad +\sum_j\gamma_j\,L_j(x,p)\star\mathcal{W}(x,p,t)\star L_j(x,p)^*\,,
\end{aligned} \tag{3.27}$$

where

$$\Phi\left[\hat{L}_j^\dagger\hat{L}_j\right] = L_j(x,p)^*\star L_j(x,p)\,, \tag{3.28}$$

is the Weyl transform of the operator $\hat{L}_j^\dagger \hat{L}_j$. In series of $\hbar$, each term reads

$$\begin{aligned}
\Phi\left[\hat{L}_j^\dagger \hat{L}_j\right] &= \left|L_j(x,p)\right|^2 \\
&\quad + \frac{i\hbar}{2}\{L(x,p)^*, L(x,p)\}_{\mathcal{PB}} + \mathcal{O}(\hbar^2)\,, \qquad (3.29)\\
\cos\left(\frac{\hbar}{2}\left(\overleftarrow{\partial}_x\overrightarrow{\partial}_p - \overleftarrow{\partial}_p\overrightarrow{\partial}_x\right)\right) &= 1 + \mathcal{O}(\hbar^2)\,, \qquad (3.30)\\
\sin\left(\frac{\hbar}{2}\left(\overleftarrow{\partial}_x\overrightarrow{\partial}_p - \overleftarrow{\partial}_p\overrightarrow{\partial}_x\right)\right) &= \frac{\hbar}{2}\left(\overleftarrow{\partial}_x\overrightarrow{\partial}_p - \overleftarrow{\partial}_p\overrightarrow{\partial}_x\right) + \mathcal{O}(\hbar^3)\,, \qquad (3.31)\\
L_j(x,p) \star \mathcal{W}(x,p,t) &= L_j(x,p)\mathcal{W}(x,p,t) \\
&\quad + \frac{i\hbar}{2}\{L(x,p), \mathcal{W}(x,p,t)\}_{\mathcal{PB}} + \mathcal{O}(\hbar^2)\,, \qquad (3.32)\\
L_j(x,p) \star \mathcal{W}(x,p,t) \star L_j(x,p)^* &= \left|L_j(x,p)\right|^2 \mathcal{W}(x,p,t) \\
&\quad + \frac{i\hbar}{2}\{L(x,p), L(x,p)^*\}_{\mathcal{PB}}\,\mathcal{W}(x,p,t) \\
&\quad + \frac{i\hbar}{2}\left\{L_j(x,p), \mathcal{W}(x,p,t)\right\}_{\mathcal{PB}} L_j(x,p)^* \\
&\quad - \frac{i\hbar}{2}\left\{L_j(x,p)^*, \mathcal{W}(x,p,t)\right\}_{\mathcal{PB}} L_j(x,p) \\
&\quad + \mathcal{O}(\hbar^2)\,. \qquad (3.33)
\end{aligned}$$

Finally, the time evolution of the Wigner function reads

$$\begin{aligned}
\partial_t \mathcal{W}(x,p,t) &= \{H(x,p), \mathcal{W}(x,p,t)\}_{\mathcal{PB}} \\
&\quad + \frac{i\hbar}{2}\sum_j \gamma_j \left(\left\{L_j(x,p), \mathcal{W}(x,p,t)\right\}_{\mathcal{PB}} L_j(x,p)^* - \text{c.c.}\right) + \mathcal{O}(\hbar^2)\,. \qquad (3.34)
\end{aligned}$$

Eq. (3.34) is the analogous to the Moyal equation for open systems and, neglecting $\mathcal{O}(\hbar^2)$, reduces onto a linear differential equation for the Wigner function $\mathcal{W}(x,p,t)$. Eq. (3.34) shows that, in general, the Lindblad jump operators affect the quantum dynamics at the first order in $\hbar$. However, if the Lindblad jump operators $\hat{L}_j$ are observables ($\hat{L}_j = \hat{L}_j^\dagger$), then $L_j(x,p) = L_j(x,p)^*$ and the first term linear in $\hbar$ is null.

Chapter 4

Growth of entanglement entropy under local projective measurements

During the last decades, quantum quenches in isolated systems have attracted a lot of interest. In quench dynamics, a quantum system is usually prepared in a stationary state, e.g. the ground state, and one of the tunable parameters of the Hamiltonian is suddenly modified, driving the system out of equilibrium. The state evolves unitarly and the spread of entanglement and correlations represents a useful tool to access the dynamical features of the state [85–87]. In particular, for short-ranged Hamiltonian operators, the propagation of information is limited by the Lieb-Robinson bound [88] and the bipartite entanglement of a semi-infinite subsystem can only grow unbounded. As predicted by the quasiparticle picture [55, 56, 89, 90], for integrable models, the exctitations are stable, each partner of the pairs propagates ballistically and the entanglement entropy grows linearly in time (see Sec. 1.6).

However, different factors may influence the dynamics, and the scaling behaviour of entanglement entropy may change in out-of-equilibrium driving [54, 91–93]. A paradigmatic example is the many-body localization (MBL), in which the entanglement transition is driven by a local disordered potential [94–101]. As a result, the entanglement grows logarithmically in time, in contrast with the linear growth in thermalized case [100, 101], and the stationary state exhibits area-law entropy. Alongside this, many different setups and dynamical protocols have been proposed to avoid thermalization. Some of them make use of local operations which perturb the unitary evolution and offer another class of dynamical behaviours, well explored in the contexts of weak measurements [27, 59], quantum circuits [102–120], quantum spin chains [121–130], trapped atoms [131] and trapped ions [132–134]. In continuous measurement scenarios, the most celebrated phenomenon is the quantum Zeno effect [135–139], where the monitoring frequency is so high that freezes the dynamics completely. This scenario has been explored in open many-body systems [59, 140–145], whose dynamics is described by a Lindblad master equation [66, 146, 147].

In light of these developments, we study a dynamical protocol involving random projective measurements of the local occupation numbers. The content of this chapter is based on our paper [A1].
The goal is to understand how entanglement and fluctuations are affected by the monitoring of local degrees of freedom. In Sec. 4.1, we present the general background, with the details of the monitoring protocol and the dynamics of the average density matrix. In Sec. 4.2, we study the entanglement dynamics, where the predicted linear growth for unitary dynamics is replaced by a logarithmic one. In Sec. 4.3, we present the main results of this work, regarding the asymptotic regime of the entanglement. We show that the volume-law is substituted by a sub-extensive growth of the entanglement entropy in the subsystem size. In the thermodynamic limit, a new area-law regime emerges for any measurement rate, with a correlation length increasing exponentially with the inverse of the monitoring frequency. In Sec. 4.4, we show the scaling of the stationary entanglement entropy by using the collapsed quasi-particle ansatz, see Ref. [59]. In Sec. 4.5, we analyse the entanglement fluctuations, with the scaling for small and large measurement rates. In Sec. 4.6, we summarise the achieved results in this work. We also stress that the collapsed quasi-particle pair ansatz is proved to be an incomplete picture, especially to extrapolate the dynamical properties of the entanglement under continuous measurements. However, many efforts have been made to approach the entanglement problem and, in this regard, Ref. [148] seems to be an encouraging theoretical attempt to face these difficulties. It is remarkable that the results of Ref. [148] are in agreement with our numerical analysis, which we shall illustrate in this chapter.

4.1 General framework

Let $|\Psi\rangle \in \mathscr{H} = \bigotimes_{j=0}^{L-1} \mathscr{H}_j$ be a pure quantum state of a one-dimensional many-body system, where the total Hilbert space $\mathscr{H}$ is the tensor product of the single-particle Hilbert spaces $\mathscr{H}_j$. In general,

$$|\Psi\rangle = \sum_{k=0}^{L-1} \sum_{i_k=1}^{d_k} A_{i_0 \dots i_k \dots i_{L-1}} |i_0\rangle \otimes \dots |i_k\rangle \otimes \dots |i_{L-1}\rangle \ , \tag{4.1}$$

where $\{|i_k\rangle\}_{i_k \in \{1,\dots,d_k\}}$ is the orthonormal set spanning $\mathscr{H}_k$, $d_k = \dim(\mathscr{H}_k)$ is the dimension of $\mathscr{H}_k$ and $A_{i_0 \dots i_k \dots i_{L-1}}$ is a tensor which verifies the normalization condition $\langle\Psi|\Psi\rangle = 1$.

In this chapter, we consider a quantum chain of hopping spinless fermions under periodic boundary conditions (PBC),

$$H = -\frac{1}{2}\sum_{i=0}^{L-1}\left(c_i^\dagger c_{i+1} + c_{i+1}^\dagger c_i\right) = \sum_{k=-L/2}^{L/2-1} \epsilon_k\, \eta_k^\dagger \eta_k\,, \tag{4.2}$$

where the c's are the fermionic annihilation operators and L is the total number of sites, which we assume to be a pair number. The total dimension of the Hilbert space $\mathscr{H}$ is 2^L, where $\dim\left(\mathscr{H}_j\right) = 2,\ \ \forall j \in \{0, ..., L-1\}$. The Hamiltonian H is diagonal in the Fourier modes

$$\eta_k = \frac{1}{\sqrt{L}}\sum_{j=0}^{L-1} e^{-\mathrm{i}2\pi kj/L} c_j\,, \tag{4.3}$$

with single particle energies $\epsilon_k = -\cos(2\pi k/L)$. The time evolution of the state is given by the Schrödinger equation

$$|\Psi(t)\rangle = e^{-\mathrm{i}Ht}\,|\Psi\rangle\,, \tag{4.4}$$

and the two-point function $C_{ij}(t) = \langle c_i^\dagger c_j\rangle_{\rho(t)} = \mathrm{tr}\Big(c_i^\dagger c_j \rho(t)\Big)$ evolves according to the unitary transformation

$$\mathbf{C}(t+s) = \mathbb{R}^\dagger(s)\,\mathbf{C}(t)\,\mathbb{R}(s)\,, \tag{4.5}$$

where the elements of the matrix $\mathbb{R}(s)$ are

$$\mathbb{R}_{mn}(s) = \frac{1}{L}\sum_{k=-L/2}^{L/2-1} e^{-\mathrm{i}2\pi(m-n)k/L - \mathrm{i}\epsilon_k s}\,. \tag{4.6}$$

4.1.1 Dynamical protocol

We shall present a protocol where the unitary dynamics (4.4) is perturbed by random interactions with local monitoring apparatus. Each single local Hilbert space $\mathscr{H}_j$ is coupled for a very short period of time with the environment, and a local observable

$$\mathcal{O}_j = \sum_{k=1}^{K} o_{jk}\mathcal{P}_j^{(k)}\,, \tag{4.7}$$

is measured, where o_{jk} is the k-th measurement outcome, $\mathcal{P}_j^{(k)}$ the projector on the k-th Hilbert subspace and K is the number of eigenvalues of $\mathcal{O}_j$. According to the completeness relation for Hermitian operators,

$$\sum_{k=1}^{K} \mathcal{P}_j^{(k)} = \mathbb{1}_j\,. \tag{4.8}$$

Following the Born rule, a measure of the local observable $\mathcal{O}_j$ projects the state $|\Psi\rangle$ on the k-th eigenvariety associated to the measurement outcome o_{jk}. The post-measured state is

$$\left|\Psi_j^{(k)}\right\rangle = \frac{\mathcal{P}_j^{(k)}|\Psi\rangle}{\sqrt{p_j^{(k)}}}, \tag{4.9}$$

where $p_j^{(k)} = \langle\Psi|\mathcal{P}_j^{(k)}|\Psi\rangle$ is the probability to get the outcome o_{jk}.

Given a time step $\mathrm{d}t$ and a characteristic rate τ^{-1}, each single local degree of freedom is independently monitored. In practice, a random number q_j with uniform distribution in $[0,1]$ is extracted for each site j of the chain, and a projection on the k-th subspace is performed whether $\sum_{l=1}^{k-1} p_l < q_j \leq \sum_{l=1}^{k} p_l$. Under this dynamical protocol, the many-body state $|\Psi(t)\rangle$ is conditioned by the set of measurement events and subsequent outcomes but it remains pure all along the trajectory. Observe that, since we are monitoring local observables, $\left[\mathcal{O}_{j_1}, \mathcal{O}_{j_2}\right] = 0$ $\forall j_1, j_2 \in \{0, \dots, L-1\}$ and the measurements may be performed in any order at fixed time t.

In this work, the local observables are the fermionic occupation numbers $\mathcal{O}_j = n_j = c_j^\dagger c_j$. Due to the Pauli exclusion principle, the Hermitian operator n_j takes only two different outcomes: 0 or 1. Thanks to the spectral decomposition (4.7) and the completeness relation (4.8),

$$n_j = 0 \cdot \mathcal{P}_j^{(0)} + 1 \cdot \mathcal{P}_j^{(1)}, \tag{4.10}$$

$$\mathbb{1}_j = \mathcal{P}_j^{(0)} + \mathcal{P}_j^{(1)}, \tag{4.11}$$

and thus

$$\mathcal{P}_j^{(0)} = \mathbb{1}_j - n_j, \qquad \mathcal{P}_j^{(1)} = n_j. \tag{4.12}$$

Using the results into Eq. (4.12), the possible post-measured states for the observable n_j are

$$\left|\Psi_j^{(0)}\right\rangle = \frac{\left(\mathbb{1}_j - n_j\right)|\Psi\rangle}{\sqrt{\langle\Psi|\mathbb{1}_j - n_j|\Psi\rangle}}, \qquad \left|\Psi_j^{(1)}\right\rangle = \frac{n_j|\Psi\rangle}{\sqrt{\langle\Psi|n_j|\Psi\rangle}}. \tag{4.13}$$

The panels in Fig. 4.1 show some examples of quantum trajectories for different values of the parameter τ. In particular, the average number operators are plotted as a function of the chain site j and time t. After quenching the Néel state, the unitary dynamics is perturbed by random interactions. Projective measurements make fermions (or holes) collapsing into the monitored chain sites (see the black and red spots into Fig. 4.1). These local excitations spread ballistically, with light cones and fronts being bounded by a maximum propagation velocity. As the

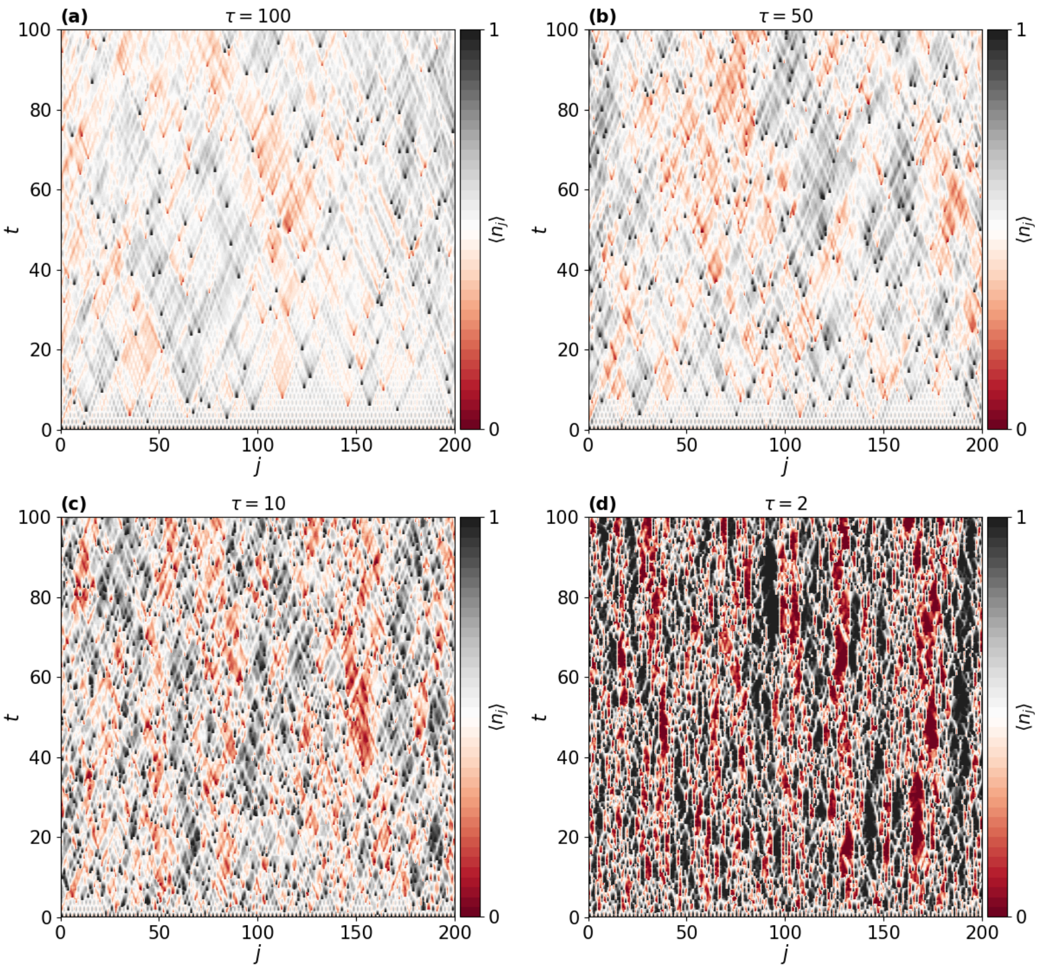

Figure 4.1: Average fermionic occupation as a function of the chain site j and time t. The quantum trajectories in each panel have been generated for different values of the parameter $\tau = 2, 10, 50, 100$.

parameter τ decreases, the average number of measurements increases, as well as the density of black and red spots. For large monitoring rates, black and red stripes emerge, since continuous measurements freeze the local dynamics and kill the correlations. In fact, in the limit $\tau \to 0$, the system reaches the celebrated Zeno regime.

Fig. 4.2 (c) shows an example of a random trajectory, using a diagrammatic representation of quantum states and operators, largely used in tensor network methods. The idea behind is that any multi-dimensional tensor may be pictorially represented by a box with a certain number of legs, one for each index with finite (possibly different) dimension. For instance, the entangled state (4.1) and the tensor $A_{i_0 \ldots i_k \ldots i_{L-1}}$ would be represented by a box with L legs, one of them

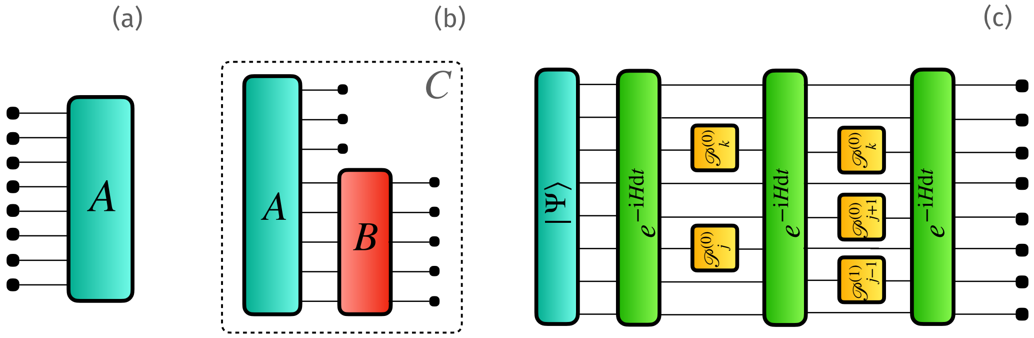

Figure 4.2: (a) Diagrammatic representation of a 8-rank tensor; (b) Contraction of a 8-rank tensor with a 10-rank tensor; (c) Example of random trajectory: the unitary evolution, here the green box, is perturbed by random interactions with a local monitoring apparatus, represented by the yellow boxes.

for each label i_k with dimension d_k (see Fig. 4.2 (a)). Graphically, if $B_{i_0 \cdots i_Q j_0 \cdots j_Q}$ is another multi-dimensional tensor, the contraction between $B_{i_0 \cdots i_Q j_0 \cdots j_Q}$ and $A_{j_0 \cdots j_Q i_{Q+1} \cdots i_{L-1}}$ is

$$C_{i_0 \dots i_{L-1}} = \sum_{j_0 \cdots j_Q} B_{i_0 \dots i_Q j_0 \dots j_Q} A_{j_0 \dots j_Q i_{Q+1} \dots i_{L-1}}\,, \qquad Q \leq L-1 \tag{4.14}$$

which is schematised in Fig. 4.2 (b). A clear application of the contraction (4.14) is the computation of the time evolved state $|\Psi(t)\rangle = \exp(-\mathrm{i}Ht)\,|\Psi\rangle$ (case $Q = L-1$), where the operator $\exp(-\mathrm{i}Ht)$ is described by a $2L$-rank tensor. Another application regards the measurement process, where the Hilbert operator n_j is represented by a 2-rank tensor and the post-measured state by the contraction (4.14) with $Q = 0$. According to this picture, a quantum trajectory is nothing but a succession of contractions, given by the unitary evolution and the random measurement events (see Fig. 4.2 (c)).

4.1.2 Stochastic samplings and average state dynamics

This work is mostly addressed to the study of the average entanglement entropy, to investigate possible transitions in the dynamical and asymptotic behaviour of the entanglement. For this reason, we need to collect a statistically significant number of trajectories. In this section, we shall illustrate the evolution of the average entanglement and the average state.

Each collection of measurement outcomes defines a quantum trajectory $\mathcal{T}_i$. Any single trajectory is not interesting by itself and we need to collect a statistically significant number of them. In this respect, let $\rho_i(t)$ denote the density operator along the trajectory $\mathcal{T}_i$. Let $\mathcal{O}[\rho]$ be a general functional of the density operator and let $\overline{\mathcal{O}}(t)$ denote the average over M trajectories,

$$\overline{\mathcal{O}}(t) = \frac{1}{M}\sum_{i=1}^{M}(\mathcal{O}[\rho_i(t)])\,. \tag{4.15}$$

If $\mathcal{O}$ is a linear functional of ρ, the relation (4.15) reduces to

$$\overline{\mathcal{O}} = \mathcal{O}[\overline{\rho}]\,, \qquad \overline{\rho} = \frac{1}{M}\sum_{i=1}^{M}\rho_i\,. \tag{4.16}$$

Let us mention that computing the average of linear functionals is much less expensive in terms of computational resources, since one can access the quantity $\overline{\mathcal{O}}$ without computing $\mathcal{O}[\rho_i(t)]$ many times along the same trajectory $\mathcal{T}_i$. Unfortunately, for nonlinear functionals, e.g. entanglement entropy, Eq. (4.16) does not hold anymore and the numerical cost increases.

Although the stochastic nature of the measurement events remains, the probabilistic outcome of a quantum projective measurement can be bypassed by introducing a statistical mixture; indeed, for measurements without sub-selection, the outcome is unknown and the state transforms according to $\rho \to \sum_{k=1}^{K} \mathcal{P}_j^{(k)}\rho\mathcal{P}_j^{(k)}$, where at the beginning $\rho(0) = |\Psi(0)\rangle\langle\Psi(0)|$. In this case, the state is not pure anymore and the two approaches are indistinguishable as far as we are considering linear functionals of the density operator $\rho(t)$.

Despite our interest in the entanglement entropy, studying the evolution of the average density matrix is sill interesting and allows us to easy access the evolution of the average N-point functions. In fact, any quantum operator can be written in terms of creation and annihilation operators and, since the trace is a linear functional of the density operator, computing the average N-point functions is equivalent to evaluate the N-point functions over the average density operator. In the next paragraphs we shall prove that, in the continuous limit, i.e. $\mathrm{d}t \to 0$, the dynamics of the mixed state $\overline{\rho}$ is governed by a Lindblad equation, with jump rate $(\tau/2)^{-1}$.

In order to get the evolution of $\overline{\rho}(t)$, we start from the analysis of the single trajectories and, at the end, we shall extrapolate the average evolution. Let $\rho(t)$ be the density operator at time t and suppose we are interested in the time-evolved state $\rho(t+\mathrm{d}t)$, under both unitary evolution (UE) and random-projective measurements (RPM). For simplicity, we shall assume the only measured observable is n_j; the corresponding generalisation to many local observables is obvious. Let $p = \mathrm{d}t/\tau$ be the probability of measurement after each time step $\mathrm{d}t$. The statistics of measurements and outcomes is expressed by the random independent variables $\{x_1, x_2\}$ with uniform distribution in $[0,1]$ and the functions

$$\mathcal{Q}_1(x_1) = \begin{cases} 1 & x_1 \in (0,p) \\ 0 & x_1 \in (p,1) \end{cases} \qquad \mathcal{Q}_2(x_2) = \begin{cases} 1 & x_2 \in (0, \langle n_j \rangle_{\rho^{\mathrm{UE}}(t+\mathrm{d}t)}) \\ 0 & x_2 \in (\langle n_j \rangle_{\rho^{\mathrm{UE}}(t+\mathrm{d}t)}, 1) \end{cases} \tag{4.17}$$

where $\rho^{\mathrm{UE}}(t+\mathrm{d}t) = \rho(t) - \mathrm{i}[H, \rho(t)]\mathrm{d}t$ is the time-evolved state under unitary evolution. For a single quantum trajectory $\mathcal{T}_i$,

$$\begin{aligned} \rho(t+\mathrm{d}t) \;&=\; \big[1-\mathcal{Q}_1(x_1)\big]\rho^{\mathrm{UE}}(t+\mathrm{d}t) + \mathcal{Q}_1(x_1)\mathcal{Q}_2(x_2)\frac{n_j \rho^{\mathrm{UE}}(t+\mathrm{d}t) n_j}{\langle n_j \rangle_{\rho^{\mathrm{UE}}(t+\mathrm{d}t)}} \\ &\quad + \mathcal{Q}_1(x_1)\big[1-\mathcal{Q}_2(x_2)\big]\frac{(\mathbb{1}_j - n_j)\rho^{\mathrm{UE}}(t+\mathrm{d}t)(\mathbb{1}_j - n_j)}{1-\langle n_j \rangle_{\rho^{\mathrm{UE}}(t+\mathrm{d}t)}}\,. \end{aligned} \tag{4.18}$$

For a number of trajectories $M \to \infty$, we get

$$\begin{aligned} \overline{\rho}(t+\mathrm{d}t) \;&=\; (1-p)\rho^{\mathrm{UE}}(t+\mathrm{d}t) + p n_j \rho^{\mathrm{UE}}(t+\mathrm{d}t) n_j \\ &\quad + p(\mathbb{1}_j - n_j)\rho^{\mathrm{UE}}(t+\mathrm{d}t)(\mathbb{1}_j - n_j)\,, \end{aligned} \tag{4.19}$$

and hence

$$\overline{\rho}(t+\mathrm{d}t) = \rho(t) - \mathrm{i}[H,\rho(t)]\mathrm{d}t + 2p\Big(n_j \rho(t) n_j - \frac{1}{2}\{n_j, \rho(t)\}\Big) + O(p^2)\,. \tag{4.20}$$

If measurements involve all the chain sites, we get

$$\frac{\mathrm{d}\overline{\rho}}{\mathrm{d}t} = -\mathrm{i}\big[H, \overline{\rho}\big] + \frac{2}{\tau}\sum_{j=0}^{L-1}\Big(n_j \overline{\rho} n_j - \frac{1}{2}\{n_j, \overline{\rho}\}\Big), \tag{4.21}$$

which is a Lindblad equation, where

$$\mathcal{D}(\overline{\rho}) = \frac{2}{\tau}\sum_{j=0}^{L-1}\Big(n_j \overline{\rho} n_j - \frac{1}{2}\{n_j, \overline{\rho}\}\Big)\,, \tag{4.22}$$

is the dissipator. The number operators n_j are the Lindblad operators, while $2/\tau$ is the jump rate. Since $[H, N] = 0$ and $\mathcal{D}(N) = 0$, the dynamics (4.21) conserves the average number of particles. Eq. (4.21) is a typical example of dephasing dynamics, where the out-of-diagonal terms of the density matrix are exponentially killed. The specific dynamical protocol described in Sec. 4.1.1 is known to be an *unravelling* of Eq. (4.21), and $\overline{\rho}(t)$ is obtained by averaging over stochastic samplings of single trajectories evolving in time as pure states.

In the last part of this paragraph, we shall evaluate the average correlator $\langle c_l^\dagger c_k \rangle_{\overline{\rho}(t)} = \mathrm{tr}\big(c_l^\dagger c_k \overline{\rho}(t)\big)$. Thanks to Eq. (4.21), we get

$$\begin{aligned} \frac{\mathrm{d}\langle c_l^\dagger c_k \rangle_{\overline{\rho}(t)}}{\mathrm{d}t} &= -\mathrm{i}\Big\langle \big[c_l^\dagger c_k, H\big] \Big\rangle_{\overline{\rho}(t)} \\ &\quad + \frac{2}{\tau} \sum_{j=0}^{L-1} \left[\langle n_j c_l^\dagger c_k n_j \rangle_{\overline{\rho}(t)} - \frac{1}{2} \Big\langle \big\{ n_j, c_l^\dagger c_k \big\} \Big\rangle_{\overline{\rho}(t)} \right]. \end{aligned} \tag{4.23}$$

Using the identities

$$\langle n_j c_l^\dagger c_k n_j \rangle = \langle c_j^\dagger c_l^\dagger c_k c_j \rangle + \delta_{jl} \delta_{jk} \langle n_j \rangle \,, \tag{4.24}$$

$$\langle n_j c_l^\dagger c_k \rangle = \langle c_j^\dagger c_l^\dagger c_k c_j \rangle + \delta_{jk} \langle c_l^\dagger c_j \rangle \,, \tag{4.25}$$

$$\langle c_l^\dagger c_k n_j \rangle = \langle c_j^\dagger c_l^\dagger c_k c_j \rangle + \delta_{jl} \langle c_j^\dagger c_k \rangle \,, \tag{4.26}$$

in Eq. (4.23), we obtain

$$\frac{\mathrm{d}\langle c_l^\dagger c_k \rangle_{\overline{\rho}(t)}}{\mathrm{d}t} = -\mathrm{i}\Big\langle \big[c_l^\dagger c_k, H\big] \Big\rangle_{\overline{\rho}(t)} + \frac{2}{\tau} \big[\delta_{lk} \langle c_l^\dagger c_k \rangle_{\overline{\rho}(t)} - \langle c_l^\dagger c_k \rangle_{\overline{\rho}(t)} \big] \,. \tag{4.27}$$

From Eqs. (4.27,4.2), we immediately get $\langle H \rangle_{\overline{\rho}(t)} = H_0 e^{-2t/\tau}$, where H_0 is the average energy at time $t = 0$. The average energy $\langle H \rangle_{\overline{\rho}(t)}$ shows an exponential decay toward zero, i.e. infinite temperature state [149].

4.1.3 Gaussianity

Computing the entanglement for large systems is the first problem to deal with. In fact, the dimension of the total Hilbert space increases exponentially with the number of sites and applying the Schmidt decomposition soon becomes numerically prohibitive.

The strategy is to prepare the system in a Gaussian state at time $t = 0$, e.g. the Néel state. Although the unitary evolution for quadratic Hamiltonians is Gaussian preserving, projective measurements could in principle destroy the Gaussianity. In this sense, the choice to detect the fermionic local occupations is not only motivated by experimental interests. In fact, we shall demonstrate that *measuring the fermionic local number operators does not spoil the Gaussianity of the state.* Hence, the Peschel's trick may be applied (see Sec. 1.5) at any time along any quantum trajectory and the calculation of the bipartite entanglement entropy reduces into the eigendecomposition of the truncated correlation matrix. In this section, we shall provide two distinct but equivalent proofs to support the Gaussianity under this specific dynamical protocol.

Proof 1

Under the initial hypothesis of Gaussianity, we want to prove that the collapsed post-measured state is still Gaussian. The first step is to write down the fermionic number operator in a useful form. According to Eq. (4.12), the observables n_j and $\mathbb{1}_j - n_j$ are projectors and then

$$n_j = \lim_{\alpha\to\infty} \frac{e^{\alpha n_j}}{e^{\alpha}-1}\,, \qquad \mathbb{1}_j - n_j = \lim_{\alpha\to\infty} e^{-\alpha n_j}\,. \tag{4.28}$$

As previously shown in Sec. 1.5, for vanishing pairing terms $\langle c_i c_j\rangle$, any Gaussian state takes the form $\rho \sim \exp\bigl(-\sum_{ij} M_{ij} c_i^\dagger c_j\bigr)$. The expression one should consider to evaluate the projected state is

$$e^{\pm\alpha n_j} e^{-\sum_{ij} M_{ij} c_i^\dagger c_j} e^{\pm\alpha n_j}\,, \tag{4.29}$$

which, thanks to the Baker-Campbell-Hausdorff formula, leads to

$$e^{-\sum_{ij} K_{ij} c_i^\dagger c_j}, \tag{4.30}$$

for another coupling matrix K_{ij}.

QED

Proof 2

An alternative proof comes from the explicit calculation of any N-point function. The goal is to verify the identity (1.31) for the post-measured states (4.13). We can directly consider the case where the indices $\alpha_k\,,\ \beta_k \neq j\ \forall k \in \{1, ..., n\}$, otherwise the Wick's theorem is trivially verified.

Firstly, let's demonstrate that $\left|\Psi_j^{(1)}\right\rangle$ is a Gaussian state. Thanks to Eq. (4.13) and the Gaussianity of the state $|\Psi\rangle$,

$$\begin{aligned}
&\sum_{k=1}^{n} (-1)^{n-k} \langle c_{\alpha_1}^\dagger c_{\beta_k}\rangle_{\Psi_j^{(1)}} \langle c_{\alpha_2}^\dagger ... c_{\alpha_n}^\dagger c_{\beta_1} ... c_{\beta_{k-1}} c_{\beta_{k+1}} ... c_{\beta_n}\rangle_{\Psi_j^{(1)}} \\
= \ & \frac{1}{\langle n_j\rangle_\Psi^2} \sum_{k=1}^{n} (-1)^{n-k} \langle c_j^\dagger c_{\alpha_1}^\dagger c_{\beta_k} c_j\rangle_\Psi \langle c_j^\dagger c_{\alpha_2}^\dagger ... c_{\alpha_n}^\dagger c_{\beta_1} ... c_{\beta_{k-1}} c_{\beta_{k+1}} ... c_{\beta_n} c_j\rangle_\Psi\,, \\
= \ & \sum_{k=1}^{n} (-1)^{n-k} \left[\frac{\langle c_{\alpha_1}^\dagger c_{\beta_k}\rangle_\Psi}{\langle n_j\rangle_\Psi} - \frac{\langle c_j^\dagger c_{\beta_k}\rangle_\Psi \langle c_{\alpha_1}^\dagger c_j\rangle_\Psi}{\langle n_j\rangle_\Psi^2} \right] \\
& \times\ \langle c_j^\dagger c_{\alpha_2}^\dagger ... c_{\alpha_n}^\dagger c_{\beta_1} ... c_{\beta_{k-1}} c_{\beta_{k+1}} ... c_{\beta_n} c_j\rangle_\Psi\,.
\end{aligned} \tag{4.31}$$

Moreover, for Gaussian states

$$
\begin{aligned}
&\sum_{k=1}^{n}(-1)^{n-k}\langle c^\dagger_{\alpha_1}c_{\beta_k}\rangle_\Psi\langle c^\dagger_j c^\dagger_{\alpha_2}...c^\dagger_{\alpha_n}c_{\beta_1}...c_{\beta_{k-1}}c_{\beta_{k+1}}...c_{\beta_n}c_j\rangle_\Psi\\
=\;&\langle c^\dagger_j c^\dagger_{\alpha_1}...c^\dagger_{\alpha_n}c_{\beta_1}...c_{\beta_n}c_j\rangle_\Psi+\langle c^\dagger_{\alpha_1}c_j\rangle_\Psi\langle c^\dagger_j c^\dagger_{\alpha_2}...c^\dagger_{\alpha_n}c_{\beta_1}...c_{\beta_n}\rangle_\Psi\,,
\end{aligned}\tag{4.32}
$$

$$
\begin{aligned}
&\sum_{k=1}^{n}(-1)^{n-k}\langle c^\dagger_j c_{\beta_k}\rangle_\Psi\langle c^\dagger_j c^\dagger_{\alpha_2}...c^\dagger_{\alpha_n}c_{\beta_1}...c_{\beta_{k-1}}c_{\beta_{k+1}}...c_{\beta_n}c_j\rangle_\Psi\\
=\;&\langle n_j\rangle_\phi\langle c^\dagger_j c^\dagger_{\alpha_2}...c^\dagger_{\alpha_n}c_{\beta_1}...c_{\beta_n}\rangle_\Psi\,.
\end{aligned}\tag{4.33}
$$

Using Eqs. (4.32), (4.33) into Eq. (4.31),

$$
\begin{aligned}
&\sum_{k=1}^{n}(-1)^{n-k}\langle c^\dagger_{\alpha_1}c_{\beta_k}\rangle_{\Psi^{(1)}_j}\langle c^\dagger_{\alpha_2}...c^\dagger_{\alpha_n}c_{\beta_1}...c_{\beta_{k-1}}c_{\beta_{k+1}}...c_{\beta_n}\rangle_{\Psi^{(1)}_j}\\
=\;&\frac{1}{\langle n_j\rangle_\Psi}\langle c^\dagger_j c^\dagger_{\alpha_1}...c^\dagger_{\alpha_n}c_{\beta_1}...c_{\beta_n}c_j\rangle_\Psi\,,\\
=\;&\langle c^\dagger_{\alpha_1}...c^\dagger_{\alpha_n}c_{\beta_1}...c_{\beta_n}\rangle_{\Psi^{(1)}_j}\,,
\end{aligned}\tag{4.34}
$$

and the Wick's theorem for $\left|\Psi^{(1)}_j\right\rangle$ is verified.

Concerning the Gaussianity of $\left|\Psi^{(0)}_j\right\rangle$, we proceed analogously to the previous case.

$$
\begin{aligned}
&\sum_{k=1}^{n}(-1)^{n-k}\langle c^\dagger_{\alpha_1}c_{\beta_k}\rangle_{\Psi^{(0)}_j}\langle c^\dagger_{\alpha_2}...c^\dagger_{\alpha_n}c_{\beta_1}...c_{\beta_{k-1}}c_{\beta_{k+1}}...c_{\beta_n}\rangle_{\Psi^{(0)}_j}\\
=\;&\frac{1}{(1-\langle n_j\rangle_\Psi)^2}\sum_{k=1}^{n}(-1)^{n-k}\left[\langle c^\dagger_{\alpha_1}c_{\beta_k}\rangle_\Psi-\langle c^\dagger_j c^\dagger_{\alpha_1}c_{\beta_k}c_j\rangle_\Psi\right]\\
&\times\left[\langle c^\dagger_{\alpha_2}...c^\dagger_{\alpha_n}c_{\beta_1}...c_{\beta_{k-1}}c_{\beta_{k+1}}...c_{\beta_n}\rangle_\Psi-\langle c^\dagger_j c^\dagger_{\alpha_2}...c^\dagger_{\alpha_n}c_{\beta_1}...c_{\beta_{k-1}}c_{\beta_{k+1}}...c_{\beta_n}c_j\rangle_\Psi\right],\\
=\;&\sum_{k=1}^{n}(-1)^{n-k}\left[\frac{\langle c^\dagger_{\alpha_1}c_{\beta_k}\rangle_\Psi}{1-\langle n_j\rangle_\Psi}-\frac{\langle c^\dagger_j c_{\beta_k}\rangle_\Psi\langle c^\dagger_{\alpha_1}c_j\rangle_\Psi}{(1-\langle n_j\rangle_\Psi)^2}\right]\left[\langle c^\dagger_{\alpha_2}...c^\dagger_{\alpha_n}c_{\beta_1}...c_{\beta_{k-1}}c_{\beta_{k+1}}...c_{\beta_n}\rangle_\Psi\right.\\
&\left.-\langle c^\dagger_j c^\dagger_{\alpha_2}...c^\dagger_{\alpha_n}c_{\beta_1}...c_{\beta_{k-1}}c_{\beta_{k+1}}...c_{\beta_n}c_j\rangle_\Psi\right],
\end{aligned}\tag{4.35}
$$

Using Eqs. (4.32,4.33) into Eq. (4.35),

$$
\begin{aligned}
&\sum_{k=1}^{n}(-1)^{n-k}\langle c^\dagger_{\alpha_1}c_{\beta_k}\rangle_{\Psi_j^{(0)}}\langle c^\dagger_{\alpha_2}...c^\dagger_{\alpha_n}c_{\beta_1}...c_{\beta_{k-1}}c_{\beta_{k+1}}...c_{\beta_n}\rangle_{\Psi_j^{(0)}} \\
=\;& \frac{1}{1-\langle n_j\rangle_\Psi}\langle c^\dagger_{\alpha_1}...c^\dagger_{\alpha_n}c_{\beta_1}...c_{\beta_n}\rangle_{\Psi_j^{(0)}} - \frac{1}{(1-\langle n_j\rangle_\Psi)^2}\langle c^\dagger_j c^\dagger_{\alpha_1}...c^\dagger_{\alpha_n}c_{\beta_1}...c_{\beta_n}c_j\rangle_{\Psi_j^{(0)}}\,, \\
=\;& \langle c^\dagger_{\alpha_1}...c^\dagger_{\alpha_n}c_{\beta_1}...c_{\beta_n}\rangle_{\Psi_j^{(0)}}\,,
\end{aligned} \tag{4.36}
$$

and the Wick's theorem for $\left|\Psi_j^{(0)}\right\rangle$ is verified.

QED

Gaussian states are fully characterised by the two-point functions, in the sense that the Wick's theorem provides any many-body quantity. Therefore, the projection rules for $|\psi\rangle$ can be translated into the following rules for $C^{(1)}_{ik}(t) := \langle c^\dagger_i c_k\rangle_{\Psi_j^{(1)}}$ and $C^{(0)}_{ik}(t) := \langle c^\dagger_i c_k\rangle_{\Psi_j^{(0)}}$, being the correlation matrices for the post-measured states $\left|\Psi_j^{(0)}\right\rangle$ and $\left|\Psi_j^{(1)}\right\rangle$,

$$
C^{(1)}_{ik}(t) = \frac{1}{\langle n_j\rangle_\Psi}\langle n_j c^\dagger_i c_k n_j\rangle_\Psi\,, \tag{4.37}
$$

$$
C^{(0)}_{ik}(t) = \frac{1}{1-\langle n_j\rangle_\Psi}\left(\langle c^\dagger_i c_k\rangle_\Psi - \langle n_j c^\dagger_i c_k\rangle_\Psi - \langle c^\dagger_i c_k n_j\rangle_\Psi + \langle n_j c^\dagger_i c_k n_j\rangle_\Psi\right). \tag{4.38}
$$

Thanks to the identities (4.24,4.25,4.26),

$$
C^{(1)}_{ik}(t) = \delta_{ij}\delta_{kj} + C_{ik}(t) - \frac{C_{ik}(t)C_{jk}(t)}{C_{jj}(t)}\,, \tag{4.39}
$$

$$
C^{(0)}_{ik}(t) = -\delta_{ij}\delta_{kj} + C_{ik}(t) + \frac{(\delta_{ij}-C_{ij}(t))(\delta_{kj}-C_{jk}(t))}{1-C_{jj}(t)}\,. \tag{4.40}
$$

Eqs. (4.39,4.40) express the correlation matrix elements of the post-measured states as a function of the values of the same elements before the measurement. Eqs. (4.39,4.40) with the unitary transformation (4.5) provide all the ingredients to generate random trajectories from initial Gaussian states.

4.2 Entanglement entropy dynamics

In this section, we shall illustrate the dynamics of the bipartite entanglement entropy (EE), which is strongly affected by random projective measurements.

Recalling the definition (see Sec. 1.1 for details), for a pure state $|\Psi(t)\rangle$, the EE between a subsystem $\mathcal{S}$ and its complementary $\mathcal{S}^*$ is $S(t) = \mathrm{tr}_{\mathcal{S}}(\rho_{\mathcal{S}}(t)\ln\rho_{\mathcal{S}}(t))$, where $\rho_{\mathcal{S}}(t) = \mathrm{tr}_{\mathcal{S}^*}|\Psi(t)\rangle\langle\Psi(t)|$ is the reduced density operator, obtained by tracing over the degrees of freedom of the complementary partition $\mathcal{S}^*$.

In this work, we always prepare the system in the Néel state at time $t = 0$, which means $\langle\psi(0)|\, n_{2j}\, |\psi(0)\rangle = 0$ and $\langle\psi(0)|\, n_{2j+1}\, |\psi(0)\rangle = 1$. This choice is motivated by three practical reasons. Firstly, the Néel state is a Guassian state and, since this dynamical protocol is Guassian preserving, the Peschel's trick may be applied along any quantum trajectory. Second, for initial Néel states and closed non-interacting systems ($\tau \to \infty$), the entanglement evolution is well captured by the quasi-particle picture (see Sec. 1.6). This is a valuable reference to better quantify the effect of projective measurements on the spread of correlations. Third, preparing the chain into any other initial Guassian state with the same filling factor 1/2 does not play any role in the long time limit. Repeated projective measurements destroy any memory effect, making the entanglement dynamics practically indistinguishable at $t \sim \infty$. In a recent work, see Ref. [150], the authors tried to go even beyond the Gaussianity, that means the dynamics is not constrained anymore into the Hilbert subspace of the Gaussian states. The Gaussianity-breaking is achieved with interacting models or even with suitable measurements. As main result, the authors found no fundamental differences as far as the entanglement transition is concerned.

According to the quasi-particle picture, when no measurements occur ($\tau \to \infty$), low-entangled and highly excited initial states behave like reservoirs of classical excitations, which are entangled in pairs. After quenching the Néel state, the quasi-particles spread ballistically with group velocity $v_p = \sin(p)$ and the EE dynamics is characterised by a linear growth for $t \leq l/2$, where l is the subsystem size of $\mathcal{S}$. For $t \geq l/2$, the linear increase is progressively replaced by a stationary regime where entanglement saturates toward an extensive value equal to $l\ln(2)$. This extensive behaviour of the asymptotic EE is referred to as *volume law*. In the opposite limit $\tau \to 0$, we keep measuring the system everywhere at every time, the Zeno regime freezes the dynamics and system collapses into a product state with zero entanglement.

In general, a finite monitoring rate should lower the entanglement production, since measurements project the state and destroy the correlations. However, how and to what extent the monitoring rate τ^{-1} affects the non-equilibrium dynamics is anything but obvious. We investigate this question by analysing the dynamics of the bipartite EE for different subsystems sizes l, embedded in a system of size L. We perform averages over 200÷1000 different quantum trajectories, depending on the system size and the monitoring rate. Indeed, the smaller τ, the larger the number of measurements and, in principle, one should average over a huge stochastic sampling to smooth down the random fluctuations.

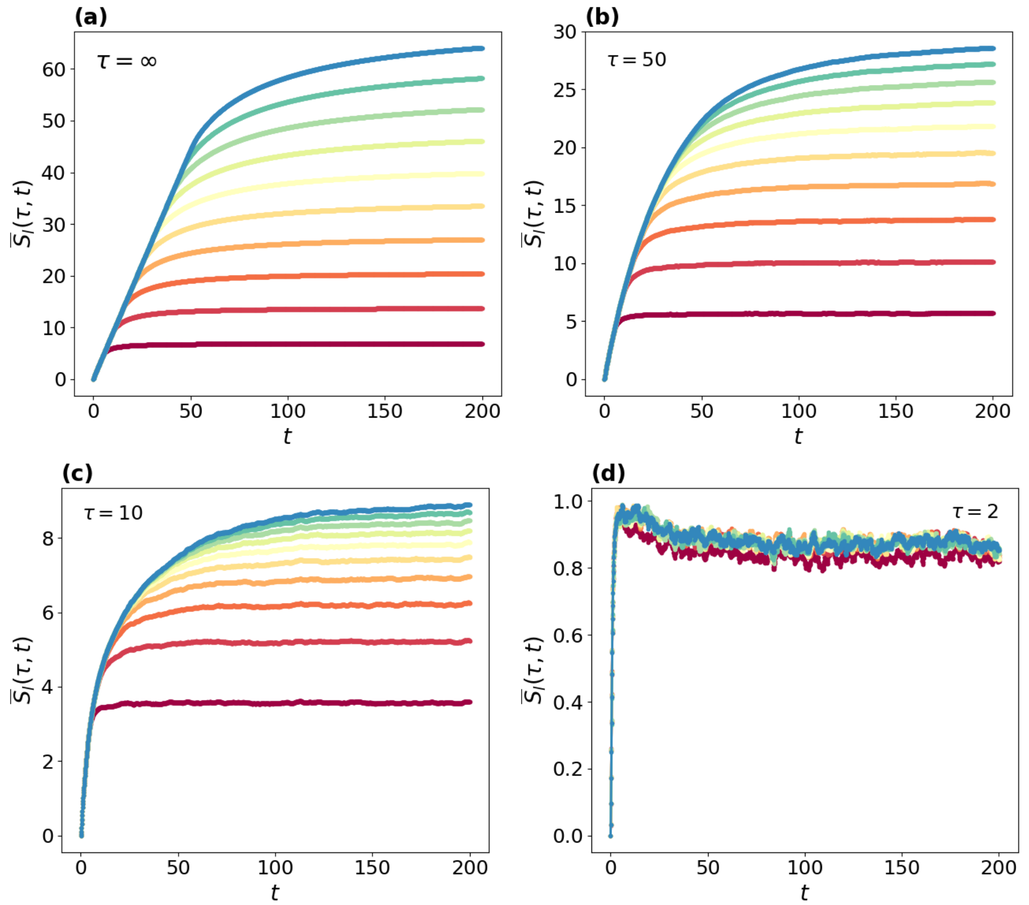

Figure 4.3: EE evolution for an initial Néel state and $L = 500$. Lines, from bottom to top, represent increasing subsystem sizes $l = 10n$, $n \in \{1, ..., 10\}$. The results for each $\tau \in \{2, 10, 50, \infty\}$ have been computed by averaging over 1000 different quantum trajectories.

In Fig. 4.3, we show the typical behaviour of the bipartite EE for $l = 10n$, $n \in \{1, ..., 10\}$. Maximum simulation time and subsystem sizes have been selected in such a way that data are not affected by finite size effects. Fig. 4.3 (a) shows the entanglement dynamics for $\tau \to \infty$, i.e. the unitary evolution, with the initial linear growth and the stationary value proportional to the subsystem size l, in agreement with the volume law. For finite values of τ, as shown into Figs. 4.3 (b,c), the linear increase is replaced by a sub-linear growth. More specifically, numerical data rule out a power growth, in favour of a logarithmic one, with $\overline{S}_l(t) = a_\tau \ln t + b_\tau$. Again, the EE saturates in the long time limit. Finally for very high monitoring rates τ^{-1} (see Fig. 4.3 (d)), we can identify a short transient regime where the average EE exhibits a fast growth, before reaching a plateau where the

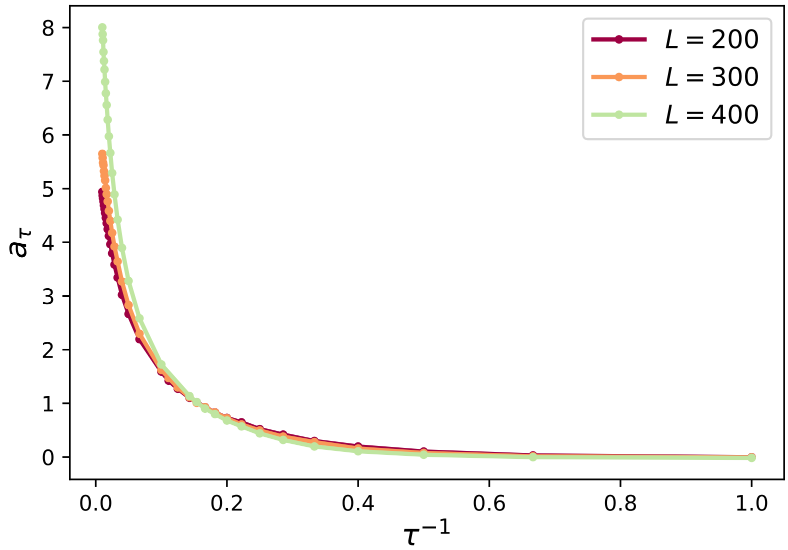

Figure 4.4: Logarithmic slope of the EE extracted from $\overline{S}_l(t) = a_\tau \ln t + b_\tau$ at $l = L/4$ as a function of τ for different system sizes ($L = 200, 300, 400$). When τ gets larger, the expected linear growth of the entanglement is restored. On the contrary, when $\tau \to 0$, a_τ is getting closer to zero suggesting an area-law phase.

EE is independent on the subsystem size, the *area-law* regime. Indeed, the density of measurements is so large that the system immediately loses memory of the initial state and approaches a dynamical regime where the spread of correlations is continuously interrupted and bounded by a finite characteristic length.

From the bipartite EE at $l = L/4$ we extract the parameter a_τ by fitting the data in the interval $t \in [0, L/8]$. In Fig. 4.4, we show a_τ as a function of the monitoring rate $1/\tau$, for different system sizes $L \in \{200, 300, 400\}$. As expected, a_τ is growing when τ is getting larger, eventually diverging for $\tau \to \infty$, restoring the linear behaviour of the entanglement under unitary dynamics. The larger τ, the larger the times and the subsystem sizes to observe any deviation from the linear growth. A low measurement density on a huge quantum chain cannot significantly change the entanglement behaviour for short time scales. On the contrary, for $\tau \to 0$, a_τ is vanishing, confirming the observed area-law regime.

4.3 Stationary entanglement entropy

Unsurprisingly, random measurements also affect the scaling of the stationary entanglement. From an inspection of the data, the asymptotic EE undergoes a qualitative change: from being extensive when $\tau = \infty$, it shows an area-law scaling for high rates τ^{-1}. However, it is much less obvious the scaling law for any finite measurement rate. At first glance, data may suggest the existence of a critical measurement rate at which a new *logarithmic* phase emerges. In this section, we shall go deeply to give an answer and justify our conclusions. The absence of rigorous theoretical tools for this new research field made it very difficult and time-consuming to came up to firm conclusions. The statements and arguments on the stationary EE should not be taken as a rigorous mathematical proof, but rather as a numerical evidence strongly supported by numerical data.

We investigate the behaviour of the stationary EE as a function of the subsystem sizes l and measurement rates τ^{-1}. By an analysis of the data, we conclude that the stationary EE is independent on l for sufficiently small values of τ (roughly speaking $\tau \lesssim 2$), which is the area-law phase; in other words, the measurement rate is so high that the time-evolved system cannot escape from a short correlated state. In the opposite limit $\tau \to \infty$, the volume-law behaviour characterises the system, with infinite correlation length. Between the two asymptotic cases, there is a large range of measurement rates where, for finite subsystem sizes l accessible from numerics, the stationary EE is characterised by a sub-linear growth (see Fig. 4.3 and Fig. 4.5 (a)). However, understanding whether this sub-linear growth survives in the thermodynamic limit or not has required many efforts and numerical analysis. In this respect, the logarithmic ansatz, typical for critical systems, was a good candidate and seemed to be in agreement with numerical data for large sizes l. The purpose of this section is to verify the existence of the logarithmic phase, and eventually identify the critical parameter $\tau_c > 0$ at which the transition between the logarithmic and the area-law phase occurs.

We analyse the stationary EE as a function of the subsystem size l for different system sizes L. In order to reduce the fluctuations, we also take the time average over the time window $[t_{\min}, t_{\max}]$ wherein the EE is almost constant. The upper and lower boundaries $t_{\min} \geq l/2$ and $t_{\max} \leq (L-l)/2$ have been chosen so that the entropy is weakly affected by finite-size effects; in fact, in that interval, the EE has essentially entered the stationary regime and is not affected by the motion of particles under PBC on a finite ring. In the following, $\langle \overline{S}_l(\tau) \rangle$ will denote the time average of the entanglement $\overline{S}_l(\tau)$ in the time window $[t_{\min}, t_{\max}]$.

In order to check whether the asymptotic scaling acquires a logarithmic dependence or not, we make use of the fit function $r \ln(l) + k$ with $l \in [l_{\min}, l_{\max}]$, from where we extract the parameter r. The fit parameter r gives an estimate of the asymptotic logarithmic slope of the entanglement, namely $l\partial_l \langle \bar{S}_l(\infty) \rangle$, as

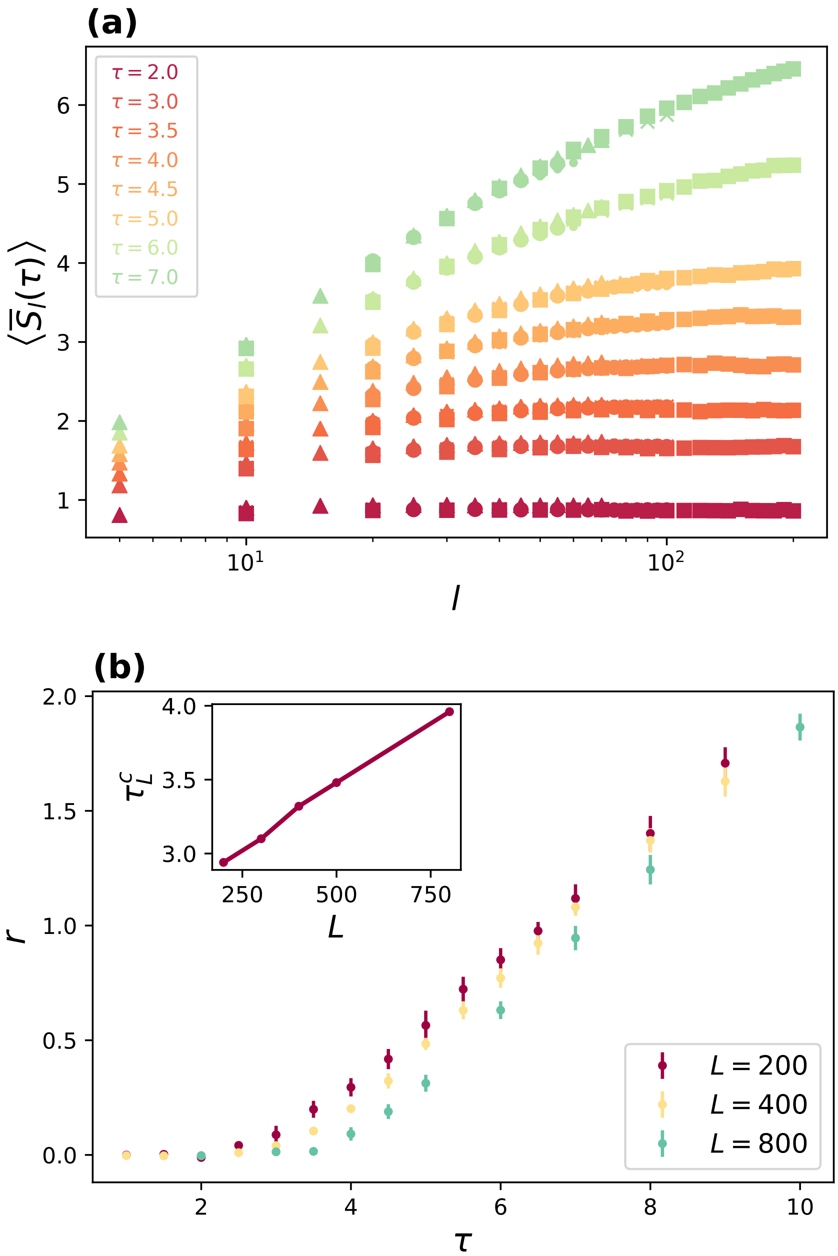

Figure 4.5: (a) We plot the stationary EE in log-linear scale, for $L \in \{200, 300, 400, 500, 800\}$ (different symbols) and several measurement rates τ^{-1} (different colors), as a function of the subsystem size $l \in [1, 200]$. (b) Logarithmic slope of the stationary EE for different system sizes L as a function of the parameter τ. The inset shows the critical value τ_L^c, which has been estimated for different system sizes L, revealing its divergent behaviour.

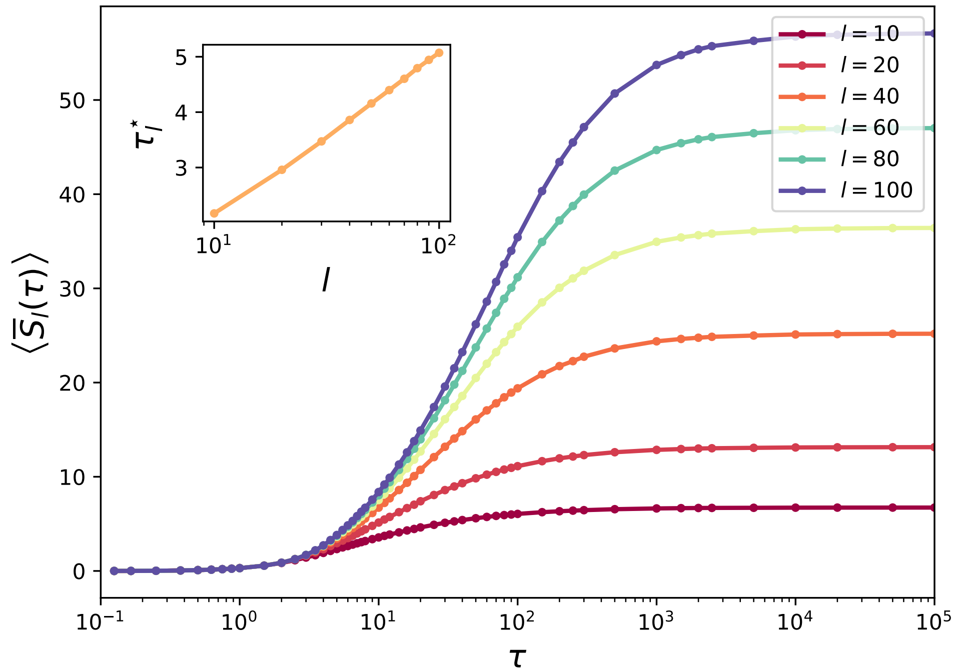

Figure 4.6: We show the stationary EE as a function of τ for different subsystem sizes l and $L = 400$; in the inset, the logarithmic growth of the inflection point $\tau_l^\star$ as a function of the subsystem size l.

a function of the measurement rate τ^{-1}. Again, the upper and lower boundaries l_{min} and l_{max} have been selected appropriately in relation to the total system size L, in order to stay in the correct regime. In Fig. 4.5 (b) we plot the best fit parameter r for $\tau \in [1, 10]$ and different system sizes $L \in \{200, 400, 800\}$. This quantity is an indicator of a possible sharp transition between the area-law and log-low phase. Similarly to what has been observed for the scaling of the time-dependent EE, the logarithmic slope r decreases for τ approaching the Zeno regime. In particular, for every system size L, we can identify a critical value τ_L^c such that, for $\tau < \tau_L^c$, the fit parameter r shows a fast convergence toward zero. To estimate τ_L^c we perform a best fit of r for every system size L whose intercept with the axis $r = 0$ gives the critical value τ_L^c separating the area-law and log-law phase. Indeed, if the limit $\lim_{L\to\infty} \tau_L^c = \tau^c$ converges to a finite value, the logarithmic phase characterises the stationary regime for $\tau > \tau_c$. However, the data in the inset of Fig. 4.5 (b) shows that τ_L^c is growing linearly with L and therefore the only stationary-EE phase that survives in the thermodynamic limit is the area-law phase.

Those results are further supported by the study of the stationary EE as a function of the parameter τ for different subsystem sizes l (see Fig. 4.6). The stationary EE is identically zero in the Zeno regime ($\tau = 0$) and approaches $l \ln(2)$ for $\tau \to \infty$. As expected, $\langle \overline{S}_l(\tau) \rangle$ is a monotonically increasing function of τ, since local measurements project the state and destroy the correlations. The stationary EE is size-independent for large rates and then changes its concavity at $\tau = \tau_l^\star$. In particular, our data show a logarithmic growth of the inflection point $\tau_l^\star$ with the subsystem size l. This observation allows us to introduce a correlation length $\xi(\tau)$ which increases exponentially with τ and determines the entanglement behaviour. In fact, if $\xi(\tau) \ll l$, only the chain sites close to the boundary are correlated with the complementary partition, which is the area-law regime. For increasing values of τ, $\xi(\tau)$ gets larger and larger, as well as the number of sites involved in generating correlations with the rest of the chain. In the limit $\xi(\tau) \gg l$, the entire subsystem contributes to the EE, approaching the volume-law regime. The exponential growth of the correlation length $\xi(\tau)$ explains why it becomes soon numerically prohibitive to observe the area-law regime.

4.4 Entanglement entropy scaling

As already shown in Sec. 1.6, the qualitative behaviour of the entanglement is captured by the quasi-particles, which are correlated in pairs and spread ballistically with opposite momenta $\pm k \in [-\pi, \pi]$. The contribution to the EE comes from these quasi-particle pairs such that one partner is inside the subsystem and the other one is outside. In this section, we shall see how this picture can be reshaped to include the effects of projective measurements.

In order to get the scaling of the stationary EE, in this work we make use of the *collapsed quasi-particle ansatz*, introduced in Ref. [59], in which the authors study a dynamical protocol where the system undergoes infinitely weak and frequent interactions with ancillas, namely *continuous weak measurements*. According to the collapsed quasi-particle ansatz, the quasi-particle pairs may be destroyed with probability $\tau \mathrm{d}t$ in every time step $\mathrm{d}t$; if this happens, one quasi-particle of the collapsed pair is chosen with equal probability $1/2$, and then a new pair is created at its position, with random momenta $\pm k$, where k is chosen uniformly in the Brillouin zone $[-\pi, \pi]$. Moreover, the contribution to the EE of the new quasiparticle pairs created at (x, t) is assumed to be $s[\rho(x, t)]$, where $\rho(x, t)$ is the particle density and s the Yang-Yang entropy (1.54). Under these hypothesis, the stationary EE reads

$$\langle \overline{S}_l(\tau) \rangle = \ln(2) \int_0^\infty \frac{\mathrm{d}y}{\tau}\, e^{-y/\tau} \int_{-\pi}^{\pi} \frac{\mathrm{d}k}{2\pi} \int_{\Omega_{k,y}} dx \,. \tag{4.41}$$

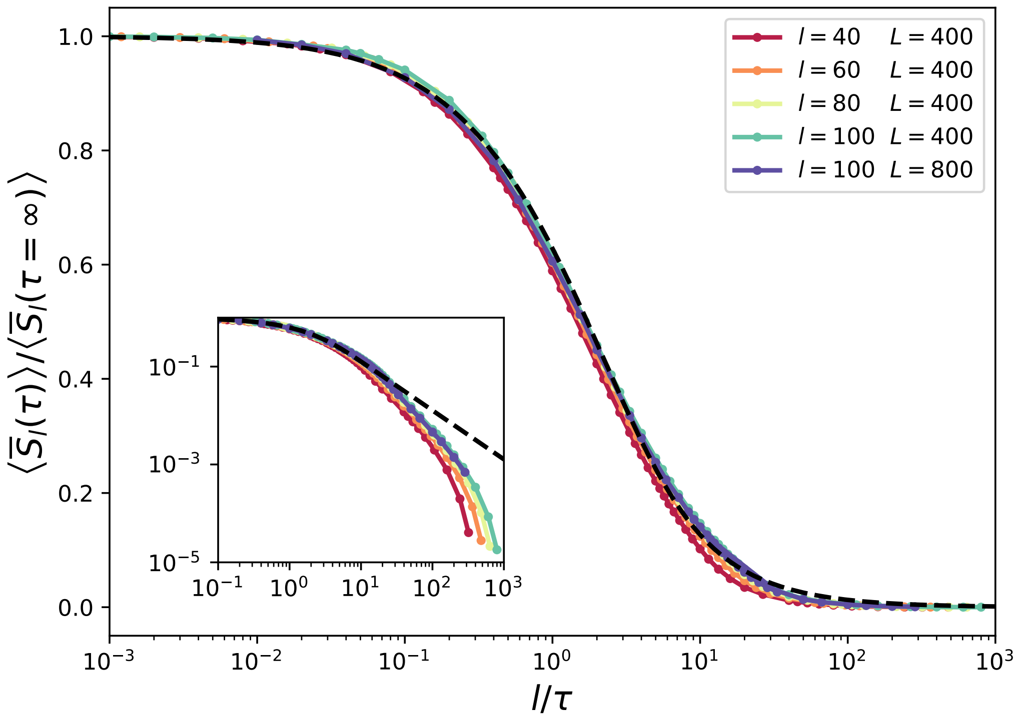

Figure 4.7: Scaling of the stationary EE: $\langle \overline{S}_l(\tau)\rangle / \langle \overline{S}_l(\tau = \infty)\rangle$ vs l/τ. The dashed line is the collapsed quasi-particle ansatz while the coloured spots are data. Note that $\langle \overline{S}_l(\tau)\rangle$ has been computed by taking the average in $[t_{\min}, t_{\max}]$ and thus $\langle \overline{S}_l(\tau = \infty)\rangle$ is very well approximated by $l \ln(2)$ only if $l \ll L$. The inset shows the same data in log-log scale, in order to emphasise the differences between the continuous limit $\mathrm{d}t \to 0$ and the discrete case.

Eq. (4.41) fits the numerical data, as shown in Fig. 4.7. Since our protocol differs from the one in Ref.[59], it is worth investigating whether our recipe agrees with their scaling result. The EE in our discrete model is very well captured by the continuous limit description (4.21) ($\mathrm{d}t/\tau \ll 1$). Although we expect a good prediction by the collapsed quasi-particle ansatz only for $\mathrm{d}t/\tau \ll 1$, we see in Fig. 4.7 that the agreement is excellent in a much wider range of measurement rates. Fig. 4.7 also shows the same ratio for different chain sizes $L \in \{400, 800\}$ to emphasise that the scaling figure is weakly affected by finite-size effects.

Unfortunately, this semi-classical approach does not match the dynamical regime and the logarithmic growth, suggesting that the mechanism behind the spread of correlations is much more complicated. As put forward in Ref. [151], the competition between coherent dynamics and random projective measurements generates multipartite quantum correlations which are inconsistent with an entangled-pair structure, then requiring the presence of larger multiplets.

4.5 Entanglement entropy fluctuations

In order to further support the results of the previous sections, we analyse the stationary fluctuations $\langle\sigma_l^2(\tau)\rangle = \langle\overline{S^2}_l(\tau)\rangle - \langle\overline{S}_l(\tau)^2\rangle$. Fig. 4.8 (a) shows the fluctuations as a function of the parameter τ for several subsystem sizes. One may immediately notice that the variance is l-independent for very high measurement rates, since the system is close to the Zeno regime. For large measurement rates, we do expect that even higher momenta of the EE are size independent. In the opposite limit ($\tau \to \infty$), the behaviour of the fluctuations may be easily understood looking at the properties of the Poisson distribution, as detailed below.

Suppose that the parameter τ is large enough so that $L\mathrm{d}t/\tau \ll 1$. This condition is equivalent to say that the probability to have multiple measurement events after each time step dt is negligible. Hence, the dynamical protocol becomes a Poisson process and $\kappa = TL/\tau$ is the average number of measurements in the time interval $[0, T]$,

$$\overline{S^n}_l(\tau, T) = \sum_j \mathcal{P}(j)\mathcal{A}_l(j, n, T)\,, \tag{4.42}$$

where $\mathcal{P}(j) = \kappa^j e^{-\kappa}/j!$ is the probability to take j measurements in $[0, T]$ and $\mathcal{A}_l(j, n, T)$ is the average of the n-th momentum of the EE over all the quantum trajectories in $[0, T]$ with fixed number of measurements j. The variance is given by

$$\sigma_l^2(\tau, T) = \overline{S^2}_l(\tau, T) - (\overline{S}_l(\tau, T))^2 \sim \mathcal{F}_l(T)\kappa(\tau, T)\,, \qquad \kappa \ll 1 \tag{4.43}$$

where $\mathcal{F}_l(T) = \mathcal{A}_l(1, 2, T) - 2\mathcal{A}_l(0, 1, T)\mathcal{A}_l(1, 1, T) + \mathcal{A}_l(0, 1, T)^2$. Since we are interested in the asymptotic quantities, the simulation time T has to be properly chosen to make sure that the entanglement moments enter the stationary regime but avoiding the finite size effects. The term $\mathcal{A}_l(1, n, T)$ represents the contribution to the EE moments for one single measurement and then it can be written in terms of small perturbations to the unitary case. In other terms, $\mathcal{F}_l(T)$ is approximately proportional to l^2 and thus the ratio $\mathrm{g}(l, \tau) = \langle\sigma_l^2(\tau)\rangle/\langle\overline{S}_l(\tau)\rangle^2$ is l-independent and proportional to τ^{-1} for very low measurement rates. This behaviour is emphasized in Fig. 4.8 (b).

Between the two asymptotic regimes, the variance shows a double-peak structure (see Fig. 4.8 (a)) which might suggest the presence of two different processes generating fluctuations. Note that this double-peak structure also reflects into

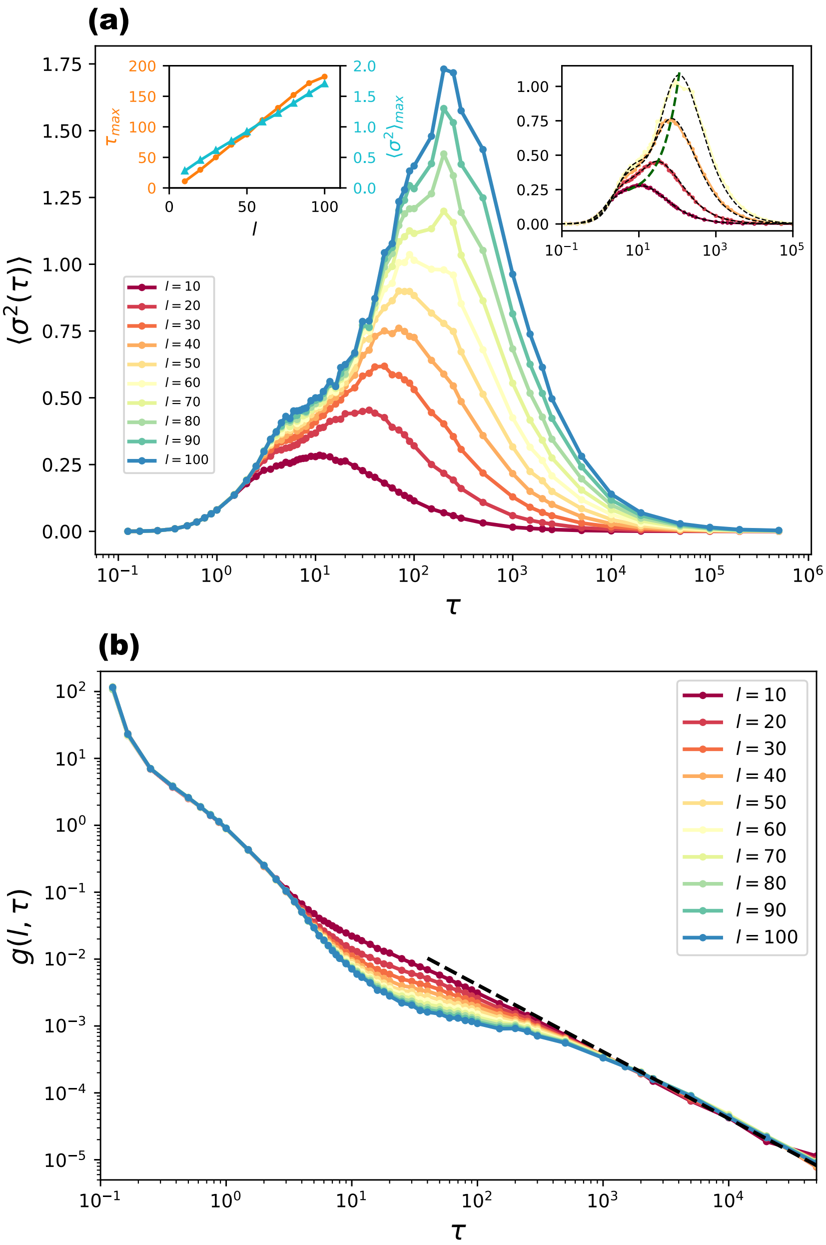

Figure 4.8: (a) Fluctuations of the stationary EE as a function of the parameter τ for $L = 400$. The absolute maximum point $\langle\sigma^2\rangle_{\text{max}}$ and the corresponding position τ_{max} grow linearly with the subsystem size l, as shown in the inset on the left. The inset on the right illustrates the fit functions (dashed lines) based on the collapsed quasi-particle ansatz; the green curve interpolates the maximum points. (b) The ratio $g(l, \tau) = \langle\sigma_l^2(\tau)\rangle / \langle\overline{S}_l(\tau)\rangle^2$ as a function of the parameter τ for $L = 400$. The dashed line is the asymptotic behaviour given by the theory, well fitting the numerical data.

the ratio $g(l,\tau) = \langle \sigma_l^2(\tau)\rangle / \langle \overline{S}_l(\tau)\rangle^2$, as shown in Fig. 4.8 (b). In particular, data suggest that the position of the first peak scales logarithmically with the subsystem size l; this is not surprising because, in that regime, fluctuations reflect the behaviour of the inflection point τ_l^* of the EE, which also scales logarithmically. Despite the fact that the total system size, as well as the number of simulated trajectories, is not large enough to proceed with a thorough analysis, data suggest that the peak position of the absolute maximum $\tau_{\max}$ and its value $\langle\sigma^2\rangle_{\max} = \langle\sigma^2(\tau_{\max})\rangle$ increase linearly with the subsystem size l, as shown in the inset of the Fig. 4.8 (a). In order to estimate the maximum points and their positions, we use as a fit function a linear combination of the square of Eq. (4.41) and the square of the average contribution to the EE by the new quasi-particle pairs randomly created by measurements (the argument of the integral (4.41)). By optimising the parameters of the fit function, we get a very good interpolation of the data, as shown in the inset of Fig. 4.8 (a). This suggests that the collapsed quasi-particle ansatz may give some insights to capture the qualitative behaviour of the fluctuations but still remains inappropriate and unsatisfactory for this kind of analysis, as put forward in Ref. [151].

4.6 Discussion and conclusion

In this numerical work, we studied the quench dynamics for the Néel state in a free fermion chain under random projective measurements of the local occupation. We found a logarithmic growth of the EE as a function on time, replacing the linear behaviour for closed systems. Moreover, we also investigated the stationary entanglement as a function of the measurement rate τ^{-1}. We ruled out a logarithmic phase and we numerically confirmed the presence of a single area-law phase for any finite value of the parameter τ. Moreover, using the collapsed quasi-particle ansatz, we found the scaling of the stationary EE. Finally, we studied the fluctuations and the scaling behaviour for very low/high measurement rates. The EE fluctuations show a very intriguing profile which, unfortunately, cannot be captured by the collapsed quasi-particle ansatz.

However, this is not the end of the story and many questions and scenarios still remain unexplored. The collapsed quasi-particle ansatz is clearly unsatisfactory for the dynamical regime and the higher moments of the EE. As proved in Ref. [151], entangled multiplets should be considered. In a recent work [148], some numerical results presented in this chapter, such as the single area-law phase, have been theoretically confirmed. Despite this, rigorous theoretical investigation methods are still missing and, most of the time, numerics is the only way to access the entanglement behaviour.

Chapter 5

Wigner dynamics for quantum gases under inhomogeneous gain and loss processes with dephasing

Unrevealing the mechanism behind the particle transport in open quantum systems is one of the most attractive challenges in out-of-equilibrium physics. The first successful attempt comes from the Wigner approach, which achieved great success in semi-classical contexts [26, 75]. As shown in Chapter 3, this alternative formulation of quantum mechanics is based on mapping quantum operators into phase-space functions and leads to the celebrated Boltzmann transport equation [152, C13, 153] for the Wigner quasi-probability distribution [152, C13, 153], elegantly defined as the Weyl transform of the density operator [154–156].

Despite the huge interest in closed systems, many other scenarios still remain totally or partially unexplored, as the k-body gain and loss processes in one dimensional systems [157–162]. Along the lines of the phase-space method in quantum optics [C8, C12, 163, 164], there have also been remarkable attempts to develop a characteristic function approach for open fermion systems [165], based on mapping the Liouville-Fock space of the fermion operators into the space of the Grassmann variables. Thus, for non-interacting Hamiltonians and linear Lindbladian operators, the master equation of the density operator may be transformed into a first order partial differential equation for the characteristic function, solvable by standard techniques. Despite the non-commutative algebra of the Grassmann variables, this approach is still interesting since the average value of one-body or two-body observables can be written in terms of partial derivatives of the characteristic function.

In this chapter, we aim to investigation particle transport in open markovian systems, as proposed in Refs. [166–174]. More specifically, we were inspired by the hydrodynamic approach [9, 10, 59, 175–193] which describes the non-equilibrium dynamics of closed systems in terms of classical non-interacting quasi-particles. In this chapter, we shall generalise this picture for the Lindblad dynamics.

The content of this chapter is based on our paper [A2]. In Sec. 5.1, we outline the general background. More specifically, we consider quantum chains of free particles (bosons or fermions) coupled to Lindblad baths, whose interaction is described by single particle gain-loss processes and dephasing, both with inhomogeneous jump rates. This choice is motivated by the huge interest in transport phenomena for boundary-driven spin chains, where fermionic jump operators determine the exchange of excitations with the external environment. In quantum optics, inhomogenous single-particle gain-loss processes may be engineered by experimentalists. For instance, coherent bosonic dynamics may be perturbed by electronic beams to remove atoms from selected sites [194], while local excitations may be created by the Raman pumping process [195]. As we saw in Chapter 4, dephasing is a kind of noise which describes continuous measurement protocols, where non-interacting fermion chains are coupled to external monitoring apparatus detecting the local occupation [A1, 59, 140, 151, 196–200]. In such a scenario, the dephasing rate in the master equation is nothing but the monitoring frequency or, using the generalized hydrodynamic approach, the collapsing rate of the quasi-particle pairs spreading ballistically along the chain. In this chapter, we also assume inhomogeneous dephasing rates, as for real experimental layouts, where the monitoring frequency is a tunable parameter. In the context of weak measurement protocols, it has already been proved that, for homogeneous setups, the inverse of the monitoring rate is the characteristic time at which the ballistic motion is replaced by a diffusive one [59, 201].

In Sec. 5.2, we expose the main results of this work. We derive the Wigner function dynamics starting from the equation of motion of the correlation matrix. Moreover, we show that the linear differential equation for the Wigner function admits a simple probabilistic interpretation in terms of non-interacting classical quasi-particles. In Sec. 5.3, we consider a simple scenario without dephasing or local potentials, for which the equation of motion is exactly solvable by standard techniques. We also provide some pedagogical examples, e.g. Gaussian jump rates, to test the hydrodynamic approach and compare the results with the exact microscopic dynamics. In Sec. 5.4, we combine gain-loss processes with a constant dephasing, which dramatically affects the quasi-particle motion at the crossover time, with a new emerging diffusive regime. Finally, the main results are summarised in Sec. 5.5, where we draw some future perspectives.

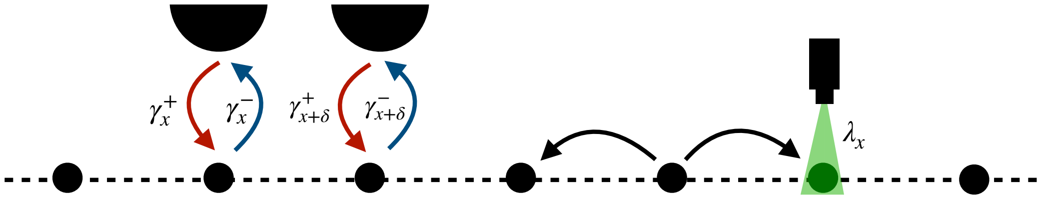

Figure 5.1: Sketch of an open quantum system: chain of hopping fermions with inhomogeneous gain-loss processes and dephasing. The exchange of particles with the bath(s) is represented by red and blue arrows, with rates γ_x^+ and γ_x^- for gain and loss, respectively. The dephasing noise is represented by the monitoring apparatus in green, detecting the local occupation of fermions with rate λ_x.

5.1 General framework

Let $\hat{\rho}$ be the density operator of a quantum system whose dynamics is generated by the Liouvillian $\mathcal{L}(\hat{\rho}) = \frac{\mathrm{d}\hat{\rho}}{\mathrm{d}t}$ of the form

$$\mathcal{L}(\hat{\rho}) = -\mathrm{i}[\widehat{H}, \hat{\rho}] + D(\hat{\rho}), \tag{5.1}$$

$$D(\hat{\rho}) = \sum_j \Upsilon_j \mathcal{D}_\rho(\hat{L}_j), \tag{5.2}$$

where $\widehat{H}$ denotes the Hamiltonian, $D(\hat{\rho})$ is the dissipator and

$$\mathcal{D}_\rho(\hat{L}_j) = \hat{L}_j \hat{\rho} \hat{L}_j^\dagger - \frac{1}{2}\{\hat{L}_j^\dagger \hat{L}_j, \hat{\rho}\}, \tag{5.3}$$

the super-operator acting on the Lindblad operators $\hat{L}_j$. We assume inhomogeneous jump rates Υ_j, which are non-negative definite. This makes Eq. (5.1) a CPTP dynamical map (see Chapter 2). Along this chapter, we shall make use of the Wigner approach and, in order to avoid confusion between quantum observables and real variables, we shall keep the symbol $\wedge$ over Hilbert operators to distinguish them from phase-space functions.

In this work, we shall consider L-site quantum chains under periodic boundary conditions. We shall derive results for spinless particles, either fermions or bosons. Since the different statistics introduces minimal modifications between the two cases, we shall address simultaneously the fermionic and bosonic problems. As a convention, every time the different algebra will generate a different sign, the one on top will label fermions and that one on bottom the bosons.

Regarding the unitary contribution to the dynamics (5.1), let $\widehat{H}$ be a non-interacting Hamiltonian. In particular, we assume that $\widehat{H} = \widehat{H}_0 + \widehat{V}$, where $\widehat{H}_0$ is

Coefficient	Interpretation
h_0	Translation-invariant Hamiltonian
ϵ_p	Single particle energies
$\mathcal{V}_{xy} = \mathcal{V}_x \delta_{xy}$	Diagonal potential
$\gamma_x^+,\ \gamma_x^-$	Injection/extraction rate at position x
$\omega_p^+,\ \omega_p^-$	Injection/extraction rate with momentum p
λ_x	Dephasing at position x
ζ_p	Dephasing with momentum p
$\Gamma_x = \gamma_x^- \pm \gamma_x^+$	Dissipation at position x
$\Omega_p = \omega_p^- \pm \omega_p^+$	Dissipation with momentum p
$n(x,p,t)$	Wigner function, Eq. (5.17)
$\rho(x,t), \tilde{\rho}(p,t)$	Densities [Eq (5.20)]
$N_{\mathrm{p}}(t) = \sum_x \rho(x,t) = \sum_{p\in\mathcal{B}} \tilde{\rho}(p,t)$	Total number of particles

Table 5.1: Description of the main coefficients entering the master equation (5.8).

a translation-invariant Hamiltonian, i.e. hopping Hamiltonian, and $\widehat{V}$ is a diagonal potential in real-space representation. For instance, $\widehat{V}$ may be a confining potential, e.g. harmonic traps, or may include tunable parameters as for non-equilibrium dynamics induced by quantum quenches. The operators $\widehat{H}_0$ and $\widehat{V}$ take the form

$$\widehat{H}_0 = \hat{\mathbf{c}}^\dagger \mathbf{h}_0 \hat{\mathbf{c}}\,, \qquad \widehat{V} = \hat{\mathbf{c}}^\dagger \boldsymbol{\mathcal{V}} \hat{\mathbf{c}}\,, \qquad \hat{\mathbf{c}} = \begin{pmatrix} \hat{c}_1 \\ \vdots \\ \hat{c}_L \end{pmatrix}, \tag{5.4}$$

where the $\hat{c}$'s are the fermionic/bosonic operators and $\mathbf{h}_0, \boldsymbol{\mathcal{V}}$ are $L\times L$ Hermitian matrices. By hypothesis, $\mathcal{V}_{xy} = \mathcal{V}_x \delta_{xy}$ and, without loss of generality, we can suppose $(\mathbf{h}_0)_{xx} = 0\ \forall x$ since any non-vanishing diagonal element may be reabsorbed into $\boldsymbol{\mathcal{V}}$. Therefore the Hamiltonian $\widehat{H} = \hat{\mathbf{c}}^\dagger \mathbf{h} \hat{\mathbf{c}}$ is fully characterised by the coefficient matrix

$$\mathbf{h} = \mathbf{h}_0 + \boldsymbol{\mathcal{V}}\,. \tag{5.5}$$

The Hamiltonian $\widehat{H}_0$ is translationally invariant and may be diagonalized by the Fourier transform

$$\hat{\eta}_p = \frac{1}{\sqrt{L}} \sum_x e^{-\mathrm{i}px} \hat{c}_x\,, \qquad \hat{\eta}_p^\dagger = \frac{1}{\sqrt{L}} \sum_x e^{\mathrm{i}px} \hat{c}_x^\dagger\,, \tag{5.6}$$

where $x \in [0, L-1]$ labels the chain sites; the p's are the Fourier modes which define the Brillouin zone $\mathcal{B} = \{p = -\pi + 2\pi l/L \,:\, l \in [0, L-1], l \in \mathbb{N}\}$; $(\hat{\eta}_p^\dagger, \hat{\eta}_p)$

are the creation and annihilation operators in reciprocal space. Hence,

$$\hat{H}_0 = \sum_{p\in\mathcal{B}} \epsilon_p \hat{\eta}_p^\dagger \hat{\eta}_p \,, \tag{5.7}$$

where ϵ_p are the single particle eigenvalues. The dissipator we shall study in this work is

$$\begin{aligned} D(\hat{\rho}) \;&=\; \sum_x \gamma_x^+ \mathcal{D}_\rho(\hat{c}_x^\dagger) + \gamma_x^- \mathcal{D}_\rho(\hat{c}_x) + \lambda_x \mathcal{D}_\rho(\hat{c}_x^\dagger \hat{c}_x) \\ &\quad + \sum_{p\in\mathcal{B}} \omega_p^+ \mathcal{D}_\rho(\hat{\eta}_p^\dagger) + \omega_p^- \mathcal{D}_\rho(\hat{\eta}_p) + \zeta_p \mathcal{D}_\rho(\hat{\eta}_p^\dagger \hat{\eta}_p) \,, \end{aligned} \tag{5.8}$$

which includes both linear and quadratic jump operators. The physical meaning of each jump rate appearing into Eq. (5.8) is provided in Table 5.1. From a microscopic perspective, all the jump rates into Eq. (5.8) depend on the specific interaction Hamiltonian and, in general, describe the coupling amplitude between the system and the bath(s). As we saw in Chapter 2, it is always desirable to get the dissipator by an ab-initio approach, requiring some expected physical properties, such as the relaxation toward a Gibbs thermal state. However, most of the time the bath's modes are not known exactly or easy to control. For this reason, sometimes the use of phenomenological dissipators is the only way to approach the problem, where jump operators and rates are conveniently chosen to describe the observed phenomenology. In the view of presenting the most general case, we shall not make any hypothesis on the jump rates, which will be considered positive independent quantities.

The super-operator (5.8) includes many different dissipative effects. In more detail, $\gamma_x^+ \mathcal{D}_\rho(\hat{c}_x^\dagger)$ and $\gamma_x^- \mathcal{D}_\rho(\hat{c}_x)$ represent one-body gain-loss processes in real space. Consistently with the local occupation on site x and the bosonic/fermionic algebra, a single particle may be injected or ejected at site x with characteristic rates γ_x^+ and γ_x^-. At the same time, we consider one-body gain-loss processes $\omega_p^+ \mathcal{D}_\rho(\hat{\eta}_p^\dagger)$, $\omega_p^- \mathcal{D}_\rho(\hat{\eta}_p)$ in momentum space, where a single particle may be injected or ejected with momentum p and characteristic rates ω_p^+, ω_p^-. Furthermore, there is the dephasing noise $\lambda_x \mathcal{D}_\rho(\hat{c}_x^\dagger \hat{c}_x)$, which has already been studied in Chapter 4. In Chapter 4, we proved that the dynamical protocol involving random projective measurements on fermionic chains is an unravelling of Eq. (4.21). This kind of noise kills exponentially the out-of-diagonal terms of the correlation matrix. Finally, we also consider dephasing $\zeta_p \mathcal{D}_\rho(\hat{\eta}_p^\dagger \hat{\eta}_p)$ in momentum space, whose physical meaning can be easily understood if one considers a dynamical protocol involving random projective measurements of the occupation $\hat{\eta}_p^\dagger \hat{\eta}_p$.

In this work, the goal is to provide a hydrodynamic description for open systems, where the system-bath(s) coupling is described by the Lindblad dissipator (5.8). As we shall see below, the hydrodynamic approach is based on the Wigner function dynamics (see also Chapter 3).

Let $C_{xy} = \langle \hat{c}_y^\dagger \hat{c}_x \rangle = \mathrm{tr}\left(\hat{c}_y^\dagger \hat{c}_x \hat{\rho}\right)$ be the elements of the correlation matrix. For the Lindblad dynamics (5.1), the time evolution of C_{xy} is given by

$$\frac{\mathrm{d}\langle \hat{c}_y^\dagger \hat{c}_x \rangle}{\mathrm{d}t} = -\mathrm{i}\left\langle [\hat{c}_y^\dagger \hat{c}_x, \hat{H}] \right\rangle + \mathrm{tr}\left(\hat{c}_y^\dagger \hat{c}_x D(\hat{\rho})\right). \tag{5.9}$$

After straightforward algebra, it is possible to prove that, for the specific dissipator (5.8), the differential equation (5.9) takes a closed form. To see this, we introduce the coefficient matrices $\boldsymbol{\gamma}^+, \boldsymbol{\gamma}^-, \boldsymbol{\lambda}, \tilde{\boldsymbol{\omega}}^+, \tilde{\boldsymbol{\omega}}^-, \tilde{\boldsymbol{\zeta}}, \tilde{\boldsymbol{\zeta}}^{(\alpha,\beta)}$ whose elements read

$$\gamma^+_{xy} = \gamma^+_x \delta_{xy}, \quad \gamma^-_{xy} = \gamma^-_x \delta_{xy}, \quad \lambda_{xy} = \lambda_x \delta_{xy}, \tag{5.10}$$

$$\tilde{\omega}^+_{xy} = \frac{1}{L}\sum_{p\in\mathcal{B}} e^{\mathrm{i}p(x-y)}\omega^+_p, \quad \tilde{\omega}^-_{xy} = \frac{1}{L}\sum_{p\in\mathcal{B}} e^{\mathrm{i}p(x-y)}\omega^-_p, \tag{5.11}$$

$$\tilde{\zeta}_{xy} = \frac{1}{L}\sum_{p\in\mathcal{B}} e^{\mathrm{i}p(x-y)}\zeta_p, \qquad \tilde{\zeta}^{(\alpha,\beta)}_{xy} = \tilde{\zeta}_{\alpha+x,\beta+y}. \tag{5.12}$$

The equation of motion of the correlation matrix is [202]

$$\frac{\mathrm{d}C_{\alpha\beta}}{\mathrm{d}t} = -\Big(\mathbf{WC} + \mathbf{CW}^\dagger - \mathbf{F} - \mathrm{diag}(\boldsymbol{\lambda}\mathbf{C})\Big)_{\alpha\beta} + \frac{1}{L}\mathrm{tr}\big(\tilde{\boldsymbol{\zeta}}^{(\alpha,\beta)}\mathbf{C}\big), \tag{5.13}$$

where

$$\begin{aligned} \mathbf{W} &= \mathrm{i}\mathbf{h} + (\boldsymbol{\gamma}^- \pm \boldsymbol{\gamma}^+ + \boldsymbol{\lambda} + \tilde{\boldsymbol{\omega}}^- \pm \tilde{\boldsymbol{\omega}}^+ + \tilde{\boldsymbol{\zeta}})/2, && (5.14)\\ \mathbf{F} &= \boldsymbol{\gamma}^+ + \tilde{\boldsymbol{\omega}}^+. && (5.15) \end{aligned}$$

Eq. (5.13) describes the exact microscopic dynamics of the correlations. As expected, for vanishing dephasing noises, Eq. (5.13) reduces to the Lyapunov equation

$$\frac{\mathrm{d}\mathbf{C}}{\mathrm{d}t} = -\mathbf{WC} - \mathbf{CW}^\dagger + \mathbf{F}. \tag{5.16}$$

The mathematical solution of Eq. (5.13) provides any two-body observable, such as the particle density or the average occupation in momentum space. However, Eq. (5.13) hides most of the non-equilibrium features. As with closed systems, the strategy is to build a one-to-one correspondence between the correlation matrix and a new real-valued function, i.e. the Wigner function. In other terms, we map Eq. (5.13) into the phase-space, obtaining the equation of motion for the Wigner function. As we shall see below, this will give us the insight to describe the non-equilibrium behaviour in terms of classical non-interacting quasi-particles.

The accuracy of the hydrodynamic approach will be tested by solving the exact microscopic dynamics (5.13).

The Wigner function, in its discrete form, is defined as

$$n(x,p,t) \;:=\; \sum_y e^{2\mathrm{i}py} C_{x-y,x+y}(t)\,, \tag{5.17}$$

$$= \sum_{k\in\mathcal{B}} e^{-2\mathrm{i}xk} \tilde{C}_{p-k,p+k}(t)\,, \tag{5.18}$$

where

$$\tilde{C}_{qp} = \langle \hat{\eta}_p^\dagger \hat{\eta}_q \rangle = \mathrm{tr}\Big(\hat{\eta}_p^\dagger \hat{\eta}_q \hat{\rho}\Big) = \frac{1}{L}\sum_{xy} e^{-\mathrm{i}qx} C_{xy} e^{\mathrm{i}py}\,, \tag{5.19}$$

and (x,p) are the discrete position-momentum variables [59, 178, 180, 193]. The Wigner function is a joint quasi-probability distribution, and its marginals coincide with the single-particle densities in real and momentum space:

$$\rho(x,t) \;=\; \langle \hat{c}_x^\dagger \hat{c}_x \rangle = \frac{1}{L}\sum_{p\in\mathcal{B}} n(x,p,t)\,, \tag{5.20}$$

$$\tilde{\rho}(p,t) \;=\; \langle \hat{\eta}_p^\dagger \hat{\eta}_p \rangle = \frac{1}{L}\sum_{x} n(x,p,t)\,, \tag{5.21}$$

which follow from the Kronecker delta relations

$$\delta_{xy} = \frac{1}{L}\sum_{k\in\mathcal{B}} e^{\mathrm{i}k(x-y)}\,, \qquad \delta_{pq} = \frac{1}{L}\sum_{x} e^{\mathrm{i}x(p-q)}\,. \tag{5.22}$$

The total number of particles is

$$N_{\mathrm{p}}(t) = \frac{1}{L}\sum_x \sum_{p\in\mathcal{B}} n(x,p,t)\,, \tag{5.23}$$

which is an extensive quantity.

The function in Eq. (5.17) is the Weyl transform of the correlation matrix. For this reason, strictly speaking, Eq. (5.17) does not coincide with the standard definition of the Wigner function for many-body systems that we provided into Chapter 3. However, in this work, we shall follow the conventions used in the hydrodynamic approaches, where people 'improperly' refer to Eq. (5.17) as the Wigner function. Nevertheless, the Lindblad dynamics (5.8) without dephasing is Gaussian preserving. In such a case, if the system is properly prepared in a Gaussian state at time $t = 0$ then the Wigner function (5.17) provides a complete description of the quantum dynamics. Indeed, any Gaussian state is fully described by the correlation matrix and the Wick's theorem applies for any many-body quantity (see Chapter 1).

5.2 Hydrodynamics for open systems

In this section, we derive the equation of motion of the Wigner function from the differential equation (5.13). According to Eqs. (5.1,5.17),

$$\partial_t n(x,p,t) = \sum_y e^{2ipy}\,\mathrm{tr}\left\{\hat{c}^\dagger_{x+y}\hat{c}_{x-y}\mathcal{L}(\hat{\rho}(t))\right\}. \tag{5.24}$$

To compute Eq. (5.24), we start from the unitary contribution $-\mathrm{i}\left[\widehat{H},\hat{\rho}\right]$ into Eq. (5.1), which describes the dynamics of closed systems. By hypothesis, the Hamiltonian $\widehat{H}_0$ is diagonal in the Fourier space (see Eq. (5.7)),

$$(h_0)_{xy} = \frac{1}{L}\sum_{p\in\mathcal{B}} e^{\mathrm{i}p(x-y)}\epsilon_p\,, \tag{5.25}$$

where ϵ_p are the single particle eigenvalues of $\widehat{H}_0$. Combining Eqs. (5.6,5.25) with Eq. (5.17),

$$\begin{aligned}\sum_y e^{2ipy}\,\mathrm{tr}\left\{[\hat{c}^\dagger_{x+y}\hat{c}_{x-y},\widehat{H}]\hat{\rho}(t)\right\} &= \sum_{k\in\mathcal{B}} e^{-2ikx}(\epsilon_{p-k}-\epsilon_{p+k})\tilde{C}_{p-k,p+k}(t)\\ &\quad+\sum_y e^{2ipy}(\mathcal{V}_{x-y}-\mathcal{V}_{x+y})C_{x-y,x+y}(t)\,.\end{aligned} \tag{5.26}$$

Proceeding similarly for the one-body gain-loss terms,

$$\begin{gathered}\sum_y e^{2ipy}\sum_z \mathrm{tr}\left\{\hat{c}^\dagger_{x+y}\hat{c}_{x-y}\left(\gamma_z^+\mathcal{D}_\rho[\hat{c}^\dagger_z]+\gamma_z^-\mathcal{D}_\rho[\hat{c}_z]\right)\right\} =\\ \gamma_x^+ - \frac{1}{2}\sum_y e^{2ipy}\left[\gamma^-_{x-y}+\gamma^-_{x+y}\pm(\gamma^+_{x-y}+\gamma^+_{x+y})\right]C_{x-y,x+y}(t)\,,\end{gathered} \tag{5.27}$$

and

$$\begin{gathered}\sum_y e^{2ipy}\sum_{k\in\mathcal{B}} \mathrm{tr}\left\{\hat{c}^\dagger_{x+y}\hat{c}_{x-y}\left(\omega_k^+\mathcal{D}_\rho[\hat{\eta}^\dagger_k]+\omega_k^-\mathcal{D}_\rho[\hat{\eta}_k]\right)\right\} =\\ \omega_p^+ - \frac{1}{2}\sum_{k\in\mathcal{B}} e^{-2ikx}\left[\omega^-_{p-k}+\omega^-_{p+k}\pm(\omega^+_{p-k}+\omega^+_{p+k})\right]\tilde{C}_{p-k,p+k}(t)\,.\end{gathered} \tag{5.28}$$

For the dephasing noise, we get

$$\begin{gathered}\sum_y e^{2ipy}\sum_z \mathrm{tr}\left\{\hat{c}^\dagger_{x+y}\hat{c}_{x-y}\left(\lambda_z\mathcal{D}_\rho[\hat{c}^\dagger_z\hat{c}_z]\right)\right\} =\\ \lambda_x C_{xx}(t) - \frac{1}{2}\sum_y e^{2ipy}(\lambda_{x-y}+\lambda_{x+y})C_{x-y,x+y}(t)\,,\end{gathered} \tag{5.29}$$

and

$$\sum_{y} e^{2\mathrm{i}py} \sum_{k\in\mathcal{B}} \operatorname{tr}\left\{\hat{c}^{\dagger}_{x+y}\hat{c}_{x-y}\left(\zeta_k \mathcal{D}_\rho[\hat{\eta}^{\dagger}_k\hat{\eta}_k]\right)\right\} =$$
$$\zeta_p \tilde{C}_{pp}(t) - \frac{1}{2}\sum_{k\in\mathcal{B}} e^{-2\mathrm{i}kx}(\zeta_{p-k} + \zeta_{p+k})\tilde{C}_{p-k,p+k}(t)\,. \tag{5.30}$$

Up to now, any calculation has been performed exactly without any approximation. However, Eqs. (5.26,5.27,5.28,5.29,5.30) are difficult to handle and, for this reason, we shall go to a continuous limit for the position-momentum variables. One of the main assumptions of hydrodynamics is the *separation of length scales*, which states the existence of mesoscopic fluid cells. These cells are much bigger than the microscopic scales, defined by the lattice spacing (here equal to 1) and the distance $\mathrm{d}p = 2\pi/L$ between two consecutive Fourier modes in the Brillouin zone, and much smaller than the macroscopic scales, where the inhomogeneities of the system become important. We assume the Wigner function, as well as the jump rates, the eigenvalues ϵ_p and the potential $\mathcal{V}_x$, to be slowly varying quantities at microscopic scale, so that position and momentum may be treated as continuous variables and all the discrete quantities into Table 5.1 as smooth analytical functions with domain in the phase space (x, p).

For analytic functions, the series expansion reads

$$\frac{g_{p-k} + (-1)^j g_{p+k}}{2} = (-1)^j \sum_{n=0}^{\infty} \frac{\partial^{2n+\delta_{j,1}} g_p}{(2n+\delta_{j,1})!} k^{2n+\delta_{j,1}}\,, \tag{5.31}$$
$$\frac{f_{x-y} + (-1)^j f_{x+y}}{2} = (-1)^j \sum_{n=0}^{\infty} \frac{\partial^{2n+\delta_{j,1}} f_x}{(2n+\delta_{j,1})!} y^{2n+\delta_{j,1}}\,, \tag{5.32}$$

for $j \in \{0, 1\}$, $f_x = \mathcal{V}_x, \gamma^+_x, \gamma^-_x, \lambda_x$ and $g_p = \epsilon_p, \omega^+_p, \omega^-_p, \zeta_p$. In this limit, the real and momentum space densities are

$$\rho(x,t) = \frac{1}{2\pi}\int_{-\pi}^{\pi} \mathrm{d}p\, n(x,p,t)\,, \tag{5.33}$$
$$\tilde{\rho}(p,t) = \frac{1}{L}\int \mathrm{d}x\, n(x,p,t)\,, \tag{5.34}$$

with total number of particles

$$N_\mathrm{p} = \int \mathrm{d}x\, \rho(x) = \frac{L}{2\pi}\int_{-\pi}^{\pi} \mathrm{d}p\, \tilde{\rho}(p) = \frac{1}{2\pi}\int \mathrm{d}x \int_{-\pi}^{\pi} \mathrm{d}p\, n(x,p,t)\,. \tag{5.35}$$

Finally, using Eqs. (5.31,5.32) into Eqs. (5.26,5.27,5.28,5.29,5.30), one obtains

$$\begin{aligned}\partial_t n(x,p,t) &= 2\Big(\epsilon_p + \mathcal{V}_x\Big)\sin\!\Big(\frac{1}{2}\Big(\overleftarrow{\partial}_x\overrightarrow{\partial}_p - \overleftarrow{\partial}_p\overrightarrow{\partial}_x\Big)\Big)n(x,p,t)\\ &\quad -(\omega_p^- \pm \omega_p^+ + \zeta_p + \gamma_x^- \pm \gamma_x^+ + \lambda_x)\cos\!\Big(\frac{1}{2}\Big(\overleftarrow{\partial}_x\overrightarrow{\partial}_p - \overleftarrow{\partial}_p\overrightarrow{\partial}_x\Big)\Big)n(x,p,t)\\ &\quad + \int \mathrm{d}x' \int_{-\pi}^{\pi} \mathrm{d}p' \Big(\frac{\zeta_{p'}}{L}\delta(p-p') + \frac{\lambda_{x'}}{2\pi}\delta(x-x')\Big)n(x',p',t)\\ &\quad +\gamma_x^+ + \omega_p^+ , \end{aligned} \tag{5.36}$$

which is a linear differential equation in $n(x,p,t)$.

The operator $\sin\left(\frac{1}{2}\left(\overleftarrow{\partial}_x\overrightarrow{\partial}_p - \overleftarrow{\partial}_p\overrightarrow{\partial}_x\right)\right)$ is the Moyal product [26, 75, 84, 179], e.g. see Chapter 3, and describes the unitary contribution to the dynamics. On the other hand, the operator $\cos\left(\frac{1}{2}\left(\overleftarrow{\partial}_x\overrightarrow{\partial}_p - \overleftarrow{\partial}_p\overrightarrow{\partial}_x\right)\right)$, the non-local terms and the source terms into Eq. (5.36) come from the Lindblad dissipator (5.8).

In order to simplify Eq. (5.36), we observe that all the quantities involved into Eq. (5.36) are, by hypothesis, slowly varying functions of position and momentum. For this reason, we shall truncate Eq. (5.36) at the lowest non-trivial order in ∂_x and ∂_p derivatives. Hence, Eq. (5.36) becomes

$$\begin{aligned}\partial_t n(x,p,t) &= \{\epsilon_p + \mathcal{V}_x, n(x,p,t)\}_{\mathcal{PB}} - \Big(\Omega_p + \zeta_p + \Gamma_x + \lambda_x\Big)n(x,p,t)\\ &\quad +\zeta_p\tilde{\rho}(p,t) + \lambda_x\rho(x,t) + \gamma_x^+ + \omega_p^+ ,\end{aligned} \tag{5.37}$$

where $\Omega_p = \omega_p^- \pm \omega_p^+$, $\Gamma_x = \gamma_x^- \pm \gamma_x^+$ and

$$\{\mathcal{F},\mathcal{G}\}_{\mathcal{PB}} = \partial_x\mathcal{F}\partial_p\mathcal{G} - \partial_p\mathcal{F}\partial_x\mathcal{G}, \qquad \forall\mathcal{F},\mathcal{G} \tag{5.38}$$

indicates the Poisson bracket. As we proved into Chapter 3, the Poisson bracket describes the Wigner function's dynamics for closed systems [75, 84, 156, 179, 203]. For a recap of the meaning of each symbol into Eq. (5.37), see Table 5.1.

Eq. (5.37) is our main result, which is a compact partial differential equation for the Wigner function, describing inhomogeneous gain-loss processes and dephasing. Unfortunately, dephasing introduces non-local terms into Eq. (5.37), i.e. $\rho(x,t)$ and $\tilde{\rho}(p,t)$, which are the marginals of the Wigner function. Those terms make it difficult to solve Eq. (5.37) by standard analytical methods.

The range of applicability of the truncation of higher order derivatives into Eq. (5.36) needs to be carefully discussed. For closed systems, the Wigner dynamics is given by the classical evolution plus quantum corrections at the third order in the ∂_x and ∂_p derivatives, which come from the series expansion of the Moyal product. Nevertheless, Eq. (5.37) neglects contributions at the second order in the partial derivatives, which derive from the series expansion of the operator $\cos\left(\frac{1}{2}\left(\overleftarrow{\partial}_x\overrightarrow{\partial}_p - \overleftarrow{\partial}_p\overrightarrow{\partial}_x\right)\right)$. We conclude that the truncation of Eq. (5.36) is less efficient for open systems. The analytic form of the jump rates has to be evaluated case by case in order to stay in the correct regime. However, as we shall illustrate below, Eq. (5.37) is very efficient in a wide range of physical scenarios, unless one takes very discontinuous profiles.

In the last part of this section, we shall describe Eq. (5.37) as a stochastic average over classical trajectories. In the same spirit of the generalized hydrodynamics, weakly-entangled but highly excited initial states can be viewed as a reservoir of classical non-interacting quasi-particles. In this perspective, the Wigner function becomes the joint distribution of these exitations in the phase space. For closed systems, after quenching the state, the particle motion is governed by the Newton's laws: any excitation in the phase-space point (x_0, p_0) at time t_0 moves to $(x_0 + v_{p_0}\mathrm{d}t, p_0 + \mathcal{F}_{x_0}\mathrm{d}t)$ at time $t_0 + \mathrm{d}t$, where $v_p = \partial_p \epsilon_p$ is the group velocity and $\mathcal{F}_x = -\partial_x \mathcal{V}_x$ (see Fig. 5.2 (a)). For instance, for vanishing potentials, the quasi-particles spread ballistically along the chain and the momentum is conserved. On the other hand, inhomogeneous potentials affect the momentum conservation accelerating particles. This simple characterisation of the Wigner function dynamics turns to be very useful in the understanding of the non-equilibrium behaviour.

For clarity, we shall discuss the effects of the dissipators one by one, starting from one-body gain-loss processes. In such a case, the total number of particles is not a constant of motion anymore, i.e. $\mathcal{L}^\dagger(\widehat{N}) \neq 0$. According to the hydrodynamic equation (5.37), the classical particles crossing the phase-space point (x, p) are destroyed with local rate $\alpha_{(x,p)} = \Gamma_x + \Omega_p$. Moreover, the source term $\gamma_x^+ + \omega_p^+$ creates new excitations in the phase space: $\gamma_x^+\mathrm{d}t$ represents the probability in every interval $\mathrm{d}t$ of injecting quasi-particles at position x and random momentum p chosen uniformly in the Brillouin zone; $\omega_p^+\mathrm{d}t$ is the probability of creating quasi-particles with momentum p and random site x chosen uniformly along the chain (see Fig. 5.2 (b)). One fundamental aspect of the dissipative dynamics emerges: one-body gain-loss processes by themselves cannot change the transport features. The classical particles keep moving according to Newton's laws while the dissipators only add or remove excitations with specific rates.

The dephasing noise changes that and makes the dynamics much more interesting. The mean lifetime is reduced even more, with annihilation rate $\alpha'_{(x,p)} = \alpha_{(x,p)} + \lambda_x + \zeta_p$, while the last two non local terms $\lambda_x \rho(x,t)$ and $\zeta_p \tilde{\rho}(p,t)$ into Eq. (5.37) further complicate the dynamics. For any quasi-particle crossing the site x, a new excitation is created with rate λ_x, at the same position and random momentum p in the Brillouin zone. Finally, for any quasi-particle with mo-

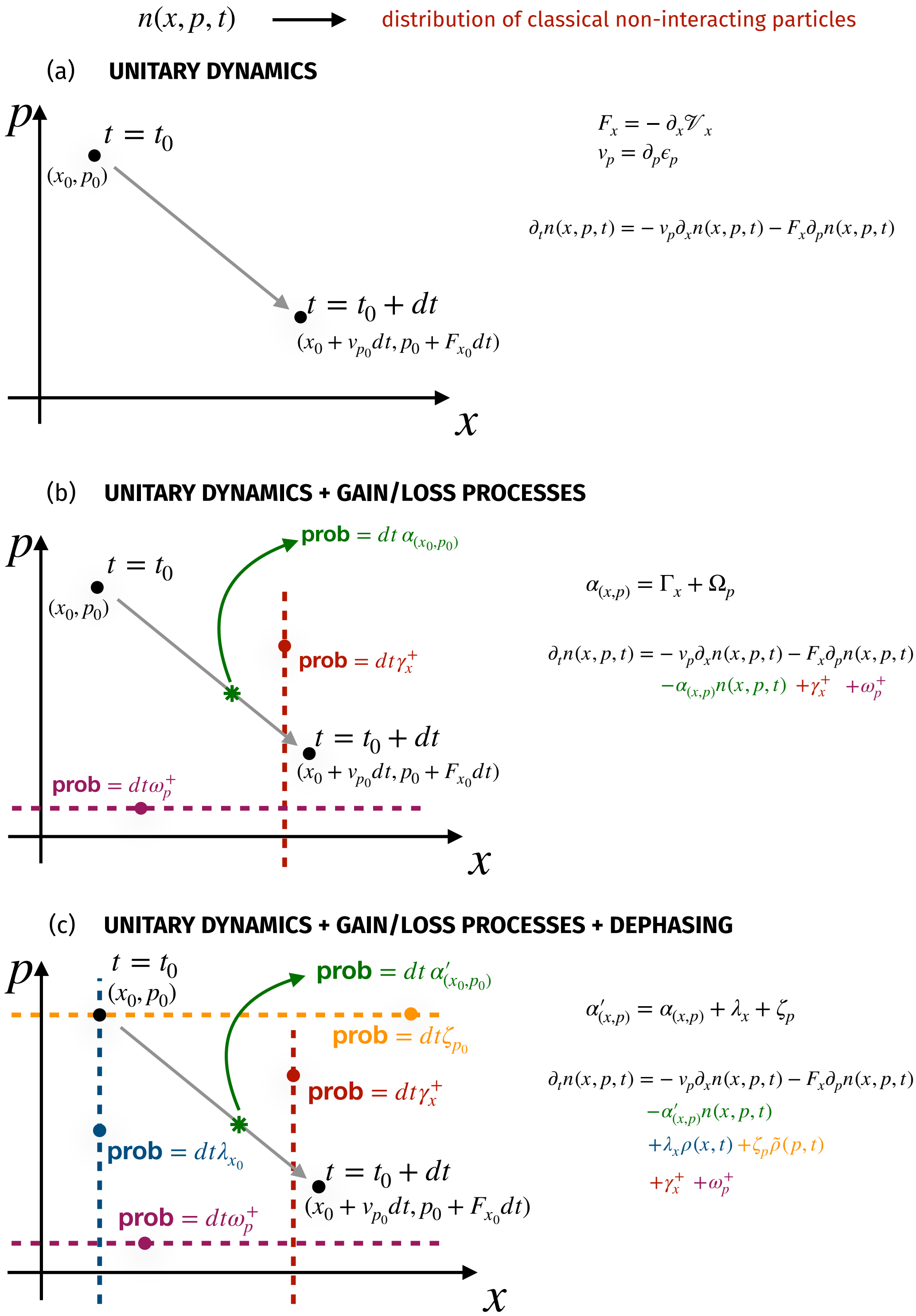

Figure 5.2: Sketch of the quasi-particle's motion in the phase-space. We assume an excitation in (x_0, p_0) at time t_0 and we study how it behaves under the action of dissipators; (a) unitary dynamics; (b) unitary dynamics perturbed by single particle gain and loss processes; (c) open dynamics with gain-loss processes and dephasing.

mentum p, a new excitation is created with rate ζ_p, momentum p and random site x along the chain (see Fig. 5.2 (c)). We conclude that dephasing strongly affects the transport features. For instance, we quote the dephasing dynamics (4.21) into Chapter 4, which describes the evolution of the average state for a specific dynamical protocol involving random projective measurements. The dephasing rate is homogeneous ($\lambda_x = \lambda$) since all the chain sites were assumed to be monitored with the same frequency. In the limit $t\lambda \gg 1$, the dynamics of the average density $\rho(x,t)$ is well captured by a Fokker-Planck differential equation

$$\partial_t \rho(x,t) = \frac{D}{2}\partial_{xx}\,\rho(x,t)\,, \tag{5.39}$$

with diffusion coefficient $D = \lambda^{-1}$ [59, 201].

The generalized hydrodynamic description for open systems represents the second main result of this work. In the next sections, we shall test this picture in some concrete examples, comparing the microscopic dynamics with the hydrodynamic approach.

5.3 Wigner dynamics without dephasing

In order to gain some intuition about one-body gain-loss processes, we first focus on the Wigner function evolution for vanishing potentials and dephasing ($\mathcal{V}_x = \zeta_p = \lambda_x = 0$). Under these hypothesis, Eq. (5.37) reduces to

$$\partial_t n(x,p,t) = -v_p \partial_x n(x,p,t) + \gamma_x^+ + \omega_p^+ - \Big(\Omega_p + \Gamma_x\Big) n(x,p,t)\,. \tag{5.40}$$

The analytical solution of Eq. (5.40) comes from the ansatz

$$n(x,p,t) = \exp\left\{-\frac{\Omega_p}{v_p}x - \frac{1}{v_p}\int_0^x \mathrm{d}s\,\Gamma_s\right\} f(x,p,t)\,. \tag{5.41}$$

for a given analytic function $f(x,p,t)$ to be determined. Using this ansatz into Eq. (5.40), we get

$$f(x,p,t) = \tilde{n}(x,p,t) + \frac{1}{v_p}\int_0^x \mathrm{d}s\,(\gamma_s^+ + \omega_p^+)\exp\left\{\frac{\Omega_p}{v_p}s + \frac{1}{v_p}\int_0^s \mathrm{d}y\,\Gamma_y\right\}\,, \tag{5.42}$$

where $\tilde{n}(x,p,t)$ solves the differential equation

$$\partial_t \tilde{n}(x,p,t) = -v_p \partial_x \tilde{n}(x,p,t)\,. \tag{5.43}$$

Eq. (5.43) is the hydrodynamic equation for closed system and its solution is $\tilde{n}(x,p,t) = \tilde{n}(x - tv_p, p, 0)$, where $\tilde{n}(x,p,0)$ depends on the initial condition

$n(x,p,0)$ of the Cauchy problem. After some manipulations, the full solution reads

$$\begin{aligned} n(x,p,t) &= \exp\left\{-\Omega_p t - \int_0^t \mathrm{d}s_1\, \Gamma(x-s_1 v_p)\right\} n(x-tv_p,p,0) \\ &\quad + \int_0^t \mathrm{d}s_1 \gamma^+(x-s_1 v_p) \exp\left\{-\Omega_p s_1 - \int_0^{s_1} \mathrm{d}s_2 \Gamma(x-s_2 v_p)\right\} \\ &\quad + \omega_p^+ \int_0^t \mathrm{d}s_1 \exp\left\{-\Omega_p s_1 - \int_0^{s_1} \mathrm{d}s_2 \Gamma(x-s_2 v_p)\right\}. \end{aligned} \tag{5.44}$$

Eq. (5.44) is the exact solution without local potentials and dephasing noises.

5.3.1 Jump operators creating/destroying delocalized particles

As first example, we assume $\gamma_x^+ = \gamma_x^- = 0$, so that particles can be injected-ejected as plane waves, with rates ω_p^+ and ω_p^-. Eq. (5.40) reduces to

$$\partial_t n(x,p,t) = -v_p \partial_x n(x,p,t) - \Omega_p n(x,p,t) + \omega_p^+ \,, \tag{5.45}$$

with solution

$$n(x,p,t) = \begin{cases} \left(n(x-tv_p,p,0) - \frac{\omega_p^+}{\Omega_p}\right) e^{-\Omega_p t} + \frac{\omega_p^+}{\Omega_p}\,, & \Omega_p \neq 0 \\ n(x-tv_p,p,0) + \omega_p^+ t\,. & \Omega_p = 0 \end{cases} \tag{5.46}$$

According to Eq. (5.46), the system exponentially reaches a steady state for $\Omega_p > 0$. For bosons, $\Omega_p = \omega_p^- - \omega_p^+$ and the system is stable if $\omega_p^- > \omega_p^+$. For fermions $\Omega_p = \omega_p^+ + \omega_p^- \geq 0$ and no such restriction applies.

In the long time limit, the filling factor is

$$\varkappa_\infty := \lim_{t\to\infty} \frac{N_\mathrm{p}(t)}{L} = \frac{1}{2\pi} \int_{-\pi}^{\pi} \mathrm{d}k \frac{\omega_k^+}{\Omega_k}\,. \tag{5.47}$$

For fermionic chains, $\varkappa_\infty \in [0,1]$. In particular, if $\omega_p^+ \neq 0, \omega_p^- = 0$ then $\varkappa_\infty = 1$. In this case, the system starts absorbing particles until it is completely filled and the Pauli exclusion principle freezes the dynamics. In the opposite case $\omega_p^+ = 0, \omega_p^- \neq 0$, the Winger function goes exponentially to zero until reaching the vacuum steady state, with $\varkappa_\infty = 0$. Another interesting case is $\omega_p^+ = \omega_p^- \neq 0$, where the system tends to a maximally mixed state with particle number $N_\mathrm{p} = L/2$, which is the half filling condition.

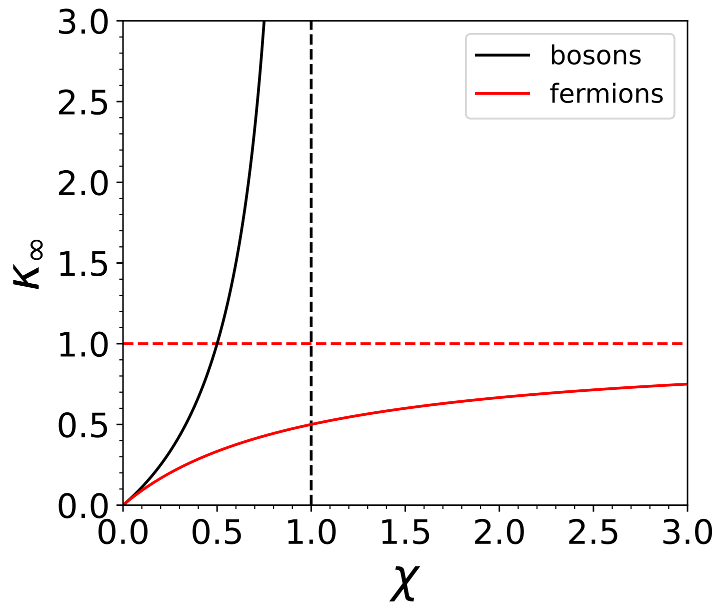

Figure 5.3: Filling factor κ_∞ as a function of $\chi = \omega^+/\omega^-$, for fermions and bosons.

For bosonic chains, the filling factor κ_∞ may take any positive value and the constraint $\omega_p^- > \omega_p^+$ guarantees the existence of the steady state in the long time limit. As in the fermionic case, if $\omega_p^+ = 0, \omega_p^- \neq 0$, the system approaches exponentially the vacuum steady state.

For homogeneous rates, $\omega_p^+ = \omega^+, \omega_p^- = \omega^-$ and $\kappa_\infty = \chi/(1 \pm \chi)$, where $\chi := \omega^+/\omega^-$ is the ratio between the absorption and emission rates. For bosonic systems, the constraint $\omega_p^- > \omega_p^+$ implies that $\chi \in [0, 1)$. In Fig. 5.3, we show the asymptotic filling factor κ_∞ as a function of χ, for bosons and fermions.

5.3.2 Jump operators creating/destroying localized particles

Here and below, our interest will be on spinless fermions. Moreover, we shall always take $\hat{H}_0$ to be a tight-binding Hamiltonian with nearest neighbour interactions, viz. $(\mathbf{h}_0)_{ij} = -(\delta_{i,j+1} + \delta_{i,j-1})/2$. This hypothesis on $\hat{H}_0$ leads to the single particle eigenvalues $\epsilon_p = -\cos(p)$ and the group velocity $v_p = \partial_p \epsilon_p = \sin(p)$.

In this paragraph, we deal with one-body gain-loss processes in real space ($\omega_p^+ = \omega_p^- = 0$), where localised particles are injected and ejected with inhomogeneous rates γ_x^+, γ_x^-. Under these assumptions, the differential equation (5.40) becomes

$$\partial_t n(x,p,t) = -\sin(p)\partial_x n(x,p,t) - \Gamma_x n(x,p,t) + \gamma_x^+ \,, \tag{5.48}$$

with analytical solution

$$\begin{aligned} n(x,p,t) &= \exp\left\{-\int_0^t \mathrm{d}s_1\, \Gamma(x-s_1\sin(p))\right\} n(x-t\sin(p),p,0) \\ &+ \int_0^t \mathrm{d}s_1 \gamma^+(x-s_1\sin(p)) \exp\left\{-\int_0^{s_1} \mathrm{d}s_2 \Gamma(x-s_2\sin(p))\right\}. \end{aligned} \tag{5.49}$$

In Figs. 5.4 (a-b), we consider the gain and loss rates

$$\gamma_x^\alpha = \frac{A_\alpha}{\sqrt{2\pi}\sigma_{x,\alpha}} e^{-\frac{(x-x_\alpha)^2}{2\sigma_{x,\alpha}^2}} \,, \tag{5.50}$$

where $\alpha = +,-$ and $A_\alpha, \sigma_{x,\alpha}, x_\alpha$ are three tunable parameters. More specifically, the parameter A_α is related to the coupling amplitude between the system and the external environment; the standard deviation $\sigma_{x,\alpha}$ introduces a dispersion along the real axis and has to be chosen so that the Gaussian distribution (5.50) is a slowly varying function compared to the lattice spacing (here equal to 1); the parameter x_α defines the peak position of γ_x^α.

We prepare the system in the double domain wall

$$n(x,p,0) = \Theta(L/2+\delta-x) - \Theta(L/2-\delta-x). \tag{5.51}$$

After quenching the state, the double domain wall (5.51) starts melting inside the light cones $|x-L/2-\delta| < t$ and $|x-L/2+\delta| < t$. The quasi-particle motion is ballistic and characterised by a finite lifetime t_{life}, which is a random variable following the exponential distribution

$$P(t_{\text{life}}; x_0, p_0) = \mathcal{Z} \exp\left\{-\int_0^{t_{\text{life}}} \mathrm{d}s\; \Gamma(x_0 + \sin(p_0)s)\right\}, \tag{5.52}$$

where $\mathcal{Z}$ is a normalization constant. The probability distribution $P(t_{\text{life}}; x_0, p_0)$ depends on the initial position and momentum (x_0, p_0) of the quasi-particle and the analytic form of the jump rates (5.50). This implies that the average lifetime $\langle t_{\text{life}}\rangle = \int_0^\infty s\,P(s; x_0, p_0)\,\mathrm{d}s$ is not identical for any excitation. At the same time, in average, a new quasi-particle is created at position x after any time interval $(\gamma_x^+)^{-1}$.

In Figs. 5.4 (a-b), we plot the particle density and the Wigner joint distribution as a function of time. In particular, we consider a 200-site chain and we set

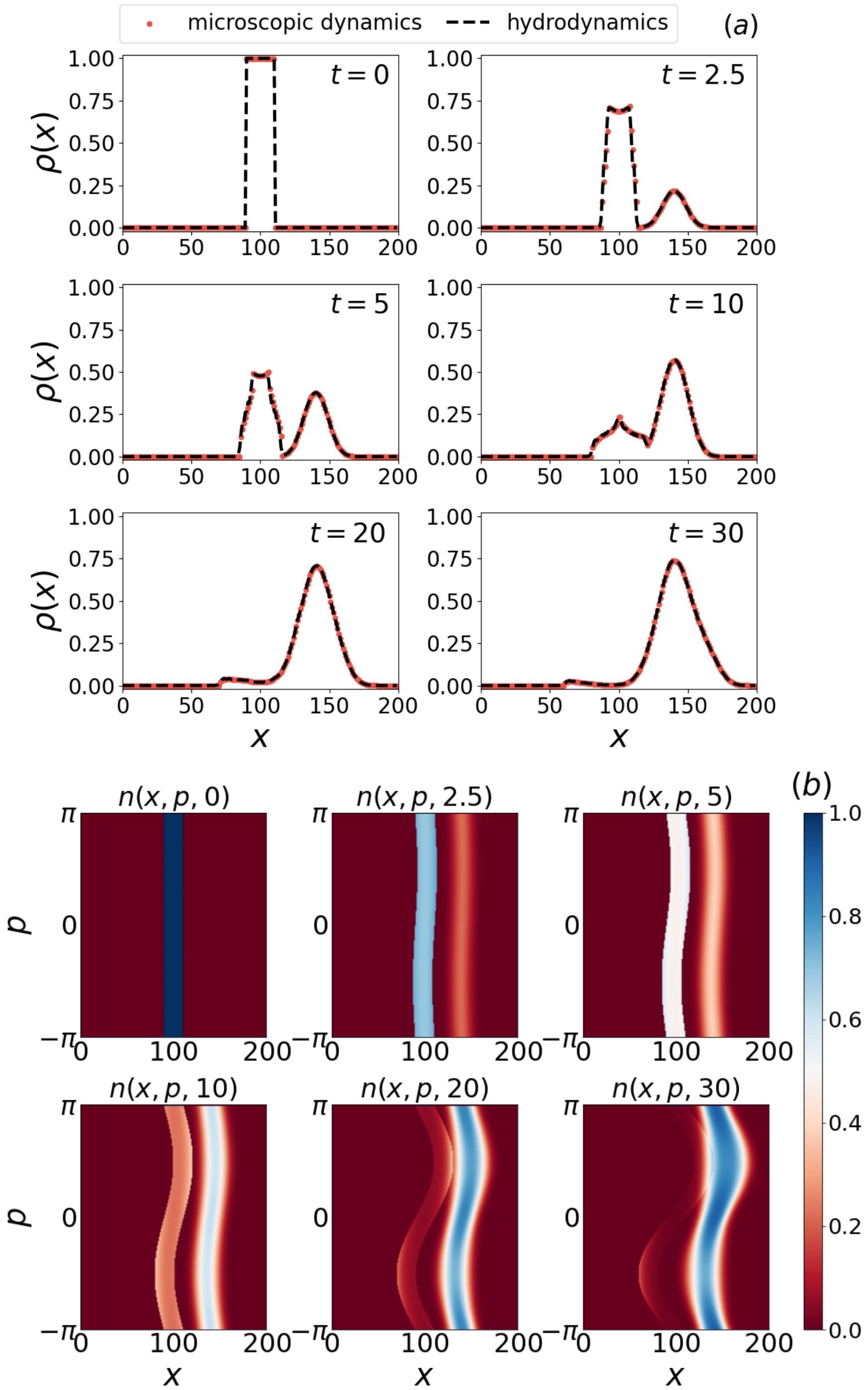

Figure 5.4: 200-site chain of hopping fermions with Gaussian-like jump rates (5.50). We prepare the system in the double domain wall (5.51) and we set $\delta = 10, A_+ = 2.0, \sigma_{x,+} = 8.0, x_+ = 140.0, A_- = 6.0, \sigma_{x,-} = 16.0, x_- = 100.0$. (a) Time evolution of the density $\rho(x,t)$; we compare the microscopic dynamics (5.16) (red spots) with the hydrodynamic approach (5.49) (black dashed lines); (b) Evolution of the phase-space Wigner function.

$\delta = 10, A_+ = 2.0, \sigma_{x,+} = 8.0, x_+ = 140.0, A_- = 6.0, \sigma_{x,-} = 16.0, x_- = 100.0$. For this specific choice of parameters and the initial condition (5.51), the Wigner function become more and more asymmetric over time, with new exitations created in the right hand side of the chain and others being destroyed in the middle. Only a few residual particles with negative velocity manage to overcome the chain section dominated by the jump rate γ_x^-.

In Fig. 5.5 (a), we pictorially show the density evolution for a domain wall initial configuration $n(x, p, t) = \Theta(-x)$. We assume a chain of hopping fermions ($v_p = \sin(p)$) with a single-particle loss process

$$\gamma_x^- = \gamma^- \Big(\Theta(x_0 + l/2 - x) - \Theta(x_0 - l/2 - x) \Big), \tag{5.53}$$

where $x_0 = l/2$ and l is the length of the subsystem where particles are destroyed with rate γ^-. Eq. (5.48) reduces to

$$\partial_t n(x, p, t) = -\sin(p) \partial_x n(x, p, t) - \gamma_x^- n(x, p, t) \,. \tag{5.54}$$

After quenching the states, the particle start flowing toward the empty sites in the right hand side of the chain. Hence, any quasi-particle crossing the section $[0, l]$ is destroyed with rate γ^-. The bigger the rate γ^-, the higher the probability for the particles with positive momentum of being destroyed. One quantity which is definitely affected by the loss process (5.53) is $N_p([0, \infty], t)$, which is the number of particles in $[0, \infty]$ at time t,

$$\begin{aligned} N_p([0, \infty], t) \;\; = \;\; & \Theta(t - l) \frac{1}{\pi \gamma^-} \left[1 - e^{-\gamma^- t} \left(1 - \sqrt{1 - \left(\frac{l}{t}\right)^2} \right) \right] \\ & + \Theta(t - l) \frac{1}{\pi \gamma^-} \int_{\arcsin(l/t)}^{\pi/2} dk \;\; [(\gamma^- t - 1) \sin(k) - l \gamma^-] \, e^{-\frac{\gamma^- l}{\sin(k)}} \\ & + \Theta(l - t) \frac{1}{\pi \gamma^-} (1 - e^{-\gamma^- t}) \,. \end{aligned} \tag{5.55}$$

In Fig. 5.5 (b), we plot $N_p([0, \infty], t)$ as a function of time and several values of γ^-. For large times ($t/l \gg 1$), the number of particles $N_p([0, \infty], t)$ grows linearly in time, with proportionality constant

$$m(\gamma^- l) = \frac{1}{\pi} \int_0^{\pi/2} dk \;\; \sin(k) e^{-\frac{\gamma^- l}{\sin(k)}} \,. \tag{5.56}$$

If $\gamma^- l \ll 1$ then $\exp\left\{ -\frac{\gamma^- l}{\sin(k)} \right\} \simeq 1$ for $p \in (0, \pi/2)$, and $m \simeq 1/\pi$. In the opposite limit $\gamma^- l \gg 1$, $\exp\left\{ -\frac{\gamma^- l}{\sin(k)} \right\} \simeq 0$ and $m \simeq 0$. The inset into Fig. 5.5 (b) shows the proportionality constant as a function of γ^- for $l = 20$, which goes exponentially to zero for large γ^- and verifies $m(0) = 1/\pi$, as expected for closed systems.

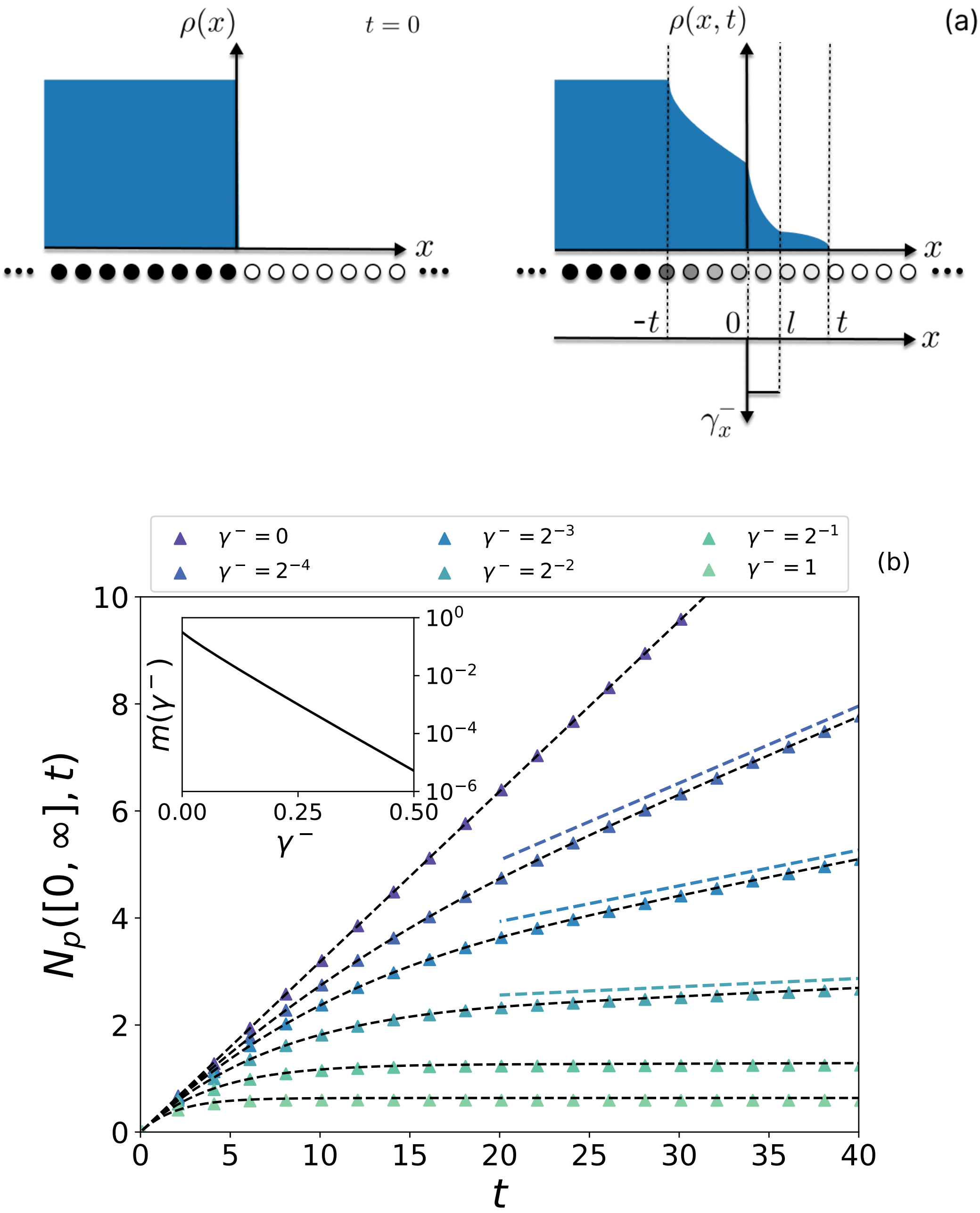

Figure 5.5: (a) Illustration of the domain wall setting. At $t = 0$ the system is filled entirely on the left half of the chain and empty on the right one; the fermionic density at time $t = 0$ is $\rho(x) = \Theta(-x)$ and the loss process is modulated by the jump frequency (5.53). At $t > 0$ the domain wall melts inside the light cone region $|x| \leq t$ and the density profile is given by Eq. (5.54). (b) Number of particles in $[0, \infty]$ for $x_0 = l/2 = 10$. The black dashed line and the coloured spots refer to the microscopic dynamics (5.16) and the quasi-particle ansatz (5.55), respectively. In the inset, the coefficient (5.56) as a function of γ^- for $l = 20$.

5.3.3 Transport phenomena

To connect the previous analysis with transport features, we shall consider a single particle state with Wigner function $n(x, p, 0) = \delta(x)$. After quenching the state, we focus on the average displacement $d(t) = \sqrt{\langle x^2 \rangle - \langle x \rangle^2}$, which measures the deviation of the particle position over time. For closed systems and vanishing potentials, the motion is ballistic and $d(t) \propto t$. In this paragraph, we would like to explore the transport for one-body gain-loss processes affecting the particle number conservation. We assume the dynamics is described by Eq. (5.54) with $v_p = \sin(p)$ and $\gamma_x^+ = 0$ to avoid particle injection. We also consider symmetric jump rates γ_x^- under $x = 0$, so that $\langle x \rangle = 0$ and

$$d(t) = \left[\int_{-\infty}^{+\infty} \mathrm{d}x\, x^2 \rho(x, t) \right]^{1/2}. \tag{5.57}$$

From the solution of the hydrodynamic equation (5.54), the particle density reads

$$\rho(x, t) = \frac{1}{\pi t} \frac{e^{-t \int_0^1 \mathrm{d}s\, \gamma^-(x - xs)}}{\sqrt{1 - (x/t)^2}} \Big(\Theta(t - x) - \Theta(-t - x) \Big). \tag{5.58}$$

By hypothesis, we assume γ_x^- equal to (5.53), with $x_0 = 0$. The average displacement is

$$d(t) = \Theta\left(\frac{l}{2} - t\right) \frac{t}{\sqrt{2}} e^{-\gamma^- t/2} + \Theta\left(t - \frac{l}{2}\right) \sqrt{\frac{2}{\pi}} t \, \times$$
$$\times \left[\int_{\frac{l}{2t}}^1 \mathrm{d}y \, \frac{y^2}{\sqrt{1 - y^2}} e^{-\gamma^- l/2y} + \frac{1}{2} e^{-\gamma^- t} \left(\arcsin\left(\frac{l}{2t}\right) - \frac{l}{2t} \sqrt{1 - \left(\frac{l}{2t}\right)^2} \right) \right]^{1/2}. \tag{5.59}$$

Observe that $d(t) = t/\sqrt{2}$ for $\gamma_x^- = 0$, as expected for closed systems. In the long time limit ($t/l \gg 1$), $d(t) \simeq \widetilde{m}(\gamma^- l) t$, with

$$\widetilde{m}(\gamma^- l) = \sqrt{\frac{2}{\pi}} \left[\int_0^1 \mathrm{d}y \, \frac{y^2}{\sqrt{1 - y^2}} e^{-\gamma^- l/2y} \right]^{1/2}. \tag{5.60}$$

Following the hydrodynamic description into Sec. 5.2, the transport is still ballistic but the average displacement cannot be linear in time anymore, since the dissipator may destroy the excitation in the interval $(-l/2, l/2)$. Notice that there is a crossover at $t = l/2$, coinciding with the distance covered by the particle with maximum velocity after the quench. In the long time limit, the average displacement is linear again. As before, we distinguish two asymptotic cases. For $\gamma^- l \ll 1$, $\exp\{-\gamma^- l/2y\} \simeq 1$ and $\widetilde{m} \simeq 1/\sqrt{2}$; for $\gamma^- l \gg 1$, $\exp\{-\gamma^- l/2y\} \simeq 0$ and $\widetilde{m} \simeq 0$.

5.4 Wigner dynamics with dephasing

In this section we include a constant dephasing noise in the dynamics, which may be viewed in the light of continuous measurement processes (see Chapter 4), where the system undergoes random projective measurements or infinitely weak and frequent interactions with ancillas [C6].

5.4.1 Homogeneous dephasing

In this brief paragraph, we just recall some known results about open dynamics with homogeneous dephasing noise (see also Chapter 4 and Ref. [59]). In Fig. 5.6, we prepare a 200-site chain of hopping fermions ($v_p = \sin(p)$) in the initial condition $n(x, p, 0) = \delta(x - L/2) = \rho(x, 0)$. The Wigner function solves

$$\partial_t n(x, p, t) = -\sin(p)\partial_x n(x, p, t) - \lambda n(x, p, t) + \lambda \rho(x, t)\,. \tag{5.61}$$

In Fig. 5.6, we assume $\lambda = 0.2$ and we compare the microscopic dynamics (5.13) with the Gaussian distribution

$$\sqrt{\frac{\lambda}{2\pi t}} \exp\left\{-\frac{\lambda(x - L/2)^2}{2t}\right\}. \tag{5.62}$$

Eq. (5.62) is a solution of the heat equation (5.39). In Fig. 5.6, we observe that the microscopic dynamics converges to the Gaussian distribution (5.62) in the long time limit $t\lambda \gg 1$.

In Fig. 5.7, we prepare the system in the single particle state $n(x, p, 0) = \delta(x - L/2)$ and we show the scaling of the integrated current

$$\mathcal{C}(t) = \sum_{x>L/2} \langle c_x^\dagger c_x \rangle(t)\,. \tag{5.63}$$

Fig. 5.7 clearly shows the ballistic and diffusive regimes, with crossover time $t = \lambda^{-1}$. The coloured spots represent data collected by numerical experiments involving random projective measurements (see Sec. 4.1.2), while the black line comes from the numerical solution of Eq. (5.61). An interesting open problem is to prove analytically the crossover between the ballistic and diffusive regimes, which should emerge from the solution of Eq. (5.61).

5.4.2 Homogeneous dephasing and losses in real space

Although the dynamics with homogeneous dephasing has been abundantly explored, it is much less explicit how dephasing and gain-loss processes jointly

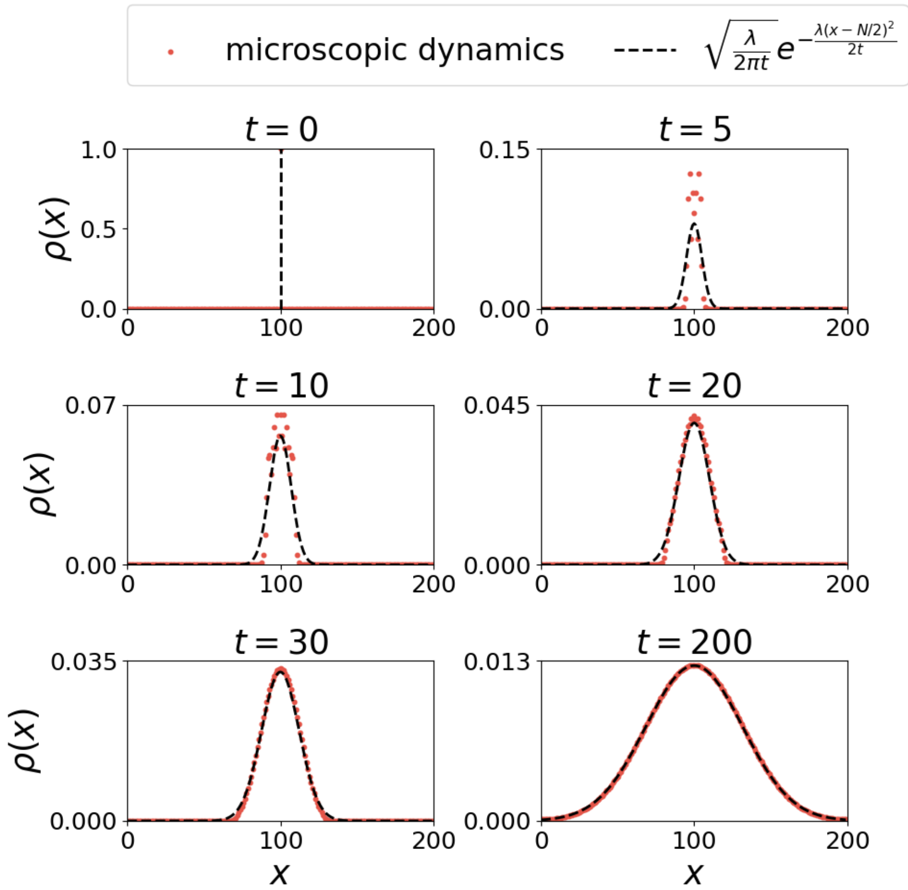

Figure 5.6: Evolution of the particle density for hopping fermions and homogeneous dephasing rates. We set $\lambda = 0.2$ and $L = 200$. We prepare the system in the state $n(x, p, 0) = \delta(x - L/2)$. The red spots and the dashed black line represent the exact microscopic dynamics and the Gaussian function (5.62), which is solution of the heat equation (5.39). The microscopic evolution converges to the solution of the diffusive equation (5.39) in the limit $t\lambda \gg 1$.

affect the Wigner evolution. To explore this scenario, we take a chain of hopping fermions ($v_p = \sin(p)$), under homogeneous dephasing and losses in real space ($\lambda_x = \lambda$, $\gamma_x^+ = 0$, $\omega_p^+ = \omega_p^- = \zeta_p = 0$). In particular, we assume a loss rate γ_x^- given by Eq. (5.53), with $x_0 = L/2$. Under these hypothesis, the Wigner function satisfies

$$\partial_t n(x, p, t) = -\sin(p)\partial_x n(x, p, t) - (\lambda + \gamma_x^-)n(x, p, t) + \lambda\rho(x, t). \tag{5.64}$$

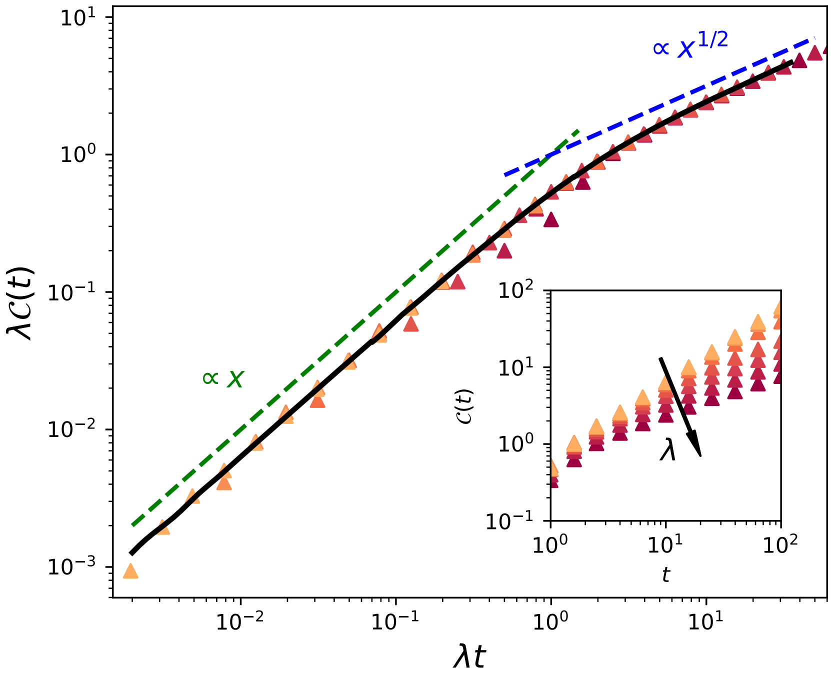

Figure 5.7: Scaling of the integrated current $\mathcal{C}(t)$. We plot $\lambda\mathcal{C}(t)$ vs $x = \lambda t$. We can distinguish the ballistic regime ($\lambda\mathcal{C}(t) \propto x$) and the diffusive regime ($\lambda\mathcal{C}(t) \propto x^{1/2}$), with a crossover at $x = 1$. The coloured spots are data collected by numerical experiments involving random measurements; the black line comes from the numerical solution of the differential equation (5.61).

We prepare the system in the Wigner function

$$n(x, p, 0) = \begin{cases} 1 & |x - L/2| < l/2 \wedge |p| < \pi/2 \\ 0 & |x - L/2| \geq l/2 \vee |p| \geq \pi/2 \end{cases} \tag{5.65}$$

and we study its time evolution.

In Figs. 5.8 (a), 5.9, we show the density and the Wigner function dynamics for several values of λ. For $\lambda = 0$, the motion is purely ballistic and the number of destroyed particles is finite and always different from zero. As the dephasing constant λ increases, excitations spend more and more time inside the chain section with $\gamma_x^- \neq 0$ until they are destroyed. In the large λ limit, the Zeno regime freezes the dynamics and the system exponentially converges to the vacuum state. In conclusion, any finite value $\lambda > 0$ leads the system to the vacuum state.

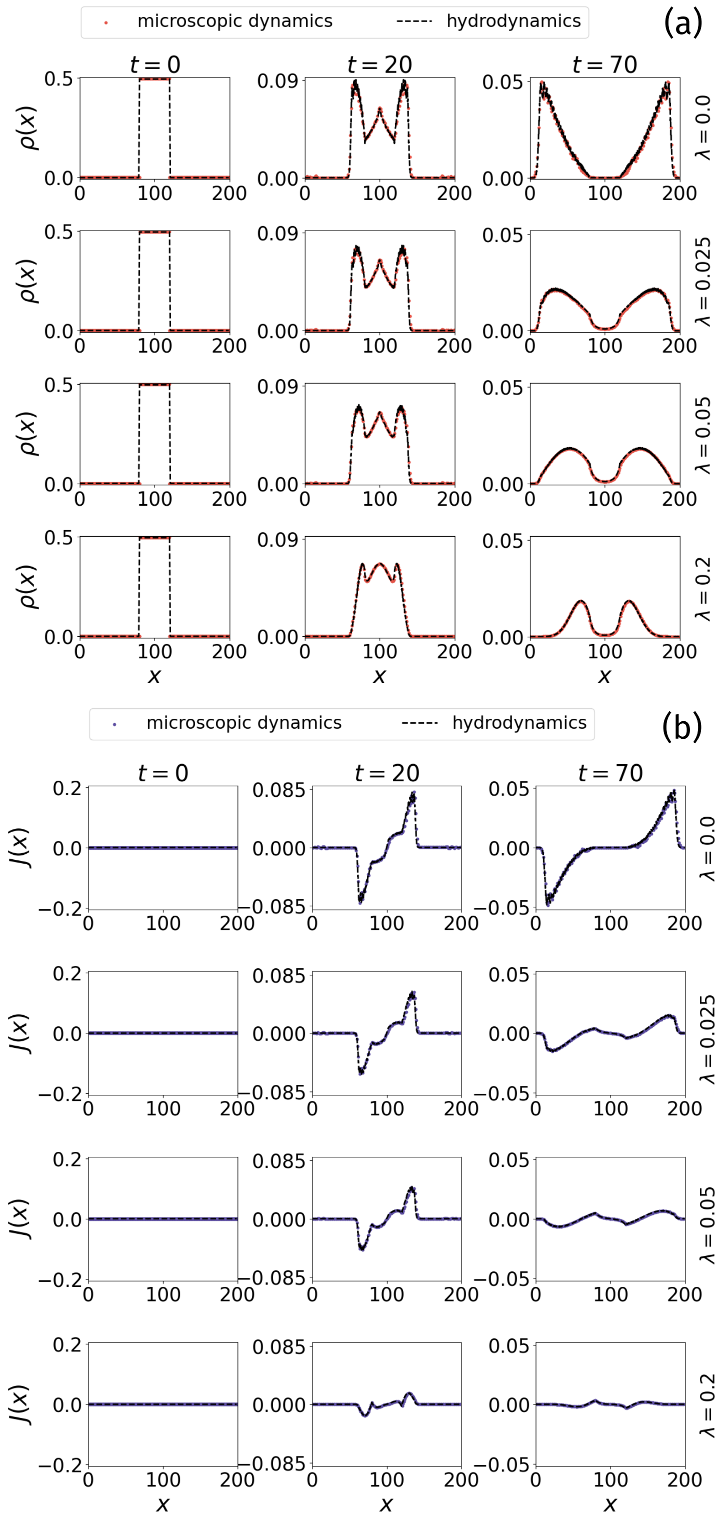

Figure 5.8: 200-site chain of hopping fermions under homogeneous monitoring and loss processes (5.53), with $x_0 = 100$, $l = 40$, $\gamma^- = 0.1$. For the initial conditions (5.65), we compare the hydrodynamic description with the microscopic dynamics; (a) Time evolution of the particle density; (b) Time evolution of the current.

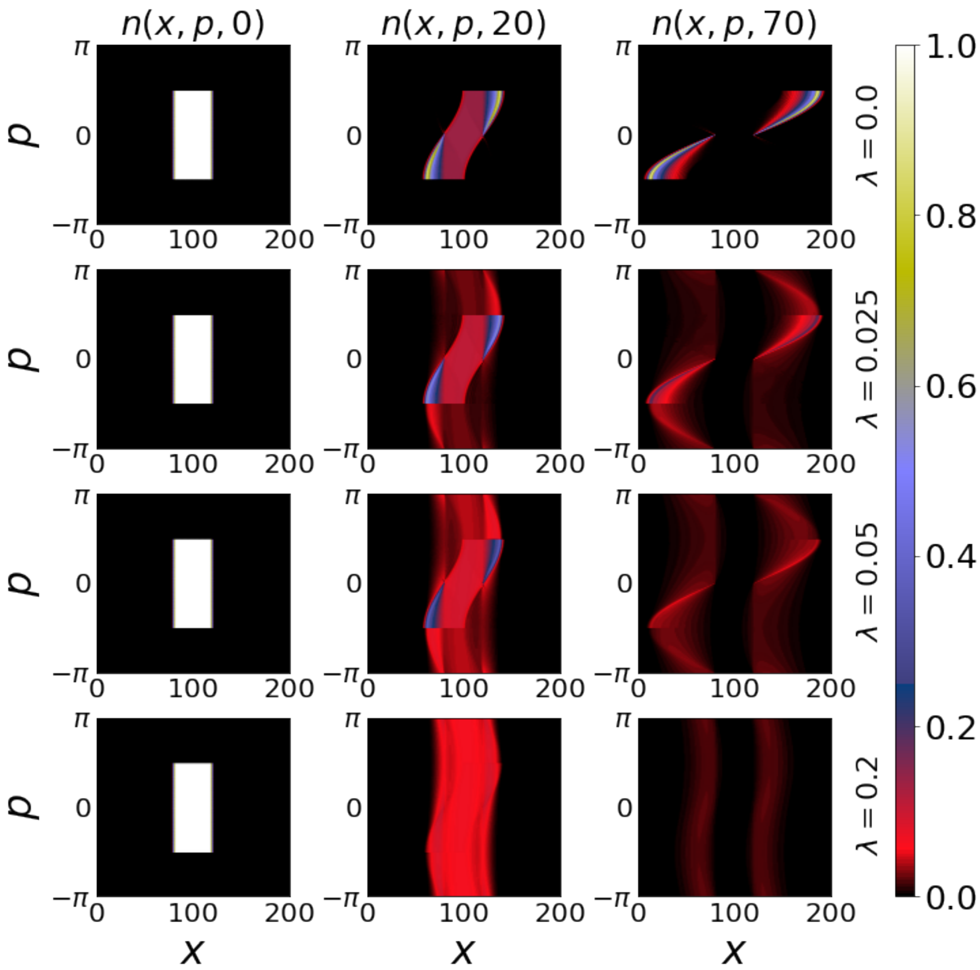

Figure 5.9: 200-site chain of hopping fermions under homogeneous monitoring and local loss processes (5.53), with $x_0 = 100$, $l = 40$, $\gamma^- = 0.1$. For the initial conditions (5.65), we show the full Wigner function time evolution for different values of the dephasing constant λ.

In Fig. 5.8 (b) we also show the current

$$J(x,t) = \int_{-\pi}^{\pi} \frac{\mathrm{d}p}{2\pi} \sin(p)\, n(x,p,t)\,, \tag{5.66}$$

as a function of time t and several measurement rates λ. The current solves the differential equation

$$\partial_t \rho(x,t) + \partial_x J(x,t) + \gamma_x^- \rho(x,t) = 0. \tag{5.67}$$

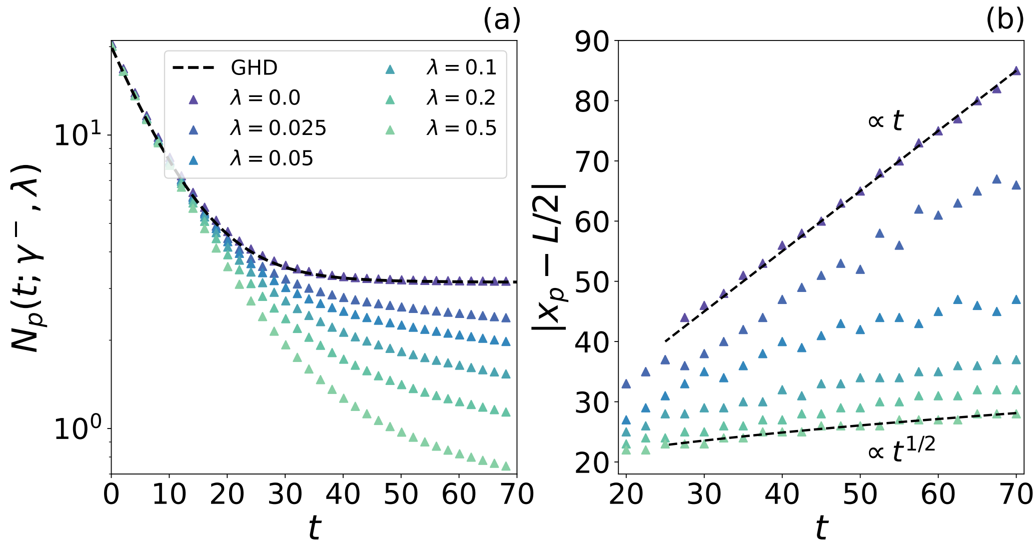

Figure 5.10: 200-site chain of hopping fermions under homogeneous monitoring and local loss processes (5.53), $x_0 = 100$, $l = 40$, $\gamma^- = 0.1$. We prepare the system in the Wigner function (5.65) at time $t = 0$. (a) Total number of particles as a function of time for different values of the parameter λ. The spots represent the data collected by solving Eq. (5.13). The black dashed line refers to the hydrodynamic prediction (5.69). (b) Displacement of the density peaks as a function of time. Observe the linear growth for $\lambda t \ll 1$ and the square root behaviour for $\lambda t \gg 1$.

As expected, the loss processes break the continuity equation. Integrating Eq. (5.67) with the boundary condition $J(L,t) \xrightarrow{L\to\infty} 0$, we find

$$J(x,t) = \partial_t N_\mathrm{p}([x,L],t) + \int_x^\infty \mathrm{d}y\, \gamma_y^- \rho(y,t), \tag{5.68}$$

where $N_\mathrm{p}([x,L],t)$ is the particle number in $[x,L]$ at time t.

In Fig. 5.10 (a), we plot the total number of particles $N_\mathrm{p}(t;\gamma^-,\lambda)$ for different values of the parameter λ. $N_\mathrm{p}(t;\gamma^-,\lambda)$ is a monotonically decreasing function of λ at fixed values (t,γ^-). For vanishing dephasing ($\lambda = 0$), the analytic solution reads

$$
\begin{aligned}
N_{\mathrm{p}}(t;\gamma^-,0) \quad = \quad & \Theta(l-t)\left[N_{\mathrm{p}}^0 e^{-\gamma^- t} - \frac{t}{\pi}e^{-\gamma^- t} + \frac{1}{\pi\gamma^-}(1-e^{-\gamma^- t})\right] \\
& +\Theta(t-l)\frac{1}{\pi\gamma^-}\left[1 + l\gamma^- \arcsin\left(\frac{l}{t}\right)e^{-\gamma^- t}\right] \\
& -\Theta(t-l)\frac{1}{\pi\gamma^-}e^{-\gamma^- t}(1+\gamma^- t)\left(1-\sqrt{1-\left(\frac{l}{t}\right)^2}\right) \\
& -\Theta(t-l)\frac{1}{\pi\gamma^-}\int_{\arcsin(l/t)}^{\pi/2} \mathrm{d}p\ \sin(p)\, e^{-\frac{\gamma^- l}{\sin(p)}}\,,
\end{aligned}
\tag{5.69}
$$

where $N_{\mathrm{p}}^0 = l/2$ is the initial number of particles, according to the half filling condition (5.65). If $t \to \infty$, the number of residual particles goes to $m(\gamma^- l)/\gamma^-$, approaching $1/\pi\gamma^-$ for $\gamma^- l \ll 1$. In Fig. 5.10 (b), we show $|x_p - L/2|$ as a function of time, where x_p corresponds to the peak position of the wave front of the density. As for the integrated current into Fig. 5.7, we numerically find the initial linear regime and the $t^{1/2}$ behaviour for $\lambda t \gg 1$. Observe that the peak position (coloured spots in Fig. 5.10 (b)) has been obtained by solving the exact microscopic dynamics. The higher order terms in the derivatives ∂_x and ∂_p, neglected into Eq. (5.64), are the reason behind the not complete monotonicity of the function $|x_p - L/2|$. Indeed, this behaviour cannot be captured by Eq. (5.64). The main purpose of Fig. 5.10 (b) is to emphasise that the peak position slows down for increasing dephasing constants λ, approaching the diffusive regime (5.39) for $\lambda t \gg 1$.

5.4.3 Homogeneous dephasing and losses in momentum space

In Fig. 5.11, we consider a chain of hopping fermions ($v_p = \sin(p)$), under homogeneous dephasing and losses in reciprocal space ($\zeta_p = \zeta$, $\omega_p^+ = \gamma_x^- = \gamma_x^+ = \lambda_x = 0$). The particle exchange is modulated by the jump rate

$$
\omega_p^- = \omega^-\left(\Theta\left(\frac{\pi}{2} - p\right) - \Theta\left(-\frac{\pi}{2} - p\right)\right), \tag{5.70}
$$

which selects the emission channels. The hydrodynamic equation is

$$
\partial_t n(x,p,t) = -\sin(p)\partial_x n(x,p,t) - (\zeta + \omega_p^-)n(x,p,t) + \zeta\tilde{\rho}(p,t)\,, \tag{5.71}
$$

with the initial Wigner function (5.65). In Fig. 5.11, we show the particle density evolution for different values of the monitoring rate ζ. The specific dynamical

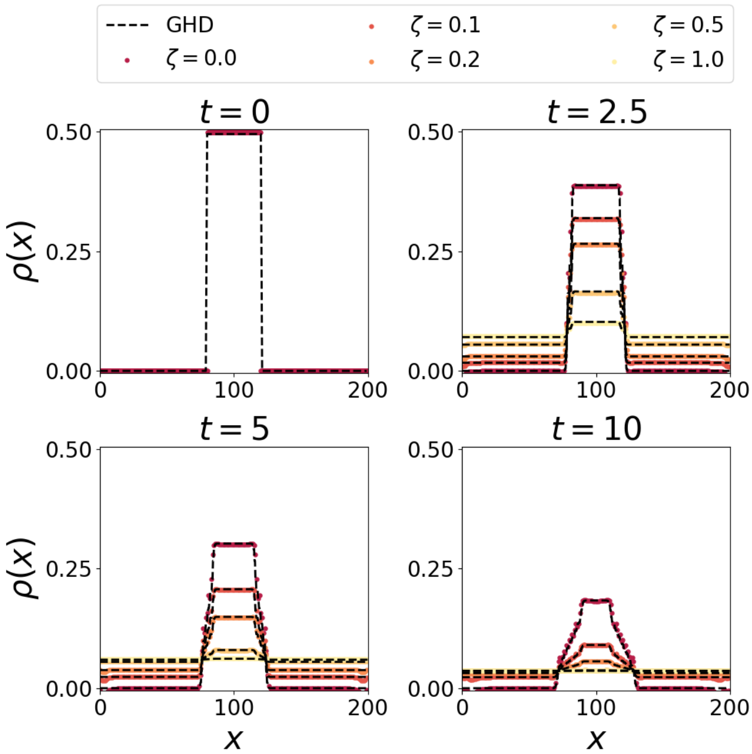

Figure 5.11: 200-site chain of hopping fermions under homogeneous dephasing and loss processes (5.70). We set $\omega^- = 0.1$ and we prepare the system in the Wigner function (5.65) at time $t = 0$. We plot the density time evolution for different values of the parameter ζ. The coloured spots and the black dashed lines refer to the microscopic dynamics (5.13) and the hydrodynamic approach (5.71), respectively.

protocol into Eq. (5.71) conserves the particle momentum and thus, for the initial conditions (5.65), the system exponentially converges to the vacuum state for any dephasing rate ζ. However, the larger parameter ζ, the greater the number of delocalized particles over time.

5.5 Discussion and conclusion

In this work, we generalised the hydrodynamic approach for quantum chains of non-interacting particles coupled to external Lindblad baths. We studied the case of inhomogeneous one-body gain-loss processes and dephasing. As main result, we got the equation of motion of the Wigner function, whose dynamics may be pictorially viewed in terms of classical non-interacting quasi-particles:

the gain and loss processes make the average lifetime finite while the dephasing affects the transport features. Through several examples, we showed that the Wigner dynamics reproduces the same results of the microscopic dynamics. In particular cases, we provided analytical solutions of the hydrodynamic equations, giving unique physical insights. Finally, we studied the combined effects of constant dephasing noises and single particle loss processes. In this context, a natural working direction for the future would be to analyse the effects of inhomogeneous monitoring rates, as for real experimental layouts, where more interesting transport features may emerge.

Chapter 6

From Lindblad master equations to Langevin dynamics and back

The description of the non-equilibrium dynamics of open quantum systems, even at a fundamental level, continues to present many challenges [C6, 204, C14–C16, 205, 206, C17]. Modelling the interaction system-bath is usually tough and depends on the physical background. Following the proposal by Ford, Kac and Mazur, see e.g. Ref. [72] and Sec. 2.2, the Langevin equations are derived from an ab-initio approach, where the quantum fluctuation-dissipation theorem (QFDT) holds and the relaxation towards the thermodynamic equilibrium state is guaranteed. However, the resulting dynamics cannot be markovian [14, 72, 74, C14, C17, 207–209]. As previously mentioned in Sec. 2.2, the Langevin dynamics may also be derived by approaching the problem from a phenomenological perspective, introducing a deterministic damping term and some stochastic noises, whose correlators are to be determined by peculiar properties of the stationary state [C17, C18, 210]. Although a proper langevian description is intrinsically non-markovian, in Sec. 2.2 we quoted the Bedeaux-Mazur proposal, where Langevin equations with markovian noises may still be obtained by relaxing some physical requirements. In this chapter, the focus is on these physical situations where the characteristic time scales between the system and the bath are compatible with an effective markovian description of the system dynamics.

In Chapter 2, we introduced the Lindblad evolution, which is a prototypical example of markovian dynamics specified in terms of dynamical semigroups [61]. The Lindblad dynamics arises from second-order perturbation theory and other assumptions, such as uncorrelated initial states, the rotating wave approximation and, of course, the Markov hypothesis. Under these conditions, the Liouvillian generator for the reduced dynamics verifies the complete positivity [61, C19, 211–214]. However, the need of complete positivity as dynamical postulate has been questioned and recent approaches try to circumvent this controversial topic [60, 212, 213, 215–224].

For open quantum systems with effective markovian dynamics, both the lindbladian and langevinian descriptions co-exist but the relation between them is much less explored. For this purpose, we consider a single particle quantum harmonic oscillator, which lends itself well to many applications, e.g. Refs. [C6, C8, 67, 68, C14, C17, 210, 225]. The Lindblad dynamics for a quantum oscillator is usually based on quantum optics, to describe a single mode in an optical cavity [C6, C8, C14]. On the other hand, the physical picture for the Langevin equations is a massive particle in a confining potential, which is submitted to friction and random impulsive forces. In this work, we use the proposal by Bedeaux and Mazur [67, 68] with markovian noises (see Sec. 2.2), keeping in mind that the Langevin and Lindblad dynamics are considered equivalent if they reproduce the same dynamics of the average observables.

The content of this chapter is based on our paper [A3]. In Sec. 6.1, we recall the Bedeaux-Mazur formulation of the markovian quantum Langevin dynamics, hereinafter the *friction model* [67]. Afterwards, we define the *cavity model*, as a quantum harmonic oscillator with different deterministic damping terms and stochastic noises to be determined [C6]. As we shall see, both models are strictly connected to more general systems studied long time ago [225]. In order to determine the noise correlators, we shall use the same phenomenological criteria discussed in Sec. 2.2 and Ref. [14], with the exception of the requirement (D) about the QFDT, which is modified to generate markovian noises. Whatever microscopic justification might be found in either models, these must lead to certain phenomenological consequences which we use to circumvent any explicit discussion of complete positivity, rather than having to rely on rather abstract mathematically-inspired systems usually discussed in the literature. Although the friction and cavity models share some common features, the explicit dynamics is not identical. For instance, the friction model also contains an over-damped dynamical regime which is absent in the cavity model. In Sec. 6.2, we show that the cavity model is equivalent to the dampening of a single electromagnetic mode inside a cavity [C6, C8, C14], which is described by a completely positive map [C19]. Similarly, we build the Liouvillian generator of the reduced dynamics of the friction model, which is manifestly not completely positive. Strictly speaking, the dynamical map is not even positive [226]. However, unless we consider very squeezed initial states, we get physical density matrices at any time t. Nevertheless, as we shall show later, positive semi-definite density matrices are always recovered in the long-time limit. In Sec. 6.3, we make use of the Wigner function approach to solve the master equation for the friction and cavity models. In Sec. 6.4, we study the relaxation toward the stationary state, which is identical for both models without an external field. In Sec. 6.5, we recast both models as mean-field approximations of a many-body interacting magnet, deriving the phase diagrams at zero temperature. While the friction model relaxes to a proper equilibrium state independently on the damping parameter γ, this is not true for the cavity model, whose stationary state is γ-dependent. Our main results are summarised in Sec. 6.6.

6.1 Quantum Langevin equations

Our study concerns a single harmonic oscillator, with Hamiltonian

$$\begin{aligned} \widehat{H} &= \frac{g}{2}\widehat{p}^2 + \frac{\omega^2}{2g}\hat{x}^2 - B\hat{x}\,, && (6.1) \\ &= \hbar\omega\left(\hat{a}^\dagger\hat{a} + \frac{1}{2}\right) - B\sqrt{\frac{\hbar g}{2\omega}}\,(\hat{a} + \hat{a}^\dagger)\,, && (6.2) \end{aligned}$$

where g is the quantum coupling and ω is the angular frequency. The operators $\hat{x}$, $\widehat{p}$ are the position and momentum observables which obey the commutation relation $[\hat{x}, \widehat{p}] = \mathrm{i}\hbar$ and can be re-expressed through bosonic creation and annihilation operators

$$\hat{x} = \sqrt{\frac{\hbar g}{2\omega}}\,(\hat{a}^\dagger + \hat{a})\,, \qquad \widehat{p} = \mathrm{i}\sqrt{\frac{\hbar\omega}{2g}}\,(\hat{a}^\dagger - \hat{a})\,, \tag{6.3}$$

which leads to Eq. (6.2). In application to quantum magnets, where the position operator $\hat{x}$ becomes the quantum spin operator $\hat{s}$, B is interpreted as an external magnetic field. In this chapter, we shall compare two dissipative protocols generated by the Langevin equations, namely the *friction model*

$$\begin{aligned} \partial_t\hat{x} &= \frac{\mathrm{i}}{\hbar}\left[\widehat{H}, \hat{x}\right] + \hat{\eta}^{(x)}\,, && (6.4) \\ \partial_t\widehat{p} &= \frac{\mathrm{i}}{\hbar}\left[\widehat{H}, \widehat{p}\right] - \gamma\widehat{p} + \hat{\eta}^{(p)}\,, && (6.5) \end{aligned}$$

and the *cavity model*

$$\begin{aligned} \partial_t\hat{x} &= \frac{\mathrm{i}}{\hbar}\left[\widehat{H}, \hat{x}\right] - \frac{\gamma}{2}\hat{x} + \hat{\eta}^{(x)}\,, && (6.6) \\ \partial_t\widehat{p} &= \frac{\mathrm{i}}{\hbar}\left[\widehat{H}, \widehat{p}\right] - \frac{\gamma}{2}\widehat{p} + \hat{\eta}^{(p)}\,, && (6.7) \end{aligned}$$

for the particular Hamiltonian $\widehat{H}$ of the harmonic oscillator (6.1). In both models, we combine the unitary dynamics with phenomenological noises and deterministic damping terms with amplitude γ.

As we saw in Sec. 2.2, the friction model arises from the quantization of the classical Langevin equations for a particle of mass g^{-1} in a fluid. In this perspective, the particle is subject to classical harmonic potentials, damping forces proportional to the momentum variable and random impulsive interactions parameterised by white noises.

The choice (6.4,6.5) could appear more natural and intuitive than (6.6,6.7). In this respect, Eqs. (6.6,6.7) look artificial and the classical counterpart is not easily identifiable. However, along this chapter we shall prove that Eqs. (6.6,6.7) reproduce the dynamics of an oscillator in an optical cavity.

The coupling with the external bath(s) is encoded by the markovian noises $\hat{\eta}^{(x)}$, $\hat{\eta}^{(p)}$, being operator-valued centred random variables with a joint probability distribution and non-vanishing second moments. In this work, we shall follow the Bedeaux and Mazur proposal [67, 68], which is equivalent to the axiomatic construction of Ref. [14]. The noise correlators are specified by four phenomenological requirements

(A) the canonical equal-time commutator $\left\langle\left[\hat{x}(t), \hat{p}(t)\right]\right\rangle = \mathrm{i}\hbar$;

(B) the *Kubo formula* of linear response theory ;

(C) the *virial theorem*, both classical [C9–C11] and quantum-mechanical [14, 73], characterising the stationary regime. For a quantum oscillator with $B = 0$, it reads $\left\langle \hat{p}^2\right\rangle = \frac{\omega^2}{g^2}\left\langle \hat{x}^2\right\rangle$;

(D) the quantum equilibrium state condition, which reads $\left\langle \hat{x}^2\right\rangle_{\mathrm{eq}} - \left\langle \hat{x}\right\rangle_{\mathrm{eq}}^2 = \frac{\hbar g}{2\omega}\coth\left(\frac{\hbar\omega}{2T}\right)$ for the harmonic oscillator. This requirement replaces the QFDT, which is not compatible with markovian noises [14, 74, C14, C17, 207–209].

The conditions (A) and (B) fix the noise commutators, while the conditions (C) and (D) fix the noise anti-commutators.

As we shall prove in Sec. 6.1.2, the non-vanishing noise correlators of the friction model (6.4,6.5) are [67, 68]

$$\left\langle\left[\hat{\eta}^{(x)}(t), \hat{\eta}^{(p)}(t')\right]\right\rangle = \mathrm{i}\gamma\hbar\,\delta(t-t')\,, \tag{6.8}$$

$$\left\langle\left\{\hat{\eta}^{(p)}(t), \hat{\eta}^{(p)}(t')\right\}\right\rangle = \frac{2\gamma\hbar\omega}{g}\coth\left(\frac{\hbar\omega}{2T}\right)\delta(t-t')\,, \tag{6.9}$$

with units such that $k_{\mathrm{B}} = 1$. We can see that, in the classical limit $\hbar \to 0$, the friction model reduces to a linearly damped harmonic oscillator subject to white noise. Concerning the cavity model (6.6,6.7), the noise correlators take the form

$$\langle[\hat{\eta}^{(x)}(t),\hat{\eta}^{(p)}(t')]\rangle = \mathrm{i}\gamma\hbar\,\delta(t-t')\,, \tag{6.10}$$

$$\langle\{\hat{\eta}^{(p)}(t),\hat{\eta}^{(p)}(t')\}\rangle = \frac{\gamma\hbar\omega}{g}\coth\left(\frac{\hbar\omega}{2T}\right)\delta(t-t')\,, \tag{6.11}$$

$$\langle\{\hat{\eta}^{(x)}(t),\hat{\eta}^{(x)}(t')\}\rangle = \frac{\gamma\hbar g}{\omega}\coth\left(\frac{\hbar\omega}{2T}\right)\delta(t-t')\,, \tag{6.12}$$

which are explicitly derived in Sec. 6.1.1 below. Notice that, for both models, the Markov property is encoded by the delta functions. In Sec. 6.2 we shall show that Eqs. (6.6,6.7) are related to a CPTP Lindblad map whereas the master equation corresponding to the dynamics (6.4,6.5) is positive, but manifestly not completely positive.

In order to express the requirements (A-D) in a compact form, we define the averages

$$C_-^{(\mathcal{A},\mathcal{B})}(t,t') := \frac{1}{2}\langle[\hat{\mathcal{A}}(t),\hat{\mathcal{B}}(t')]\rangle\,, \tag{6.13}$$

$$C_+^{(\mathcal{A},\mathcal{B})}(t,t') := \frac{1}{2}\langle\{\hat{\mathcal{A}}(t),\hat{\mathcal{B}}(t')\}\rangle\,, \tag{6.14}$$

and the connected correlator

$$C_{+,c}^{(\mathcal{A},\mathcal{B})}(t,t') := C_+^{(\mathcal{A},\mathcal{B})}(t,t') - \langle\mathcal{A}(t)\rangle\langle\mathcal{B}(t')\rangle\,, \tag{6.15}$$

for any Hilbert operator $\hat{\mathcal{A}}$ and $\hat{\mathcal{B}}$. In terms of the functions $C_+^{(x,x)}(t,t')$, $C_+^{(p,p)}(t,t')$, the virial theorem reads [14]

$$C_+^{(p,p)}(t,t')=\frac{\omega^2}{g^2}C_+^{(x,x)}(t,t')\,, \tag{6.16}$$

which, for non-vanishing magnetic fields, is expressed by the connected correlators

$$C_{+,c}^{(p,p)}(t,t') = \frac{\omega^2}{g^2}C_{+,c}^{(x,x)}(t,t')\,. \tag{6.17}$$

On the other hand, the Kubo formula [204, C20] involves the *response functions*

$$R^{(x)}(t,s) := \left.\frac{\delta\langle\hat{x}(t)\rangle}{\delta B(s)}\right|_{B=0}\,, \tag{6.18}$$

$$Q^{(p)}(t,s) := \left.\frac{\delta\langle\hat{p}(t)\rangle}{\delta B(s)}\right|_{B=0}\,, \tag{6.19}$$

where t is the observation time and s the waiting time. In terms of the commutator $C_-^{(x,x)}(t,t')$, the Kubo formula reads

$$R^{(x)}(t,s)=\frac{2\mathrm{i}}{\hbar}\Theta(t-s)C_-^{(x,x)}(t,s)\,. \tag{6.20}$$

6.1.1 Cavity model

In this section, we shall provide the formal solution of the cavity model (6.6,6.7). In particular, we shall derive the second moments of the noises (6.10,6.11,6.12), following Ref. [14] as guideline.

The dynamics of the cavity model is given by Eqs. (6.6,6.7), with the harmonic oscillator Hamiltonian (6.1). Computing the commutator, one gets

$$\begin{aligned}\partial_t\hat{x} &= g\hat{p}-\frac{\gamma}{2}\hat{x}+\hat{\eta}^{(x)}\,, &(6.21)\\ \partial_t\hat{p} &= -\frac{\omega^2}{g}\hat{x}-\frac{\gamma}{2}\hat{p}+B+\hat{\eta}^{(p)}\,. &(6.22)\end{aligned}$$

The formal solution of the linear differential equations (6.21,6.22) is

$$\begin{aligned}\hat{x}(t) &= \hat{x}_+(0)\mathrm{e}^{-\Lambda_+t}+\hat{x}_-(0)\mathrm{e}^{-\Lambda_-t}\\ &+\frac{1}{2}\int_0^t \mathrm{d}\tau\,\mathrm{e}^{-\Lambda_+(t-\tau)}\left(\hat{\eta}^{(x)}(\tau)+\frac{\mathrm{i}g}{\omega}\left(\hat{\eta}^{(p)}(\tau)+B\right)\right)\\ &+\frac{1}{2}\int_0^t \mathrm{d}\tau\,\mathrm{e}^{-\Lambda_-(t-\tau)}\left(\hat{\eta}^{(x)}(\tau)-\frac{\mathrm{i}g}{\omega}\left(\hat{\eta}^{(p)}(\tau)+B\right)\right)\,, &(6.23)\end{aligned}$$

$$\begin{aligned}\hat{p}(t) &= -\mathrm{i}\frac{\omega}{g}\hat{x}_+(0)\mathrm{e}^{-\Lambda_+t}+\mathrm{i}\frac{\omega}{g}\hat{x}_-(0)\mathrm{e}^{-\Lambda_-t}\\ &-\mathrm{i}\frac{\omega}{2g}\int_0^t \mathrm{d}\tau\,\mathrm{e}^{-\Lambda_+(t-\tau)}\left(\hat{\eta}^{(x)}(\tau)+\frac{\mathrm{i}g}{\omega}\left(\hat{\eta}^{(p)}(\tau)+B\right)\right)\\ &+\mathrm{i}\frac{\omega}{2g}\int_0^t \mathrm{d}\tau\,\mathrm{e}^{-\Lambda_-(t-\tau)}\left(\hat{\eta}^{(x)}(\tau)-\frac{\mathrm{i}g}{\omega}\left(\hat{\eta}^{(p)}(\tau)+B\right)\right)\,, &(6.24)\end{aligned}$$

with eigenvalues $\Lambda_\pm=\frac{\gamma}{2}\pm\mathrm{i}\omega$ and initial conditions $\hat{x}_+(0)$, $\hat{x}_-(0)$.

The goal of this section is to derive the second moments (6.10,6.11,6.12). For the average noise commutator, we use the ansatz

$$\left\langle\left[\hat{\eta}^{(x)}(t),\hat{\eta}^{(p)}(t')\right]\right\rangle=\kappa\delta(t-t')\,. \tag{6.25}$$

Thanks to Eqs. (6.23, 6.24), one may compute the average commutator between position and momentum,

$$\begin{aligned}2C_-^{(x,p)}(t,t') &= \langle[\hat{x}(t),\hat{p}(t')]\rangle\\ &= \left(\frac{\mathrm{i}\omega}{g}\langle[\hat{x}_+(0),\hat{x}_-(0)]\rangle-\frac{\kappa}{2\gamma}\right)\left(\mathrm{e}^{-\Lambda_+t-\Lambda_-t'}+\mathrm{e}^{-\Lambda_-t-\Lambda_+t'}\right)\\ &+\frac{\kappa}{2\gamma}\left(\mathrm{e}^{-\Lambda_+|t-t'|}+\mathrm{e}^{-\Lambda_-|t-t'|}\right)\,, &(6.26)\end{aligned}$$

which contains a stationary part depending only on $|t-t'|$ and a rapidly decaying transient term. The requirement (A) holds if the transient term is zero, and this is true for the choice

$$\langle [\hat{x}_+(0), \hat{x}_-(0)] \rangle = -\mathrm{i}\frac{\kappa g}{2\gamma\omega}. \tag{6.27}$$

Thus, the average equal-time commutator

$$\langle [\hat{x}(t), \hat{p}(t)] \rangle = \frac{\kappa}{\gamma}, \tag{6.28}$$

is time-independent. For the specific choice $\kappa = i\hbar\gamma$, the requirement (A) is verified and

$$\left\langle \left[\hat{\eta}^{(x)}(t), \hat{\eta}^{(p)}(t')\right] \right\rangle = \mathrm{i}\hbar\gamma\delta(t-t'). \tag{6.29}$$

Next, we check the validity of the Kubo formula for the linear response theory (B). Using the definitions (6.18,6.19), the evolution of the response functions is

$$\partial_t R^{(x)}(t,s) = gQ^{(p)}(t,s) - \frac{\gamma}{2}R^{(x)}(t,s), \tag{6.30}$$

$$\partial_t Q^{(p)}(t,s) = -\frac{\omega^2}{g}R^{(x)}(t,s) - \frac{\gamma}{2}Q^{(p)}(t,s) + \delta(t-s). \tag{6.31}$$

Since these functions only depend on the time difference $\tau = t - s$, we define $\mathscr{R}(\tau) := R^{(x)}(t,s)$ which obeys to the second-order differential equation

$$\partial_\tau^2 \mathscr{R}(\tau) + \gamma\partial_\tau \mathscr{R}(\tau) + \left(\omega^2 + \frac{\gamma^2}{4}\right)\mathscr{R}(\tau) = g\delta(\tau). \tag{6.32}$$

The standard technique to solve the differential equation (6.32) makes use of the Fourier transform

$$\widehat{\mathscr{R}}(\nu) = \frac{1}{\sqrt{2\pi}}\int_{\mathbb{R}} \mathrm{d}\tau\, \mathrm{e}^{-\mathrm{i}\nu\tau}\mathscr{R}(\tau). \tag{6.33}$$

The Fourier transforms of $\partial_\tau\mathscr{R}(\tau)$, $\partial_\tau^2\mathscr{R}(\tau)$ and $\delta(\tau)$ are $\mathrm{i}\nu\widehat{\mathscr{R}}(\nu)$, $-\nu^2\widehat{\mathscr{R}}(\nu)$ and $1/\sqrt{2\pi}$, respectively. Hence, Eq. (6.32) maps into

$$-\nu^2\widehat{\mathscr{R}}(\nu) + \mathrm{i}\gamma\nu\widehat{\mathscr{R}}(\nu) + \left(\omega^2 + \frac{\gamma^2}{4}\right)\widehat{\mathscr{R}}(\nu) = \frac{g}{\sqrt{2\pi}}, \tag{6.34}$$

with solution

$$\widehat{\mathscr{R}}(\nu) = -\frac{g}{\sqrt{2\pi}}\frac{1}{\nu^2 - \mathrm{i}\gamma\nu - \omega^2 - \gamma^2/4}. \tag{6.35}$$

Eq. (6.35) shows two pôles $\nu_\pm = \mathrm{i}\frac{\gamma}{2} \pm \omega$ in the upper complex ν-half-plane. Consequently, inverting Eq. (6.35) via the residue theorem, the response of the position x is

$$\mathscr{R}(\tau) = R^{(x)}(\tau+s,s) = \frac{g}{\omega}\,\mathrm{e}^{-\gamma\tau/2}\sin\big(\omega\tau\big)\,\Theta\big(\tau\big)\,, \tag{6.36}$$

where the Heaviside function $\Theta(\tau)$ expresses the causality. The commutator (6.13) is

$$\begin{aligned} C_-^{(x,x)}(t,t') &= \frac{1}{2}\left(\big\langle[\hat{x}_+(0),\hat{x}_-(0)]\big\rangle - \frac{\hbar g}{2\omega}\right)\left(e^{-\Lambda_+ t-\Lambda_- t'} - e^{-\Lambda_+ t'-\Lambda_- t}\right) \\ &\quad + \frac{\hbar}{2\mathrm{i}}\frac{g}{\omega}\mathrm{e}^{-\gamma|t-t'|/2}\sin\big(\omega|t-t'|\big)\,. \end{aligned} \tag{6.37}$$

Eq. (6.27) and $\varkappa = \mathrm{i}\hbar\gamma$ imply that the first term into Eq. (6.37) is equal to zero and the Kubo formula (B)

$$R^{(x)}(\tau+s,s) = \frac{2\mathrm{i}}{\hbar}C_-^{(x,x)}(\tau+s,s)\Theta(\tau)\,, \tag{6.38}$$

is automatically verified.

Now, it is the turn of the virial theorem (C), which reads $C^{(p,p)}_{+,\mathrm{c,stat}}(t,t') = \frac{\omega^2}{g^2}C^{(x,x)}_{+,\mathrm{c,stat}}(t,t')$. If $B \neq 0$, we must analyse the connected correlators $C^{(x,x)}_{+,\mathrm{c}}(t,t')$ and $C^{(p,p)}_{+,\mathrm{c}}(t,t')$. Following the guidelines of Ref. [14], we use the ansatz

$$\begin{aligned} \frac{1}{2}\big\langle\{\hat{\eta}^{(p)}(t),\hat{\eta}^{(p)}(t')\}\big\rangle &= \alpha\,\delta(t-t')\,, & (6.39)\\ \frac{1}{2}\big\langle\{\hat{\eta}^{(x)}(t),\hat{\eta}^{(x)}(t')\}\big\rangle &= \beta\,\delta(t-t')\,, & (6.40)\\ \big\langle\{\hat{\eta}^{(x)}(t),\hat{\eta}^{(p)}(t')\}\big\rangle &= 0\,, & (6.41) \end{aligned}$$

for some real coefficients α, β. The virial theorem requires to evaluate the connected correlator

$$\begin{aligned} C^{(x,x)}_{+,\mathrm{c}}(t,t') &= \left(\big\langle\hat{x}_+(0)^2\big\rangle - \frac{\beta-\alpha g^2/\omega^2}{8\Lambda_+}\right)e^{-\Lambda_+(t+t')} \\ &\quad + \left(\big\langle\hat{x}_-(0)^2\big\rangle - \frac{\beta-\alpha g^2/\omega^2}{8\Lambda_-}\right)e^{-\Lambda_-(t+t')} \\ &\quad + \left(\frac{1}{2}\big\langle\{\hat{x}_+(0),\hat{x}_-(0)\}\big\rangle - \frac{\beta+\alpha g^2/\omega^2}{4(\Lambda_+ + \Lambda_-)}\right)\left(e^{-\Lambda_+ t-\Lambda_- t'} + e^{-\Lambda_+ t'-\Lambda_- t}\right) \\ &\quad + \frac{1}{4}\left(\frac{\beta-\alpha g^2/\omega^2}{2\Lambda_+} + \frac{\beta+\alpha g^2/\omega^2}{\Lambda_+ + \Lambda_-}\right)e^{-\Lambda_+|t-t'|} \\ &\quad + \frac{1}{4}\left(\frac{\beta-\alpha g^2/\omega^2}{2\Lambda_-} + \frac{\beta+\alpha g^2/\omega^2}{\Lambda_+ + \Lambda_-}\right)e^{-\Lambda_-|t-t'|}\,. \end{aligned} \tag{6.42}$$

The terms in the first three lines are rapidly decaying contributions whereas the stationary terms are collected in the fourth and fifth lines; the non-connected terms $\propto B^2$ vanish. Similarly, we compute the connected correlator

$$\begin{aligned}
C^{(p,p)}_{+,\mathrm{c}}(t,t') &= \frac{\omega^2}{g^2}\left(-\langle \hat{x}_+(0)^2\rangle + \frac{\beta-\alpha g^2/\omega^2}{8\Lambda_+}\right)e^{-\Lambda_+(t+t')} \\
&+\frac{\omega^2}{g^2}\left(-\langle \hat{x}_-(0)^2\rangle + \frac{\beta-\alpha g^2/\omega^2}{8\Lambda_-}\right)e^{-\Lambda_-(t+t')} \\
&+\frac{\omega^2}{g^2}\left(\frac{1}{2}\langle\{\hat{x}_+(0),\hat{x}_-(0)\}\rangle - \frac{\beta+\alpha g^2/\omega^2}{4(\Lambda_++\Lambda_-)}\right)\left(e^{-\Lambda_+t-\Lambda_-t'}+e^{-\Lambda_+t'-\Lambda_-t}\right) \\
&+\frac{\omega^2}{4g^2}\left(-\frac{\beta-\alpha g^2/\omega^2}{2\Lambda_+}+\frac{\beta+\alpha g^2/\omega^2}{\Lambda_++\Lambda_-}\right)e^{-\Lambda_+|t-t'|} \\
&+\frac{\omega^2}{4g^2}\left(-\frac{\beta-\alpha g^2/\omega^2}{2\Lambda_-}+\frac{\beta+\alpha g^2/\omega^2}{\Lambda_++\Lambda_-}\right)e^{-\Lambda_-|t-t'|}\,,
\end{aligned} \tag{6.43}$$

with transient terms in the first three lines and the stationary contributions in the fourth and fifth lines. Comparing Eqs. (6.42,6.43), the condition for the validity of the virial theorem is

$$\frac{1}{4}\left(\frac{\beta-\alpha g^2/\omega^2}{2\Lambda_\pm}+\frac{\beta+\alpha g^2/\omega^2}{\Lambda_++\Lambda_-}\right)\overset{!}{=}\frac{1}{4}\left(-\frac{\beta-\alpha g^2/\omega^2}{2\Lambda_\pm}+\frac{\beta+\alpha g^2/\omega^2}{\Lambda_++\Lambda_-}\right), \tag{6.44}$$

and leads to

$$\alpha = \frac{\omega^2}{g^2}\beta\,. \tag{6.45}$$

Finally, using the stationary part of Eq. (6.42), the condition (D) implies that the position (connected) auto-correlator at equilibrium is

$$C^{(x,x)}_{+,\mathrm{c,eq}}(t,t) = \frac{\beta}{2\gamma} \overset{!}{=} \frac{\hbar g}{2\omega}\coth\left(\frac{\hbar\omega}{2T}\right), \tag{6.46}$$

and hence

$$\beta = \frac{\hbar\gamma\omega}{g}\coth\left(\frac{\hbar\omega}{2T}\right). \tag{6.47}$$

Thus the anti-commutators (6.39,6.40) are

$$\begin{aligned}
\langle\{\hat{\eta}^{(p)}(t),\hat{\eta}^{(p)}(t')\}\rangle &= \frac{\gamma\hbar\omega}{g}\coth\left(\frac{\hbar\omega}{2T}\right)\delta(t-t')\,, &(6.48)\\
\langle\{\hat{\eta}^{(x)}(t),\hat{\eta}^{(x)}(t')\}\rangle &= \frac{\gamma\hbar g}{\omega}\coth\left(\frac{\hbar\omega}{2T}\right)\delta(t-t')\,. &(6.49)
\end{aligned}$$

To finish, for the sake of completeness, we also compute the connected anti-commutator $C_{+,c}^{(x,p)}(t,t')$ which once more follows from (6.23, 6.24),

$$
\begin{aligned}
C_{+,c}^{(x,p)}(t,t') &= -i\frac{\omega}{g}\langle \hat{x}_+(0)^2\rangle e^{-\Lambda_+(t+t')} + i\frac{\omega}{g}\langle \hat{x}_-(0)^2\rangle e^{-\Lambda_-(t+t')} \\
&\quad +i\frac{\omega}{2g}\left(\langle\{\hat{x}_+(0),\hat{x}_-(0)\}\rangle - \frac{\beta}{\gamma}\right)\left(e^{-\Lambda_+ t-\Lambda_- t'} - e^{-\Lambda_- t-\Lambda_+ t'}\right) \\
&\quad +i\frac{\omega\beta}{2\gamma g}\left(e^{-\Lambda_+|t-t'|} - e^{-\Lambda_-|t-t'|}\right) . \qquad (6.50)
\end{aligned}
$$

In particular, the stationary equal-time contribution $C_{+,c,\text{eq}}^{(x,p)}(t,t)$ vanishes, independently of the initial conditions. In the next sections, the dynamical behaviour of those correlators will be valued case by case (see Figs. 6.1,6.2,6.3).

6.1.2 Friction model

In this section, we shall provide the formal solution of the friction model (6.4,6.5). The second moments of the noises (6.8,6.9) were already known in literature and identical to the Bedeaux and Mazur proposal [67, 68]. However, for the sake of completeness, we shall sum up the results already presented in Ref. [14].

Eqs. (6.4,6.5) are equivalent to

$$
\begin{aligned}
\partial_t \hat{x} &= g\hat{p} + \hat{\eta}^{(x)} , \qquad (6.51)\\
\partial_t \hat{p} &= -\frac{\omega^2}{g}\hat{x} - \gamma\hat{p} + B + \hat{\eta}^{(p)} , \qquad (6.52)
\end{aligned}
$$

whose formal solution reads

$$
\begin{aligned}
\hat{x}(t) &= \hat{x}_+(0)e^{-\Lambda_+ t} + \hat{x}_-(0)e^{-\Lambda_- t} \\
&\quad -\frac{1}{\Lambda_+ - \Lambda_-}\int_0^t d\tau\, e^{-\Lambda_+(t-\tau)}\left[g\big(\hat{\eta}^{(p)}(\tau) + B\big) + \Lambda_-\hat{\eta}^{(x)}(\tau)\right] \\
&\quad +\frac{1}{\Lambda_+ - \Lambda_-}\int_0^t d\tau\, e^{-\Lambda_-(t-\tau)}\left[g\big(\hat{\eta}^{(p)}(\tau) + B\big) + \Lambda_+\hat{\eta}^{(x)}(\tau)\right] , \qquad (6.53)
\end{aligned}
$$

$$
\begin{aligned}
\hat{p}(t) &= -\frac{\Lambda_+}{g}\hat{x}_+(0)e^{-\Lambda_+ t} - \frac{\Lambda_-}{g}\hat{x}_-(0)e^{-\Lambda_- t} \\
&\quad +\frac{\Lambda_+}{g(\Lambda_+ - \Lambda_-)}\int_0^t d\tau\, e^{-\Lambda_+(t-\tau)}\left[g\big(\hat{\eta}^{(p)}(\tau) + B\big) + \Lambda_-\hat{\eta}^{(x)}(\tau)\right] \\
&\quad -\frac{\Lambda_-}{g(\Lambda_+ - \Lambda_-)}\int_0^t d\tau\, e^{-\Lambda_-(t-\tau)}\left[g\big(\hat{\eta}^{(p)}(\tau) + B\big) + \Lambda_+\hat{\eta}^{(x)}(\tau)\right] , \qquad (6.54)
\end{aligned}
$$

with eigenvalues $\Lambda_\pm = \frac{\gamma}{2} \pm \sqrt{\frac{\gamma^2}{4} - \omega^2}$ and initial conditions $\hat{x}_+(0)$, $\hat{x}_-(0)$. Contrary to the cavity model, the eigenvalues $\Lambda_\pm$ may take real or complex values, depending on the parameters (ω, γ). The eigenvalues $\Lambda_\pm$ govern the qualitative behaviour of the position-momentum observables. If $\omega < \gamma/2$ we have an *over-damped phase*, with real and positive eigenvalues. On the other hand, if $\omega > \gamma/2$ we find an *under-damped phase*, where the eigenvalues are complex and the dynamics contains oscillations. In the cavity model, only the under-damped regime exists.

As already done for the cavity model, we start from the ansatz (6.25) and we impose the condition for the equal time position-momentum commutator (A). Eqs. (6.53,6.54) imply

$$
\begin{aligned}
2C_-^{(x,p)}(t,t') &= \left\langle [\hat{x}(t), \hat{p}(t')] \right\rangle \\
&= \frac{1}{g}\left(\left\langle [\hat{x}_+(0), \hat{x}_-(0)] \right\rangle - \frac{\kappa g}{(\Lambda_+ - \Lambda_-)(\Lambda_+ + \Lambda_-)} \right) \\
&\quad \times \left(\Lambda_+ \mathrm{e}^{-\Lambda_- t - \Lambda_+ t'} - \Lambda_- \mathrm{e}^{-\Lambda_+ t - \Lambda_- t'} \right) \\
&\quad + \frac{\kappa}{(\Lambda_+ - \Lambda_-)(\Lambda_+ + \Lambda_-)} \\
&\quad \times \left(\Lambda_+ \mathrm{e}^{-\Lambda_- |t-t'|} - \Lambda_- \mathrm{e}^{-\Lambda_+ |t-t'|} \right), \qquad (6.55)
\end{aligned}
$$

which contains a stationary part depending only on $|t-t'|$ and a rapidly decaying term. The equal time commutator (A) requires

$$
\left\langle [\hat{x}_+(0), \hat{x}_-(0)] \right\rangle = \frac{\kappa g}{(\Lambda_+ - \Lambda_-)(\Lambda_+ + \Lambda_-)}, \qquad (6.56)
$$

and

$$
\left\langle [\hat{x}(t), \hat{p}(t)] \right\rangle = \frac{\kappa}{\Lambda_+ + \Lambda_-} = \frac{\kappa}{\gamma} \stackrel{!}{=} \mathrm{i}\hbar, \qquad (6.57)
$$

which leads to

$$
\left\langle \left[\hat{\eta}^{(x)}(t), \hat{\eta}^{(p)}(t') \right] \right\rangle = \mathrm{i}\hbar\gamma\delta(t-t'). \qquad (6.58)
$$

Next, we check the validity of the Kubo formula for the linear response theory (B). The equations of motion of the response functions (6.18,6.19) are

$$
\begin{aligned}
\partial_t R^{(x)}(t,s) &= g Q^{(p)}(t,s), \qquad (6.59) \\
\partial_t Q^{(p)}(t,s) &= -\frac{\omega^2}{g} R^{(x)}(t,s) - \gamma Q^{(p)}(t,s) + \delta(t-s). \qquad (6.60)
\end{aligned}
$$

Since these functions only depend on the time difference $\tau = t - s$, we define $\mathscr{R}(\tau) := R^{(x)}(t,s)$, which obeys to the second-order differential equation

$$
\partial_\tau^2 \mathscr{R}(\tau) + \gamma \partial_\tau \mathscr{R}(\tau) + \omega^2 \mathscr{R}(\tau) = g\delta(\tau). \qquad (6.61)
$$

The standard technique to solve the differential equation (6.61) makes use of the Fourier transforms. Eq. (6.61) is mapped into

$$-\nu^2\widehat{\mathscr{R}}(\nu) + \mathrm{i}\gamma\nu\widehat{\mathscr{R}}(\nu) + \omega^2\widehat{\mathscr{R}}(\nu) = \frac{g}{\sqrt{2\pi}}\,, \tag{6.62}$$

where $\widehat{\mathscr{R}}(\nu)$ is the Fourier transform (6.33). Eq. (6.62) has solution

$$\widehat{\mathscr{R}}(\nu) = -\frac{g}{\sqrt{2\pi}}\frac{1}{\nu^2 - \mathrm{i}\gamma\nu - \omega^2}\,, \tag{6.63}$$

with two simple poles in the upper complex ν-plane. Consequently, inverting (6.63) via the residue theorem, the response of the position x is

$$\mathscr{R}(\tau) = R^{(x)}(\tau + s, s) = \frac{g}{\Lambda_+ - \Lambda_-}\left(\mathrm{e}^{-\Lambda_-\tau} - \mathrm{e}^{-\Lambda_+\tau}\right)\Theta(\tau)\,, \tag{6.64}$$

where the Heaviside function $\Theta(\tau)$ encodes the causality. On the other hand, we need the commutator (6.13), which is

$$C_-^{(x,x)}(t,t') = \frac{\hbar}{2\mathrm{i}}\frac{g}{\Lambda_+ - \Lambda_-}\Theta(t-t')(\mathrm{e}^{-\Lambda_-|t-t'|} - \mathrm{e}^{-\Lambda_+|t-t'|})\,. \tag{6.65}$$

and then the Kubo formula (B) is automatically verified.

In order to check the virial theorem, we evaluate the connected correlators $C_{+,\mathrm{c}}^{(x,x)}(t,t')$ and $C_{+,\mathrm{c}}^{(p,p)}(t,t')$. Again, we use the ansatz (6.39,6.40,6.41) and we get

$$\begin{aligned}
C_{+,\mathrm{c}}^{(x,x)}(t,t') = {} & \frac{1}{2}\left(\left\langle \hat{x}_+(0)^2\right\rangle - \frac{\beta\Lambda_-^2 + \alpha g^2}{\Lambda_+(\Lambda_+ - \Lambda_-)^2}\right)\mathrm{e}^{-\Lambda_+(t+t')} \\
& + \frac{1}{2}\left(\left\langle \hat{x}_-(0)^2\right\rangle - \frac{\beta\Lambda_+^2 + \alpha g^2}{\Lambda_-(\Lambda_+ - \Lambda_-)^2}\right)\mathrm{e}^{-\Lambda_-(t+t')} \\
& + \frac{1}{2}\left(\left\langle\{\hat{x}_+(0), \hat{x}_-(0)\}\right\rangle + \frac{2\beta\Lambda_+\Lambda_- + 2\alpha g^2}{(\Lambda_+ + \Lambda_-)(\Lambda_+ - \Lambda_-)^2}\right) \\
& \times\left(\mathrm{e}^{-\Lambda_+ t - \Lambda_- t'} + \mathrm{e}^{-\Lambda_+ t' - \Lambda_- t}\right) \\
& + \left(\frac{\alpha g^2 + \beta\Lambda_-^2}{2\Lambda_+} - \frac{\alpha g^2 + \beta\Lambda_-\Lambda_+}{2(\Lambda_+ + \Lambda_-)}\right)\frac{\mathrm{e}^{-\Lambda_+|t-t'|}}{(\Lambda_+ - \Lambda_-)^2} \\
& + \left(\frac{\alpha g^2 + \beta\Lambda_+^2}{2\Lambda_-} - \frac{\alpha g^2 + \beta\Lambda_-\Lambda_+}{2(\Lambda_+ + \Lambda_-)}\right)\frac{\mathrm{e}^{-\Lambda_-|t-t'|}}{(\Lambda_+ - \Lambda_-)^2}\,.
\end{aligned} \tag{6.66}$$

The terms in the first four lines are rapidly decaying transient contributions whereas the stationary terms are collected in the fifth and sixth lines; again, the non-connected terms $\propto B^2$ vanish. Similarly, we compute the connected correlator

$$\begin{aligned}
C^{(p,p)}_{+,\mathrm{c}}(t,t') \;=\; & \frac{\Lambda_+^2}{2g^2}\left(\langle \hat{x}_+(0)^2\rangle - \frac{\beta\Lambda_-^2+\alpha g^2}{\Lambda_+(\Lambda_+-\Lambda_-)^2}\right)\mathrm{e}^{-\Lambda_+(t+t')} \\
& +\frac{\Lambda_-^2}{2g^2}\left(\langle \hat{x}_-(0)^2\rangle - \frac{\beta\Lambda_+^2+\alpha g^2}{\Lambda_-(\Lambda_+-\Lambda_-)^2}\right)\mathrm{e}^{-\Lambda_-(t+t')} \\
& +\frac{\Lambda_+\Lambda_-}{2g^2}\left(\langle\{\hat{x}_+(0),\hat{x}_-(0)\}\rangle + \frac{2\beta\Lambda_+\Lambda_-+2\alpha g^2}{(\Lambda_++\Lambda_-)(\Lambda_+-\Lambda_-)^2}\right) \\
& \times\left(\mathrm{e}^{-\Lambda_+t-\Lambda_-t'}+\mathrm{e}^{-\Lambda_+t'-\Lambda_-t}\right) \\
& +\frac{\Lambda_+(\alpha g^2+\beta\Lambda_-^2)}{2g^2(\Lambda_+-\Lambda_-)^2}\mathrm{e}^{-\Lambda_+|t-t'|}+\frac{\Lambda_-(\alpha g^2+\beta\Lambda_+^2)}{2g^2(\Lambda_+-\Lambda_-)^2}\mathrm{e}^{-\Lambda_-|t-t'|} \\
& -\frac{\Lambda_+\Lambda_-(\alpha g^2+\beta\Lambda_-\Lambda_+)}{g^2(\Lambda_++\Lambda_-)(\Lambda_+-\Lambda_-)^2}(\mathrm{e}^{-\Lambda_+|t-t'|}+\mathrm{e}^{-\Lambda_-|t-t'|})\,,
\end{aligned} \tag{6.67}$$

with transient terms in the first four lines and the stationary contributions in the fifth and sixth lines. Comparing Eqs. (6.66,6.67), the virial theorem holds true for

$$\Lambda_+\left(\alpha g^2+\beta\Lambda_-^2\right)+\Lambda_-\left(\alpha g^2+\beta\Lambda_+^2\right)\overset{!}{=}\Lambda_-\left(\alpha g^2+\beta\Lambda_-^2\right)+\Lambda_+\left(\alpha g^2+\beta\Lambda_+^2\right), \tag{6.68}$$

which leads to

$$\beta\Lambda_-^2\Lambda_+ + \beta\Lambda_+^2\Lambda_- \overset{!}{=} \beta\Lambda_-^3+\beta\Lambda_+^3\,. \tag{6.69}$$

If $\beta\neq 0$, Eq. (6.69) is verified for $(\Lambda_++\Lambda_-)(\Lambda_+-\Lambda_-)^2=0$. However, since the angular frequency ω and the damping constant γ are independent parameters, the solution $\beta\neq 0$ is impossible. Hence we conclude $\beta=0$ and Eq. (6.69) is automatically satisfied. Having shown that $\beta=0$, it remains to find α. For the variance at equilibrium (D),

$$C^{(x,x)}_{+,\mathrm{c,eq}}(t,t)=\frac{\alpha g^2}{2\gamma\omega^2}\overset{!}{=}\frac{\hbar g}{2\omega}\coth\left(\frac{\hbar\omega}{2T}\right), \tag{6.70}$$

and hence

$$\alpha=\frac{\hbar\gamma\omega}{g}\coth\left(\frac{\hbar\omega}{2T}\right). \tag{6.71}$$

Finally, the second moments of the noises are

$$\left\langle\{\hat{\eta}^{(p)}(t),\hat{\eta}^{(p)}(t')\}\right\rangle \;=\; \frac{\hbar\gamma\omega}{g}\coth\left(\frac{\hbar\omega}{2T}\right)\delta(t-t')\,, \tag{6.72}$$

$$\left\langle\{\hat{\eta}^{(x)}(t),\hat{\eta}^{(x)}(t')\}\right\rangle \;=\; 0\,. \tag{6.73}$$

For the sake of completeness, we also compute the connected anti-commutator $C_{+,c}^{(x,p)}(t,t')$ which once more follows from (6.53, 6.54),

$$\begin{aligned}
C_{+,c}^{(x,p)}(t,t') &= \left(-\frac{\Lambda_+}{g}\langle\hat{x}_+(0)^2\rangle + \frac{g\alpha}{2(\Lambda_+-\Lambda_-)^2}\right)\mathrm{e}^{-\Lambda_+(t+t')} \\
&+\left(-\frac{\Lambda_-}{g}\langle\hat{x}_-(0)^2\rangle + \frac{g\alpha}{2(\Lambda_+-\Lambda_-)^2}\right)\mathrm{e}^{-\Lambda_-(t+t')} \\
&-\left(\frac{1}{2g}\langle\{\hat{x}_+(0),\hat{x}_-(0)\}\rangle + \frac{g\alpha}{\gamma(\Lambda_+-\Lambda_-)^2}\right) \\
&\times\left(\Lambda_-\mathrm{e}^{-\Lambda_+t-\Lambda_-t'} + \Lambda_+\mathrm{e}^{-\Lambda_-t-\Lambda_+t'}\right) \\
&+\frac{g\alpha}{\gamma(\Lambda_+-\Lambda_-)^2}\left(\Lambda_- - \frac{\gamma}{2}\right)\mathrm{e}^{-\Lambda_+|t-t'|} \\
&+\frac{g\alpha}{\gamma(\Lambda_+-\Lambda_-)^2}\left(\Lambda_+ - \frac{\gamma}{2}\right)\mathrm{e}^{-\Lambda_-|t-t'|}, \qquad (6.74)
\end{aligned}$$

The stationary equal-time anticommutator $C_{+,c,\text{stat}}^{(x,p)}(t,t)$ vanishes. In the next sections, we shall compute the time evolution of the connected correlators for different initial conditions, e.g. vacuum state and coherent states (see Figs. 6.1,6.2,6.3).

6.1.3 Lowering and raising operators

Since the Lindblad equations (see Sec. 6.2) are conveniently formulated in terms of the lowering and raising operators (see Eq. (6.3)), here we rewrite the Langevin equations for these operators

$$\partial_t\hat{a} = -\left(\mathrm{i}\omega + \frac{\gamma}{2}\right)\hat{a} + \frac{\gamma}{2}\hat{a}^\dagger + \mathrm{i}B\sqrt{\frac{g}{2\hbar\omega}} + \hat{\eta}^{(a)}, \quad \text{friction model} \qquad (6.75)$$

$$\partial_t\hat{a} = -\left(\mathrm{i}\omega + \frac{\gamma}{2}\right)\hat{a} + \mathrm{i}B\sqrt{\frac{g}{2\hbar\omega}} + \hat{\eta}^{(a)}, \quad \text{cavity model} \qquad (6.76)$$

where the equation for $\hat{a}^\dagger$ is obtained by formal complex conjugation. The noise operator $\hat{\eta}^{(a)}$ is for both models

$$\hat{\eta}^{(a)} := \sqrt{\frac{\omega}{2\hbar g}}\,\hat{\eta}^{(x)} + \mathrm{i}\sqrt{\frac{g}{2\hbar\omega}}\,\hat{\eta}^{(p)}, \qquad (6.77)$$

such that the non-vanishing second moments are

$$\left\langle\left[\hat{\eta}^{(a)}(t),\hat{\eta}^{(a^\dagger)}(t')\right]\right\rangle = \gamma\,\delta(t-t'), \qquad (6.78)$$

$$\left\langle\left\{\hat{\eta}^{(a)}(t),\hat{\eta}^{(a^\dagger)}(t')\right\}\right\rangle = \gamma\coth\left(\frac{\hbar\omega}{2T}\right)\delta(t-t'), \qquad (6.79)$$

and

$$\begin{aligned}\left\langle\{\hat{\eta}^{(a)}(t),\hat{\eta}^{(a)}(t')\}\right\rangle &= \left\langle\left\{\hat{\eta}^{(a^\dagger)}(t),\hat{\eta}^{(a^\dagger)}(t')\right\}\right\rangle \\ &= \begin{cases} -\gamma\coth\!\left(\frac{\hbar\omega}{2T}\right)\delta(t-t') & \text{friction model} \\ 0 & \text{cavity model}\end{cases}, \end{aligned} \tag{6.80}$$

where the hermitian conjugate $\hat{\eta}^{(a^\dagger)} = \hat{\eta}^{(a)\dagger}$ is obtained from (6.77). The noises average to zero ($\langle\hat{\eta}^{(a)}\rangle = 0$) and the equation of motion for $\langle\hat{a}\rangle$ is directly read off from Eqs. (6.75,6.76). The equations for the two-point functions can be obtained by Eqs. (6.75,6.76) with the noise correlators (6.78,6.79,6.80).

In a compact form, the equations of motion can be written as a matrix differential equation

$$\partial_t\mathbf{v} = \mathbf{A}\mathbf{v}+\mathbf{b} \quad , \quad \mathbf{v} := \begin{pmatrix}\langle\hat{a}\rangle \\ \langle\hat{a}^\dagger\rangle \\ \langle\hat{a}\hat{a}\rangle \\ \langle\hat{a}^\dagger\hat{a}^\dagger\rangle \\ \langle\hat{a}^\dagger\hat{a}\rangle\end{pmatrix}, \tag{6.81}$$

where each component of the vector $\mathbf{v}$ refers to a different average value. The formal solution of Eq. (6.81) is

$$\mathbf{v}(t) = e^{\mathbf{A}t}\left(\mathbf{v}(0)+\mathbf{A}^{-1}\mathbf{b}\right)-\mathbf{A}^{-1}\mathbf{b} \tag{6.82}$$

For the friction model, the matrix $\mathbf{A}$ and the vector $\mathbf{b}$ take the form

$$\mathbf{A} = \gamma\begin{pmatrix} -\frac{1}{2} & \frac{1}{2} & 0 & 0 & 0 \\ \frac{1}{2} & -\frac{1}{2} & 0 & 0 & 0 \\ 0 & 0 & -1 & 0 & 1 \\ 0 & 0 & 0 & -1 & 1 \\ 0 & 0 & \frac{1}{2} & \frac{1}{2} & -1 \end{pmatrix} + \mathrm{i}\begin{pmatrix} -\omega & 0 & 0 & 0 & 0 \\ 0 & \omega & 0 & 0 & 0 \\ \sqrt{2g/\omega\hbar}\,B & 0 & -2\omega & 0 & 0 \\ 0 & -\sqrt{2g/\omega\hbar}\,B & 0 & 2\omega & 0 \\ -\sqrt{g/2\omega\hbar}\,B & \sqrt{g/2\omega\hbar}\,B & 0 & 0 & 0 \end{pmatrix}, \tag{6.83}$$

$$\mathbf{b} = \gamma n_\omega\begin{pmatrix}0 \\ 0 \\ -1 \\ -1 \\ 1\end{pmatrix} + \mathrm{i}\sqrt{\frac{g}{2\omega\hbar}}\,B\begin{pmatrix}1 \\ -1 \\ 0 \\ 0 \\ 0\end{pmatrix}, \tag{6.84}$$

where $n_\omega = (e^{\hbar\omega/T}-1)^{-1}$ is the Bose-Einstein distribution. For the cavity model, the same quantities are

$$\mathbf{A} = \gamma \begin{pmatrix} -\frac{1}{2} & 0 & 0 & 0 & 0 \\ 0 & -\frac{1}{2} & 0 & 0 & 0 \\ 0 & 0 & -1 & 0 & 0 \\ 0 & 0 & 0 & -1 & 0 \\ 0 & 0 & 0 & 0 & -1 \end{pmatrix} + \mathrm{i} \begin{pmatrix} -\omega & 0 & 0 & 0 & 0 \\ 0 & \omega & 0 & 0 & 0 \\ \sqrt{2g/\omega\hbar}\, B & 0 & -2\omega & 0 & 0 \\ 0 & -\sqrt{2g/\omega\hbar}\, B & 0 & 2\omega & 0 \\ -\sqrt{g/2\omega\hbar}\, B & \sqrt{g/2\omega\hbar}\, B & 0 & 0 & 0 \end{pmatrix}, \tag{6.85}$$

$$\mathbf{b} = \gamma n_\omega \begin{pmatrix} 0 \\ 0 \\ 0 \\ 0 \\ 1 \end{pmatrix} + \mathrm{i}\sqrt{\frac{g}{2\omega\hbar}}\, B \begin{pmatrix} 1 \\ -1 \\ 0 \\ 0 \\ 0 \end{pmatrix}. \tag{6.86}$$

For vanishing external magnetic fields, the matrix $\mathbf{A}$ of the cavity model is diagonal and the dynamics turns to be very simple.

6.2 Equivalent master equations

In this section, we shall derive the effective master equations for the friction and cavity models. In this way, we build an equivalent formalism to the Langevin dynamics, at the level of the one-point and two-point functions. We shall find out that, for the cavity model, the correlators are generated by a Lindblad-type deterministic equation for a single mode in an optical cavity. On the other hand, for the friction model, the dynamical map is not completely positive but it is still generated by quadratic operators in the bosonic creation and annihilation operators.

The dynamical maps for the friction and cavity models may be solved by standard analytical methods, as presented in Sec. 6.3.

6.2.1 Cavity model

The correlators of the cavity model turn to be equivalent to those generated by the dampening of a single electromagnetic mode inside a cavity [C6, C8, C14, C15]. The external environment is a bosonic bath at thermal equilibrium, i.e. the modes outside the cavity. The Liouvillian $\mathcal{L}(\hat\rho_c) = \mathrm{d}\hat\rho_c/\mathrm{d}t$ takes the form

$$\mathcal{L}(\hat\rho_c) = -\frac{\mathrm{i}}{\hbar}\left[\hat{H}, \hat\rho_c\right] + \mathcal{D}(\hat\rho_c), \tag{6.87}$$

$$\mathcal{D}(\hat\rho_c) = \gamma(n_\omega + 1) D_{\rho_c}(\hat a, \hat a^\dagger) + \gamma n_\omega D_{\rho_c}(\hat a^\dagger, \hat a), \tag{6.88}$$

where here and below we shall use the super-operator

$$D_\rho(\widehat{\mathcal{A}},\widehat{\mathcal{B}}) = \widehat{\mathcal{A}}\,\hat\rho\,\widehat{\mathcal{B}} - \frac{1}{2}\widehat{\mathcal{B}}\,\widehat{\mathcal{A}}\,\hat\rho - \frac{1}{2}\hat\rho\,\widehat{\mathcal{B}}\,\widehat{\mathcal{A}}\,, \tag{6.89}$$

for any Hilbert operator $\widehat{\mathcal{A}}$, $\widehat{\mathcal{B}}$. In the formalism of the quantum trajectories, the dissipator $\mathcal{D}(\hat\rho_c)$ describes one-body gain-loss processes with jump rates γn_ω and $\gamma(n_\omega+1)$, where $n_\omega = \left[e^{\hbar\omega/T}-1\right]^{-1} > 0$ is the Bose-Einstein distribution. This choice of the jump rates guarantees stability in the long time limit (see Chapter 5).

For any operator $\widehat{\mathcal{O}}$, the equation of motion reads

$$\begin{aligned}\partial_t\langle\widehat{\mathcal{O}}\rangle = \partial_t\,\mathrm{tr}\big(\widehat{\mathcal{O}}\hat\rho_c\big) \;&=\; \frac{\mathrm{i}}{\hbar}\langle\big[\widehat{H},\widehat{\mathcal{O}}\big]\rangle + \gamma(n_\omega+1)\Big(\langle\hat a^\dagger\widehat{\mathcal{O}}\hat a\rangle - \frac{1}{2}\langle\{\widehat{\mathcal{O}},\hat a^\dagger\hat a\}\rangle\Big)\\ &\quad + \gamma n_\omega\Big(\langle\hat a\widehat{\mathcal{O}}\hat a^\dagger\rangle - \frac{1}{2}\langle\{\widehat{\mathcal{O}},\hat a\hat a^\dagger\}\rangle\Big).\end{aligned} \tag{6.90}$$

If we identify $\langle\widehat{\mathcal{O}}\rangle$ as one of the components of the vector $\mathbf{v}$ into Eq. (6.81), we get the equations of motion for the one-point and two-point functions, which are equivalent to Eqs. (6.85,6.86) generated by the Langevin dynamics.

In Chapter 2, we have repeatedly pointed out that the Lindblad equation is a completely positive dynamical map, and this statement is mathematically equivalent to the condition of non-negative jump rates. Thus, the cavity model is a CPTP map [60, 61, 205, C19, 211–219, 224] and the generator $\mathcal{L}$ makes positive any extended dynamical map $\mathcal{L}' = \mathcal{L}\otimes\mathbb{1}_N$ for the composite system given by the harmonic oscillator and any other N-level ancilla. As we shall illustrate in the next paragraph, complete positivity does not hold for the friction model. The microscopic reasons behind this can be many, e.g. initially correlated states. However, we prefer to bypass this long controversy, moving directly to the study of the internal dynamics. The Langevin equations and the markovian stochastic noises verify the same physical requirements (A-D) and those criteria make the friction and cavity models physically acceptable, regardless of the complete positivity.

6.2.2 Friction model

For the generator of the friction model, we try the ansatz

$$\mathcal{L}(\hat\rho_f) \;=\; -\frac{\mathrm{i}}{\hbar}\big[\widehat{H}_f,\hat\rho_f\big] + \mathcal{D}(\hat\rho_f)\,, \tag{6.91}$$

$$\mathcal{D}(\hat\rho_f) \;=\; \sum_{j=1,2}\varepsilon_j D_{\rho_f}(\widehat{V}_j,\widehat{V}_j^\dagger)\,, \tag{6.92}$$

where $\widehat{H}_f$ is an effective Hamiltonian, $D_{\rho_f}(\widehat{V}_j, \widehat{V}_j^\dagger)$ is the super-operator in Eq. (6.89), $\widehat{V}_j$ are Hilbert operators to be determined and ε_j play the role of two real coefficients. As we shall see below, $\varepsilon_1 = -\varepsilon_2 = 1$ and then Eq. (6.91) with the dissipator (6.92) is not a Lindblad equation or even a completely positive map.

In order to make this description consistent with the Langevin equations (6.4,6.5), we proceed in two steps. Firstly, we build the effective hamiltonian $\widehat{H}_f$, second we define the Hilbert operators $\widehat{V}_j$, showing that the constants ε_j must be chosen appropriately to avoid mathematical inconsistencies.

Following Refs. [225, 227], the jump operators $\widehat{V}_j$ should be linear functions of position $\hat{x}$ and momentum $\widehat{p}$. This is because the space of the first-degree polynomials spanned by the average position and momentum must be closed under the action of the dissipative dynamics generated by $\mathcal{L}$ [225, 227–229]. For this reason, we try the ansatz

$$\widehat{V}_j = \mathfrak{a}_j\, \hat{x} + \mathfrak{b}_j\, \widehat{p} = \alpha_j\, \hat{a} + \beta_j^*\, \hat{a}^\dagger \quad ; \quad j = 1, 2 \tag{6.93}$$

where the complex numbers α_j, β_j (or equivalently $\mathfrak{a}_j, \mathfrak{b}_j$) must be fixed. Any additional constant term into Eq. (6.93) can be absorbed into the effective Hamiltonian $\widehat{H}_f$, since $\mathcal{L}$ is invariant under the inhomogeneous transformation (2.35). The Liouvillian $\mathcal{L}$ generates the right equations of motion for $\langle\hat{a}\rangle$ and $\langle\hat{a}^\dagger\rangle$ if we assume [61, 225, 228]

$$\widehat{H}_f = \widehat{H} + \widehat{H}_\gamma\,, \tag{6.94}$$

where $\widehat{H}$ is the Hamiltonian (6.1) and

$$\widehat{H}_\gamma = \frac{\gamma}{4}\,(\widehat{p}\hat{x} + \hat{x}\widehat{p}) = \frac{i\hbar}{4}\gamma\left(\hat{a}^\dagger\hat{a}^\dagger - \hat{a}\hat{a}\right)\,. \tag{6.95}$$

Notice that $\widehat{H}_\gamma$ is not a Lamb shift since $\widehat{H}_\gamma$ does not commute with the system Hamiltonian $\widehat{H}$, viz. $\left[\widehat{H}_\gamma, \widehat{H}\right] \neq 0$ [227]. Concerning the dissipator, for simplicity we define four constants

$$E_1 \;:=\; \frac{1}{\hbar}\sum_{j=1,2} \varepsilon_j|\alpha_j|^2\,, \tag{6.96}$$

$$E_2 \;:=\; \frac{1}{\hbar}\sum_{j=1,2} \varepsilon_j|\beta_j|^2\,, \tag{6.97}$$

$$E_3 \;:=\; \frac{1}{\hbar}\sum_{j=1,2} \varepsilon_j\alpha_j\beta_j = E_4^*\,, \tag{6.98}$$

where, without loss of generality, we may assume $\varepsilon_j = \pm 1$. Hence the master equation (6.91) with the effective Hamiltonian (6.94) and the ansatz (6.93) becomes

$$
\begin{aligned}
\frac{\mathrm{d}\hat{\rho}_f(t)}{\mathrm{d}t} &= E_1\hat{a}\hat{\rho}_f\hat{a}^\dagger - \frac{1}{2}(E_1 + \mathrm{i}\omega)\hat{a}^\dagger\hat{a}\hat{\rho}_f - \frac{1}{2}(E_1 - \mathrm{i}\omega)\hat{\rho}_f\hat{a}^\dagger\hat{a} \\
&+E_2\hat{a}^\dagger\hat{\rho}_f\hat{a} - \frac{1}{2}(E_2 + \mathrm{i}\omega)\hat{a}\hat{a}^\dagger\hat{\rho}_f - \frac{1}{2}(E_2 - \mathrm{i}\omega)\hat{\rho}_f\hat{a}\hat{a}^\dagger \\
&+E_3\hat{a}\hat{\rho}_f\hat{a} - \frac{1}{2}\left(E_3 + \frac{\gamma}{2}\right)\hat{a}\hat{a}\hat{\rho}_f - \frac{1}{2}\left(E_3 - \frac{\gamma}{2}\right)\hat{\rho}_f\hat{a}\hat{a} \\
&+E_4\hat{a}^\dagger\hat{\rho}_f\hat{a}^\dagger - \frac{1}{2}\left(E_4 - \frac{\gamma}{2}\right)\hat{a}^\dagger\hat{a}^\dagger\hat{\rho}_f - \frac{1}{2}\left(E_4 + \frac{\gamma}{2}\right)\hat{\rho}_f\hat{a}^\dagger\hat{a}^\dagger\,. \qquad (6.99)
\end{aligned}
$$

In order to determine the coefficients E_i, $\forall i \in \{1, ..., 4\}$, we compare the equations generated by the Liouvillian (6.99) with the matrix differential equation (6.81) and Eqs. (6.83,6.84). Let's start with the dynamics of the first-order polynomials,

$$
\frac{\mathrm{d}\langle\hat{a}\rangle}{\mathrm{d}t} = \frac{\mathrm{d}}{\mathrm{d}t}\,\mathrm{tr}\big(\hat{a}\hat{\rho}_f\big) = -\left(\frac{1}{2}(E_1 - E_2) + \mathrm{i}\omega\right)\langle\hat{a}\rangle + \frac{\gamma}{2}\langle\hat{a}^\dagger\rangle\,, \qquad (6.100)
$$

which requires

$$
E_1 - E_2 \overset{!}{=} \gamma\,. \qquad (6.101)
$$

Since $\langle\hat{a}^\dagger\rangle = \langle\hat{a}\rangle^*$ the equation for $\langle\hat{a}^\dagger\rangle$ does not yield any further information. Next, the average $\langle\hat{a}\hat{a}\rangle$ obeys

$$
\frac{\mathrm{d}\langle\hat{a}\hat{a}\rangle}{\mathrm{d}t} = \frac{\mathrm{d}}{\mathrm{d}t}\,\mathrm{tr}\big(\hat{a}\hat{a}\hat{\rho}_f\big) = -(E_1 - E_2 + 2\mathrm{i}\omega)\langle\hat{a}\hat{a}\rangle + \gamma\langle\hat{a}^\dagger\hat{a}\rangle - \left(E_4 - \frac{\gamma}{2}\right)\,, \qquad (6.102)
$$

and the comparison with the equation of motion (6.81) and Eqs. (6.83,6.84) implies

$$
E_4 \overset{!}{=} \frac{\gamma}{2}\coth\left(\frac{\hbar\omega}{2T}\right) = \gamma(n_\omega + 1/2) = E_3\,. \qquad (6.103)
$$

Since $\langle\hat{a}^\dagger\hat{a}^\dagger\rangle = \langle\hat{a}\hat{a}\rangle^*$, we move to the equation of motion of $\langle\hat{a}^\dagger\hat{a}\rangle$, which is

$$
\frac{\mathrm{d}\langle\hat{a}^\dagger\hat{a}\rangle}{\mathrm{d}t} = \frac{\mathrm{d}}{\mathrm{d}t}\,\mathrm{tr}\big(\hat{a}^\dagger\hat{a}\hat{\rho}_f\big) = -(E_1 - E_2)\langle\hat{a}^\dagger\hat{a}\rangle + \frac{\gamma}{2}\langle\hat{a}^\dagger\hat{a}^\dagger + \hat{a}\hat{a}\rangle + E_2\,. \qquad (6.104)
$$

Eq. (6.104) implies

$$
\begin{aligned}
E_2 &\overset{!}{=} \frac{\gamma}{2}\left(\coth\left(\frac{\hbar\omega}{2T}\right) - 1\right) = \gamma n_\omega\,, \qquad (6.105)\\
E_1 &= \frac{\gamma}{2}\left(\coth\left(\frac{\hbar\omega}{2T}\right) + 1\right) = \gamma(n_\omega + 1)\,. \qquad (6.106)
\end{aligned}
$$

and the equivalence between the Langevin equations (6.4,6.5) and the dynamical map (6.99) is established at the level of the one-point and two-point functions, as required. The full Liouvillian reads

$$\begin{aligned}\mathcal{L}(\hat{\rho}_f) &= -\frac{\mathrm{i}}{\hbar}\left[\widehat{H}_f,\hat{\rho}_f\right]+\gamma(n_\omega+1)D_{\rho_f}(\hat{a},\hat{a}^\dagger)+\gamma n_\omega D_{\rho_f}(\hat{a}^\dagger,\hat{a}) \\ &\quad +\gamma\left(n_\omega+\frac{1}{2}\right)D_{\rho_f}(\hat{a},\hat{a})+\gamma\left(n_\omega+\frac{1}{2}\right)D_{\rho_f}(\hat{a}^\dagger,\hat{a}^\dagger)\,, \qquad (6.107)\end{aligned}$$

where the first two dissipators coincide with those of the cavity model, while the last two terms are specific for the friction model.

It remains to find the constants α_j,β_j from Eqs. (6.103,6.105,6.106). Firstly, we shall prove that the choice $\varepsilon_1=\varepsilon_2=+1$ is not admissible. In fact, this assumption implies that

$$\sum_{j=1,2}\left|\alpha_j-\beta_j^*\right|^2=0\,, \qquad (6.108)$$

and hence $\alpha_1=\beta_1^*$ and $\alpha_2=\beta_2^*$. Eqs. (6.108,6.96,6.97) imply $E_1=E_2$, which is in contradiction with Eq. (6.101) for $\gamma>0$. For this reason, $\varepsilon_1=\varepsilon_2=+1$ is inadmissible and the dynamical map for the friction model is not completely positive. For a physical solution, we must rather take $\varepsilon_1=+1$ and $\varepsilon_2=-1$. For this choice, we get

$$\begin{aligned}\alpha_1^2-\alpha_2^2 &= \gamma(n_\omega+1)\,, & (6.109)\\ \beta_1^2-\beta_2^2 &= \gamma n_\omega\,, & (6.110)\\ \alpha_1\beta_1-\alpha_2\beta_2 &= \gamma(n_\omega+1/2)\,. & (6.111)\end{aligned}$$

Since we have three independent equations and four parameters, we have the freedom to fix one of them. A simple parametrisation is

$$\begin{aligned}\alpha_1&=\alpha\cosh\phi \qquad \alpha_2=\alpha\sinh\phi\,, & (6.112)\\ \beta_1&=\beta\cosh\psi \qquad \beta_2=\beta\sinh\psi\,, & (6.113)\end{aligned}$$

with $\alpha>0$ and $\beta>0$, from which it follows

$$\alpha^2=\gamma(n_\omega+1)\,,\quad \beta^2=\gamma n_\omega\,,\quad \cosh(\phi-\psi)=\cosh\frac{\omega}{2T}\,, \qquad (6.114)$$

and the parameter $\phi+\psi$ is fixed arbitrary. Then, the Liouvillian (6.107) can be rewritten as

$$\begin{aligned}\mathcal{L}(\hat{\rho}_f) &= -\frac{\mathrm{i}}{\hbar}[\widehat{H}_f,\hat{\rho}_f] \\ &\quad +D_{\rho_f}\big(\alpha\cosh\phi\,\hat{a}+\beta\cosh\psi\,\hat{a}^\dagger,\alpha\cosh\phi\,\hat{a}^\dagger+\beta\cosh\psi\,\hat{a}\big) \\ &\quad -D_{\rho_f}\big(\alpha\sinh\phi\,\hat{a}+\beta\sinh\psi\,\hat{a}^\dagger,\alpha\sinh\phi\,\hat{a}^\dagger+\beta\sinh\psi\,\hat{a}\big)\,. \qquad (6.115)\end{aligned}$$

For $\varepsilon_1=-\varepsilon_2=1$, $\mathcal{L}$ is not a CPTP map. Moreover, as shown into Sec. 6.3 and put forward into Refs. [226, 230], simple positivity holds true in the friction model only if either time is large enough or else if the initial states are not squeezed too much.

6.3 Wigner function dynamics

In this section, we aim to solve the equivalent master equations of the friction and cavity models by using the Wigner function formalism (see Chapter 3). We shall prove that the dynamics of both models is described by a Fokker-Planck differential equation, which gives access to the entire probability distributions rather than just few average values.

6.3.1 General formalism

To get the analytical solution of Eqs. (6.91,6.87), we use the Wigner function approach (see Sec. 3 for details), based on mapping Hilbert operators into real-valued phase-space functions [75–78, 154–156, 163, 164, C14, 231]. The Weyl transform of the density matrix is the Wigner function,

$$\mathcal{W}_\alpha(x,p) = \int_{\mathbb{R}} \mathrm{e}^{\mathrm{i}\, pw/\hbar} \, \langle x - w/2 \mid \hat{\rho}_\alpha \mid x + w/2 \rangle \, \mathrm{d}w \quad , \tag{6.116}$$

where $\alpha = f, c$ labels the friction (f) and cavity (c) models.

In this section, we shall compute the Weyl transform of Eqs. (6.91, 6.87) in order to get their phase-space representation. The dissipators of the friction and cavity models have the generic structure

$$\begin{aligned}
\mathcal{D}(\hat{\rho}) &= E_1 D_\rho(\hat{a},\hat{a}^\dagger) + E_2 D_\rho(\hat{a}^\dagger,\hat{a}) + E_3 D_\rho(\hat{a},\hat{a}) + E_3^* D_\rho(\hat{a}^\dagger,\hat{a}^\dagger)\,, \\
&= \left(E_1 + E_2 + E_3 + E_3^*\right)\frac{\omega}{2\hbar g} D_\rho(\hat{x},\hat{x}) + \left(E_1 + E_2 - E_3 - E_3^*\right)\frac{g}{2\hbar\omega} D_\rho(\hat{p},\hat{p}) \\
&\quad + (E_1 - E_2)\hat{\rho} - \frac{\mathrm{i}}{2\hbar}(E_1 - E_2)(\hat{x}\hat{\rho}\hat{p} - \hat{p}\hat{\rho}\hat{x}) \\
&\quad + \frac{\mathrm{i}}{2\hbar}(E_3 - E_3^*) D_\rho(\hat{x},\hat{p}) + \frac{\mathrm{i}}{2\hbar}(E_3 - E_3^*) D_\rho(\hat{p},\hat{x})\,,
\end{aligned} \tag{6.117}$$

where

$$D_\rho(\hat{a},\hat{a}^\dagger) = \frac{\omega}{2\hbar g} D_\rho(\hat{x},\hat{x}) + \frac{g}{2\hbar\omega} D_\rho(\hat{p},\hat{p}) + \frac{1}{2}\hat{\rho} - \frac{\mathrm{i}}{2\hbar}(\hat{x}\hat{\rho}\hat{p} - \hat{p}\hat{\rho}\hat{x})\,, \tag{6.118}$$

$$D_\rho(\hat{a}^\dagger,\hat{a}) = \frac{\omega}{2\hbar g} D_\rho(\hat{x},\hat{x}) + \frac{g}{2\hbar\omega} D_\rho(\hat{p},\hat{p}) - \frac{1}{2}\hat{\rho} + \frac{\mathrm{i}}{2\hbar}(\hat{x}\hat{\rho}\hat{p} - \hat{p}\hat{\rho}\hat{x})\,, \tag{6.119}$$

$$D_\rho(\hat{a},\hat{a}) = \frac{\omega}{2\hbar g} D_\rho(\hat{x},\hat{x}) - \frac{g}{2\hbar\omega} D_\rho(\hat{p},\hat{p}) + \frac{\mathrm{i}}{2\hbar} D_\rho(\hat{x},\hat{p}) + \frac{\mathrm{i}}{2\hbar} D_\rho(\hat{p},\hat{x})\,, \tag{6.120}$$

$$D_\rho(\hat{a}^\dagger,\hat{a}^\dagger)^\dagger = \frac{\omega}{2\hbar g} D_\rho(\hat{x},\hat{x}) - \frac{g}{2\hbar\omega} D_\rho(\hat{p},\hat{p}) - \frac{\mathrm{i}}{2\hbar} D_\rho(\hat{x},\hat{p}) - \frac{\mathrm{i}}{2\hbar} D_\rho(\hat{p},\hat{x})\,. \tag{6.121}$$

and the constants E_1, E_2, E_3 are specific for the friction and cavity models. According to the results into Sec. 6.2, we get

$$\text{friction model} \quad \begin{cases} E_1 = \gamma(n_\omega + 1)\,, \quad E_2 = \gamma n_\omega\,, \quad E_3 = \gamma(n_\omega + 1/2)\,, \\ \mathcal{D}(\hat{\rho}) = (2n_\omega + 1)\frac{\omega\gamma}{\hbar g} D_\rho(\hat{x}, \hat{x}) + \frac{\gamma}{2}\hat{\rho} - \frac{\mathrm{i}\gamma}{2\hbar}(\hat{x}\hat{\rho}\hat{p} - \hat{p}\hat{\rho}\hat{x})\,, \end{cases} \tag{6.122}$$

$$\text{cavity model} \quad \begin{cases} E_1 = \gamma(n_\omega + 1)\,, \quad E_2 = \gamma n_\omega\,, \quad E_3 = 0\,, \\ \mathcal{D}(\hat{\rho}) = (2n_\omega + 1)\frac{\omega\gamma}{2\hbar g} D_\rho(\hat{x}, \hat{x}) + (2n_\omega + 1)\frac{g\gamma}{2\hbar\omega} D_\rho(\hat{p}, \hat{p}) \\ \qquad + \frac{\gamma}{2}\hat{\rho} - \frac{\mathrm{i}\gamma}{2\hbar}(\hat{x}\hat{\rho}\hat{p} - \hat{p}\hat{\rho}\hat{x})\,. \end{cases} \tag{6.123}$$

The next step is to compute the Weyl transforms of the Hamiltonian operators and the dissipators into Eqs. (6.122,6.123), which are explicitly written in Table 6.1. The master equations (6.91,6.87) are finally mapped into

$$\begin{aligned} \partial_t \mathcal{W}_f &= (2n_\omega + 1)\frac{\hbar\gamma}{2}\frac{\omega}{g}\partial_p^2 \mathcal{W}_f + \left(\frac{\omega^2}{g}x + \gamma p - B\right)\partial_p \mathcal{W}_f \\ &\quad - gp\partial_x \mathcal{W}_f + \gamma\, \mathcal{W}_f\,, \end{aligned} \tag{6.124}$$

$$\begin{aligned} \partial_t \mathcal{W}_c &= \frac{\hbar\gamma}{4}(2n_\omega + 1)\left[\frac{g}{\omega}\partial_x^2 \mathcal{W}_c + \frac{\omega}{g}\partial_p^2 \mathcal{W}_c\right] \\ &\quad + \left(\frac{\omega^2}{g}x + \frac{\gamma}{2}p - B\right)\partial_p \mathcal{W}_c + \left(\frac{\gamma}{2}x - gp\right)\partial_x \mathcal{W}_c + \gamma\, \mathcal{W}_c\,, \end{aligned} \tag{6.125}$$

with $\mathcal{W}_\alpha = \mathcal{W}_\alpha(t, x, p)$. Eqs. (6.124,6.125) may be written in compact form as

$$\partial_t \mathcal{W}_\alpha(t, x, p) = \boldsymbol{\nabla}\cdot\left[\frac{\mathbf{D}_\alpha}{2}\boldsymbol{\nabla}\mathcal{W}_\alpha(t, x, p) + \boldsymbol{\Theta}_\alpha \begin{pmatrix} x \\ p \end{pmatrix} \mathcal{W}_\alpha(t, x, p) - \boldsymbol{\Theta}_\alpha \boldsymbol{\mu}_\alpha \mathcal{W}_\alpha(t, x, p)\right], \tag{6.126}$$

with $\boldsymbol{\nabla} = \begin{pmatrix} \partial_x \\ \partial_p \end{pmatrix}$ and

$$\mathbf{D}_f = \begin{pmatrix} 0 & 0 \\ 0 & \frac{\omega\hbar\gamma}{g}\left(2n_\omega + 1\right) \end{pmatrix}, \qquad \mathbf{D}_c = \begin{pmatrix} \frac{g\hbar\gamma}{2\omega}\left(2n_\omega + 1\right) & 0 \\ 0 & \frac{\omega\hbar\gamma}{2g}\left(2n_\omega + 1\right) \end{pmatrix}, \tag{6.127}$$

$$\boldsymbol{\Theta}_f = \begin{pmatrix} 0 & -g \\ \omega^2/g & \gamma \end{pmatrix}, \qquad \boldsymbol{\Theta}_c = \begin{pmatrix} \gamma/2 & -g \\ \omega^2/g & \gamma/2 \end{pmatrix}, \tag{6.128}$$

$$\boldsymbol{\mu}_f = B\begin{pmatrix} g/\omega^2 \\ 0 \end{pmatrix}, \qquad \boldsymbol{\mu}_c = B\left(\omega^2 + \gamma^2/4\right)^{-1}\begin{pmatrix} g \\ \gamma/2 \end{pmatrix}, \tag{6.129}$$

Quantum operator	Weyl transform
$\widehat{H}$	$\frac{g}{2}p^2 + \frac{\omega^2}{2g}x^2 - Bx$
$\widehat{H}_f$	$\frac{g}{2}p^2 + \frac{\omega^2}{2g}x^2 - Bx + \frac{\gamma}{2}xp$
$\left[\widehat{H}, \hat{\rho}\right]$	$\mathrm{i}\hbar\left(\frac{\omega^2}{g}x\partial_p\mathcal{W} - B\partial_p\mathcal{W} - gp\partial_x\mathcal{W}\right)$
$\left[\widehat{H}_f, \hat{\rho}\right]$	$\mathrm{i}\hbar\left(\frac{\omega^2}{g}x\partial_p\mathcal{W} - B\partial_p\mathcal{W} - gp\partial_x\mathcal{W} - \frac{\gamma}{2}x\partial_x\mathcal{W} + \frac{\gamma}{2}p\partial_p\mathcal{W}\right)$
$\hat{x}\hat{\rho}\hat{x}$	$x^2\mathcal{W} + \left(\frac{\hbar}{2}\right)^2\partial_p^2\mathcal{W}$
$\widehat{p}\hat{\rho}\widehat{p}$	$p^2\mathcal{W} + \left(\frac{\hbar}{2}\right)^2\partial_x^2\mathcal{W}$
$\widehat{p}\hat{\rho}\hat{x}$	$xp\mathcal{W} - \frac{\mathrm{i}\hbar}{2}\left(x\partial_x\mathcal{W} + p\partial_p\mathcal{W}\right) - \frac{\mathrm{i}\hbar}{2}\mathcal{W} - \left(\frac{\hbar}{2}\right)^2\partial_x\partial_p\mathcal{W}$
$\hat{x}\hat{\rho}\widehat{p}$	$xp\mathcal{W} + \frac{\mathrm{i}\hbar}{2}\left(x\partial_x\mathcal{W} + p\partial_p\mathcal{W}\right) + \frac{\mathrm{i}\hbar}{2}\mathcal{W} - \left(\frac{\hbar}{2}\right)^2\partial_x\partial_p\mathcal{W}$
$\hat{x}\hat{\rho}\widehat{p} - \widehat{p}\hat{\rho}\hat{x}$	$\mathrm{i}\hbar\left(x\partial_x\mathcal{W} + p\partial_p\mathcal{W}\right) + \mathrm{i}\hbar\mathcal{W}$
$\frac{1}{2}\{\widehat{p}^2, \hat{\rho}\}$	$p^2\mathcal{W} - \left(\frac{\hbar}{2}\right)^2\partial_x^2\mathcal{W}$
$\frac{1}{2}\{\hat{x}^2, \hat{\rho}\}$	$x^2\mathcal{W} - \left(\frac{\hbar}{2}\right)^2\partial_p^2\mathcal{W}$
$\frac{1}{2}\{\hat{x}\widehat{p}, \hat{\rho}\}$	$xp\mathcal{W} + \frac{\mathrm{i}\hbar}{2}\mathcal{W} - \left(\frac{\hbar}{2}\right)^2\partial_x\partial_p\mathcal{W}$
$\frac{1}{2}\{\widehat{p}\hat{x}, \hat{\rho}\}$	$xp\mathcal{W} - \frac{\mathrm{i}\hbar}{2}\mathcal{W} - \left(\frac{\hbar}{2}\right)^2\partial_x\partial_p\mathcal{W}$
$D_\rho(\hat{x}, \hat{x})$	$\frac{\hbar^2}{2}\partial_p^2\mathcal{W}$
$D_\rho(\widehat{p}, \widehat{p})$	$\frac{\hbar^2}{2}\partial_x^2\mathcal{W}$
$D_\rho(\hat{x}, \widehat{p})$	$\mathrm{i}\hbar\left(\mathcal{W} + \frac{1}{2}(x\partial_x\mathcal{W} + p\partial_p\mathcal{W})\right)$
$D_\rho(\widehat{p}, \hat{x})$	$-\mathrm{i}\hbar\left(\mathcal{W} + \frac{1}{2}(x\partial_x\mathcal{W} + p\partial_p\mathcal{W})\right)$

Table 6.1: Quantum operators with their Weyl transforms.

for the friction (f) and cavity (c) models. Eq. (6.126) is the linear partial differential equation governing the Wigner function evolution. The Fokker-Plank equation (6.126) is solved by mapping the problem into the Fourier space,

$$\widetilde{W}_\alpha(t,\mathbf{k}) = \int_{\mathbb{R}^2} \mathrm{d}\mathbf{r}\; W_\alpha(t,\mathbf{r})\,\mathrm{e}^{-\mathrm{i}\mathbf{r}\cdot\mathbf{k}/\hbar}\,, \qquad \mathbf{r} = \begin{pmatrix} x \\ p \end{pmatrix}, \quad \mathbf{k} = \begin{pmatrix} \tilde{p} \\ \tilde{x} \end{pmatrix}. \tag{6.130}$$

where $\widetilde{W}_\alpha(t,\mathbf{k})$ is the Fourier transform and $\mathbf{k}$ is the reciprocal space variable. After some algebra, the time-dependent transformed Wigner function reads [232]

$$\widetilde{W}_\alpha(t,\mathbf{k}) = \widetilde{W}_\alpha\Big(0,\mathrm{e}^{-\mathbf{\Theta}_\alpha^T t}\mathbf{k}\Big)\exp\Big\{-\frac{\mathrm{i}}{\hbar}\mathbf{k}^T\Big(\mathbf{1}-\mathrm{e}^{-\mathbf{\Theta}_\alpha t}\Big)\boldsymbol{\mu}_\alpha - \frac{1}{2\hbar^2}\mathbf{k}^T\mathbf{\Sigma}_\alpha(t)\mathbf{k}\Big\}, \tag{6.131}$$

where

$$\mathbf{\Sigma}_\alpha(t) := \int_0^t \mathrm{d}s\; \mathrm{e}^{-s\mathbf{\Theta}_\alpha}\mathbf{D}_\alpha\,\mathrm{e}^{-s\mathbf{\Theta}_\alpha^T}\,. \tag{6.132}$$

The inverse Fourier transforms of $\exp\Big\{-\frac{\mathrm{i}}{\hbar}\mathbf{k}^T\Big(\mathbf{1}-\mathrm{e}^{-\mathbf{\Theta}_\alpha t}\Big)\boldsymbol{\mu}_\alpha - \frac{1}{2\hbar^2}\mathbf{k}^T\mathbf{\Sigma}_\alpha(t)\mathbf{k}\Big\}$ and $\widetilde{W}_\alpha(t,\mathbf{k})$ are

$$\begin{aligned} f_\alpha(t,\mathbf{r}) \;&:=\; \int_{\mathbb{R}^2}\frac{\mathrm{d}\mathbf{k}}{(2\pi\hbar)^2}\exp\Big\{-\frac{\mathrm{i}}{\hbar}\mathbf{k}^T\Big(\mathbf{1}-\mathrm{e}^{-\mathbf{\Theta}_\alpha t}\Big)\boldsymbol{\mu}_\alpha - \frac{1}{2\hbar^2}\mathbf{k}^T\mathbf{\Sigma}_\alpha(t)\mathbf{k}\Big\}\mathrm{e}^{\mathrm{i}\mathbf{k}\cdot\mathbf{r}/\hbar} \\ &=\; \frac{(2\pi)^{-1}}{\sqrt{\det\mathbf{\Sigma}_\alpha(t)}}\exp\Big\{-\frac{1}{2}\Big(\mathbf{r}-\mathbf{m}_\alpha(t)\Big)^T\mathbf{\Sigma}_\alpha^{-1}(t)\Big(\mathbf{r}-\mathbf{m}_\alpha(t)\Big)\Big\}, \qquad (6.133) \\ W'_\alpha(t,\mathbf{r}) \;&:=\; \int_{\mathbb{R}^2}\frac{\mathrm{d}\mathbf{k}}{(2\pi\hbar)^2}\widetilde{W}_\alpha\Big(0,\mathrm{e}^{-\mathbf{\Theta}_\alpha^T t}\mathbf{k}\Big)\mathrm{e}^{\mathrm{i}\mathbf{k}\cdot\mathbf{r}/\hbar} \;=\; \mathrm{e}^{\mathrm{tr}(\mathbf{\Theta}_\alpha)t}\,W_\alpha(0,\mathrm{e}^{\mathbf{\Theta}_\alpha t}\mathbf{r})\,, \qquad (6.134) \end{aligned}$$

where $W_\alpha(0,\mathbf{r})$ is the initial distribution and

$$\mathbf{m}_\alpha(t) := \Big(\mathbf{1}-\mathrm{e}^{-\mathbf{\Theta}_\alpha t}\Big)\boldsymbol{\mu}_\alpha\,. \tag{6.135}$$

Using the convolution theorem, the general solution is given by

$$W_\alpha(t,\mathbf{r}) = \int_{\mathbb{R}^2}\mathrm{d}\mathbf{r}'\; f_\alpha(t,\mathbf{r}-\mathbf{r}')W'_\alpha(t,\mathbf{r}')\,. \tag{6.136}$$

The dynamics generated by the two Liouvillian operators (6.107,6.87) is Gaussian-preserving. This feature clearly emerges from the solution into Eq. (6.136): $f_\alpha(t,\mathbf{r})$ is a Gaussian function and the convolution of two Gaussian functions is a Gaussian function as well.

For the time evolution of $f_\alpha(t, \mathbf{r})$, we need to evaluate the matrix $\boldsymbol{\Sigma}_\alpha(t)$. Using the Cayley–Hamilton theorem [C21, C22], the 2×2 exponential matrix $\mathrm{e}^{-\boldsymbol{\Theta}_\alpha t}$ may be written as

$$\mathrm{e}^{-\boldsymbol{\Theta}_\alpha t} = s_0^\alpha(t)\mathbb{1} + s_1^\alpha(t)\boldsymbol{\Theta}_\alpha \tag{6.137}$$

with

$$s_0^\alpha(t) = \frac{\Lambda_+^{(\alpha)}\mathrm{e}^{-\Lambda_-^{(\alpha)}t} - \Lambda_-^{(\alpha)}\mathrm{e}^{-\Lambda_+^{(\alpha)}t}}{\Lambda_+^{(\alpha)} - \Lambda_-^{(\alpha)}}\,, \qquad s_1^\alpha(t) = \frac{\mathrm{e}^{-\Lambda_+^{(\alpha)}t} - \mathrm{e}^{-\Lambda_+^{(\alpha)}t}}{\Lambda_+^{(\alpha)} - \Lambda_-^{(\alpha)}}\,, \tag{6.138}$$

and the eigenvalues $\Lambda_\pm^{(\alpha)}$ of $\boldsymbol{\Theta}_\alpha$, for the friction ($f$) and cavity ($c$) models. Eq. (6.132) reduces to

$$\begin{aligned}\boldsymbol{\Sigma}_\alpha(t) &= \int_0^t \mathrm{d}t'\; s_0^\alpha(t')^2\mathbf{D}_\alpha + \int_0^t \mathrm{d}t'\; s_1^\alpha(t')^2\boldsymbol{\Theta}_\alpha\mathbf{D}_\alpha\boldsymbol{\Theta}_\alpha^T \\ &\quad + \int_0^t \mathrm{d}t'\; s_0^\alpha(t')s_1^\alpha(t')\Big(\boldsymbol{\Theta}_\alpha\mathbf{D}_\alpha + \mathbf{D}_\alpha\boldsymbol{\Theta}_\alpha^T\Big).\end{aligned} \tag{6.139}$$

It can be proved that the long-time limit is the same in both models,

$$\begin{aligned}\boldsymbol{\Lambda}_T &:= \lim_{t\to\infty} \boldsymbol{\Sigma}_\alpha(t) \\ &= \int_0^\infty \mathrm{d}t\; \mathrm{e}^{-\boldsymbol{\Theta}_\alpha t}\mathbf{D}_\alpha\, \mathrm{e}^{-\boldsymbol{\Theta}_\alpha^T t} = \frac{\hbar}{2}\begin{pmatrix} g/\omega & 0 \\ 0 & \omega/g\end{pmatrix}\coth\frac{\omega\hbar}{2T}\,,\end{aligned} \tag{6.140}$$

$\forall\alpha = f, c$. The matrix $\boldsymbol{\Lambda}_T$ characterises thermal equilibrium for quantum harmonic oscillators, with a one-to-one map [233] onto the Gibbs state of temperature T

$$\lim_{t\to\infty} f_\alpha(t,\mathbf{r}) = \frac{1}{2\pi\hbar}\mathcal{W}_\alpha^T(\mathbf{r})\,, \qquad \mathcal{W}_\alpha^T(\mathbf{r}) \longleftrightarrow \hat{\rho}_\alpha^T = \frac{\mathrm{e}^{-\hat{\mathcal{H}}_\alpha/T}}{Z}\,, \tag{6.141}$$

where $Z = \mathrm{tr}\Big(\mathrm{e}^{-\hat{\mathcal{H}}_\alpha/T}\Big)$ is a normalisation constant,

$$\mathcal{W}_\alpha^T(\mathbf{r}) = \frac{\hbar}{\sqrt{\det\boldsymbol{\Lambda}_T}}\exp\Big\{-\frac{1}{2}(\mathbf{r}-\boldsymbol{\mu}_\alpha)^T\boldsymbol{\Lambda}_T^{-1}(\mathbf{r}-\boldsymbol{\mu}_\alpha)\Big\}, \tag{6.142}$$

and $\hat{\mathcal{H}}_\alpha$ is an effective Hamiltonian,

$$\hat{\mathcal{H}}_f = \hat{H}\,, \qquad \hat{\mathcal{H}}_c = \hat{H} + B\frac{\gamma^2}{\gamma^2+4\omega^2}\hat{x} - B\frac{2g\gamma}{\gamma^2+4\omega^2}\hat{p}\,. \tag{6.143}$$

In order to show the equivalence between the two objects in Eq. (6.141), we expand the equilibrium thermal state

$$\hat{\rho}_\alpha^T = \frac{\mathrm{e}^{-\widehat{\mathcal{H}}_\alpha/T}}{Z} = \frac{1}{Z}\sum_{n=0}^{\infty}\frac{1}{n!}(-\widehat{\mathcal{H}}_\alpha/T)^n\,, \tag{6.144}$$

which is mapped onto

$$\mathcal{W}_\alpha^T(x,p) = \frac{1}{Z}\sum_{n=0}^{\infty}\frac{1}{n!}\Phi[(-\widehat{\mathcal{H}}_\alpha/T)^n]\,, \tag{6.145}$$

where T is the bath temperature and Φ indicates the Weyl transform. For the quantum harmonic oscillator, Eq. (6.145) is proved to be equivalent to [233]

$$\mathcal{W}_\alpha^T(x,p) = \frac{1}{Z^*}\sum_{n=0}^{\infty}\frac{1}{n!}(-\mathcal{H}_\alpha(x,p)/T_{\text{eff}})^n = \frac{e^{-\mathcal{H}_\alpha(x,p)/T_{\text{eff}}}}{Z^*}\,, \tag{6.146}$$

where $\mathcal{H}_\alpha(x,p) = \Phi[\widehat{\mathcal{H}}_\alpha]$ is the Weyl transform of the effective Hamiltonian $\widehat{\mathcal{H}}_\alpha$, $T_{\text{eff}} = \frac{\hbar\omega}{2}\coth\frac{\hbar\omega}{2T}$ and $Z^* = (2\pi\hbar)^{-1}\int \mathrm{d}x\mathrm{d}p\,\exp(-\mathcal{H}_\alpha(x,p)/T_{\text{eff}})$. As expected, $T_{\text{eff}} \to T$ in the classical limit $\hbar \to 0$.

In the long-time limit,

$$\lim_{t\to\infty}\mathcal{W}'(t,\mathbf{r}) = 2\pi\hbar\delta(\mathbf{r})\,, \tag{6.147}$$

and Eq. (6.136) implies

$$\lim_{t\to\infty}\mathcal{W}_\alpha(t,\mathbf{r}) = \int_{\mathbb{R}^2}\mathrm{d}\mathbf{r}'\;\mathcal{W}_\alpha^T(\mathbf{r}-\mathbf{r}')\delta(\mathbf{r}') = \mathcal{W}_\alpha^T(\mathbf{r})\,. \tag{6.148}$$

According to Eq. (6.148), the system always relaxes to a formal 'equilibrium state' with the bath, for both models. More specifically, if $B=0$, the effective Hamiltonians and the equilibrium states coincide ($\widehat{\mathcal{H}}_c = \widehat{\mathcal{H}}_f = \widehat{H}$). However, for non-vanishing magnetic fields $B \neq 0$, the effective Hamiltonian $\widehat{\mathcal{H}}_c$ of the cavity model depends on γ (see Eq. (6.143)), which means the stationary state is not a physical equilibrium state in the usual sense. The failure of full equilibration arises in the cavity model although the connected correlators $C_{+,c}^{(x,x)}(t,t)$ and $C_{+,c}^{(p,p)}(t,t)$ in Sec. 6.1 were required to take their equilibrium values.

6.3.2 Dynamics of Gaussian states

A pedagogic and important example is provided by initial Gaussian states, e.g. any Gibbs thermal state for $\widehat{H}$, since the dissipative dynamics is Gaussian preserving and the convolution theorem makes it easy to derive the time evolution.

Nevertheless, this choice is not so restrictive as it might appear at first sight, since states represented as an infinite sum of shifted Gaussian functions are dense in the space of (square-)integrable functions [C23, C24, 234].

Suppose to prepare the system into the initial state

$$\mathcal{W}(0,\mathbf{r}) = \frac{\hbar}{\sqrt{\det\mathbf{\Gamma}}}\exp\left\{-\frac{1}{2}(\mathbf{r}-\boldsymbol{\nu})^T\mathbf{\Gamma}^{-1}(\mathbf{r}-\boldsymbol{\nu})\right\}, \tag{6.149}$$

where $\mathbf{\Gamma}$ is any 2×2 invertible matrix. According to Eq. (6.136), the full solution is

$$\mathcal{W}_\alpha(t,\mathbf{r}) = \frac{\hbar}{\sqrt{\det\mathbf{\Omega}_\alpha(t)}}\exp\left\{-\frac{1}{2}\Big(\mathbf{r}-\mathbf{M}_\alpha(t)\Big)^T\mathbf{\Omega}_\alpha^{-1}(t)\Big(\mathbf{r}-\mathbf{M}_\alpha(t)\Big)\right\}, \tag{6.150}$$

where

$$\mathbf{M}_\alpha(t) = \mathrm{e}^{-\mathbf{\Theta}_\alpha t}\boldsymbol{\nu} + \mathbf{m}_\alpha(t)\,, \qquad \mathbf{\Omega}_\alpha(t) = \mathrm{e}^{-\mathbf{\Theta}_\alpha t}\mathbf{\Gamma}\mathrm{e}^{-\mathbf{\Theta}_\alpha^T t} + \mathbf{\Sigma}_\alpha(t)\,. \tag{6.151}$$

For any observable with Weyl transform $\mathrm{g}(\mathbf{r})$, the average value is

$$\begin{aligned}\int_{\mathbb{R}^2}\frac{\mathrm{d}\mathbf{r}}{2\pi\hbar}\,\mathrm{g}(\mathbf{r})\mathcal{W}_\alpha(t,\mathbf{r}) &= \frac{1}{2\pi\sqrt{\det\mathbf{\Omega}_\alpha(t)}}\int_{\mathbb{R}^2}\mathrm{d}\mathbf{r}\,\mathrm{g}\Big(\mathbf{r}+\mathbf{M}_\alpha(t)\Big)\exp\left\{-\frac{1}{2}\mathbf{r}^T\mathbf{\Omega}_\alpha^{-1}(t)\mathbf{r}\right\}\\ &= \exp\left\{\frac{1}{2}\sum_{i,j=1}^{2}(\mathbf{\Omega}_\alpha)_{ij}\partial_{r_i}\partial_{r_j}\right\}\mathrm{g}\Big(\mathbf{r}+\mathbf{M}_\alpha(t)\Big)\Big|_{\mathbf{r}=0}\,.\end{aligned} \tag{6.152}$$

Thanks to Eq. (6.152), we find

$$\langle\hat{\mathbf{r}}\rangle_\alpha(t) = \mathbf{M}_\alpha(t) = \begin{pmatrix} M_\alpha^x(t)\\ M_\alpha^p(t)\end{pmatrix}, \tag{6.153}$$

$$\langle\hat{x}^2\rangle_\alpha(t) = \Big(M_\alpha^x(t)\Big)^2 + \Big(\mathbf{\Omega}_\alpha(t)\Big)_{11}, \tag{6.154}$$

$$\langle\hat{p}^2\rangle_\alpha(t) = \Big(M_\alpha^p(t)\Big)^2 + \Big(\mathbf{\Omega}_\alpha(t)\Big)_{22}. \tag{6.155}$$

The structure of the 2×2 matrix $\mathbf{\Omega}_\alpha(t)$ is important to discuss the positivity of the dynamical map. The matrix $\mathbf{\Omega}_\alpha(t)$ must be positive to generate physically admissible density matrices, which means the eigenvalues of $\mathbf{\Omega}_\alpha(t)$ must be strictly positive and compatible with the Heisenberg principle. While the positivity of $\mathbf{\Omega}_\alpha(t)$ is automatically guaranteed for the cavity model [61], the same does not hold for the friction model, as put forward into Ref. [226]. On the other hand, since the long-time limit $\mathbf{\Lambda}_T = \lim_{t\to\infty}\mathbf{\Sigma}_\alpha(t)$ is positive definite, both models will be positive for large enough times and non-positivity can only arise in a short-time regime in the friction model. For a given set of parameters ω, g, B, T, γ characterising the experimental conditions, we shall focus on the initial state, deriving the minimal conditions to generate positive semi-definite density matrices after quenching the state. More specifically, consider the space of 2×2 physically admissible matrices $\mathbf{\Gamma}$ which generate positive semi-definite density operators $\hat{\rho}$. The initial state (6.149) is described by the positive, real and symmetric matrix

$$\mathbf{\Gamma} = \begin{pmatrix} \Gamma_1 & \Gamma_3 \\ \Gamma_3 & \Gamma_2 \end{pmatrix}, \tag{6.156}$$

For simplicity, we assume $\boldsymbol{\nu} = 0$, hence for the Heisenberg uncertainty principle $\Gamma_1\Gamma_2 \geq \hbar/2$. To linear order in the time t, the positivity of the initial state (6.149) is maintained by the markovian dynamics if the sufficient criterion

$$\left.\frac{\mathrm{d}\mathbf{\Omega}_f(t)}{\mathrm{d}t}\right|_{t=0} = \begin{pmatrix} 2g\Gamma_3 & g\Gamma_2 - \gamma\Gamma_3 - \frac{\omega^2}{g}\Gamma_1 \\ g\Gamma_2 - \gamma\Gamma_3 - \frac{\omega^2}{g}\Gamma_1 & \frac{\omega\hbar\gamma}{g}(2n_\omega + 1) - 2\gamma\Gamma_2 - 2\frac{\omega^2}{g}\Gamma_3 \end{pmatrix} > 0\,, \tag{6.157}$$

is obeyed, that means $\left.\frac{\mathrm{d}\mathbf{\Omega}_f(t)}{\mathrm{d}t}\right|_{t=0}$ is a positive matrix. Clearly, if $\mathbf{\Gamma}$ were diagonal, one of the eigenvalues of $\left.\frac{\mathrm{d}\mathbf{\Omega}_f(t)}{\mathrm{d}t}\right|_{t=0}$ would be negative such that (6.157) were not satisfied. Therefore, we must admit $\Gamma_3 > 0$ and look for the region in the parameter space $(\Gamma_1, \Gamma_2, \Gamma_3)$ such that all the conditions

$$\begin{cases} \left.\begin{array}{l} \Gamma_1 + \Gamma_2 > 0 \\ \Gamma_1\Gamma_2 > \Gamma_3^2 \end{array}\right\} \quad \mathbf{\Gamma} > 0 \\ \left.\Gamma_1\Gamma_2 \geq \hbar/2 \quad\right\} \quad \text{Validity of the Heisenberg principle at } t = 0 \\ \left.\begin{array}{l} \frac{\omega\hbar\gamma}{g}(2n_\omega + 1) - 2\gamma\Gamma_2 - 2\left(\frac{\omega^2}{g} + g\right)\Gamma_3 > 0 \\ 2g\Gamma_3\left[\frac{\omega\hbar\gamma}{g}(2n_\omega + 1) - 2\gamma\Gamma_2 - 2\frac{\omega^2}{g}\Gamma_3\right] > \left[g\Gamma_2 - \gamma\Gamma_3 - \frac{\omega^2}{g}\Gamma_1\right]^2 \end{array}\right\} \quad \left.\frac{\mathrm{d}\mathbf{\Omega}_f(t)}{\mathrm{d}t}\right|_{t=0} > 0 \end{cases} \tag{6.158}$$

are verified.

6.4 Relaxation behaviour

From Eqs. (6.139,6.151), the relaxation time is expressed through the eigenvalues $\Lambda_\pm^{(\alpha)}$ of $\mathbf{\Theta}_\alpha$. For the cavity model, the eigenvalues $\Lambda_\pm^{(c)} = \gamma/2 \pm \mathrm{i}\omega$ are al-

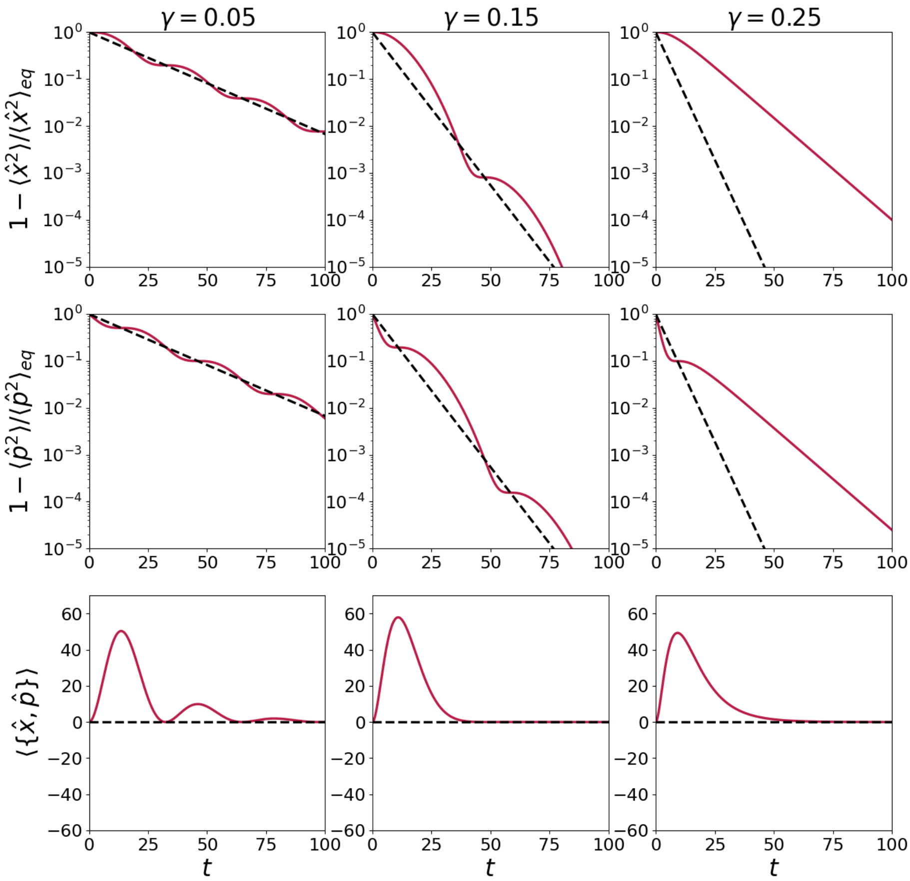

Figure 6.1: Time evolution of the equal-time correlators $\langle \hat{x}^2(t) \rangle = C_+^{(x,x)}(t,t)$, $\langle \hat{p}^2(t) \rangle = C_+^{(p,p)}(t,t)$ and $2C_+^{(x,p)}(t,t) = \langle \{\hat{x}(t), \hat{p}(t)\} \rangle$. The system is initially prepared in the ground state $\hat{a}\,|0\rangle = 0$ of the quantum harmonic oscillator. The red lines refer to the friction model and the black dashed lines to the cavity model. The columns correspond to different values of the damping constant $\gamma = [0.05, 0.15, 0.25]$, with the expected transition at $\gamma = 2\omega$. Here we set $B = 0$, $g = 1$, $\hbar = 1$, $\omega = 0.1$ and $T = 10$.

ways complex numbers, which means the system approaches exponentially the stationary state with relaxation time $2/\gamma$ while the imaginary part of $\Lambda_\pm^{(c)}$ is responsible of the oscillatory behaviour. For the friction model we distinguish between over-damped and under-damped regimes: if $\gamma < 2\omega$, the eigenvalues $\Lambda_\pm^{(f)} = (\gamma \pm \mathrm{i}\sqrt{4\omega^2 - \gamma^2})/2$ are complex numbers and the relaxation time is still $2/\gamma$; however, if $\gamma > 2\omega$, the eigenvalues $\Lambda_\pm^{(f)} = (\gamma \pm \sqrt{\gamma^2 - 4\omega^2})/2$ are always

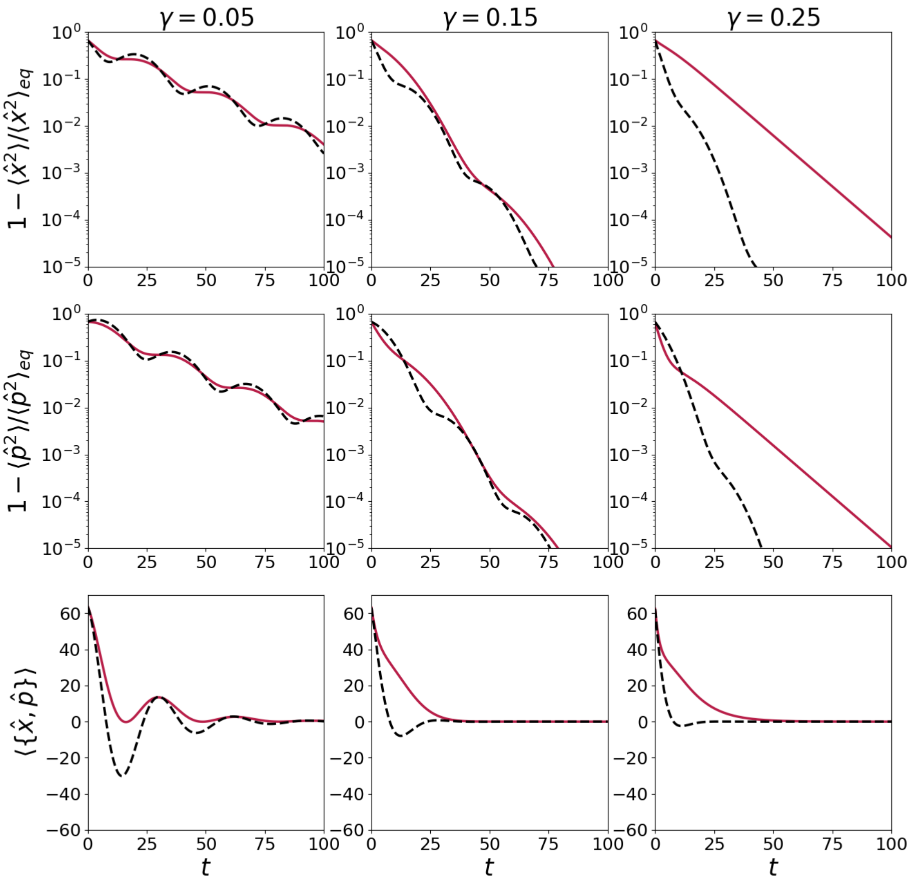

Figure 6.2: Time evolution of the equal-time correlators $\langle \hat{x}^2(t) \rangle = C_+^{(x,x)}(t,t)$, $\langle \widehat{p}^2(t) \rangle = C_+^{(p,p)}(t,t)$ and $2C_+^{(x,p)}(t,t) = \langle \{\hat{x}(t), \widehat{p}(t)\} \rangle$. The system is initially prepared in the coherent state $|4+4\mathrm{i}\rangle$: $\hat{a}\,|4+4\mathrm{i}\rangle = (4+4\mathrm{i})\,|4+4\mathrm{i}\rangle$. The red lines refer to the friction model and the black dashed lines to the cavity model. The columns correspond to different values of the damping constant $\gamma = [0.05, 0.15, 0.25]$, with the expected transition at $\gamma = 2\omega$. Here we set $B = 0$, $\mathrm{g} = 1$, $\hbar = 1$, $\omega = 0.1$ and $T = 10$.

real, with a dominant relaxation time $2/(\gamma - \sqrt{\gamma^2 - 4\omega^2})$.

The resulting relaxation behaviour of the averages $\langle \hat{x}^2 \rangle(t) = C_+^{(x,x)}(t,t)$, $\langle \widehat{p}^2 \rangle(t) = C_+^{(p,p)}(t,t)$ and $\langle \{\hat{x}(t), \widehat{p}(t)\} \rangle$ is illustrated in Figs. 6.1, 6.2 and 6.3, for different values of γ. The first two columns refer to the under-damped regime $\gamma < 2\omega$ and the last one to the over-damped regime $\gamma > 2\omega$. If we set $B = 0$,

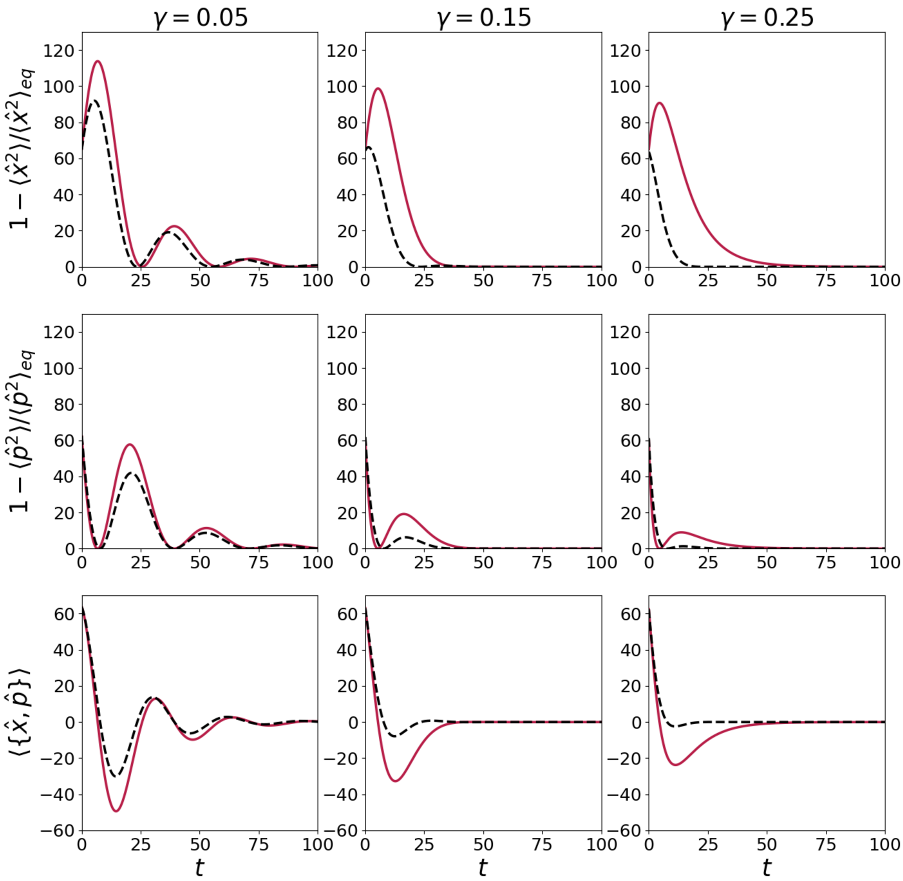

Figure 6.3: Time evolution of the equal-time correlators $\langle \hat{x}^2(t) \rangle = C_+^{(x,x)}(t,t)$, $\langle \hat{p}^2(t) \rangle = C_+^{(p,p)}(t,t)$ and $2C_+^{(x,p)}(t,t) = \langle \{\hat{x}(t), \hat{p}(t)\} \rangle$. The system is initially prepared in the coherent state $|4+4\mathrm{i}\rangle$: $\hat{a}\,|4+4\mathrm{i}\rangle = (4+4\mathrm{i})\,|4+4\mathrm{i}\rangle$. The red lines refer to the friction model and the dashed black lines to the cavity model. The columns correspond to different values of the damping constant $\gamma = [0.05, 0.15, 0.25]$, with the expected transition at $\gamma = 2\omega$. Here we use $B = 0$, $g = 1$, $\hbar = 1$, $\omega = 0.1$ and $T = 0$.

both models evolve towards the same equilibrium Gibbs state (6.142). In Fig. 6.1, the initial state is the vacuum state $|0\rangle$, namely the harmonic oscillator ground state $\hat{a}\,|0\rangle = 0$. In Figs. 6.2, 6.3, the initial state is the coherent state $|4+4\mathrm{i}\rangle$: $\hat{a}\,|4+4\mathrm{i}\rangle = \big(4+4\mathrm{i}\big)\,|4+4\mathrm{i}\rangle$.

The time evolution at the bath temperature $T = 10$ in Figs. 6.1,6.2 look globally similar, while the dynamics at $T = 0$ in Fig. 6.3 looks different. In the cavity model, the characteristic relaxation time for the quadratic observables is γ^{-1}, while for the friction model one has to distinguish between over-damped and under-damped regimes: for the under-damped case $\gamma < 2\omega$, one finds γ^{-1} as relaxation time; for the over-damped regime $\gamma > 2\omega$, one gets $\left(\gamma - \sqrt{\gamma^2 - 4\omega^2}\,\right)^{-1}$, approximated by ω^2/γ for $\gamma \gg 1$.

In Figs. 6.1, 6.2, 6.3, we chose to plot $1-\langle\hat{x}^2(t)\rangle/\langle\hat{x}^2\rangle_{\rm eq}$ and $1-\langle\hat{p}^2(t)\rangle/\langle\hat{p}^2\rangle_{\rm eq}$, to better emphasise the deviations from the equilibrium values. In Figs. 6.1, 6.2 we see that, by construction, at the bath temperature $T = 10$, both $\langle\hat{x}^2\rangle(t)$ and $\langle\hat{p}^2\rangle(t)$ approach their equilibrium values from below, which means $\langle\hat{x}^2\rangle(t) \leq \langle\hat{x}^2\rangle_{\rm eq}$ and $\langle\hat{p}^2\rangle(t) \leq \langle\hat{p}^2\rangle_{\rm eq}$. On the other hand, at zero temperature $T = 0$, the opposite holds true, viz. $\langle\hat{x}^2\rangle(t) \geq \langle\hat{x}^2\rangle_{\rm eq}$ and $\langle\hat{p}^2\rangle(t) \geq \langle\hat{p}^2\rangle_{\rm eq}$, and thus equilibrium is approached from above, see Fig. 6.3. These observations are in agreement to the condition (D) which guarantees that, for both models, the stationary values of these two observables relax towards their equilibrium value. This is confirmed by the fact that at thermal equilibrium no evolution occurs.

We remark that the Lindblad dynamics (6.87) describing a single mode in an optical cavity comes directly from the second-order Born approximation in γ. In this sense, it is not surprising that the cavity model is characterised only by the under-damped regime. The existence of the over-damped regime in the friction model may suggest that, from a microscopic perspective, some hypothesis can be relaxed. We also observe that, in the weak coupling limit $\gamma \ll 1$, the relaxation in both models is almost identical, with some damped oscillations in the friction model.

If the system is initially prepared in the vacuum state $|0\rangle$, the equal time anti-commutator $\langle\{\hat{x}(t), \hat{p}(t)\}\rangle$ of the friction model is always positive and goes toward zero in the long time limit. On the other hand, the same quantity is identically zero in the cavity model. For the coherent initial state $|4 + 4\mathrm{i}\rangle$, the anti-commutator $\langle\{\hat{x}(t), \hat{p}(t)\}\rangle$ oscillates around its equilibrium value for both models, as predicted by Eqs. (6.50,6.74).

If the bath is at zero temperature, see Fig. 6.3, both $1 - \langle\hat{x}^2\rangle(t)/\langle\hat{x}^2\rangle_{\rm eq}$ and $1 - \langle\hat{p}^2\rangle(t)/\langle\hat{p}^2\rangle_{\rm eq}$ vanish in the under-damped regime at certain times. It is also interesting to notice that the decaying oscillations into $1 - \langle\hat{x}^2\rangle(t)/\langle\hat{x}^2\rangle_{\rm eq}$ and $1 - \langle\hat{p}^2\rangle(t)/\langle\hat{p}^2\rangle_{\rm eq}$ are phase-shifted in such a way that a plateau in one corresponds to the maximal value in the other. Moreover, the anti-commutator $\langle\{\hat{x}(t), \hat{p}(t)\}\rangle$ of the friction model displays a sequence of damped oscillations and it goes to zero for $t \sim \infty$.

In the over-damped case (friction model), there is a clear crossover between a rapid short-time dynamics towards a more slow long-time decay, notably visible for $\langle\hat{p}^2(t)\rangle$.

6.5 Effective mean-field theories

Mean-field descriptions [C5] of phase transitions often provide a first qualitative appreciation of cooperative effects in many-body systems. In the most simple form, they emerge by replacing the interaction terms by a self-consistently determined external field. In this section, we make a step more towards the understanding of the cavity and friction models, by interpreting their long-time behaviour as mean-field approximations of a many-body magnet, where the average position $m = \langle \hat{x} \rangle$ becomes the magnetisation. In the following, we set the bath temperature $T = 0$ and we take the *quantum spherical model* as a reference, whose equilibrium and non-equilibrium critical behaviour are already known in literature and share many qualitative features with more realistic models [235–243, C25, 244–252]. The quantum spherical model introduces the constraint $\langle \hat{x}^2 \rangle = 1$ to the one-body oscillator (6.1), making the angular frequency a time-dependent quantity,

$$\omega(t) = \frac{\hbar g}{2} \left(\langle \hat{a}^\dagger \hat{a}^\dagger \rangle + \langle \hat{a}\hat{a} \rangle + \langle \hat{a}^\dagger \hat{a} \rangle + 1 \right) . \tag{6.159}$$

The interpretation of this one-body problem as an effective mean-field approximation goes through the self-consistent magnetic field

$$B = \kappa \langle x \rangle = \kappa \sqrt{\frac{\hbar g}{2\omega}} \langle \hat{a}^\dagger + \hat{a} \rangle = \kappa \sqrt{\frac{2\hbar g}{\omega}}\, x_1 , \tag{6.160}$$

for the real constant $\kappa > 0$ and the real parameter x_1 to be determined. We also define

$$\langle \hat{a} \rangle = x_1 + \mathrm{i} x_2 , \qquad \langle \hat{a}\hat{a} \rangle = x_3 + \mathrm{i} x_4 , \qquad \langle \hat{a}^\dagger \hat{a} \rangle = x_5 , \tag{6.161}$$

where, by hypothesis, $x_2, \dots, x_5$ are real parameters. Below, the spherical constraint into Eq. (6.159) will be used to eliminate x_5. Since we are interested in the phase diagramme of the stationary state, we take the asymptotic value $\omega := \lim_{t\to\infty} \omega(t)$. In the next paragraphs, we briefly discuss the results, which come from the solution of the stationary equations of motion of the friction and cavity models (see Sec. 6.1.3).

6.5.1 Friction model

For the friction models, we find two distinct solutions, both independent on the damping constant γ, as it should be for a proper equilibrium state. The first solution coincides with a disordered, paramagnetic state with magnetisation $m =$

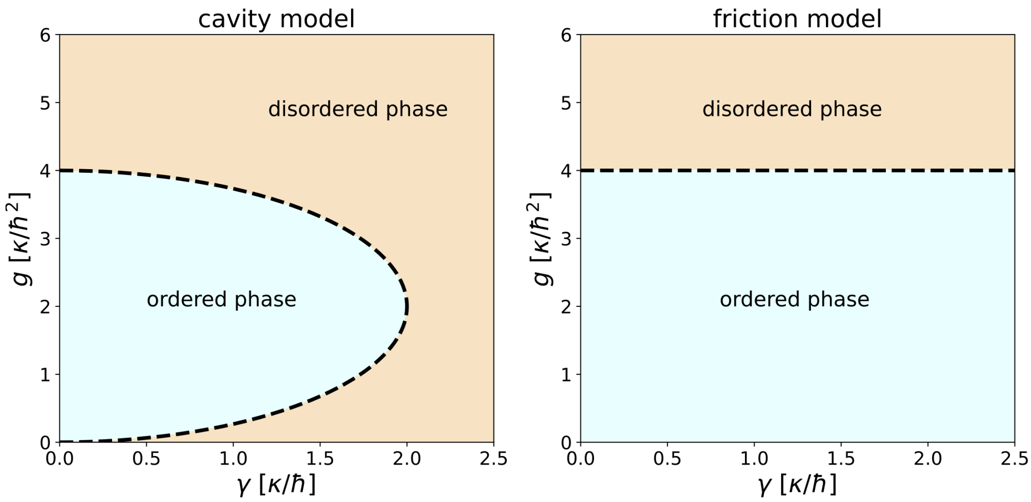

Figure 6.4: Mean-field phase diagrammes of a single quantum spherical spin at $T = 0$, for the cavity model (left) and the friction model (right).

0, $x_i = 0$, $\forall i \in \{1, ..., 5\}$ and $\omega = \omega_d = \hbar g/2$; the second one corresponds to an ordered, magnetic state with $x_1 \neq 0$ and $\omega = \omega_o = \sqrt{\kappa g}$. We find $x_2 = x_4 = 0$ and

$$m^2 = x_1^2 = \frac{1}{4\sqrt{g}}\left(\frac{2\sqrt{\kappa}}{\hbar} - \sqrt{g}\right) = x_3\,, \tag{6.162}$$

At the critical point $\omega_d = \omega_o$, we get the critical value $g_c = 4\kappa/\hbar^2$. In this way, the magnetization may be rewritten as

$$m^2 = \left(g_c^{1/2} - g^{1/2}\right)/4g^{1/2}\,, \tag{6.163}$$

such that the system is magnetically ordered for $g < g_c$ (see Fig. 6.4). Since close to criticality, one expects $m^2 \sim \left(g_c - g\right)^{2\beta}$, recovering the standard mean-field exponent $\beta = 1/2$.

6.5.2 Cavity model

Also for the cavity model, there are two different stationary solutions [253]. The first one for the disordered phase $x_i = 0$, $\forall i \in \{1, ..., 5\}$ and $\omega = \omega_d = \hbar g/2$. The second solution is expressed in terms of the damping constant γ and $\omega_o' = \sqrt{g\kappa - \gamma^2/4}$, where all the other coefficients $x_1, \dots, x_4$ are non-vanishing. The condition of criticality $\omega_d = \omega_o'$ implies two distinct solutions for $\gamma < 2\kappa/\hbar$, which leads to two distinct critical points [253],

$$g_{c,\pm}(\gamma) = \frac{2\kappa}{\hbar^2} \pm \sqrt{\frac{4\kappa^2}{\hbar^4} - \frac{\gamma^2}{\hbar^2}}\,. \tag{6.164}$$

In the limit $\gamma \to 0$, the upper critical point $\lim_{\gamma\to 0} g_{c,+}(\gamma) = g_c$ coincides with that one of the friction model; for a finite $\gamma < 2\kappa/\hbar$, we also find a lower critical point $g_{c,-}(\gamma)$, as shown in Fig. 6.4. The magnetisation is [253]

$$m^2 = x_1^2 = \frac{\gamma^2}{4\kappa g}\left(1 + \frac{4\omega^2}{\gamma}\right)\left(1 - \frac{\hbar g}{2\omega}\right), \tag{6.165}$$

which does not vanish only for $g_{c,-}(\gamma) < g < g_{c,+}(\gamma)$ (see Fig. 6.4). These re-entrant transitions are a purely kinetic effect and cannot characterise an equilibrium state.

As already discussed in Sec. 6.3, this example remarks that, contrary to the friction model, for non-vanishing external magnetic fields the cavity model does not guarantee the relaxation toward a proper equilibrium state.

6.6 Discussion and conclusion

The study carried out in this chapter is framed into the wide context of open markovian dynamics. The commonly used ab-initio approach derives the reduced dynamics from the microscopic system-bath(s) interactions. In this respect, the Lindblad evolution is a typical example of markovian dynamics which turns to be completely positive thanks to the initial uncorrelated state hypothesis. However, the need of complete positivity as dynamical postulate is controversial. In our study we bypass these difficulties by using a phenomenological formalism based on the Langevin equations, where a deterministic damping term and two stochastic noises encode the system-bath(s) interactions. The noises are specified by a set of physical requirements which, in this work, make the dynamics markovian. More specifically, we studied two simple but representative toy models based on the single quantum harmonic oscillator, namely the *friction model* and the *cavity model*, specified by Eqs. (6.4,6.5) and (6.6,6.7), respectively. The main results are summarised into Tab. 6.2.

The models present distinct friction terms and stochastic noises but verify the same physical criteria (A-D). In the classical limit $\hbar \to 0$, the friction model leads back the brownian motion of a particle in a confining harmonic potential. On the other hand, there is no known classical counterpart for the cavity model. From the quantum Langevin equations, we derived two effective master equations for the density operator, which are equivalent at the level of the one-point and two-point functions. The liouvillian is completely positive for the cavity model, but manifestly not completely positive for the friction model. We reformulated the master equations as a Fokker-Planck equation for the Wigner function, showing

	CAVITY MODEL	FRICTION MODEL
Ehrenfest theorem	✗	✓
Classical limit	?	Linearly damped harmonic oscillator subject to white noise
Complete positivity	✓	✗
Simple positivity	✓	✓ positive map only if either (i) initial state is not squeezed too much or (ii) for times t large enough
Dynamical behaviour	Only under-damped phase	Under-damped phase for $\gamma < 2\omega$ Over-damped phase for $\gamma > 2\omega$
Thermal equilibrium	✗	✓

Table 6.2: Comparison between cavity model and friction model.

that, for vanishing magnetic fields, both models evolve towards the same Gibbs thermal state.

Explicit solutions of the Fokker-Planck equation show the differences between the friction and cavity models. In particular, the relaxation behaviour is illustrated in Figs. 6.1, 6.2 and 6.3, where we prepared the system in some specific initial states, such as the ground state or coherent states. We explicitly showed the under-damped and over-damped regimes of the friction model, and the single under-damped regime of the cavity model. We also recast the two models as mean-field approximation of a magnetic system, which are distinguished through a determination of the stationary state in an external field and the ensuing phase transition (see Fig. 6.4). For weak damping $\gamma \ll 1$, both models reproduce the same phenomenology of time-dependent averages.

Formally, there is no obvious criterion to prefer the friction model over the cavity model, or any other model with different noises that satisfies the physical criteria (A-D). However, the 'natural requirement' of complete positivity is sometimes limiting to describe the dynamics of open quantum systems. This is strongly supported by the fact that, in the classical limit $\hbar \to 0$, complete positivity does not lead back to the motion of a damped particle subjected to harmonic potentials and white noises. Above all, even the Ehrenfest theorem is not verified (see Eqs. (6.6,6.7)).

This study paves the way to the many-body generalisation, notably the quantum spherical model. Even the comparison with the non-markovian quantum dynamics, e.g. [208, 244, 249, 252], may offer interesting working directions.

Chapter 7

Conditional no-jump dynamics of non-interacting quantum chains

Open quantum systems far from equilibrium continue to raise many physical challenges. One of the most common proposals to investigate the transport phenomena is to prepare a localised wave-packet and study its evolution along the chain. However, due to the coupling system-environment, e.g. Lindblad-type dissipators, accessing the dynamics may not be simple [254]. In the formalism of the quantum trajectories [62–66], quantum jumps may be pictorially viewed as the action of some detectors monitoring the exchange of particles between the system and the bath(s). The statistics of jumps is expressed by the theory of Full Counting Statistics [255–258].

The no-jump probabilities and the waiting-time distributions (WTDs) [167, 258, 259] are useful tools to access the statistics of the next jumps by the knowledge of the previous ones [258]. For instance, Ref. [167] is a precious example of how these techniques can be successfully applied. In Ref. [167], the author computed the WTDs for Gaussian-preserving Lindblad dynamics and, more specifically, for boundary driven chains of free fermions subject to single particle gain-loss processes at the edges. The work we present in this chapter aims to generalise the results of Ref. [167] from different perspectives. Firstly, we study the more general case of partial monitoring. In other terms, we associate to each quantum channel j a real number $\Gamma_j \in [0, 1]$ revealing how much the detection process is close to be ideal: $\Gamma_j = 1$ when the monitoring is perfect and any occurred quantum jump is detected and $\Gamma_j = 0$ when the channel j is not monitored at all. Hence, the conditional no-jump evolution is a dynamical map with the constraint of no jumps being detected; some jump events may be lost cause of the non-ideal efficiency of the monitoring apparatus. This study is clearly useful to experimentalists, where the monitoring efficiency is not ideal and may change with the work conditions. Second, we also contribute with the no-jump probability and not only the WTDs. In the context of partial monitoring, the no-jump probability $P_{\rm no}(t)$ is the probability of not detecting jumps in the time interval $[0,t]$, while the waiting-time distribution $W_k(t)$ is the probability distribution of detecting the first jump in the quantum channel k at time t. Third, we also derive results for particle non-conserving Hamiltonian operators and, fourth, we also study the bosonic case, which offers interesting applications in optomechanical systems [260].

In the first part of this chapter (Sec. 7.1), we define the no-jump dynamics, as well as the no-jump probabilities and the WTDs, generalising the definitions in Ref. [167] in light of non ideal measurements. In Sec. 7.2, we study two physical setups involving a single qubit, either incoherently or coherently driven, identifying oscillatory and non-oscillatory regimes. In Sec. 7.3, we focus on the many-body physics, considering a chain of free particles with one-body gain-loss processes. Using a Gaussian ansatz, we derived a Riccati differential equation for the correlation matrix, which gives access to the WTDs and the no-jump probabilities (Sec. 7.4). As an application (Sec. 7.5), we consider a chain of hopping fermions with nearest neighbour interactions and special absorption-emission channels. In Sec. 7.6 and Sec. 7.7, we generalise the results to particle non-conserving Hamiltonian operators (pairing terms). Finally, in Sec. 7.8 we study a specific example of no-jump dynamics involving a 2-site boundary driven fermionic/bosonic system. Our main findings are summarised in Sec. 7.9.

7.1 General framework

Let ρ be the density operator of a quantum system whose dynamics is generated by the Liouvillian $\mathcal{L}(\rho)$

$$\frac{\mathrm{d}\rho}{\mathrm{d}t} = \mathcal{L}(\rho) = -\mathrm{i}[H,\rho] + \mathcal{D}(\rho)\,, \tag{7.1}$$

where H denotes the Hamiltonian, $\mathcal{D}(\rho)$ is a Lindblad-type dissipator

$$\mathcal{D}(\rho) = \sum_k D_\rho[L_k] = \sum_k L_k\rho L_k^\dagger - \frac{1}{2}\{L_k^\dagger L_k,\rho\}\,, \tag{7.2}$$

with a generic set of jump operators L_k. In the quantum jump unravelling [63], the terms $L_k\rho L_k^\dagger$ represent quantum jumps and the dynamics can be viewed as a series of discrete jumps, followed by a smooth no-jump evolution (see Fig. 7.1). Each Lindblad operator L_k corresponds to a different channel where the jump might occur, which we assume can be directly linked to a click in a classical detector.

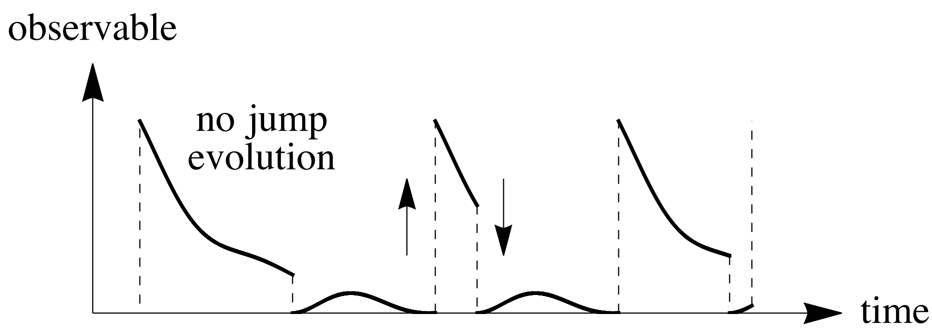

Figure 7.1: We illustrate a typical evolution along a quantum jump trajectory, as viewed from the perspective of a pictorial system observable. Abrupt jumps occur at random times and, in between, the observable evolves smoothly, governed by the so-called no-jump conditional evolution (7.5).

In this work, we study a simple but apparently unexplored scenario, where one can independently choose to measure each L_k with different efficiencies $\Lambda_k \in [0,1]$. In particular, $\Lambda_k = 1$ for perfect monitoring and $\Lambda_k = 0$ if the channel is not monitored at all. We split Eq. (7.1) as

$$\mathcal{L} = \mathcal{L}_0 + \mathcal{L}_1 \,, \tag{7.3}$$

where

$$\mathcal{L}_1(\rho) = \sum_k \mathcal{J}_k \rho = \sum_k \Lambda_k L_k \rho L_k^\dagger \,, \tag{7.4}$$

and each jump channel specified by the super-operator $\mathcal{J}_k$. The *conditional no-jump operator* is

$$\mathcal{L}_0(\rho) = -\,\mathrm{i}[H,\rho] + \sum_k \Big[(1-\Lambda_k) L_k \rho L_k^\dagger - \frac{1}{2}\{L_k^\dagger L_k, \rho\}\Big] \,. \tag{7.5}$$

If all jumps are perfectly monitored, $\Lambda_k = 1\ \forall k$, then $\mathcal{L}_0$ can also be written as

$$\mathcal{L}_0(\rho) = -\mathrm{i}\Big(H_\mathrm{e}\rho - \rho H_\mathrm{e}^\dagger\Big) \,, \tag{7.6}$$

where

$$H_e = H - \frac{\mathrm{i}}{2} \sum_k L_k^\dagger L_k \,, \tag{7.7}$$

is a non-Hermitian Hamiltonian.

In general, the solution of Eq. (7.1) is $\rho(t) = e^{\mathcal{L}t}\rho_0$, where ρ_0 is the initial state at time $t = 0$. $\rho(t) = e^{\mathcal{L}t}\rho_0$ is called the *unconditional dynamics*, since the full

Liouvillian $\mathcal{L}$ is ignorant whether jumps occur or not. Using the Dyson series, it is possible to expand the solution as

$$\begin{aligned}\rho(t) &= e^{\mathcal{L}_0 t}\rho_0 + \int_0^t dt_1 e^{\mathcal{L}_0(t-t_1)}\mathcal{L}_1 e^{\mathcal{L}_0 t_1}\rho_0 \\ &\quad + \int_0^t dt_2 \int_0^{t_2} dt_1 e^{\mathcal{L}_0(t-t_2)}\mathcal{L}_1 e^{\mathcal{L}_0(t_2-t_1)}\mathcal{L}_1 e^{\mathcal{L}_0 t_1}\rho_0 + \dots \,. \end{aligned} \tag{7.8}$$

The first term $e^{\mathcal{L}_0 t}\rho_0$ into Eq. (7.8) is the evolution conditioned on no jumps detected up to time t, the second one contains exactly one jump at time t_1 and so on [254, 261]. In this work, we focus on the first term, i.e. the conditional no-jump dynamics. Since $\mathcal{L}_0$ is not a proper Liouvillian, $\mathcal{L}_0$ is not trace preserving and the evolved state is not normalized. We define the unnormalized density matrix

$$\tilde{\rho}_{\rm no}(t) = e^{\mathcal{L}_0 t}\rho_0\,, \qquad \frac{d\tilde{\rho}_{\rm no}}{dt} = \mathcal{L}_0(\tilde{\rho}_{\rm no})\,. \tag{7.9}$$

If all channels are monitored ($\Lambda_k = 1$), this reduces to

$$\tilde{\rho}_{\rm no}(t) = e^{-\mathrm{i}H_e t}\rho_0 e^{\mathrm{i}H_e^\dagger t}, \tag{7.10}$$

which represents a non-Hermitian dynamics. The conditional evolution is indeed a very natural way of implementing non-Hermitian physics [262]. The trace of $\tilde{\rho}_{\rm no}(t)$ is precisely the *no-jump probability* $P_{\rm no}(t)$, which is the probability that no jumps are detected in $[0, t]$:

$$P_{\rm no}(t) = \mathrm{tr}\ \tilde{\rho}_{\rm no}(t)\,. \tag{7.11}$$

$P_{\rm no}(t)$ will play a key role in this chapter and most of our efforts will be addressed to evaluate this quantity. The normalised conditional state is

$$\rho_{\rm no}(t) = \frac{\tilde{\rho}_{\rm no}(t)}{P_{\rm no}(t)}\,. \tag{7.12}$$

Since the initial quantum state ρ_0 is normalised, the probability $P_{\rm no}(t)$ satisfies the boundary condition $P_{\rm no}(0) = 1$. In the limit $t \to \infty$, it may either tend to zero or a finite value. If $P_{\rm no}(\infty) = 0$ it means a jump must eventually occur. Conversely, $P_{\rm no}(\infty) \neq 0$ means it might never do. This may happen in particular scenarios where the system has a dark subspace, which is immune to the dissipator in Eq. (7.2).

The unconditional evolution of any quantum observable $\mathcal{O}$ can be derived from Eq. (7.1) and reads

$$\frac{\mathrm{d}\langle\mathcal{O}\rangle}{\mathrm{d}t} = \langle\mathcal{L}^{\dagger}(\mathcal{O})\rangle\,, \tag{7.13}$$

where

$$\mathcal{L}^{\dagger}(\mathcal{O}) = \mathrm{i}[H,\mathcal{O}] + \sum_k \left[L_k^{\dagger}\mathcal{O}L_k - \frac{1}{2}\{L_k^{\dagger}L_k,\mathcal{O}\}\right], \tag{7.14}$$

is the so-called adjoint dissipator and $\langle\mathcal{O}\rangle$ denotes the expectation value of the operator $\mathcal{O}$ over the unconditional normalised state $\rho(t)$. We can also write down a similar equation for the conditional expectation value

$$\langle\mathcal{O}\rangle_{\mathrm{no}} := \frac{\mathrm{tr}(\mathcal{O}\tilde{\rho}_{\mathrm{no}}(t))}{P_{\mathrm{no}}(t)}\,. \tag{7.15}$$

Thanks to Eqs. (7.5,7.15), one obtains

$$\frac{\mathrm{d}\langle\mathcal{O}\rangle_{\mathrm{no}}}{\mathrm{d}t} = \langle\mathcal{L}^{\dagger}(\mathcal{O})\rangle_{\mathrm{no}} - \sum_k \Lambda_k\Big[\langle L_k^{\dagger}\mathcal{O}L_k\rangle_{\mathrm{no}} - \langle\mathcal{O}\rangle_{\mathrm{no}}\langle L_k^{\dagger}L_k\rangle_{\mathrm{no}}\Big]. \tag{7.16}$$

The first term into Eq. (7.16) is the same as in the unconditional evolution (7.13), while the others are new contributions stemming from monitoring the jumps.

The quantity $\langle L_k^{\dagger}L_k\rangle_{\mathrm{no}}(t)$ provides the no-jump probability. In fact, if we differentiate Eq. (7.11) and we substitute $\mathcal{L}_0 = \mathcal{L} - \mathcal{L}_1$, we obtain

$$\frac{\mathrm{d}P_{\mathrm{no}}}{\mathrm{d}t} = \mathrm{tr}\Big((\mathcal{L}-\mathcal{L}_1)\tilde{\rho}_{\mathrm{no}}(t)\Big)\,. \tag{7.17}$$

Since $\mathcal{L}$ is the full Liouvillian then $\mathrm{tr}(\mathcal{L}\tilde{\rho}_{\mathrm{no}}(t)) = 0$. Therefore Eq. (7.17) becomes

$$\frac{\mathrm{d}P_{\mathrm{no}}}{\mathrm{d}t} = -\,\mathrm{tr}(\mathcal{L}_1\tilde{\rho}_{\mathrm{no}})\,. \tag{7.18}$$

Using Eq. (7.4) and including the proper state normalization, we find

$$\frac{\mathrm{d}P_{\mathrm{no}}}{\mathrm{d}t} = -P_{\mathrm{no}}\sum_k \left[\Lambda_k\langle L_k^{\dagger}L_k\rangle_{\mathrm{no}}\right]. \tag{7.19}$$

Assuming that $\langle L_k^{\dagger}L_k\rangle_{\mathrm{no}}$ is known, the solution of Eq. (7.19) is

$$P_{\mathrm{no}}(t) = \exp\left\{-\int_0^t \mathrm{d}t'\beta(t')\right\}, \tag{7.20}$$

$$\beta(t) = \sum_k \Lambda_k\langle L_k^{\dagger}L_k\rangle_{\mathrm{no}}(t)\,. \tag{7.21}$$

This result relates the no-jump probability with the expectation values $\langle L_k^\dagger L_k\rangle_{\rm no}$, which is given by Eq. (7.16). Eq. (7.20) can also be used to establish a criteria for the existence of a dark subspace.

Assuming the long time limit for β exists, let β^∞ denote the asymptotic value: $\beta^\infty = \lim_{t\to\infty}\beta(t)$. Hence, the long behaviour of the no-jump probability is $P_{\rm no}(t) \sim e^{-\beta^\infty t}$. This implies that $P_{\rm no}(\infty) = 0$ if at least one term $\lim_{t\to\infty}\Lambda_k\langle L_k^\dagger L_k\rangle_{\rm no}(t) = \Lambda_k\langle L_k^\dagger L_k\rangle_{\rm no}^\infty \neq 0$. Notice that the existence of dark subspaces is not only a property of the master equation (7.1), but also of the monitoring efficiencies Λ_k. As a sanity check, if nothing is monitored ($\Lambda_k = 0\ \forall k$) we simply find $P_{\rm no}(t) = 1$.

Computing the no-jump probability $P_{\rm no}(t)$ is crucial to have access to the waiting-time distribution $W_k(t)$ which, in the spirit of the Dyson series (7.8), is the probability distribution of detecting the first jump in the channel k at time t. The WTDs play a key role in the study of transport along quantum chains, e.g. boundary driven spin chains, and are defined as

$$\begin{aligned} W_k(t) &:= \operatorname{tr}\left\{\mathcal{J}_k e^{\mathcal{L}_0 t}(\rho_0)\right\}, \\ &= P_{\rm no}(t)\operatorname{tr}\left\{\mathcal{J}_k\,\rho_{\rm no}(t)\right\}, && (7.22) \\ &= \Lambda_k P_{\rm no}(t)\langle L_k^\dagger L_k\rangle_{\rm no}(t), && (7.23) \end{aligned}$$

For the normalisation condition,

$$\sum_k \int_0^\infty W_k(t)\,{\rm d}t = 1\,. \tag{7.24}$$

From these results we conclude that both $P_{\rm no}(t)$ and $W_k(t)$ can be computed by the conditional evolution of the averages $\langle L_k^\dagger L_k\rangle_{\rm no}(t)$.

7.2 Qubit example

In this section, we shall use the results in Sec. 7.1 for a single qubit under different absorbtion and emission channels. Even for such a simple systems, the conditional no-jump dynamics is quite involved.

7.2.1 Rabi drive with a single emission channel

Let's consider a single qubit with Rabi drive

$$H = \frac{\Omega}{2}\sigma_x\,, \tag{7.25}$$

where $\Omega > 0$ and the σ's are the Pauli matrices. Assume a single emission channel described by the Lindblad operator $L = \sqrt{\Gamma}\sigma_-$, with jump frequency $\Gamma > 0$ and efficiency Λ^-. The unconditional dynamics is generated by the Liouvillian

$$\mathcal{L}(\rho) = -\mathrm{i}\frac{\Omega}{2}[\sigma_x, \rho] + \Gamma\Big[\sigma_-\rho\sigma_+ - \frac{1}{2}\{\sigma_+\sigma_-, \rho\}\Big]. \tag{7.26}$$

Now, we would like to explore the conditional dynamics by applying Eq. (7.16). For the dynamics (7.26), the natural operators to evaluate are the population $\sigma_+\sigma_-$ and the coherence σ_-. For simplicity, let's define the conditional expectation values $q = \langle\sigma_+\sigma_-\rangle_{\mathrm{no}}$ and $c = \langle\sigma_-\rangle_{\mathrm{no}}$. Eq. (7.16) then yields a system of two coupled non-linear equations

$$\frac{\mathrm{d}q}{\mathrm{d}t} = \frac{\mathrm{i}\Omega}{2}(c - c^*) - \Gamma q + \Gamma\Lambda^- q^2\,, \tag{7.27}$$
$$\frac{dc}{dt} = \frac{\mathrm{i}\Omega}{2}(2q-1) - \frac{\Gamma}{2}c + \Gamma\Lambda^- cq\,. \tag{7.28}$$

Solving the coupled differential equations (7.27,7.28), we can immediately obtain the no-jump probability (7.20) with

$$\beta(t) = \Lambda^-\Gamma q(t)\,. \tag{7.29}$$

Suppose to prepare the system in the eigenstate $|\downarrow\rangle_z$ of σ_z: $\sigma_z\,|\downarrow\rangle_z = -|\downarrow\rangle_z$. The parameters (Ω, Γ) affect the no-jump dynamics in a non-trivial way, but Eqs. (7.27, 7.28) clearly show that the steady state, if it exists, is only determined by the rate $r = \Gamma/\Omega > 0$.

Fig. 7.2 shows the evolution of $q(t)$ (left column) and $|c(t)|$ (right column) as a function of time for $\Omega = 1$ and different values of the rate r. In the next paragraphs, we shall discuss the results for different values of the monitoring efficiency Λ^-.

The unconditional dynamics ($\Lambda^- = 0$; no monitoring) shows the typical behaviour of a damped oscillator and always relaxes to a steady-state,

$$q^\infty_{\Lambda^-=0} = \frac{1}{2+r^2}\,, \tag{7.30}$$
$$|c^\infty_{\Lambda^-=0}| = r q^\infty_{\Lambda^-=0}\,. \tag{7.31}$$

The general case $\Lambda^- \in (0,1)$ is more difficult but still shares the same features with $\Lambda^- = 0$. The oscillations are damped and $q^\infty_{\Lambda^-}$ is the real and positive solution of the cubic equation

$$2r^2(\Lambda^-)^2(q^\infty_{\Lambda^-})^3 - 3\Lambda^- r^2(q^\infty_{\Lambda^-})^2 + (r^2+2)q^\infty_{\Lambda^-} - 1 = 0\,, \tag{7.32}$$

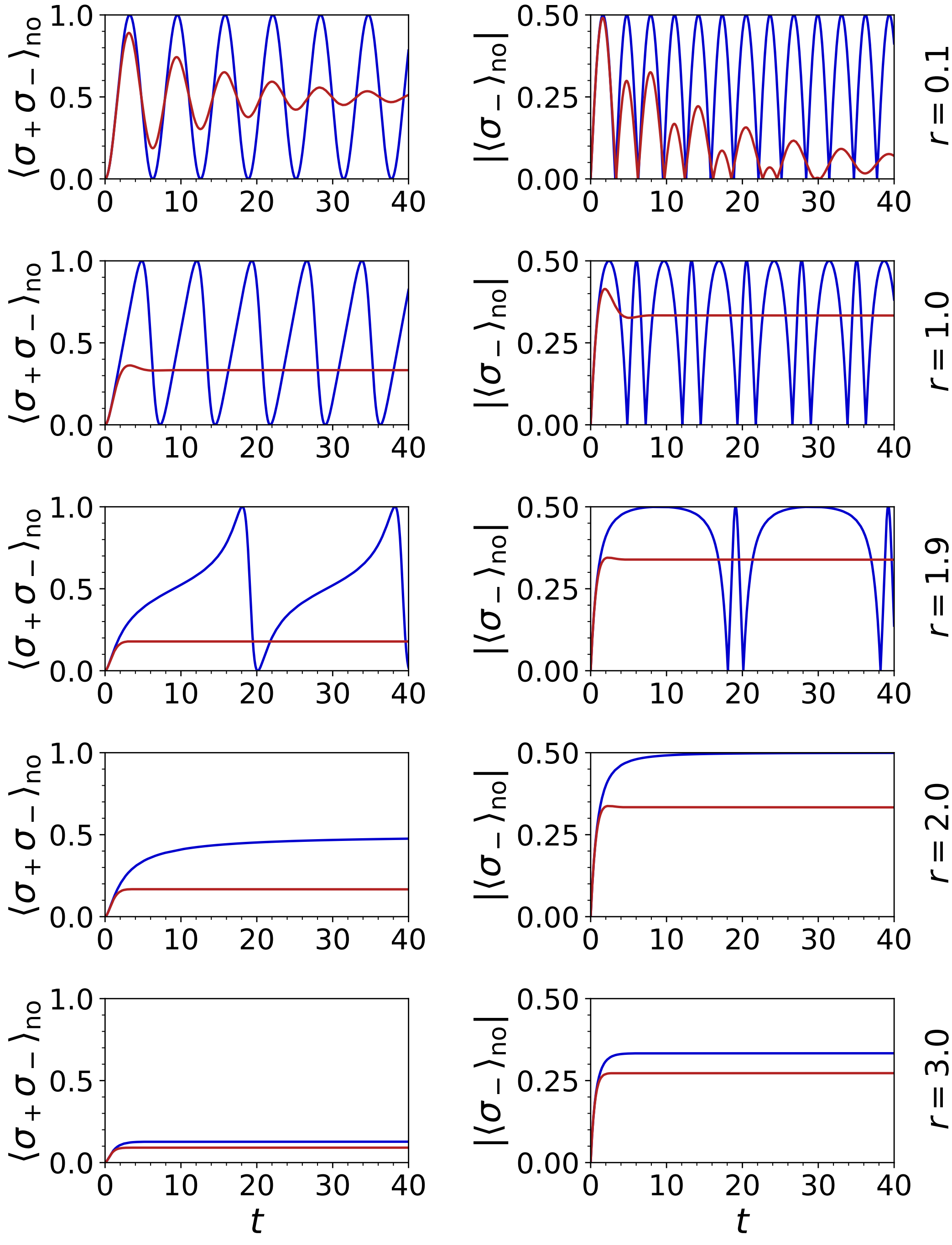

Figure 7.2: $q = \langle\sigma_+\sigma_-\rangle_{\rm no}$ (left column) and $|c| = |\langle\sigma_-\rangle_{\rm no}|$ (right column) as a function of time for the conditional ($\Lambda = 1$; blue line) and unconditional ($\Lambda = 0$; red line) cases. The dynamics of the qubit is governed by the master equation (7.26). Each row is for $\Omega = 1$ and a different value of the ratio $r = \Gamma/\Omega = 0.1, 1.0, 1.9, 2.0, 3.0$ (from top to bottom).

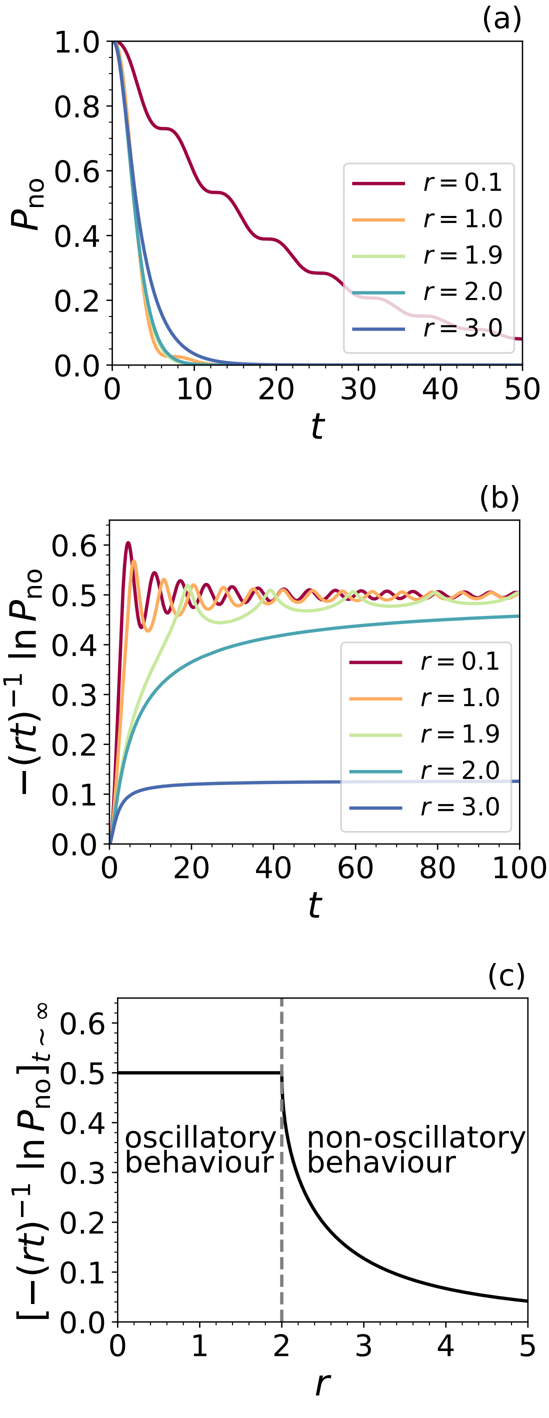

Figure 7.3: (a) Time evolution of the no-jump probability $P_{\rm no}$ for $\Lambda^- = 1.0$ (perfect monitoring), $\Omega = 1$ and $r = 0.1, 1.0, 1.9, 2.0, 3.0$; ($b$) time evolution of $-(rt)^{-1} \ln P_{\rm no}(t)$; ($c$) $\alpha(r)/r$ vs r (see Eq. (7.36)).

with

$$|c^{\infty}_{\Lambda^-}| = r q^{\infty}_{\Lambda^-}(1 - \Lambda^- q^{\infty}_{\Lambda^-}) \,. \tag{7.33}$$

Conversely, the full monitoring case ($\Lambda^- = 1$) contains more interesting physics. We can identify a critical rate $r_c = 2$ which distinguishes two different regimes. If $r < r_c$, $q(t)$ and $|c(t)|$ are periodic functions, the system exhibits an oscillatory phase and never relaxes; if $r \geq r_c$, the oscillations are suppressed and the system relaxes toward the stationary state with

$$q^{\infty}_{\Lambda^-=1} = \frac{1}{2} - \frac{1}{2}\sqrt{1 - \frac{4}{r^2}} \,, \tag{7.34}$$

$$|c^{\infty}_{\Lambda^-=1}| = r q^{\infty}_{\Lambda^-=1}(1 - q^{\infty}_{\Lambda^-=1}) \,. \tag{7.35}$$

In Fig. 7.3 (a), we show the no-jump probability $P_{\mathrm{no}}(t)$ as a function of time for $\Lambda^- = 1$, $\Omega = 1$ and several values of the parameter r. Under these hypothesis, in the long-time limit, the no-jump probability reads

$$P_{\mathrm{no}} \sim e^{-\alpha(r)t} \,, \qquad \alpha(r) = \begin{cases} r/2 \,, & r < r_c \\ r q^{\infty}_{\Lambda^-=1} \,, & r \geq r_c \end{cases} \tag{7.36}$$

Fig. 7.3 (b) illustrates the time evolution of $-(rt)^{-1} \ln P_{\mathrm{no}}(t)$ and the differences between the oscillatory phase $r < r_c = 2$ and the damped phase $r > r_c$. Finally, in Fig. 7.3 (c), we plot $\alpha(r)/r$ as a function of r, which showcases the sharp transition at $r = r_c = 2$.

7.2.2 Incoherent dynamics with emission and absorption

Next we consider a two-level system with trivial Hamiltonian

$$H = \frac{\Omega}{2}\sigma_z \,, \tag{7.37}$$

interacting with a fermionic bath described by two jump operators $L_- = \sqrt{\Gamma^-}\sigma_-$ and $L_+ = \sqrt{\Gamma^+}\sigma_+$ representing, respectively, the emission and the absorption of an excitation. We shall adopt the following parametrization:

$$\Gamma^+ = \Gamma f, \qquad \Gamma^- = \Gamma(1 - f), \tag{7.38}$$

where $\Gamma > 0$ is the coupling strength to the reservoir and $f = (e^{\Omega/T} + 1)^{-1} \in [0, 1]$ is the Fermi-Dirac distribution of the reservoir (with T being the temperature and $k_B = 1$). We again apply Eq. (7.16) with $\mathcal{O} = \sigma_+\sigma_-$, but now there are two

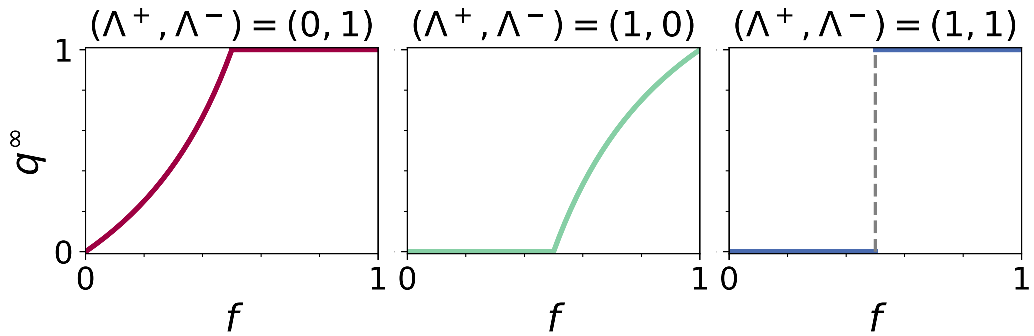

Figure 7.4: Steady-state population q^∞ of the conditional dynamics (7.39) as a function of the Fermi-Dirac occupation f, for different choices of (Λ^+, Λ^-).

monitoring efficiencies, which we denote as Λ^- and Λ^+. The qubit population $q = \langle\sigma_+\sigma_-\rangle_{\rm no}$ is described by the non-linear equation

$$\frac{1}{\Gamma}\frac{\mathrm{d}q}{\mathrm{d}t} = f - q + (1-f)\Lambda^- q^2 - f\Lambda^+(1-q)^2. \tag{7.39}$$

Plugging the solution in Eq (7.20) also yields the no-jump probability in the form (7.20), with

$$\beta(t) = \Gamma(1-f)\Lambda^- q(t) + \Gamma f\Lambda^+(1-q(t)). \tag{7.40}$$

The steady state is determined by $\frac{\mathrm{d}q}{\mathrm{d}t} = 0$. From Eq. (7.39), one gets

$$\begin{aligned} q^\infty =& \frac{\sqrt{(2f\Lambda^+-1)^2 - 4f(1-\Lambda^+)(\Lambda^- - f(\Lambda^-+\Lambda^+))}}{2(f\Lambda^- + f\Lambda^+ - \Lambda^-)} \\ &+ \frac{2f\Lambda^+-1}{2(f\Lambda^- + f\Lambda^+ - \Lambda^-)}, \end{aligned} \tag{7.41}$$

where the result is independent of Γ. In the next lines, we discuss the cases $\Lambda^+, \Lambda^- \in \{0,1\}$ (see Fig. 7.4). If $\Lambda^+ = \Lambda^- = 0$ we get the unconditional steady-state $q^\infty = f$. If we only monitor emissions, but not absorptions ($\Lambda^- = 1$, $\Lambda^+ = 0$),

$$q^\infty = \begin{cases} \frac{f}{1-f} & f < 1/2 \\ 1 & f > 1/2 \end{cases}, \tag{7.42}$$

which is the red curve in Fig. 7.4. The rational is that, since the conditional evolution does not allow to detect emission events, it is more likely that there is an excitation present, leading to a population $q^\infty \geqslant f$. In the opposite scenario ($\Lambda^+ = 1$, $\Lambda^- = 0$) we get

$$q^\infty = \begin{cases} 0 & f < 1/2 \\ \frac{2f-1}{f} & f > 1/2 \end{cases}, \tag{7.43}$$

which is the green curve in Fig. 7.4. In this case, the observer knows with certainty that no excitations can be absorbed, leading to a population $q^\infty \leqslant f$, which is lower than in the unconditional case. Finally, if $\Lambda^- = \Lambda^+ = 1$, we get a step function (blue curve), which reflects the non-trivial interplay of conditioning on both channels.

7.3 No-jump dynamics of non-interacting particles

The previous examples show that, even for a single qubit, the conditional no-jump dynamics is quite involved. In order to provide further analytical insights, we now study the conditional dynamics of many-body one dimensional systems with Gaussian-preserving dynamics, i.e. single particle gain-loss processes.

Let's consider a L-site quantum chain, either bosonic or fermionic. The creation and annihilation operators verify the commutation/anti-commutation rules

$$\{c_i, c_j^\dagger\} = \delta_{ij}\,, \quad \{c_i, c_j\} = 0\,, \qquad \text{fermions} \tag{7.44}$$

$$\left[c_i, c_j^\dagger\right] = \delta_{ij}\,, \quad \left[c_i, c_j\right] = 0\,. \qquad \text{bosons} \tag{7.45}$$

By hypothesis, the system is subject to the Lindblad master equation (7.1) with dissipator of the form

$$\mathcal{D}(\rho) = \sum_{i=1}^{L} \Gamma_i^- D_\rho[L_i] + \Gamma_i^+ D_\rho[L_i^\dagger]\,. \tag{7.46}$$

The jump rates $\Gamma_i^\pm \geqslant 0$ and the operators L_i are assumed to be linear in the creation-annihilation operators, that is, $\mathbf{L} = \boldsymbol{\alpha}^\dagger \mathbf{c}$ for $\mathbf{c}^\dagger = (c_1^\dagger, \dots, c_L^\dagger)$ and some unitary matrix $\boldsymbol{\alpha}$. This hypothesis makes the dynamics Gaussian preserving. In terms of the $\mathbf{c}$'s operators, the dissipator (7.46) reads

$$\mathcal{D}(\rho) = \sum_{i=1}^{L} (\gamma^-)_{ij} \widetilde{D}_\rho[c_j, c_i^\dagger] + (\gamma^+)_{ij} \widetilde{D}_\rho[c_i^\dagger, c_j]\,, \tag{7.47}$$

where $\boldsymbol{\gamma}^- = \boldsymbol{\alpha}\boldsymbol{\Gamma}^-\boldsymbol{\alpha}^\dagger$, $\boldsymbol{\gamma}^+ = \boldsymbol{\alpha}\boldsymbol{\Gamma}^+\boldsymbol{\alpha}^\dagger$ and

$$\widetilde{D}_\rho[A, B] = A\rho B - \frac{1}{2}\{BA, \rho\}\,, \tag{7.48}$$

for any Hilbert operators A, B. If the diagonal matrices $\boldsymbol{\Lambda}^+$, $\boldsymbol{\Lambda}^-$ quantify the monitoring efficiencies related to the Lindblad operators L_i, the no-jump super-operator $\mathcal{L}_0$ becomes

$$\begin{aligned}\mathcal{L}_0(\rho) &= -\mathrm{i}[H,\rho] + \sum_{i=1}^{L}\Big[[\boldsymbol{\gamma}^-(\mathbb{1}-\boldsymbol{\lambda}^-)]_{ij}c_j\rho c_i^\dagger - \frac{(\boldsymbol{\gamma}^-)_{ij}}{2}\{c_i^\dagger c_j,\rho\}\Big] \\ &\quad + \sum_{i=1}^{L}\Big[[\boldsymbol{\gamma}^+(\mathbb{1}-\boldsymbol{\lambda}^+)]_{ij}c_i^\dagger\rho c_j - \frac{(\boldsymbol{\gamma}^+)_{ij}}{2}\{c_j c_i^\dagger,\rho\}\Big]. \end{aligned} \tag{7.49}$$

where $\boldsymbol{\lambda}^+ = \boldsymbol{\alpha}\boldsymbol{\Lambda}^+\boldsymbol{\alpha}^\dagger$, $\boldsymbol{\lambda}^- = \boldsymbol{\alpha}\boldsymbol{\Lambda}^-\boldsymbol{\alpha}^\dagger$ and H is any free particle Hamiltonian.

The goal of the next sections is to compute the normalized no-jump density matrix $\rho_{\mathrm{no}}(t)$ from Eq. (7.49). In particular, we start from $H = \sum_{ij} h_{ij}c_i^\dagger c_j$ and then we shall generalise the dynamics to particle non-conserving Hamiltonian operators. As we shall see, the pairing terms make the dynamics more involved and computationally expensive.

7.4 No-jump dynamics without pairing terms - fermionic and bosonic chains

In this section, we shall study the conditional no-jump evolution (7.49) with the quadratic Hamiltonian

$$H = \mathbf{c}^\dagger\mathbf{h}\mathbf{c}\,. \qquad \mathbf{h} = \mathbf{h}^\dagger\,, \tag{7.50}$$

where the $\mathbf{c}$'s verify either the fermionic or bosonic algebra. For the moment, we do not include pair creation terms in Eq. (7.50), which will be discussed below, in Sec. 7.6 and Sec. 7.7.

7.4.1 Full monitoring

The most naive case is when all channels are perfectly monitored, that is $\boldsymbol{\Lambda}^+ = \boldsymbol{\Lambda}^- = \mathbb{1}$. The no-jump Liouvillian (7.49) reduces to

$$\mathcal{L}_0(\rho) = -\mathrm{i}[H,\rho] - \frac{1}{2}\sum_{ij}(\boldsymbol{\gamma}^- \mp \boldsymbol{\gamma}^+)_{ij}\{c_i^\dagger c_j,\rho\} - \mathrm{tr}(\boldsymbol{\gamma}^+)\rho\,, \tag{7.51}$$

where the $-$ sign is for fermions and the $+$ sign for bosons. Since it is possible to solve simultaneously the fermionic and bosonic cases with minimal modifications, in this chapter the sign on top will refer to the fermionic case and the sign on bottom to the bosonic one. Following the prescriptions in Sec. 7.1, the dynamics generated by Eq. (7.6) is governed by an effective non-Hermitian Hamiltonian

$$H_{\mathrm{e}} = \sum_{ij} (\mathbf{h}_{\mathrm{e}})_{ij} c_i^\dagger c_j - \mathrm{i}\,\mathrm{tr}(\boldsymbol{\gamma}^+)/2\,, \tag{7.52}$$

where

$$\mathbf{h}_{\mathrm{e}} = \mathbf{h} - \frac{\mathrm{i}}{2}(\boldsymbol{\gamma}^- \mp \boldsymbol{\gamma}^+)\,. \tag{7.53}$$

7.4.2 Dynamics under partial monitoring

In this section, we address the problem of the conditional dynamics under partial monitoring $\boldsymbol{\lambda}^+, \boldsymbol{\lambda}^- \neq \mathbb{1}$, where the no-jump Liouvillian takes the form (7.49). Differently from the full monitoring case, we need additional hypotheses on the initial state.

As we already stressed before, the Lindblad dissipator (7.47) has been carefully chosen to be Gaussian preserving. Therefore, assuming the initial state ρ_0 is a Gaussian state, the density operator at time t is

$$\rho(t) := e^{\mathcal{L}t}(\rho_0) = \frac{e^{-\mathbf{c}^\dagger \cdot \mathbf{M}_t \cdot \mathbf{c}}}{Z_t}\,, \tag{7.54}$$

where

$$Z_t = \mathrm{tr}\Big(e^{-\mathbf{c}^\dagger \cdot \mathbf{M}_t \cdot \mathbf{c}}\Big) = [\det(\mathbb{1} \pm e^{-\mathbf{M}_t})]^{\pm 1}\,, \tag{7.55}$$

$$\mathbf{M}_t = \ln\left(\frac{\mathbb{1} \mp \mathbf{C}}{\mathbf{C}}\right), \tag{7.56}$$

and $(\mathbf{C})_{ij} = \mathrm{tr}\Big\{c_j^\dagger c_i\, \rho(t)\Big\} = \langle c_j{}^\dagger c_i \rangle(t)$ is the correlation matrix, which is supposed to be invertible. The unconditional dynamics is described by a Lyapunov equation for the correlation matrix $\mathbf{C}$ [A2, 202],

$$\frac{\mathrm{d}\mathbf{C}}{\mathrm{d}t} = -(\mathbf{W}\mathbf{C} + \mathbf{C}\mathbf{W}^\dagger) + \boldsymbol{\gamma}^+\,, \tag{7.57}$$

with

$$\mathbf{W} = \mathrm{i}\mathbf{h} + (\boldsymbol{\gamma}^- \pm \boldsymbol{\gamma}^+)/2\,. \tag{7.58}$$

However, the goal is to solve the more general non trace-preserving dynamics (7.49). Here we shall demonstrate that (7.49) is solved by a Gaussian ansatz or, more precisely, that

$$\tilde{\rho}_{\mathrm{no}}(t) := e^{\mathcal{L}_0 t}(\rho_0) = \frac{e^{-\mathbf{c}^\dagger \cdot \mathbf{M}_t^{\mathrm{no}} \cdot \mathbf{c}}}{\zeta_t}, \tag{7.59}$$

for some matrix $\mathbf{M}_t^{\text{no}}$ and some c-number ζ_t, which must satisfy specific differential equations, to be determined. The properly normalized state is then

$$\rho_{\text{no}}(t) := \frac{\tilde{\rho}_{\text{no}}(t)}{P_{\text{no}}(t)} = \frac{e^{-\mathbf{c}^\dagger \cdot \mathbf{M}_t^{\text{no}} \cdot \mathbf{c}}}{Z_t}, \tag{7.60}$$

$$Z_t = \operatorname{tr}\left(e^{-\mathbf{c}^\dagger \cdot \mathbf{M}_t^{\text{no}} \cdot \mathbf{c}}\right) = [\det(\mathbb{1} \pm e^{-\mathbf{M}_t^{\text{no}}})]^{\pm 1}. \tag{7.61}$$

The operator ρ_{no} is independent on ζ_t, but the knowledge of ζ_t is still relevant, since it determines the no-jump probability

$$P_{\text{no}}(t) = \frac{Z_t}{\zeta_t}. \tag{7.62}$$

In this paragraph, we shall prove that the ansatz (7.59) is a solution of Eq. (7.49). Therefore, the evolution of the no-jump operator (7.59) is specified by two independent differential equations for ζ_t and the conditional covariance matrix

$$\begin{aligned}(\mathbf{C}_{\text{no}})_{ij} &= \operatorname{tr}\left\{c_j^\dagger c_i\, \rho_{\text{no}}(t)\right\} = \langle c_j{}^\dagger c_i \rangle_{\text{no}}(t), \\ &= [(e^{\mathbf{M}_t^{\text{no}}} \pm \mathbb{1})^{-1}]_{ij}. \end{aligned}\tag{7.63}$$

Proof

The starting point is the Baker-Campbell-Hausdorff formula,

$$\frac{\mathrm{d}e^{K(t)}}{\mathrm{d}t} = \left\{\frac{\mathrm{d}K}{\mathrm{d}t} + \frac{1}{2!}\left[K, \frac{\mathrm{d}K}{\mathrm{d}t}\right] + \frac{1}{3!}\left[K, \left[K, \frac{\mathrm{d}K}{\mathrm{d}t}\right]\right] + \ldots\right\} e^K, \tag{7.64}$$

for any Hilbert operator K. Moreover, for any $L \times L$ matrix $\mathbf{A}, \mathbf{B}$,

$$[\mathbf{c}^\dagger \cdot \mathbf{A} \cdot \mathbf{c},\ \mathbf{c}^\dagger \cdot \mathbf{B} \cdot \mathbf{c}] = \mathbf{c}^\dagger \cdot [\mathbf{A}, \mathbf{B}] \cdot \mathbf{c}, \tag{7.65}$$

for both bosonic and fermionic cases. Combining the Baker-Campbell-Hausdorff formula (7.64), the Gaussian ansatz (7.59) and the result (7.65), we get

$$\frac{\mathrm{d}}{\mathrm{d}t} e^{-\mathbf{c}^\dagger \cdot \mathbf{M}_t^{\text{no}} \cdot \mathbf{c}} = \mathbf{c}^\dagger \cdot \left(\frac{\mathrm{d}e^{-\mathbf{M}_t^{\text{no}}}}{\mathrm{d}t} e^{\mathbf{M}_t^{\text{no}}}\right) \mathbf{c}\; e^{-\mathbf{c}^\dagger \cdot \mathbf{M}_t^{\text{no}} \cdot \mathbf{c}}. \tag{7.66}$$

Hence, the no-jump unnormalised state reads

$$\frac{\mathrm{d}\tilde{\rho}_{\text{no}}}{\mathrm{d}t} = \left[\mathbf{c}^\dagger \cdot \left(\frac{\mathrm{d}e^{-\mathbf{M}_t^{\text{no}}}}{\mathrm{d}t} e^{\mathbf{M}_t^{\text{no}}}\right) \mathbf{c} - \frac{\mathrm{d}}{\mathrm{d}t} \ln \zeta_t\right] \tilde{\rho}_{\text{no}}. \tag{7.67}$$

In order to compute $\mathcal{L}_0(\tilde{\rho}_{\rm no})$, we use the Baker-Campbell-Hausdorff formula (7.64) to get

$$\begin{aligned} e^{-\mathbf{c}^\dagger\cdot\mathbf{M}_t^{\rm no}\cdot\mathbf{c}}\mathbf{c} &= (e^{\mathbf{M}_t^{\rm no}}\mathbf{c})\, e^{-\mathbf{c}^\dagger\cdot\mathbf{M}_t^{\rm no}\cdot\mathbf{c}}\,, && (7.68)\\ e^{-\mathbf{c}^\dagger\cdot\mathbf{M}_t^{\rm no}\cdot\mathbf{c}}\mathbf{c}^\dagger &= (\mathbf{c}^\dagger e^{-\mathbf{M}_t^{\rm no}})\, e^{-\mathbf{c}^\dagger\cdot\mathbf{M}_t^{\rm no}\cdot\mathbf{c}}\,, && (7.69)\end{aligned}$$

to push the factors of $e^{-\mathbf{c}^\dagger\cdot\mathbf{M}_t^{\rm no}\cdot\mathbf{c}}$ to the right. This leads to the following list of factors:

$$\begin{aligned} [H,\tilde{\rho}_{\rm no}] &= \mathbf{c}^\dagger\cdot\left(\mathbf{h}-e^{-\mathbf{M}_t^{\rm no}}\mathbf{h}e^{\mathbf{M}_t^{\rm no}}\right)\cdot\mathbf{c}\,\tilde{\rho}_{\rm no}\,, && (7.70)\\ \sum_{ij}[\boldsymbol{\gamma}^-(\mathbb{1}-\boldsymbol{\lambda}^-)]_{ij}c_j\tilde{\rho}_{\rm no}c_i^\dagger &= \mp\mathbf{c}^\dagger\cdot\left(e^{-\mathbf{M}_t^{\rm no}}\boldsymbol{\gamma}^-(\mathbb{1}-\boldsymbol{\lambda}^-)\right)\cdot\mathbf{c}\,\tilde{\rho}_{\rm no} \\ &\quad +\mathrm{tr}\left(\boldsymbol{\gamma}^-(\mathbb{1}-\boldsymbol{\lambda}^-)e^{-\mathbf{M}_t^{\rm no}}\right)\tilde{\rho}_{\rm no}\,, && (7.71)\\ \sum_{ij}(\boldsymbol{\gamma})^-_{ij}\{c_i^\dagger c_j,\tilde{\rho}_{\rm no}\} &= \mathbf{c}^\dagger\cdot\left[\boldsymbol{\gamma}^-+e^{-\mathbf{M}_t^{\rm no}}\boldsymbol{\gamma}^-e^{\mathbf{M}_t^{\rm no}}\right]\cdot\mathbf{c}\,\tilde{\rho}_{\rm no}\,, && (7.72)\\ \sum_{ij}[\boldsymbol{\gamma}^+(\mathbb{1}-\boldsymbol{\lambda}^+)]_{ij}c_i^\dagger\tilde{\rho}_{\rm no}c_j &= \mathbf{c}^\dagger\cdot\left(\boldsymbol{\gamma}^+(\mathbb{1}-\boldsymbol{\lambda}^+)e^{\mathbf{M}_t^{\rm no}}\right)\cdot\mathbf{c}\,\tilde{\rho}_{\rm no}\,, && (7.73)\\ \sum_{ij}(\boldsymbol{\gamma})^+_{ij}\{c_jc_i^\dagger,\tilde{\rho}_{\rm no}\} &= \mp\mathbf{c}^\dagger\cdot\left(\boldsymbol{\gamma}^++e^{-\mathbf{M}_t^{\rm no}}\boldsymbol{\gamma}^+e^{\mathbf{M}_t^{\rm no}}\right)\cdot\mathbf{c}\,\tilde{\rho}_{\rm no} \\ &\quad +2\,\mathrm{tr}\left(\boldsymbol{\gamma}^+\right)\tilde{\rho}_{\rm no}\,, && (7.74)\end{aligned}$$

Comparing Eq. (7.67) with Eqs. (7.70,7.71,7.72,7.73,7.74), we see that both keep the form $\varkappa\,\tilde{\rho}_{\rm no}+\mathbf{c}^\dagger\cdot\boldsymbol{\mathcal{K}}\cdot\mathbf{c}\,\tilde{\rho}_{\rm no}$, for some c-numbers $\varkappa$ and $L\times L$ matrices $\boldsymbol{\mathcal{K}}$. Combining those results together, the Gaussian ansatz (7.59) is a solution of Eq. (7.49), provided that $\mathbf{M}_t^{\rm no}$ and ζ_t satisfy the differential equations

$$\frac{\mathrm{d}}{\mathrm{d}t}\ln\zeta_t = \mathrm{tr}\left\{\boldsymbol{\gamma}^+-\boldsymbol{\gamma}^-(\mathbb{1}-\boldsymbol{\lambda}^-)e^{-\mathbf{M}_t^{\rm no}}\right\}, \tag{7.75}$$

and

$$\begin{aligned}\frac{\mathrm{d}e^{-\mathbf{M}_t^{\rm no}}}{\mathrm{d}t}e^{\mathbf{M}_t^{\rm no}} &= -\mathrm{i}(\mathbf{h}-e^{-\mathbf{M}_t^{\rm no}}\mathbf{h}e^{\mathbf{M}_t^{\rm no}})\mp e^{-\mathbf{M}_t^{\rm no}}\boldsymbol{\gamma}^-(\mathbb{1}-\boldsymbol{\lambda}^-)\\ &\quad -\frac{1}{2}(\boldsymbol{\gamma}^-+e^{-\mathbf{M}_t^{\rm no}}\boldsymbol{\gamma}^-e^{\mathbf{M}_t^{\rm no}})+\boldsymbol{\gamma}^+(\mathbb{1}-\boldsymbol{\lambda}^+)e^{\mathbf{M}_t^{\rm no}}\\ &\quad \pm\frac{1}{2}(\boldsymbol{\gamma}^++e^{-\mathbf{M}_t^{\rm no}}\boldsymbol{\gamma}^+e^{\mathbf{M}_t^{\rm no}}). \end{aligned}\tag{7.76}$$

Eq. (7.76) is a differential equation for $\mathbf{M}_t^{\rm no}$, but it may be rewritten in terms of the conditional covariance matrix $\mathbf{C}_{\rm no}$. Given the Gaussian ansatz (7.60), $\mathbf{M}_t^{\rm no}$

and $\mathbf{C}_{\text{no}}$ verify

$$\mathbf{C}_{\text{no}}(t) = \left(\frac{1}{e^{\mathbf{M}_t^{\text{no}}} \pm \mathbb{1}}\right), \qquad e^{\mathbf{M}_t^{\text{no}}} = \frac{\mathbb{1} \mp \mathbf{C}_{\text{no}}(t)}{\mathbf{C}_{\text{no}}(t)}. \tag{7.77}$$

Eq. (7.77) implies

$$\frac{\mathrm{d}\mathbf{C}_{\text{no}}}{\mathrm{d}t} = (\mathbb{1} \mp \mathbf{C}_{\text{no}})\frac{\mathrm{d}e^{-\mathbf{M}_t^{\text{no}}}}{\mathrm{d}t}(\mathbb{1} \mp \mathbf{C}_{\text{no}}). \tag{7.78}$$

Next, we use Eq. (7.78) into Eq. (7.76) to get a differential equation for $\mathbf{C}_{\text{no}}$. After simplifying the results, Eq. (7.75) and Eq. (7.76) become

$$\frac{\mathrm{d}}{\mathrm{d}t}\ln\zeta_t = \mathrm{tr}\left\{\gamma^+ - \gamma^-(\mathbb{1} - \lambda^-)\frac{\mathbf{C}_{\text{no}}(t)}{\mathbb{1} \mp \mathbf{C}_{\text{no}}(t)}\right\}, \tag{7.79}$$

and

$$\frac{\mathrm{d}\mathbf{C}_{\text{no}}}{\mathrm{d}t} = -(\mathbf{W}\mathbf{C}_{\text{no}} + \mathbf{C}_{\text{no}}\mathbf{W}^\dagger) + \gamma^+ \pm \mathbf{C}_{\text{no}}(\gamma^-\lambda^-)\mathbf{C}_{\text{no}} - (\mathbb{1} \mp \mathbf{C}_{\text{no}})(\gamma^+\lambda^+)(\mathbb{1} \mp \mathbf{C}_{\text{no}}), \tag{7.80}$$

where $\mathbf{W}$ is the matrix into Eqs. (7.58). Eq. (7.80) is a Riccati-type equation.

QED

If there is no monitoring, $\mathbf{\Lambda}^+ = \mathbf{\Lambda}^- = 0$, $\mathbf{C}_{\text{no}} = \mathbf{C}$ and we recover the Lyapunov equation (7.57) for the unconditional dynamics. Conversely, partial monitoring introduces two new terms, which are non-linear and individually positive semi-definite. In the language of quantum optics, they are called *information matrices*, as they establish how our knowledge about the state of the system changes given the information that no jump occurred [263, 264]. Under full monitoring, $\mathbf{\Lambda}^+ = \mathbf{\Lambda}^- = \mathbb{1}$, and Eq. (7.80) becomes

$$\frac{\mathrm{d}\mathbf{C}_{\text{no}}}{\mathrm{d}t} = -(\mathbf{K}\mathbf{C}_{\text{no}} + \mathbf{C}_{\text{no}}\mathbf{K}^\dagger) - \mathbf{C}_{\text{no}}(\gamma^+ \mp \gamma^-)\mathbf{C}_{\text{no}}, \tag{7.81}$$

where

$$\mathbf{K} = \mathbf{W} \mp \gamma^+ = \mathrm{i}\mathbf{h} + (\gamma^- \mp \gamma^+)/2. \tag{7.82}$$

However, in order to determine the no-jump probability $P_{\text{no}}(t)$, one must also compute ζ_t. Assuming the evolution of the no-jump correlation matrix $\mathbf{C}_{\text{no}}$ is known by Eq. (7.80), the formal solution of Eq. (7.79) is

$$\zeta_t = Z_0 \exp\left\{-\int_0^t \mathrm{d}t'\,\mathrm{tr}\left[\gamma^-(\mathbb{1} - \lambda^-)\frac{\mathbf{C}_{\text{no}}(t')}{\mathbb{1} \mp \mathbf{C}_{\text{no}}(t')} - \gamma^+\right]\right\}. \tag{7.83}$$

Eq. (7.83) and Eq. (7.61) determine the no-jump probability. However, Eq. (7.83) is complicated to handle, for two reasons: it depends on the integral over all previous times and it requires to compute $(\mathbb{1} \mp \mathbf{C}_{\text{no}})^{-1}$. To simplify Eq. (7.83), we use Eq. (7.80) and, after straightforward algebra, the argument of Eq. (7.83) can be written as

$$\begin{aligned} \mathrm{tr}\left\{\boldsymbol{\gamma}^-(\mathbb{1}-\boldsymbol{\lambda}^-)e^{-\mathbf{M}_t^{\text{no}}}-\boldsymbol{\gamma}^+\right\} &= -\,\mathrm{tr}\left[(\mathbb{1}\mp\mathbf{C}_{\text{no}})^{-1}\frac{\mathrm{d}\mathbf{C}_{\text{no}}}{\mathrm{d}t}\right] \\ &\quad -\mathrm{tr}\left\{\boldsymbol{\gamma}^+\boldsymbol{\lambda}^+(\mathbb{1}\mp\mathbf{C}_{\text{no}})+\boldsymbol{\gamma}^-\boldsymbol{\lambda}^-\mathbf{C}_{\text{no}}\right\}. \end{aligned} \tag{7.84}$$

To proceed further, we use the Jacobi identity

$$\frac{\mathrm{d}}{\mathrm{d}t}\ln\det(\mathbf{A}) = \mathrm{tr}\left(\mathbf{A}^{-1}\frac{\mathrm{d}\mathbf{A}}{\mathrm{d}t}\right), \tag{7.85}$$

for any matrix $\mathbf{A}$. Using Eq. (7.85) in our specific case, we get

$$\frac{\mathrm{d}}{\mathrm{d}t}\ln Z_t = \mathrm{tr}\left[(1\mp\mathbf{C}_{\text{no}})^{-1}\frac{\mathrm{d}\mathbf{C}_{\text{no}}}{\mathrm{d}t}\right]. \tag{7.86}$$

We can write Eq. (7.79) as

$$\frac{\mathrm{d}}{\mathrm{d}t}\ln\zeta_t/Z_t = \mathrm{tr}\left\{\boldsymbol{\gamma}^+\boldsymbol{\lambda}^+(\mathbb{1}\mp\mathbf{C}_{\text{no}})+\boldsymbol{\gamma}^-\boldsymbol{\lambda}^-\mathbf{C}_{\text{no}}\right\}. \tag{7.87}$$

Solving the differential equation (7.87), we find

$$P_{\text{no}}(t) = \frac{\zeta_t}{Z_t} = \exp\left(-\int_0^t \mathrm{d}t'\,\mathrm{tr}\left[\boldsymbol{\gamma}^+\boldsymbol{\lambda}^+(\mathbb{1}\mp\mathbf{C}_{\text{no}}(t'))+\boldsymbol{\gamma}^-\boldsymbol{\lambda}^-\mathbf{C}_{\text{no}}(t')\right]\right). \tag{7.88}$$

Unfortunately, the no-jump probability still depends on the entire history of $\mathbf{C}_{\text{no}}$ and $(\mathbb{1}\mp\mathbf{C}_{\text{no}})$, weighed by the emission monitoring rates $\boldsymbol{\gamma}^-\boldsymbol{\lambda}^-$ and the absorption monitoring rates $\boldsymbol{\gamma}^+\boldsymbol{\lambda}^+$, with a manifest non-markovian behaviour; however, at least, Eq. (7.88) does not require to compute the inverse correlation matrix $(\mathbb{1}\mp\mathbf{C}_{\text{no}})$ for any time $t'\in(0,t)$. In other terms, the no-jump probability takes the general form (7.20) with

$$\beta(t) = \mathrm{tr}\left[\boldsymbol{\gamma}^+\boldsymbol{\lambda}^+(\mathbb{1}\mp\mathbf{C}_{\text{no}}(t))+\boldsymbol{\gamma}^-\boldsymbol{\lambda}^-\mathbf{C}_{\text{no}}(t)\right]. \tag{7.89}$$

Now, we would like to introduce some criteria for the existence of dark subspaces; given the steady-state solution $\mathbf{C}_{\text{no}}^{\infty}$ for Eq. (7.80), the no-jump probability shows an exponential decay to 0 for large times,

$$\int_0^t \mathrm{d}t'\,\beta(t') \overset{t\sim\infty}{\simeq} t\;\mathrm{tr}\left\{\boldsymbol{\gamma}^+\boldsymbol{\lambda}^+(\mathbb{1}\mp\mathbf{C}_{\text{no}}^{\infty})+\boldsymbol{\gamma}^-\boldsymbol{\lambda}^-\mathbf{C}_{\text{no}}^{\infty}\right\}. \tag{7.90}$$

However, if the steady state verifies

$$\mathrm{tr}\left\{\boldsymbol{\gamma}^+\boldsymbol{\lambda}^+(\mathbb{1}\mp\mathbf{C}_{\mathrm{no}}^{\infty})+\boldsymbol{\gamma}^-\boldsymbol{\lambda}^-\mathbf{C}_{\mathrm{no}}^{\infty}\right\}=0\,, \tag{7.91}$$

then P_{no} approaches a finite asymptotic value and a jump can never occur.

7.5 Example: tight-binding model

As an application, we consider a chain of hopping fermions with open boundary conditions (OBC) and Hamiltonian

$$H=-\sum_{i=1}^{L-1}\left(c_i^\dagger c_{i+1}+c_{i+1}^\dagger c_i\right)\,, \tag{7.92}$$

being a typical example of ballistic transport. In Fig. 7.5, we draw a sketch of the gain-loss channels: the first edge on site 1 is coupled to an injection (gain) bath with jump operator $c_1^\dagger$ and rate $\Gamma_1^+=\Gamma$. All other sites are connected to emission (loss) baths with jump operators c_i and rates $\Gamma_j^-=\Gamma\ \forall j\in\{2,\dots,L\}$. By hypothesis, we assume perfect monitoring on site 1 ($\Lambda_1^+=1$) and a non-ideal monitoring $\Lambda_j^-=\Lambda^-\ \forall j\in\{2,\dots,L\}$ for all the other channels. In this view, the no-jump conditional dynamics is given by

$$\mathcal{L}_0(\rho)=-\mathrm{i}[H,\rho]-\frac{\Gamma}{2}\{c_1c_1^\dagger,\rho\}+\Gamma\sum_{j=2}^{L}\left((1-\Lambda^-)c_j\rho c_j^\dagger-\frac{1}{2}\{c_j^\dagger c_j,\rho\}\right)\,. \tag{7.93}$$

Suppose the system is prepared in the vacuum state $|0\rangle$ and undergoes a jump in the channel $(1,+)$ at time $t=0$. $\rho(0)=c_1^\dagger|0\rangle\langle 0|c_1$ is still a Gaussian state. This is a paradigmatic example for transport protocols, where a wavepacket is injected in an empty chain, and one watches how it propagates. According to the quasi-particle picture (see Chapter 5), after the quench the excitation moves ballistically to the RHS of the chain and is destroyed with rate Γ, eventually reaching the second boundary after time $L/2$ [9, 10, A2, 59, 157–161, 175–193]. In the meantime, however, other excitations can also be injected at site 1.

Since $\Lambda^-\neq 1$, not all emission clicks are detected; for this reason, P_{no} is a decreasing function of the monitoring efficiency Λ^-. Since we are interested in the thermodynamic limit, we study the dynamics in the time window $t\in[0,L/2]$. In this way, we avoid all the secondary processes due to finite size effects, with the wavepackets moving back and forth multiple times within the chain.

In Fig. 7.6 (a), we plot the no-jump probability $P_{\mathrm{no}}(t)$ for $\Gamma=0.1$, system size $L=50$ and efficiency $\Lambda^-=\{0,0.1,0.5,1.0\}$. At early times, $P_{\mathrm{no}}(t)$ is roughly

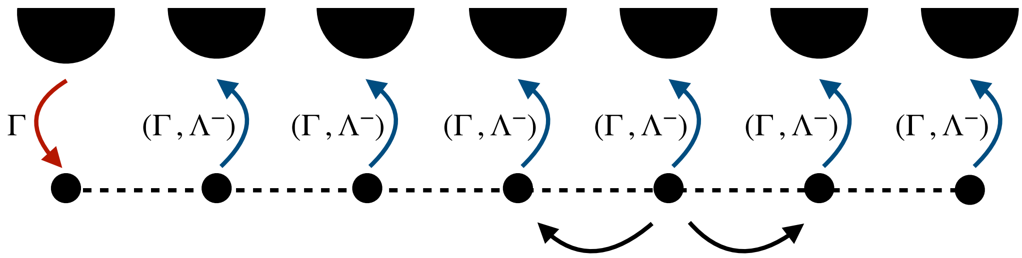

Figure 7.5: Sketch of a quantum chain of hopping particles coupled to a thermal bath. We inject excitations at the first site with rate Γ and perfect efficiency, and we lose particles at site $j \in [2, L]$ with homogeneous rate Γ and monitoring efficiency Λ^-.

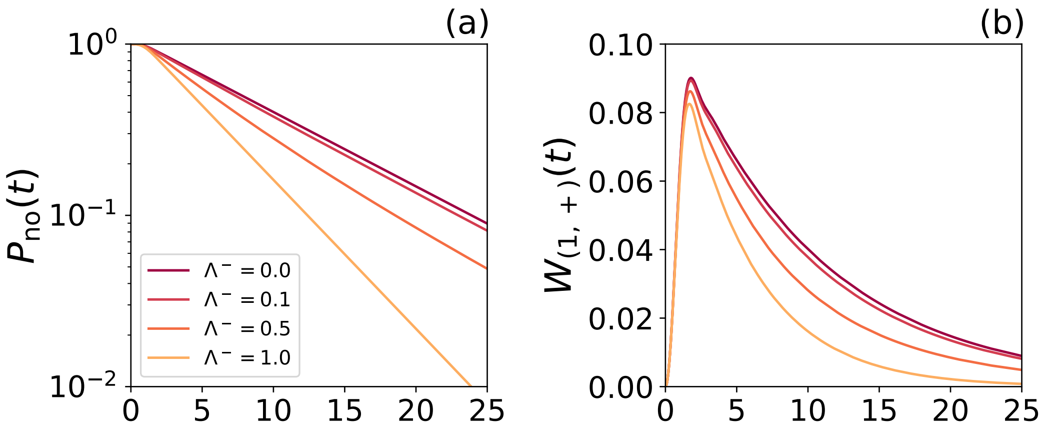

Figure 7.6: Conditional dynamics for a quantum chains of hopping fermions, $\Gamma = 0.1$ and several values of the monitoring efficiency $\Lambda^- = \{0, 0.1, 0.5, 1.0\}$. (a) no-jump probability $P_{no}(t)$ as a function of time in semi-log scale; (b) Waiting-time distribution $W_{(1,+)}(t)$ between two consecutive jumps in the channel $(1, +)$.

independent of Λ^-. This phenomenon finds a simple explanation in generalized hydrodynamics; for the specific Hamiltonian into Eq. (7.92), any particle located on site 1 needs at least $\Delta t = 0.5$ to reach the consecutive site and eventually be ejected. According to this rough picture, for $t < 0.5$ no particles may be ejected, independently on the monitoring efficiency. For large times the dynamical behaviour is dominated by the parameter Λ^-. Fig. 7.6 (a) shows the exponential decay of P_{no}. This is an indication of the fact that the system has already reached the steady state $\mathbf{C}_{no}^{\infty}$.

In Fig. 7.6 (b) we plot the waiting-time distribution $W_{(1,+)}(t)$ between two consecutive jumps. In fact, $W_{(1,+)}(t)$ is the conditional probability distribution to observe the second injection at site 1 and time t, known that one fermion has

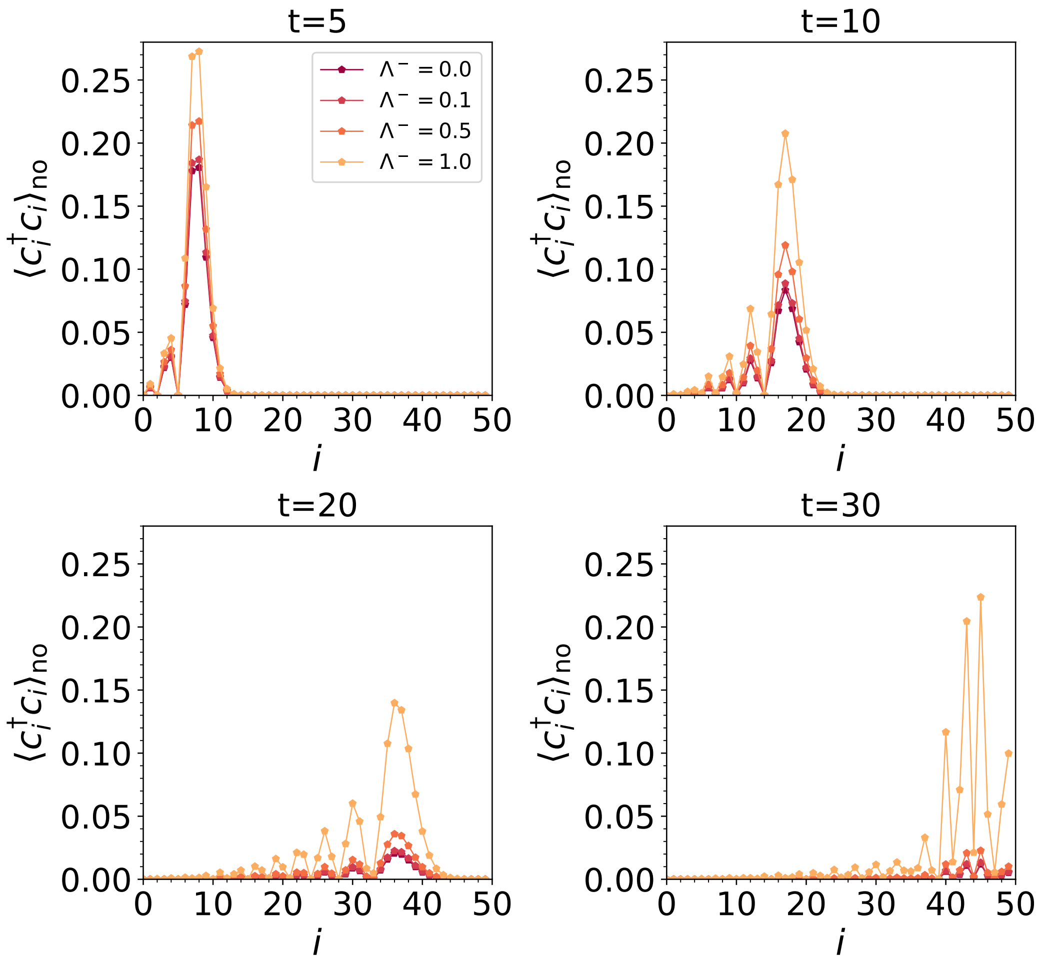

Figure 7.7: Time evolution of the local occupation for $\Gamma = 0.1$ and monitoring efficiency $\Lambda^- = \{0, 0.1, 0.5, 1.0\}$. As expected, the larger the efficiency the bigger the fermionic occupation, since the no-jump evolution does not allow to detect particle loss in $[0, t]$. Starting from $t \sim 25$, we observe finite size effects and the front wave is reflected according to the open boundary conditions.

been absorbed at site 1 and time $t = 0$. From Eq. (7.23), $W_{(1,+)}(t)$ reads

$$W_{(1,+)}(t) = \Gamma P_{\text{no}}(t)\,(1 - (\mathbf{C}_{\text{no}}(t))_{11})\,, \tag{7.94}$$

The behaviour of $W_{(1,+)}(t)$ clearly reflects the fermionic algebra (7.44). In fact, due to the finite capacity, the WTD starts at zero and then increases. As for the no-jump probability, the WTD is also independent on Λ^- at early times.

Fig. 7.7 shows the conditional time evolution of the local occupation $\langle c_i^\dagger c_i \rangle_{\text{no}}$. At time $t = 0$, we have $\langle c_1^\dagger c_1 \rangle_{\text{no}} = 1$ since there is a particle on site 1. After the quench, the system evolves with the no-jump operator (7.93). As expected, the

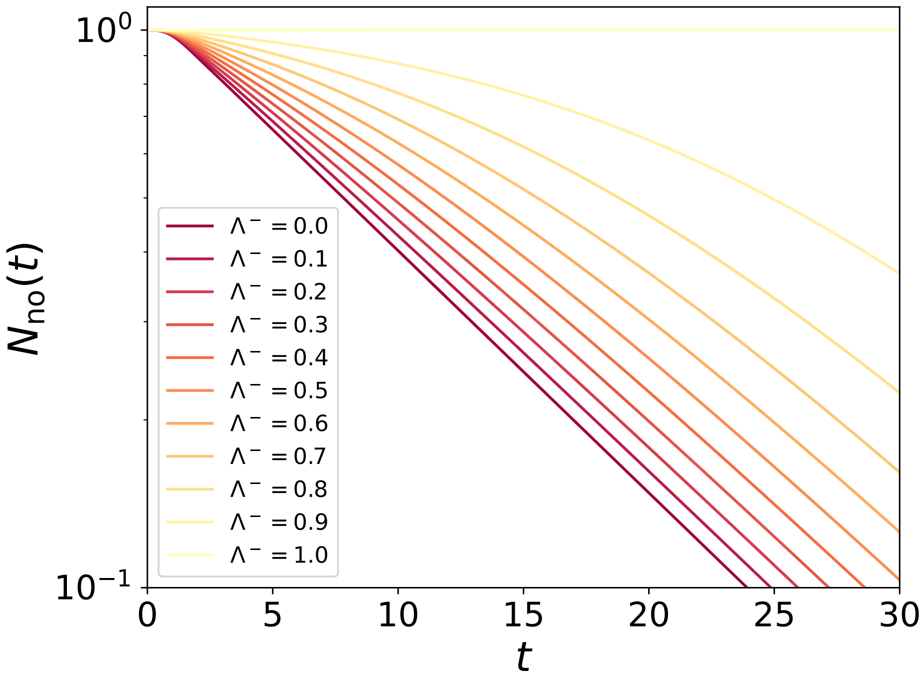

Figure 7.8: The number of particles $N_{\rm no}(t) = \sum_{i=1}^{L} \langle c_i^\dagger c_i \rangle_{\rm no}$ as a function of time t in semi-log scale.

density increases with Λ^- because perfect monitoring avoids missed detection in $[0, t]$.

In Fig. 7.8, we plot the total number of particles $N_{\rm no}(t) = \sum_{i=1}^{L} \langle c_i^\dagger c_i \rangle_{\rm no}$ under the conditional dynamics (7.93). For $\Lambda^- = 1$ (ideal monitoring), the average number of particles is a constant of motion because any particle exchange with the environment is detected. In the opposite case $\Lambda^- = 0$ (no monitoring), once the particle leaves the site 1, the statistics of the emission events follows a Poisson distribution and $N_{\rm no}(t) \simeq e^{-\Gamma t}$ is the probability of finding the particle in the chain at time t. For any $\Lambda^- \in (0, 1)$ the dynamics of $N_{\rm no}(t)$ is more involved and, in general, specified by the trace of Eq. (7.80). It is interesting to observe that, in the long time limit, $N_{\rm no}(t) \sim e^{-\Gamma t}$, independently on Λ^-.

7.6 No-jump dynamics with pairing terms - fermionic chains

We now generalize the dynamics to include pairing terms $c_i c_j$ in the Hamiltonian operator. For clarity, we decide to treat the fermionic and bosonic cases in two different sections.

If the $\mathbf{c}$'s are fermionic operators and L is the chain size, it is convenient to introduce the $2L$ Majorana operators

$$y_n^1 = c_n^\dagger + c_n\,, \qquad y_n^2 = \mathrm{i}(c_n^\dagger - c_n)\,. \qquad n = 1, \dots, L \tag{7.95}$$

The Majorana operators are Hermitian ($y_k^{1\dagger} = y_k^1$, $y_k^{2\dagger} = y_k^2$) and satisfy the Clifford algebra

$$\{y_k^1, y_\ell^1\} = 2\delta_{k\ell}\,, \qquad \{y_k^2, y_\ell^2\} = 2\delta_{k\ell}\,, \qquad \{y_k^1, y_\ell^2\} = 0\,. \tag{7.96}$$

From Eq. (7.96), it follows that

$$(y_k^1)^2 = (y_k^2)^2 = \mathbb{1}\,. \tag{7.97}$$

Below, we work with the vector $\mathbf{Y}^\dagger = (y_1^1, \dots, y_L^1, y_1^2, \dots, y_L^2)$, which then satisfies the identity $\mathbf{Y}^\dagger \cdot \mathbf{Y} = 2L$.

For fermionic systems, any quadratic Hamiltonian $\frac{1}{4}\mathbf{Y}^\dagger \cdot \mathcal{T} \cdot \mathbf{Y}$ may be represented by $2L \times 2L$ anti-symmetric ($\mathcal{T}^{\mathrm{T}} = -\mathcal{T}$) and Hermitian matrices ($\mathcal{T}^\dagger = \mathcal{T}$). Indeed, if $\mathcal{T}$ is not anti-symmetric, we can always write

$$\mathbf{Y}^\dagger \cdot \mathcal{T} \cdot \mathbf{Y} = \mathrm{tr}(\mathcal{T}) + \frac{1}{2}\mathbf{Y}^\dagger \cdot (\mathcal{T} - \mathcal{T}^{\mathrm{T}}) \cdot \mathbf{Y}\,. \tag{7.98}$$

As an example, we can take the most general Gaussian-preserving Hamiltonian

$$H = \sum_{n,m} \left\{ h_{nm} c_n^\dagger c_m + \frac{1}{2}\Big(G_{nm} c_n^\dagger c_m^\dagger + G_{mn}^* c_n c_m \Big) \right\}, \tag{7.99}$$

where $\mathbf{h} = \mathbf{h}^\dagger$ and $\mathbf{G}^{\mathrm{T}} = -\mathbf{G}$. In terms of Majorana operators, the Hamiltonian (7.99) becomes

$$H = \frac{1}{4}\mathbf{Y}^\dagger \cdot \mathcal{K} \cdot \mathbf{Y}\,, \tag{7.100}$$

where

$$\mathcal{K} = \begin{pmatrix} \mathbf{h} + (\mathbf{G} + \mathbf{G}^\dagger)/2 & \mathrm{i}\mathbf{h} - \mathrm{i}(\mathbf{G} - \mathbf{G}^\dagger)/2 \\ -\mathrm{i}\mathbf{h} - \mathrm{i}(\mathbf{G} - \mathbf{G}^\dagger)/2 & \mathbf{h} - (\mathbf{G} + \mathbf{G}^\dagger)/2 \end{pmatrix}, \tag{7.101}$$

$$= \mathbb{1} \otimes \mathbf{h} - \sigma_y \otimes \mathbf{h} + \sigma_z \otimes \left(\frac{\mathbf{G} + \mathbf{G}^\dagger}{2} \right) - \mathrm{i}\sigma_x \otimes \left(\frac{\mathbf{G} - \mathbf{G}^\dagger}{2} \right), \tag{7.102}$$

and $\otimes$ indicates the outer product. Since $\mathbf{h}^{\mathrm{T}} = \mathbf{h}^*$ and $\mathbf{G}^\dagger = -\mathbf{G}^*$,

$$\frac{1}{2}(\mathcal{K} - \mathcal{K}^{\mathrm{T}}) = \frac{1}{2}\begin{pmatrix} (\mathbf{h}-\mathbf{h}^*)+(\mathbf{G}-\mathbf{G}^*) & \mathrm{i}(\mathbf{h}+\mathbf{h}^*)-\mathrm{i}(\mathbf{G}+\mathbf{G}^*) \\ -\mathrm{i}(\mathbf{h}+\mathbf{h}^*)-\mathrm{i}(\mathbf{G}+\mathbf{G}^*) & (\mathbf{h}-\mathbf{h}^*)-(\mathbf{G}-\mathbf{G}^*) \end{pmatrix}, \tag{7.103}$$

$$\mathrm{tr}(\mathcal{K}) = 2\,\mathrm{tr}(\mathbf{h})\,. \tag{7.104}$$

If $\mathbf{h}$ and $\mathbf{G}$ are real, the anti-symmetrized $\mathcal{K}$ reduces to

$$\frac{1}{2}(\mathcal{K} - \mathcal{K}^{\mathrm{T}}) = \mathrm{i}\begin{pmatrix} 0 & \mathbf{h}-\mathbf{G} \\ -\mathbf{h}-\mathbf{G} & 0 \end{pmatrix} \tag{7.105}$$

$$= -\sigma_y \otimes \mathbf{h} - \mathrm{i}\sigma_x \otimes \mathbf{G}\,, \tag{7.106}$$

and finally

$$H = \frac{1}{4}\mathbf{Y}^\dagger \cdot \mathcal{T} \cdot \mathbf{Y} + \frac{1}{2}\,\mathrm{tr}(\mathbf{h})\,, \qquad \mathcal{T} := \mathrm{i}\begin{pmatrix} 0 & \mathbf{h}-\mathbf{G} \\ -\mathbf{h}-\mathbf{G} & 0 \end{pmatrix}. \tag{7.107}$$

Therefore, without loss of generality, we may consider the Hamiltonian

$$H = \frac{1}{4}\mathbf{Y}^\dagger \cdot \mathcal{T} \cdot \mathbf{Y}\,, \tag{7.108}$$

where $\mathcal{T}$ is a $2L \times 2L$ anti-symmetric and Hermitian matrix.

Assuming the same Lindblad dissipator (7.1), we can recast Eq. (7.47) in terms of the Majorana operators,

$$\mathcal{D}(\rho) = \sum_{i,j=1}^{2L} \Psi_{ij}\Big[Y_i \rho Y_j - \frac{1}{2}\{Y_j Y_i, \rho\}\Big], \tag{7.109}$$

where $\mathbf{\Psi}$ is a $2L \times 2L$ matrix. In order to find $\mathbf{\Psi}$ which makes $\mathcal{L}$ completely positive and trace preserving, we decompose $\mathbf{\Psi}$ in a block form, following the ordering for the Majorana operators $\mathbf{Y}$:

$$\mathbf{\Psi} = \begin{pmatrix} \mathbf{A} & \mathbf{B} \\ \mathbf{C} & \mathbf{D} \end{pmatrix}, \tag{7.110}$$

where the matrices $\mathbf{A}\,,\mathbf{B}\,,\mathbf{C}\,,\mathbf{D}$ are to be determined. One can verify that the dissipator (7.109) is the bilinear superoperator,

$$\begin{aligned}\mathcal{D}(\rho) = \sum_{ij}\Big\{&(\mathbf{A}-\mathbf{D}+\mathrm{i}\mathbf{B}+\mathrm{i}\mathbf{C})_{ij}\tilde{\mathcal{D}}[c_i^\dagger, c_j^\dagger] + (\mathbf{A}-\mathbf{D}-\mathrm{i}\mathbf{B}-\mathrm{i}\mathbf{C})_{ij}\tilde{\mathcal{D}}[c_i, c_j] \\ &+(\mathbf{A}+\mathbf{D}+\mathrm{i}\mathbf{B}-\mathrm{i}\mathbf{C})_{ji}\tilde{\mathcal{D}}[c_j, c_i^\dagger] + (\mathbf{A}+\mathbf{D}-\mathrm{i}\mathbf{B}+\mathrm{i}\mathbf{C})_{ij}\tilde{\mathcal{D}}[c_i^\dagger, c_j]\Big\}.\end{aligned} \tag{7.111}$$

In the usual thermal case, where the dissipator is given by Eq. (7.47), we get a set of four independent equations

$$\begin{cases} \mathbf{A} - \mathbf{D} + \mathrm{i}(\mathbf{B} + \mathbf{C}) = 0 \\ \mathbf{A} - \mathbf{D} - \mathrm{i}(\mathbf{B} + \mathbf{C}) = 0 \\ \mathbf{A} + \mathbf{D} + \mathrm{i}(\mathbf{B} - \mathbf{C}) = (\gamma^-)^{\mathrm{T}} \\ \mathbf{A} + \mathbf{D} - \mathrm{i}(\mathbf{B} - \mathbf{C}) = \gamma^+ \end{cases} \tag{7.112}$$

which implies

$$\mathbf{A} = \mathbf{D} = \frac{\gamma^+ + (\gamma^-)^{\mathrm{T}}}{4}, \tag{7.113}$$

$$\mathbf{B} = -\mathbf{C} = \mathrm{i}\frac{\gamma^+ - (\gamma^-)^{\mathrm{T}}}{4}. \tag{7.114}$$

Hence, the matrix $\mathbf{\Psi}$ takes the form

$$\mathbf{\Psi} = \frac{1}{4}\begin{pmatrix} \gamma^+ + (\gamma^-)^{\mathrm{T}} & \mathrm{i}\left[\gamma^+ - (\gamma^-)^{\mathrm{T}}\right] \\ -\mathrm{i}\left[\gamma^+ - (\gamma^-)^{\mathrm{T}}\right] & \gamma^+ + (\gamma^-)^{\mathrm{T}} \end{pmatrix}, \tag{7.115}$$

which is Hermitian ($\mathbf{\Psi}^\dagger = \mathbf{\Psi}$) but not symmetric ($\mathbf{\Psi}^{\mathrm{T}} \neq \mathbf{\Psi}$). The generalisation to the no-jump Liouvillian (7.5) leads to

$$\mathcal{L}_0(\rho) = -\mathrm{i}[H,\rho] + \sum_{i,j=1}^{2L}\left[[\mathbf{\Psi} - \mathbf{\Phi}]_{ij} Y_i \rho Y_j - \frac{(\mathbf{\Psi})_{ij}}{2}\{Y_j Y_i, \rho\}\right], \tag{7.116}$$

where

$$\mathbf{\Phi} = \frac{1}{4}\begin{pmatrix} \gamma^+\lambda^+ + (\gamma^-\lambda^-)^{\mathrm{T}} & \mathrm{i}\left[\gamma^+\lambda^+ - (\gamma^-\lambda^-)^{\mathrm{T}}\right] \\ -\mathrm{i}\left[\gamma^+\lambda^+ - (\gamma^-\lambda^-)^{\mathrm{T}}\right] & \gamma^+\lambda^+ + (\gamma^-\lambda^-)^{\mathrm{T}} \end{pmatrix}. \tag{7.117}$$

7.6.1 Full monitoring

Again, we start from the full monitoring case, where all the channels are perfectly monitored with efficiency $\mathbf{\Lambda}^+ = \mathbf{\Lambda}^- = \mathbb{1}$ and thus $\mathbf{\Psi} = \mathbf{\Phi}$. The no-jump Liouvillian reduces to

$$\mathcal{L}_0(\rho) = -\mathrm{i}[H,\rho] - \frac{1}{2}\sum_{i,j=1}^{2L} \Psi_{ij}\{Y_j Y_i, \rho\}. \tag{7.118}$$

After some algebra, the evolution generated by the no-jump Liouvillian $\mathcal{L}_0$ may be expressed by the effective Hamiltonian

$$H_{\mathrm{e}} = \mathbf{Y}^{\dagger} \cdot \frac{\mathcal{T} + \mathrm{i}(\mathbf{\Psi} - \mathbf{\Psi}^{\mathrm{T}})}{4} \cdot \mathbf{Y} - \mathrm{i}\frac{\mathrm{tr}(\mathbf{\Psi})}{2} . \tag{7.119}$$

Hence, the no-jump operator evolves with Eq. (7.10).

7.6.2 Dynamics under partial monitoring

Next, we derive the conditional no-jump dynamics for non-vanishing pairing terms $c_i c_j$ in the Hamiltonian operator. We shall follow the same philosophy of Sec. 7.4.2: assuming the initial state is Gaussian, the dynamics is then solved by a Gaussian ansatz.

The dynamics described by Eq. (7.1) with the Hamiltonian (7.108), the dissipator (7.109) and the matrix (7.115) is Gaussian preserving, and thus

$$\rho(t) := e^{\mathcal{L}t}(\rho_0) = \frac{e^{\frac{1}{4}\mathbf{Y}^{\dagger}\cdot\mathcal{M}_t\cdot\mathbf{Y}}}{Z_t} , \tag{7.120}$$

where

$$\begin{aligned} Z_t &= \mathrm{tr}\left\{e^{\frac{1}{4}\mathbf{Y}^{\dagger}\cdot\mathcal{M}_t\cdot\mathbf{Y}}\right\} = \sqrt{\det(\mathbb{1} + e^{\mathcal{M}_t})} , && (7.121)\\ \mathcal{M}_t &= \ln\left(\frac{\mathbb{1} - \mathbf{\Theta}}{\mathbb{1} + \mathbf{\Theta}}\right), && (7.122)\end{aligned}$$

and $(\mathbf{\Theta})_{ij} = \frac{1}{2}\,\mathrm{tr}\left\{[Y_i, Y_j]\rho(t)\right\} = \frac{1}{2}\langle [Y_i, Y_j]\rangle(t)$ is the correlation matrix, which is Hermitian ($\mathbf{\Theta}^{\dagger} = \mathbf{\Theta}$) and anti-symmetric ($\mathbf{\Theta}^{\mathrm{T}} = -\mathbf{\Theta}$). The correlation matrix $\mathbf{\Theta}$ satisfies the Lyapunov differential equation [262]

$$\frac{\mathrm{d}\mathbf{\Theta}}{\mathrm{d}t} = -\left(\mathcal{W}\mathbf{\Theta} + \mathbf{\Theta}\mathcal{W}^{\dagger}\right) + \mathcal{F}, \tag{7.123}$$

with

$$\begin{aligned} \mathcal{W} &= \mathrm{i}\mathcal{T} + \mathbf{\Psi} + \mathbf{\Psi}^{\mathrm{T}} , && (7.124)\\ \mathcal{F} &= 2(\mathbf{\Psi}^{\mathrm{T}} - \mathbf{\Psi}) . && (7.125)\end{aligned}$$

In order to solve the conditional dynamics, as already done into Sec. 7.4.2, we use the Gaussian ansatz

$$\tilde{\rho}_{\mathrm{no}}(t) := e^{\mathcal{L}_0 t}(\rho_0) = \frac{e^{\frac{1}{4}\mathbf{Y}^{\dagger}\cdot\mathcal{M}_t^{\mathrm{no}}\cdot\mathbf{Y}}}{\zeta_t} , \tag{7.126}$$

for some matrix $\mathcal{M}_t^{\text{no}}$ and some c-number ζ_t, which must satisfy specific differential equations, to be determined. Again, the properly normalised state is

$$\rho_{\text{no}}(t) \;:=\; \frac{\tilde{\rho}_{\text{no}}(t)}{P_{\text{no}}(t)} = \frac{e^{\frac{1}{4}\mathbf{Y}^\dagger\cdot\mathcal{M}_t^{\text{no}}\cdot\mathbf{Y}}}{Z_t}\,, \tag{7.127}$$

$$Z_t \;=\; \operatorname{tr}\left(e^{\frac{1}{4}\mathbf{Y}^\dagger\cdot\mathcal{M}_t^{\text{no}}\cdot\mathbf{Y}}\right), \tag{7.128}$$

where ρ_{no} is independent of ζ_t. As before, the no-jump probability is given by Eq. (7.62) and the term ζ_t is still relevant.

In this paragraph, we shall prove that the ansatz (7.126) solves the dynamics (7.116) with the Hamiltonian (7.108). The dynamics of $\tilde{\rho}_{\text{no}}(t)$ is provided by two independent differential equations for ζ_t and the conditional covariance matrix

$$(\boldsymbol{\Theta}_{\text{no}})_{ij} \;=\; \frac{1}{2}\operatorname{tr}\left\{[Y_i, Y_j]\,\rho_{\text{no}}(t)\right\} = \frac{1}{2}\langle[Y_i, Y_j]\rangle_{\text{no}}(t)\,, \tag{7.129}$$

$$\;=\; -[\tanh(\mathcal{M}_t^{\text{no}}/2)]_{ij}\,. \tag{7.130}$$

Proof

Firstly, we note that Eq. (7.65) is naturally translated to Majorana operators: given two $2L\times 2L$ anti-symmetric matrices $\mathbf{A}$ and $\mathbf{B}$,

$$[\mathbf{Y}^\dagger\cdot\mathbf{A}\cdot\mathbf{Y}, \mathbf{Y}^\dagger\cdot\mathbf{B}\cdot\mathbf{Y}] = 4\mathbf{Y}^\dagger\cdot[\mathbf{A},\mathbf{B}]\cdot\mathbf{Y}\,. \tag{7.131}$$

The Baker-Campbell-Hausdorff formula (7.64) leads to

$$\frac{\mathrm{d}}{\mathrm{d}t}e^{\frac{1}{4}\mathbf{Y}^\dagger\cdot\mathcal{M}_t^{\text{no}}\cdot\mathbf{Y}} = \mathbf{Y}^\dagger\cdot\left[\frac{1}{4}\frac{\mathrm{d}e^{\mathcal{M}_t^{\text{no}}}}{\mathrm{d}t}e^{-\mathcal{M}_t^{\text{no}}}\right]\cdot\mathbf{Y}e^{\frac{1}{4}\mathbf{Y}^\dagger\cdot\mathcal{M}_t^{\text{no}}\cdot\mathbf{Y}}\,. \tag{7.132}$$

Analogously to (7.67), we get

$$\frac{\mathrm{d}\tilde{\rho}_{\text{no}}}{\mathrm{d}t} = \mathbf{Y}^\dagger\cdot\left[\frac{1}{4}\frac{\mathrm{d}e^{\mathcal{M}_t^{\text{no}}}}{\mathrm{d}t}e^{-\mathcal{M}_t^{\text{no}}}\right]\cdot\mathbf{Y}\tilde{\rho}_{\text{no}} - \left(\frac{\mathrm{d}}{\mathrm{d}t}\ln\zeta_t\right)\tilde{\rho}_{\text{no}}\,. \tag{7.133}$$

Since $\mathbb{1} = \mathbf{A}^{-1}\mathbf{A}$, any matrix $\mathbf{A}$ satisfies the obvious identity

$$\mathbf{A}^{-1}\frac{\mathrm{d}\mathbf{A}}{\mathrm{d}t} = -\frac{\mathrm{d}\mathbf{A}^{-1}}{\mathrm{d}t}\mathbf{A}\,, \tag{7.134}$$

which implies the matrix $\frac{\mathrm{d}e^{\mathcal{M}_t^{\text{no}}}}{\mathrm{d}t}e^{-\mathcal{M}_t^{\text{no}}}$ is anti-symmetric. In other words, $\mathrm{d}\tilde{\rho}_{\text{no}}/\mathrm{d}t$ has the form $\kappa\tilde{\rho}_{\text{no}} + \mathbf{Y}^\dagger\cdot\boldsymbol{\mathcal{K}}\cdot\mathbf{Y}\tilde{\rho}_{\text{no}}$, for a c-number κ and an anti-symmetric matrix $\boldsymbol{\mathcal{K}}$. In order to cast the super-operator (7.116) in the same form, use the identity

$$e^{\frac{1}{4}\mathbf{Y}^\dagger\cdot\mathcal{M}_t^{\text{no}}\cdot\mathbf{Y}}\mathbf{Y} = e^{-\mathcal{M}_t^{\text{no}}}\mathbf{Y}e^{\frac{1}{4}\mathbf{Y}^\dagger\cdot\mathcal{M}_t^{\text{no}}\cdot\mathbf{Y}}\,, \tag{7.135}$$

where the factor $e^{\frac{1}{4}\mathbf{Y}^\dagger\cdot\mathcal{M}_t^{\mathrm{no}}\cdot\mathbf{Y}}$ is pushed on the right. This leads to

$$-\mathrm{i}[H,\tilde{\rho}_{\mathrm{no}}] = \mathbf{Y}^\dagger\cdot\left[-\frac{\mathrm{i}}{4}\Big(\mathcal{T}-e^{\mathcal{M}_t^{\mathrm{no}}}\mathcal{T}e^{-\mathcal{M}_t^{\mathrm{no}}}\Big)\right]\cdot\mathbf{Y}\tilde{\rho}_{\mathrm{no}}\,, \tag{7.136}$$

$$\sum_{ij}[\mathbf{\Psi}-\mathbf{\Phi}]_{ij}Y_i\tilde{\rho}_{\mathrm{no}}Y_j = \mathbf{Y}^\dagger\cdot[\mathbf{\Psi}-\mathbf{\Phi}]e^{-\mathcal{M}_t^{\mathrm{no}}}\cdot\mathbf{Y}\tilde{\rho}_{\mathrm{no}}\,, \tag{7.137}$$

$$\begin{aligned}\sum_{ij}(\mathbf{\Psi})_{ij}\{Y_jY_i,\tilde{\rho}_{\mathrm{no}}\} &= 4\,\mathrm{tr}(\mathbf{\Psi})\tilde{\rho}_{\mathrm{no}}\\ &\quad -\mathbf{Y}^\dagger\cdot\left[\mathbf{\Psi}+e^{\mathcal{M}_t^{\mathrm{no}}}\mathbf{\Psi}e^{-\mathcal{M}_t^{\mathrm{no}}}\right]\cdot\mathbf{Y}\tilde{\rho}_{\mathrm{no}}\,.\end{aligned} \tag{7.138}$$

However, since the matrices in the quadratic forms (7.137, 7.138) are not anti-symmetric, we need to anti-symmetrize them, to get

$$\begin{aligned}\sum_{ij}[\mathbf{\Psi}-\mathbf{\Phi}]_{ij}Y_i\tilde{\rho}_{\mathrm{no}}Y_j &= \mathbf{Y}^\dagger\cdot\left[\frac{[\mathbf{\Psi}-\mathbf{\Phi}]e^{-\mathcal{M}_t^{\mathrm{no}}}-e^{\mathcal{M}_t^{\mathrm{no}}}[\mathbf{\Psi}-\mathbf{\Phi}]^{\mathrm{T}}}{2}\right]\cdot\mathbf{Y}\tilde{\rho}_{\mathrm{no}}\\ &\quad +\mathrm{tr}\Big([\mathbf{\Psi}-\mathbf{\Phi}]e^{-\mathcal{M}_t^{\mathrm{no}}}\Big)\,\tilde{\rho}_{\mathrm{no}}\,,\end{aligned} \tag{7.139}$$

$$\begin{aligned}\sum_{ij}(\mathbf{\Psi})_{ij}\{Y_jY_i,\tilde{\rho}_{\mathrm{no}}\} &= -\mathbf{Y}^\dagger\cdot\left[\frac{\mathbf{\Psi}-\mathbf{\Psi}^{\mathrm{T}}}{2}+e^{\mathcal{M}_t^{\mathrm{no}}}\frac{\mathbf{\Psi}-\mathbf{\Psi}^{\mathrm{T}}}{2}e^{-\mathcal{M}_t^{\mathrm{no}}}\right]\cdot\mathbf{Y}\tilde{\rho}_{\mathrm{no}}\\ &\quad +2\,\mathrm{tr}(\mathbf{\Psi})\,\tilde{\rho}_{\mathrm{no}}\,.\end{aligned} \tag{7.140}$$

Now the quadratic terms are in the proper form and the Gaussian ansatz applied to the no-jump Liouvillian (7.116) reads

$$\begin{aligned}\mathcal{L}_0(\tilde{\rho}_{\mathrm{no}}) &= \mathbf{Y}^\dagger\cdot\left[\frac{[\mathbf{\Psi}-\mathbf{\Phi}]e^{-\mathcal{M}_t^{\mathrm{no}}}-e^{\mathcal{M}_t^{\mathrm{no}}}[\mathbf{\Psi}-\mathbf{\Phi}]^{\mathrm{T}}}{2}\right]\cdot\mathbf{Y}\,\tilde{\rho}_{\mathrm{no}}\\ &\quad +\mathbf{Y}^\dagger\cdot\left[\frac{\mathbf{\Psi}-\mathbf{\Psi}^{\mathrm{T}}}{4}+e^{\mathcal{M}_t^{\mathrm{no}}}\frac{\mathbf{\Psi}-\mathbf{\Psi}^{\mathrm{T}}}{4}e^{-\mathcal{M}_t^{\mathrm{no}}}\right]\cdot\mathbf{Y}\,\tilde{\rho}_{\mathrm{no}}\\ &\quad +\mathbf{Y}^\dagger\cdot\left[-\frac{\mathrm{i}}{4}\Big(\mathcal{T}-e^{\mathcal{M}_t^{\mathrm{no}}}\mathcal{T}e^{-\mathcal{M}_t^{\mathrm{no}}}\Big)\right]\cdot\mathbf{Y}\,\tilde{\rho}_{\mathrm{no}}\\ &\quad +\left[\mathrm{tr}\Big([\mathbf{\Psi}-\mathbf{\Phi}]e^{-\mathcal{M}_t^{\mathrm{no}}}\Big)-\mathrm{tr}(\mathbf{\Psi})\right]\tilde{\rho}_{\mathrm{no}}\,.\end{aligned} \tag{7.141}$$

Combining Eq. (7.141) with Eq. (7.133),

$$\frac{\mathrm{d}}{\mathrm{d}t}\ln\zeta_t = \mathrm{tr}\Big(\mathbf{\Psi}-[\mathbf{\Psi}-\mathbf{\Phi}]e^{-\mathcal{M}_t^{\mathrm{no}}}\Big)\,, \tag{7.142}$$

$$\begin{aligned}\frac{\mathrm{d}e^{\mathcal{M}_t^{\mathrm{no}}}}{\mathrm{d}t} &= -\mathrm{i}\Big(\mathcal{T}e^{\mathcal{M}_t^{\mathrm{no}}}-e^{\mathcal{M}_t^{\mathrm{no}}}\mathcal{T}\Big)+2[\mathbf{\Psi}-\mathbf{\Phi}]-2e^{\mathcal{M}_t^{\mathrm{no}}}[\mathbf{\Psi}-\mathbf{\Phi}]^{\mathrm{T}}e^{\mathcal{M}_t^{\mathrm{no}}}\\ &\quad +(\mathbf{\Psi}-\mathbf{\Psi}^{\mathrm{T}})e^{\mathcal{M}_t^{\mathrm{no}}}+e^{\mathcal{M}_t^{\mathrm{no}}}(\mathbf{\Psi}-\mathbf{\Psi}^{\mathrm{T}})\,.\end{aligned} \tag{7.143}$$

As for Sec. 7.4.2, the matrix $\boldsymbol{\mathcal{M}}_t^{\mathrm{no}}$ is not so convenient to work with and it is better to rewrite the differential equations in terms of the conditional covariance matrix $\boldsymbol{\Theta}_{\mathrm{no}}$. The relation between the matrices $\boldsymbol{\Theta}_{\mathrm{no}}$ and $\boldsymbol{\mathcal{M}}_t^{\mathrm{no}}$ reads

$$\boldsymbol{\Theta}_{\mathrm{no}} = -\tanh\big(\boldsymbol{\mathcal{M}}_t^{\mathrm{no}}/2\big)\,, \qquad e^{\boldsymbol{\mathcal{M}}_t^{\mathrm{no}}} = \frac{\mathbb{1}-\boldsymbol{\Theta}_{\mathrm{no}}}{\mathbb{1}+\boldsymbol{\Theta}_{\mathrm{no}}}\,, \tag{7.144}$$

and thus

$$\frac{\mathrm{d}\boldsymbol{\Theta}_{\mathrm{no}}}{\mathrm{d}t} = -\frac{1}{2}(\mathbb{1}+\boldsymbol{\Theta}_{\mathrm{no}})\frac{\mathrm{d}e^{\boldsymbol{\mathcal{M}}_t^{\mathrm{no}}}}{\mathrm{d}t}(\mathbb{1}+\boldsymbol{\Theta}_{\mathrm{no}})\,. \tag{7.145}$$

Using Eq. (7.145) into Eq. (7.143), we get

$$\frac{\mathrm{d}\boldsymbol{\Theta}_{\mathrm{no}}}{\mathrm{d}t} = -\big(\boldsymbol{\mathcal{W}}\boldsymbol{\Theta}_{\mathrm{no}}+\boldsymbol{\Theta}_{\mathrm{no}}\boldsymbol{\mathcal{W}}^{\dagger}\big)+\boldsymbol{\mathcal{F}}-(\mathbb{1}-\boldsymbol{\Theta}_{\mathrm{no}})\boldsymbol{\Phi}^{\mathrm{T}}(\mathbb{1}-\boldsymbol{\Theta}_{\mathrm{no}})+(\mathbb{1}+\boldsymbol{\Theta}_{\mathrm{no}})\boldsymbol{\Phi}(\mathbb{1}+\boldsymbol{\Theta}_{\mathrm{no}})\,. \tag{7.146}$$

where the explicit forms of $\boldsymbol{\mathcal{W}}$ and $\boldsymbol{\mathcal{F}}$ are provided into Eqs. (7.124,7.125). Note that, if $\boldsymbol{\gamma}^+$ and $\boldsymbol{\gamma}^-$ are symmetric, $(\boldsymbol{\Psi}+\boldsymbol{\Psi}^{\mathrm{T}})$ and $(\boldsymbol{\Psi}-\boldsymbol{\Psi}^{\mathrm{T}})$ take the simple form

$$\boldsymbol{\Psi}+\boldsymbol{\Psi}^{\mathrm{T}} = \frac{1}{2}\begin{pmatrix}\boldsymbol{\gamma}^+ + \boldsymbol{\gamma}^- & 0\\ 0 & \boldsymbol{\gamma}^+ + \boldsymbol{\gamma}^-\end{pmatrix}, \tag{7.147}$$

$$\boldsymbol{\Psi}-\boldsymbol{\Psi}^{\mathrm{T}} = \frac{\mathrm{i}}{2}\begin{pmatrix}0 & \boldsymbol{\gamma}^+ - \boldsymbol{\gamma}^-\\ \boldsymbol{\gamma}^- - \boldsymbol{\gamma}^+ & 0\end{pmatrix}. \tag{7.148}$$

QED

Again, Eq. (7.146) is a Riccati-type equation. Under full monitoring ($\boldsymbol{\Lambda}^+ = \boldsymbol{\Lambda}^- = \mathbb{1}$), $\boldsymbol{\Theta}_{\mathrm{no}} = \boldsymbol{\Theta}$ and we get the Lyapunov equation (7.123) for the unconditional dynamics. In the opposite case where all the channels are not monitored at all ($\boldsymbol{\Lambda}^+ = \boldsymbol{\Lambda}^- = 0$), Eq. (7.146) becomes

$$\frac{\mathrm{d}\boldsymbol{\Theta}_{\mathrm{no}}}{\mathrm{d}t} = -\mathrm{i}[\boldsymbol{\mathcal{T}},\boldsymbol{\Theta}_{\mathrm{no}}] + \frac{1}{2}\boldsymbol{\mathcal{F}} - \frac{1}{2}\boldsymbol{\Theta}_{\mathrm{no}}\boldsymbol{\mathcal{F}}\boldsymbol{\Theta}_{\mathrm{no}}\,. \tag{7.149}$$

The solution of the Riccati-type equation (7.146) gives access the no-jump probability. According to Eq. (7.142), ζ_t satisfies

$$\frac{\mathrm{d}}{\mathrm{d}t}\ln\zeta_t = -\,\mathrm{tr}\Big\{(\boldsymbol{\Psi}-\boldsymbol{\Phi})\frac{\mathbb{1}+\boldsymbol{\Theta}_{\mathrm{no}}}{\mathbb{1}-\boldsymbol{\Theta}_{\mathrm{no}}} - \boldsymbol{\Psi}\Big\}. \tag{7.150}$$

On the other hand, the partition function reads

$$\frac{\mathrm{d}}{\mathrm{d}t}\ln Z_t = \frac{1}{2}\,\mathrm{tr}\Big\{(1+e^{\boldsymbol{\mathcal{M}}_t^{\mathrm{no}}})^{-1}\frac{\mathrm{d}e^{\boldsymbol{\mathcal{M}}_t^{\mathrm{no}}}}{\mathrm{d}t}\Big\}. \tag{7.151}$$

Again, Eqs. (7.150,7.151) require to compute some inverse matrices and we would like to bypass this difficulty. Similarly to Sec. 7.4.2, combining Eqs. (7.144, 7.143, 7.150, 7.151), the anti-symmetry of $\boldsymbol{\mathcal{M}}_t^{\mathrm{no}}$ together with the invariance of the trace under transpose, we get the simple form

$$\frac{\mathrm{d}}{\mathrm{d}t} \ln \zeta_t / Z_t = \mathrm{tr}\left\{\boldsymbol{\Phi}(\mathbb{1} + \boldsymbol{\Theta}_{\mathrm{no}})\right\}. \tag{7.152}$$

From the solution of Eq. (7.152), we see immediately that the no-jump probability takes the form (7.20) with

$$\beta(t) = \mathrm{tr}\left[\boldsymbol{\Phi}(\mathbb{1} + \boldsymbol{\Theta}_{\mathrm{no}}(t))\right]. \tag{7.153}$$

Using Eqs. (7.129,7.117), it is possible to prove that, if $\boldsymbol{\lambda}^+\boldsymbol{\gamma}^+ = \boldsymbol{\lambda}^-\boldsymbol{\gamma}^-$, the no-jump probability reduces to

$$P_{\mathrm{no}}(t) = e^{-\,\mathrm{tr}(\boldsymbol{\Phi})t}\,. \tag{7.154}$$

In this case, it is possible to talk about a *universal behaviour* since the initial state $\Theta(0)$ and the Hamiltonian operator do not enter in the no-jump probability.

In the general case, the long time limit of the no-jump probability reads

$$P_{\mathrm{no}}(t) \sim \exp\left(-\,\mathrm{tr}\left[\boldsymbol{\Phi}(\mathbb{1} + \boldsymbol{\Theta}_{\mathrm{no}}^{\infty})\right] t\right)\,, \qquad t \sim \infty\,, \tag{7.155}$$

where $\boldsymbol{\Theta}_{\mathrm{no}}^{\infty}$ is the stationary solution of the Riccati equation (7.146).

7.7 No-jump dynamics with pairing terms - bosonic chains

In this section, we focus on bosonic chains and we study the no-jump dynamics for particle non-conserving Hamiltonian operators, in analogy with Sec. 7.6.

Assuming the $\mathbf{c}$'s to be bosonic operators, we define the $2L$ quadratures,

$$x_n = c_n^\dagger + c_n, \qquad p_n = \mathrm{i}(c_n^\dagger - c_n). \qquad n = 1, \dots, L \tag{7.156}$$

which are Hermitian ($x_k = x_k^\dagger$, $p_k = p_k^\dagger$) and satisfy the algebra

$$[x_k, p_\ell] = 2\mathrm{i}\delta_{k\ell}, \qquad [x_k, x_\ell] = 0, \qquad [p_k, p_\ell] = 0. \tag{7.157}$$

Below, we work with the vector $\mathbf{R}^\dagger = (x_1, \dots, x_L, p_1, \dots, p_L)$, which then satisfies

$$\left[R_i, R_j\right] = 2\mathrm{i}\Omega_{ij}, \tag{7.158}$$

where $\mathbf{\Omega}$ is the symplectic form

$$\mathbf{\Omega} = (\mathrm{i}\sigma_y) \otimes \mathbb{1}_L = \left(\begin{array}{c|c} 0 & \mathbb{1}_L \\ \hline -\mathbb{1}_L & 0 \end{array}\right), \tag{7.159}$$

$\mathbb{1}_L$ is the $L \times L$ identity matrix and $(\mathrm{i}\mathbf{\Omega})^2 = \mathbb{1}$.

As a direct consequence of the bosonic algebra, any quadratic Hamiltonian $\frac{1}{4}\mathbf{R}^\dagger \cdot \mathcal{T} \cdot \mathbf{R}$ may be represented by $2L \times 2L$ symmetric ($\mathcal{T}^\mathrm{T} = \mathcal{T}$) and Hermitian matrices ($\mathcal{T}^\dagger = \mathcal{T}$). Indeed, if $\mathcal{T}$ is not symmetric, we can always write

$$\mathbf{R}^\dagger \cdot \mathcal{T} \cdot \mathbf{R} = -\frac{1}{2}\,\mathrm{tr}\left((\mathcal{T} - \mathcal{T}^\mathrm{T})(\mathrm{i}\mathbf{\Omega})\right) + \frac{1}{2}\mathbf{R}^\dagger \cdot (\mathcal{T} + \mathcal{T}^\mathrm{T}) \cdot \mathbf{R}\,. \tag{7.160}$$

As an example, we proceed similarly to Sec. 7.6. The most general Gaussian-preserving Hamiltonian is given by Eq. (7.99), which can be recast as into Eq. (7.100), with $\mathcal{K}$ given by Eq. (7.101). The big difference compared to the fermionic case is that now $\mathbf{G}^\mathrm{T} = \mathbf{G}$. Since $\mathbf{h}^\mathrm{T} = \mathbf{h}^*$ and $\mathbf{G}^\dagger = \mathbf{G}^*$,

$$\frac{1}{2}(\mathcal{K} + \mathcal{K}^\mathrm{T}) = \frac{1}{2}\begin{pmatrix} (\mathbf{h}+\mathbf{h}^*) + (\mathbf{G}+\mathbf{G}^*) & \mathrm{i}(\mathbf{h}-\mathbf{h}^*) - \mathrm{i}(\mathbf{G}-\mathbf{G}^*) \\ -\mathrm{i}(\mathbf{h}-\mathbf{h}^*) - \mathrm{i}(\mathbf{G}-\mathbf{G}^*) & (\mathbf{h}+\mathbf{h}^*) - (\mathbf{G}+\mathbf{G}^*) \end{pmatrix}, \tag{7.161}$$

and

$$-\frac{1}{2}\,\mathrm{tr}\left((\mathcal{K} - \mathcal{K}^\mathrm{T})(\mathrm{i}\mathbf{\Omega})\right) = -2\,\mathrm{tr}(\mathbf{h})\,. \tag{7.162}$$

If $\mathbf{h}$ and $\mathbf{G}$ are also real, the symmetrized $\mathcal{K}$ reduces to

$$\frac{1}{2}(\mathcal{K} + \mathcal{K}^\mathrm{T}) = \begin{pmatrix} \mathbf{h}+\mathbf{G} & 0 \\ 0 & \mathbf{h}-\mathbf{G} \end{pmatrix} = \mathbb{1}_2 \otimes \mathbf{h} + \boldsymbol{\sigma}_z \otimes \mathbf{G}, \tag{7.163}$$

and finally

$$H = \frac{1}{4}\mathbf{R}^\dagger \cdot \mathcal{T} \cdot \mathbf{R} - \frac{1}{2}\,\mathrm{tr}(\mathbf{h})\,, \qquad \mathcal{T} := \begin{pmatrix} \mathbf{h}+\mathbf{G} & 0 \\ 0 & \mathbf{h}-\mathbf{G} \end{pmatrix}. \tag{7.164}$$

For this reason, without loss of generality, we assume that the Hamiltonian takes the form

$$H = \frac{1}{4}\mathbf{R}^\dagger \cdot \mathcal{T} \cdot \mathbf{R}\,, \tag{7.165}$$

where $\mathcal{T}$ is a $2L \times 2L$ symmetric and Hermitian matrix.

Similarly to Sec. 7.6, we can prove that the dissipator of the Gaussian-preserving Lindblad generator (7.47) may be put in the form

$$\mathcal{D}(\rho) = \sum_{i,j=1}^{2L} \Psi_{ij}\Big[R_i\rho R_j - \frac{1}{2}\{R_jR_i,\rho\}\Big], \tag{7.166}$$

as well as the partial monitoring dynamics (7.49),

$$\mathcal{L}_0(\rho) = -\mathrm{i}[H,\rho] + \sum_{i,j=1}^{2L}\Big[[\mathbf{\Psi}-\mathbf{\Phi}]_{ij}R_i\rho R_j - \frac{(\mathbf{\Psi})_{ij}}{2}\{R_jR_i,\rho\}\Big], \tag{7.167}$$

where $\mathbf{\Psi}$ and $\mathbf{\Phi}$ are given by Eqs. (7.115,7.117), since these matrices are not sensitive to bosonic or fermionic algebra.

7.7.1 Full monitoring

When every channel is perfectly monitored, $\mathbf{\Lambda}^+ = \mathbf{\Lambda}^- = \mathbb{1}$ and $\mathbf{\Psi} = \mathbf{\Phi}$. The no-jump Liouvillian reduces to

$$\mathcal{L}_0(\rho) = -\mathrm{i}[H,\rho] - \frac{1}{2}\sum_{i,j=1}^{2L} \Psi_{ij}\{R_jR_i,\rho\}, \tag{7.168}$$

After some algebra, $\mathcal{L}_0$ takes the form (7.6) with effective Hamiltonian

$$H_e = \mathbf{R}^\dagger \cdot \frac{\mathcal{T} - \mathrm{i}(\mathbf{\Psi}+\mathbf{\Psi}^{\mathrm{T}})}{4}\cdot \mathbf{R} - -\frac{\mathrm{i}}{4}\,\mathrm{tr}(\gamma^+ - \gamma^-). \tag{7.169}$$

7.7.2 Dynamics under partial monitoring

We now derive the conditional dynamics under partial monitoring, following Sec. 7.6.2 as guideline. We assume that the initial state is Gaussian. The dynamics described by Eq. (7.1) with the quadratures (7.156), the Hamiltonian (7.165), the dissipator (7.166) and the matrix (7.115) is Gaussian preserving, which means

$$\rho(t) := e^{\mathcal{L}t}(\rho_0) = \frac{e^{\frac{1}{4}\mathbf{R}^\dagger\cdot(\mathrm{i}\mathbf{\Omega})\mathcal{M}_t\cdot\mathbf{R}}}{Z_t}, \tag{7.170}$$

where $(i\mathbf{\Omega})\boldsymbol{\mathcal{M}}_t$ is Hermitian and symmetric,

$$Z_t = \mathrm{tr}\Big\{e^{\frac{1}{4}\mathbf{R}^\dagger\cdot(\mathrm{i}\mathbf{\Omega})\mathcal{M}_t\cdot\mathbf{R}}\Big\} = \frac{1}{\sqrt{\det(\mathbb{1}-e^{\mathcal{M}_t})}}, \tag{7.171}$$

$$e^{\mathcal{M}_t} = \frac{\mathbf{\Theta}(i\mathbf{\Omega})-\mathbb{1}}{\mathbf{\Theta}(i\mathbf{\Omega})+\mathbb{1}}, \tag{7.172}$$

and

$$(\mathbf{\Theta})_{ij} = \frac{1}{2}\,\mathrm{tr}\left\{\{R_i, R_j\}\rho(t)\right\} = \frac{1}{2}\langle\{R_i, R_j\}\rangle(t)\,, \tag{7.173}$$

is the correlation matrix. The matrix $\mathbf{\Theta}$ is Hermitian ($\mathbf{\Theta}^\dagger = \mathbf{\Theta}$) and symmetric ($\mathbf{\Theta}^\mathrm{T} = \mathbf{\Theta}$) as well. It can be proved that the correlation matrix $\mathbf{\Theta}$ satisfies the Lyapunov differential equation

$$\frac{\mathrm{d}\mathbf{\Theta}}{\mathrm{d}t} = -\left(\mathcal{W}\mathbf{\Theta} + \mathbf{\Theta}\mathcal{W}^\dagger\right) + \mathcal{F}, \tag{7.174}$$

with

$$\mathcal{W} = -\mathbf{\Omega}\mathcal{T} - (\mathrm{i}\mathbf{\Omega})(\mathbf{\Psi} - \mathbf{\Psi}^\mathrm{T})\,, \tag{7.175}$$

$$\mathcal{F} = 2(\mathrm{i}\mathbf{\Omega})(\mathbf{\Psi}^\mathrm{T} + \mathbf{\Psi})(\mathrm{i}\mathbf{\Omega})\,. \tag{7.176}$$

To solve the conditional dynamics, we take the Gaussian ansatz

$$\tilde{\rho}_\mathrm{no}(t) := e^{\mathcal{L}_0 t}(\rho_0) = \frac{e^{\frac{1}{4}\mathbf{R}^\dagger\cdot(\mathrm{i}\mathbf{\Omega})\mathcal{M}_t^\mathrm{no}\cdot\mathbf{R}}}{\zeta_t}\,, \tag{7.177}$$

for some matrix $\mathcal{M}_t^\mathrm{no}$ and some c-number ζ_t which are to be determined. Again, the properly normalized state is

$$\rho_\mathrm{no}(t) := \frac{\tilde{\rho}_\mathrm{no}(t)}{P_\mathrm{no}(t)} = \frac{e^{\frac{1}{4}\mathbf{R}^\dagger\cdot(\mathrm{i}\mathbf{\Omega})\mathcal{M}_t^\mathrm{no}\cdot\mathbf{R}}}{Z_t}\,, \tag{7.178}$$

$$Z_t = \mathrm{tr}\left(e^{\frac{1}{4}\mathbf{R}^\dagger\cdot(\mathrm{i}\mathbf{\Omega})\mathcal{M}_t^\mathrm{no}\cdot\mathbf{R}}\right). \tag{7.179}$$

In this paragraph, we shall prove that the ansatz (7.177) solves the dynamics (7.167) with the Hamiltonian (7.165). The dynamics of $\tilde{\rho}_\mathrm{no}(t)$ is determined by two independent differential equations for ζ_t and the conditional covariance matrix

$$(\mathbf{\Theta}_\mathrm{no})_{ij} = -[\coth\left(\mathcal{M}_t^\mathrm{no}/2\right)(\mathrm{i}\mathbf{\Omega})]_{ij} = \frac{1}{2}\langle\{R_i, R_j\}\rangle_\mathrm{no}(t)\,. \tag{7.180}$$

Proof

Firstly, we observe that the commutator between two quadratic forms is

$$[\mathbf{R}^\dagger\cdot(\mathrm{i}\mathbf{\Omega})\mathbf{A}\cdot\mathbf{R}, \mathbf{R}^\dagger\cdot(\mathrm{i}\mathbf{\Omega})\mathbf{B}\cdot\mathbf{R}] = 4\mathbf{R}^\dagger\cdot(\mathrm{i}\mathbf{\Omega})[\mathbf{A},\mathbf{B}]\cdot\mathbf{R}\,, \tag{7.181}$$

where $(\mathrm{i}\mathbf{\Omega})\mathbf{A}$ and $(\mathrm{i}\mathbf{\Omega})\mathbf{B}$ are two symmetric matrices. The BCH formula (7.64) and Eq. (7.181) lead to

$$\frac{\mathrm{d}}{\mathrm{d}t}e^{\frac{1}{4}\mathbf{R}^\dagger\cdot(\mathrm{i}\mathbf{\Omega})\mathcal{M}_t^\mathrm{no}\cdot\mathbf{R}} = \mathbf{R}^\dagger\cdot\left[\frac{\mathrm{i}\mathbf{\Omega}}{4}\frac{\mathrm{d}e^{\mathcal{M}_t^\mathrm{no}}}{\mathrm{d}t}e^{-\mathcal{M}_t^\mathrm{no}}\right]\cdot\mathbf{R}\,e^{\frac{1}{4}\mathbf{R}^\dagger\cdot(\mathrm{i}\mathbf{\Omega})\mathcal{M}_t^\mathrm{no}\cdot\mathbf{R}}\,. \tag{7.182}$$

The time-derivative of the no-jump operator reads

$$\frac{\mathrm{d}\tilde{\rho}_{\mathrm{no}}}{\mathrm{d}t} = \mathbf{R}^{\dagger}\cdot\left[\frac{\mathrm{i}\boldsymbol{\Omega}}{4}\frac{\mathrm{d}e^{\mathcal{M}_t^{\mathrm{no}}}}{\mathrm{d}t}e^{-\mathcal{M}_t^{\mathrm{no}}}\right]\cdot\mathbf{R}\,\tilde{\rho}_{\mathrm{no}} - \left(\frac{\mathrm{d}}{\mathrm{d}t}\ln\zeta_t\right)\tilde{\rho}_{\mathrm{no}}\,. \tag{7.183}$$

Since the matrix $(\mathrm{i}\boldsymbol{\Omega})\mathcal{M}_t^{\mathrm{no}}$ is symmetric, it is possible to prove that the matrix $\left[\frac{\mathrm{i}\Omega}{4}\frac{\mathrm{d}e^{\mathcal{M}_t^{\mathrm{no}}}}{\mathrm{d}t}e^{-\mathcal{M}_t^{\mathrm{no}}}\right]$ is symmetric as well. Using the identity $(\mathrm{i}\boldsymbol{\Omega})^{\mathrm{T}} = -(\mathrm{i}\boldsymbol{\Omega})$, the transpose matrix becomes

$$\left[(\mathrm{i}\boldsymbol{\Omega})\frac{\mathrm{d}e^{\mathcal{M}_t^{\mathrm{no}}}}{\mathrm{d}t}e^{-\mathcal{M}_t^{\mathrm{no}}}\right]^{\mathrm{T}} = -e^{-(\mathcal{M}_t^{\mathrm{no}})^{\mathrm{T}}}\frac{\mathrm{d}e^{(\mathcal{M}_t^{\mathrm{no}})^{\mathrm{T}}}}{\mathrm{d}t}(\mathrm{i}\boldsymbol{\Omega})\,. \tag{7.184}$$

Thanks to the identity (7.134), $(i\boldsymbol{\Omega})^2 = 1$ and the series expansion,

$$\begin{aligned}\left[(\mathrm{i}\boldsymbol{\Omega})\frac{\mathrm{d}e^{\mathcal{M}_t^{\mathrm{no}}}}{\mathrm{d}t}e^{-\mathcal{M}_t^{\mathrm{no}}}\right]^{\mathrm{T}} &= (\mathrm{i}\boldsymbol{\Omega})\left[(\mathrm{i}\boldsymbol{\Omega})\frac{\mathrm{d}e^{-(\mathcal{M}_t^{\mathrm{no}})^{\mathrm{T}}}}{\mathrm{d}t}(\mathrm{i}\boldsymbol{\Omega})\right]\left[(\mathrm{i}\boldsymbol{\Omega})e^{(\mathcal{M}_t^{\mathrm{no}})^{\mathrm{T}}}(\mathrm{i}\boldsymbol{\Omega})\right] & (7.185)\\ &= (\mathrm{i}\boldsymbol{\Omega})\frac{\mathrm{d}e^{-(\mathrm{i}\Omega)(\mathcal{M}_t^{\mathrm{no}})^{\mathrm{T}}(\mathrm{i}\Omega)}}{\mathrm{d}t}\,e^{(\mathrm{i}\Omega)(\mathcal{M}_t^{\mathrm{no}})^{\mathrm{T}}(\mathrm{i}\Omega)}\,. & (7.186)\end{aligned}$$

Since the matrix $(\mathrm{i}\boldsymbol{\Omega})\mathcal{M}_t^{\mathrm{no}}$ is symmetric,

$$\mathcal{M}_t^{\mathrm{no}} = -(\mathrm{i}\Omega)\left(\mathcal{M}_t^{\mathrm{no}}\right)^{\mathrm{T}}(\mathrm{i}\Omega)\,, \tag{7.187}$$

we conclude that $\left[\frac{\mathrm{i}\Omega}{4}\frac{\mathrm{d}e^{\mathcal{M}_t^{\mathrm{no}}}}{\mathrm{d}t}e^{-\mathcal{M}_t^{\mathrm{no}}}\right]^{\mathrm{T}} = \left[\frac{\mathrm{i}\Omega}{4}\frac{\mathrm{d}e^{\mathcal{M}_t^{\mathrm{no}}}}{\mathrm{d}t}e^{-\mathcal{M}_t^{\mathrm{no}}}\right]$. Thus, $\mathrm{d}\tilde{\rho}_{\mathrm{no}}/\mathrm{d}t$ takes the form $\kappa\tilde{\rho}_{\mathrm{no}} + \mathbf{R}^{\dagger}\cdot\mathcal{K}\cdot\mathbf{R}\,\tilde{\rho}_{\mathrm{no}}$, where κ is a c-number and $\mathcal{K}$ is a symmetric matrix.

Hence, when we rewrite the generator (7.167) by using the Gaussian ansatz, we shall always make sure to cast it in the same form. In order to do this, we use the identity

$$e^{\frac{1}{4}\mathbf{R}^{\dagger}\cdot(\mathrm{i}\Omega)\mathcal{M}_t^{\mathrm{no}}\cdot\mathbf{R}}\,\mathbf{R} = e^{-\mathcal{M}_t^{\mathrm{no}}}\,\mathbf{R}\,e^{\frac{1}{4}\mathbf{R}^{\dagger}\cdot(\mathrm{i}\Omega)\mathcal{M}_t^{\mathrm{no}}\cdot\mathbf{R}}\,. \tag{7.188}$$

This leads, for example, to

$$-\mathrm{i}[H,\tilde{\rho}_{\mathrm{no}}] = \mathbf{R}^{\dagger}\cdot\left[-\frac{\mathrm{i}}{4}\left(\mathcal{T} - e^{-(\mathcal{M}_t^{\mathrm{no}})^{\mathrm{T}}}\mathcal{T}e^{-\mathcal{M}_t^{\mathrm{no}}}\right)\right]\cdot\mathbf{R}\,\tilde{\rho}_{\mathrm{no}}\,, \tag{7.189}$$

which is the unitary contribution to the dynamics. The matrix $\mathcal{T} - e^{-(\mathcal{M}_t^{\mathrm{no}})^{\mathrm{T}}}\mathcal{T}e^{-\mathcal{M}_t^{\mathrm{no}}}$ is already in the proper symmetric form. The dissipators take the form

$$\begin{aligned}\sum_{ij}[\boldsymbol{\Psi}-\boldsymbol{\Phi}]_{ij}R_i\tilde{\rho}_{\mathrm{no}}R_j &= \mathbf{R}^{\dagger}\cdot[\boldsymbol{\Psi}-\boldsymbol{\Phi}]e^{-\mathcal{M}_t^{\mathrm{no}}}\cdot\mathbf{R}\,\tilde{\rho}_{\mathrm{no}}\,, & (7.190)\\ \sum_{ij}(\boldsymbol{\Psi})_{ij}\{R_jR_i,\tilde{\rho}_{\mathrm{no}}\} &= \mathbf{R}^{\dagger}\cdot\left[\boldsymbol{\Psi} + e^{-(\mathcal{M}_t^{\mathrm{no}})^{\mathrm{T}}}\boldsymbol{\Psi}e^{-\mathcal{M}_t^{\mathrm{no}}}\right]\cdot\mathbf{R}\,\tilde{\rho}_{\mathrm{no}} & \\ &\quad +4\mathrm{i}\,\mathrm{tr}(\boldsymbol{\Psi}\boldsymbol{\Omega})\,\tilde{\rho}_{\mathrm{no}}\,. & (7.191)\end{aligned}$$

These terms, however, do not have symmetric matrices in their quadratic forms. We must therefore use Eq. (7.160), which leads to

$$\begin{aligned}\sum_{ij}[\mathbf{\Psi}-\mathbf{\Phi}]_{ij}R_i\tilde{\rho}_{\text{no}}R_j &= \mathbf{R}^\dagger\cdot\left[\frac{[\mathbf{\Psi}-\mathbf{\Phi}]e^{-\mathcal{M}_t^{\text{no}}}+e^{-(\mathcal{M}_t^{\text{no}})^{\mathrm{T}}}[\mathbf{\Psi}-\mathbf{\Phi}]^{\mathrm{T}}}{2}\right]\cdot\mathbf{R}\,\tilde{\rho}_{\text{no}}\\ &\quad -\operatorname{tr}\left([\mathbf{\Psi}-\mathbf{\Phi}]e^{-\mathcal{M}_t^{\text{no}}}(\mathrm{i}\mathbf{\Omega})\right)\tilde{\rho}_{\text{no}}\,, \qquad (7.192)\end{aligned}$$

$$\begin{aligned}\sum_{ij}(\mathbf{\Psi})_{ij}\{R_jR_i,\tilde{\rho}_{\text{no}}\} &= \mathbf{R}^\dagger\cdot\left[\frac{\mathbf{\Psi}+\mathbf{\Psi}^{\mathrm{T}}}{2}+e^{-(\mathcal{M}_t^{\text{no}})^{\mathrm{T}}}\frac{\mathbf{\Psi}+\mathbf{\Psi}^{\mathrm{T}}}{2}e^{-\mathcal{M}_t^{\text{no}}}\right]\cdot\mathbf{R}\,\tilde{\rho}_{\text{no}}\\ &\quad +2\operatorname{tr}\left(\mathbf{\Psi}(\mathrm{i}\mathbf{\Omega})\right)\tilde{\rho}_{\text{no}}\,. \qquad (7.193)\end{aligned}$$

The no-jump operator (7.167) applied to the Gaussian ansatz becomes

$$\begin{aligned}\mathcal{L}_0(\tilde{\rho}_{\text{no}}) &= \mathbf{R}^\dagger\cdot\left[\frac{[\mathbf{\Psi}-\mathbf{\Phi}]e^{-\mathcal{M}_t^{\text{no}}}+e^{-(\mathcal{M}_t^{\text{no}})^{\mathrm{T}}}[\mathbf{\Psi}-\mathbf{\Phi}]^{\mathrm{T}}}{2}\right]\cdot\mathbf{R}\,\tilde{\rho}_{\text{no}}\\ &\quad -\mathbf{R}^\dagger\cdot\left[\frac{\mathbf{\Psi}+\mathbf{\Psi}^{\mathrm{T}}}{4}+e^{-(\mathcal{M}_t^{\text{no}})^{\mathrm{T}}}\frac{\mathbf{\Psi}+\mathbf{\Psi}^{\mathrm{T}}}{4}e^{-\mathcal{M}_t^{\text{no}}}\right]\cdot\mathbf{R}\,\tilde{\rho}_{\text{no}}\\ &\quad +\mathbf{R}^\dagger\cdot\left[-\frac{\mathrm{i}}{4}\left(\mathcal{T}-e^{-(\mathcal{M}_t^{\text{no}})^{\mathrm{T}}}\mathcal{T}e^{-\mathcal{M}_t^{\text{no}}}\right)\right]\cdot\mathbf{R}\,\tilde{\rho}_{\text{no}}\\ &\quad -\operatorname{tr}\left(\left[\mathbf{\Psi}+[\mathbf{\Psi}-\mathbf{\Phi}]e^{-\mathcal{M}_t^{\text{no}}}\right](\mathrm{i}\mathbf{\Omega})\right)\tilde{\rho}_{\text{no}}\,. \qquad (7.194)\end{aligned}$$

Combining Eq. (7.194) with Eq. (7.183), we get the differential equations

$$\begin{aligned}\frac{\mathrm{d}}{\mathrm{d}t}\ln\zeta_t &= \operatorname{tr}\left(\left[\mathbf{\Psi}+[\mathbf{\Psi}-\mathbf{\Phi}]e^{-\mathcal{M}_t^{\text{no}}}\right](\mathrm{i}\mathbf{\Omega})\right)\,, \qquad (7.195)\\ (\mathrm{i}\mathbf{\Omega})\frac{\mathrm{d}e^{\mathcal{M}_t^{\text{no}}}}{\mathrm{d}t} &= -\mathrm{i}\left(\mathcal{T}e^{\mathcal{M}_t^{\text{no}}}-e^{-(\mathcal{M}_t^{\text{no}})^{\mathrm{T}}}\mathcal{T}\right)+2[\mathbf{\Psi}-\mathbf{\Phi}]+2e^{-(\mathcal{M}_t^{\text{no}})^{\mathrm{T}}}[\mathbf{\Psi}-\mathbf{\Phi}]^{\mathrm{T}}e^{\mathcal{M}_t^{\text{no}}}\\ &\quad -(\mathbf{\Psi}+\mathbf{\Psi}^{\mathrm{T}})e^{\mathcal{M}_t^{\text{no}}}-e^{-(\mathcal{M}_t^{\text{no}})^{\mathrm{T}}}(\mathbf{\Psi}+\mathbf{\Psi}^{\mathrm{T}})\,. \qquad (7.196)\end{aligned}$$

Again, the matrix $\mathcal{M}_t^{\text{no}}$ is not so convenient to work with. For this reason, we recast Eq. (7.196) in terms of the conditional covariance matrix $(\mathbf{\Theta}_{\text{no}})_{ij} = \frac{1}{2}\operatorname{tr}\left\{\{R_i,R_j\}\rho_{\text{no}}(t)\right\}$. For the Gaussian ansatz (7.178), the matrix $\mathcal{M}_t^{\text{no}}$ and the correlation matrix $\mathbf{\Theta}_{\text{no}}$ are related by

$$\mathbf{\Theta}_{\text{no}} = -\coth\left(\mathcal{M}_t^{\text{no}}/2\right)(\mathrm{i}\mathbf{\Omega})\,, \qquad e^{\mathcal{M}_t^{\text{no}}} = \frac{\mathbf{\Theta}_{\text{no}}(\mathrm{i}\mathbf{\Omega})-\mathbb{1}}{\mathbf{\Theta}_{\text{no}}(\mathrm{i}\mathbf{\Omega})+\mathbb{1}}\,. \qquad (7.197)$$

One can also readily show that

$$\frac{\mathrm{d}\mathbf{\Theta}_{\text{no}}}{\mathrm{d}t}(\mathrm{i}\mathbf{\Omega}) = \frac{1}{2}\left(\mathbb{1}+\mathbf{\Theta}_{\text{no}}(\mathrm{i}\mathbf{\Omega})\right)\frac{\mathrm{d}e^{\mathcal{M}_t^{\text{no}}}}{\mathrm{d}t}\left(\mathbb{1}+\mathbf{\Theta}_{\text{no}}(\mathrm{i}\mathbf{\Omega})\right)\,. \qquad (7.198)$$

Using Eq. (7.198) to rewrite Eq. (7.196), we get

$$\frac{\mathrm{d}\mathbf{\Theta}_{\mathrm{no}}}{\mathrm{d}t}=-(\mathcal{W}\mathbf{\Theta}_{\mathrm{no}}+\mathbf{\Theta}_{\mathrm{no}}\mathcal{W}^{\dagger})+\mathcal{F}-(\mathrm{i}\mathbf{\Omega}-\mathbf{\Theta}_{\mathrm{no}})\,\mathbf{\Phi}^{\mathrm{T}}\,(\mathrm{i}\mathbf{\Omega}-\mathbf{\Theta}_{\mathrm{no}})-(\mathrm{i}\mathbf{\Omega}+\mathbf{\Theta}_{\mathrm{no}})\,\mathbf{\Phi}\,(\mathrm{i}\mathbf{\Omega}+\mathbf{\Theta}_{\mathrm{no}})\,, \tag{7.199}$$

with $\mathcal{W}$ and $\mathcal{F}$ are the same into Eqs. (7.175,7.176).

QED

Eq. (7.199) is another Riccati-type equation. If there is no monitoring, $\mathbf{\Lambda}^{+}=\mathbf{\Lambda}^{-}=0$, $\mathbf{\Theta}_{\mathrm{no}}=\mathbf{\Theta}$ and we recover the Lyapunov equation (7.174) for the unconditional dynamics. When $\mathbf{\Lambda}^{+}=\mathbf{\Lambda}^{-}=\mathbb{1}$, Eq. (7.199) can also be written as

$$\frac{\mathrm{d}\mathbf{\Theta}_{\mathrm{no}}}{\mathrm{d}t}=-\mathbf{\Theta}_{\mathrm{no}}\mathcal{T}\mathbf{\Omega}-(\mathcal{T}\mathbf{\Omega})^{\mathrm{T}}\mathbf{\Theta}_{\mathrm{no}}+\frac{1}{2}\mathcal{F}-\frac{1}{2}\mathbf{\Theta}_{\mathrm{no}}(\mathrm{i}\mathbf{\Omega})\mathcal{F}(\mathrm{i}\mathbf{\Omega})\mathbf{\Theta}_{\mathrm{no}}\,. \tag{7.200}$$

Again, the solution of the Riccati equation (7.199) gives access to the no-jump probability $P_{\mathrm{no}}(t)$. According to Eq. (7.195), ζ_t satisfies

$$\frac{\mathrm{d}}{\mathrm{d}t}\ln\zeta_t=\mathrm{tr}\left\{(\mathrm{i}\mathbf{\Omega})\mathbf{\Psi}+\frac{\mathbf{\Theta}_{\mathrm{no}}(\mathrm{i}\mathbf{\Omega})+\mathbb{1}}{\mathbf{\Theta}_{\mathrm{no}}(\mathrm{i}\mathbf{\Omega})-\mathbb{1}}(\mathrm{i}\mathbf{\Omega})(\mathbf{\Psi}-\mathbf{\Phi})\right\}, \tag{7.201}$$

Thanks to the Jacobi formula, the partition function evolves according to

$$\frac{\mathrm{d}}{\mathrm{d}t}\ln Z_t=\frac{1}{2}\,\mathrm{tr}\left\{(\mathbb{1}-e^{\mathcal{M}_t^{\mathrm{no}}})^{-1}\frac{\mathrm{d}e^{\mathcal{M}_t^{\mathrm{no}}}}{\mathrm{d}t}\right\}. \tag{7.202}$$

Combining Eqs. (7.197, 7.196, 7.201, 7.202, 7.187) together with the invariance of the trace under transpose, we arrive at

$$\frac{\mathrm{d}}{\mathrm{d}t}\ln\zeta_t/Z_t=\mathrm{tr}\left\{\mathbf{\Phi}(\mathrm{i}\mathbf{\Omega}+\mathbf{\Theta}_{\mathrm{no}})\right\}. \tag{7.203}$$

The no-jump probability finally takes the form (7.20) with

$$\beta(t)=\mathrm{tr}\left[\mathbf{\Phi}(\mathrm{i}\mathbf{\Omega}+\mathbf{\Theta}_{\mathrm{no}}(t))\right]. \tag{7.204}$$

Contrary to the fermionic case (see Sec. 7.6), if $\lambda^{+}\gamma^{+}=\lambda^{-}\gamma^{-}$, the bosonic case does not show any universal behaviour. In fact, the no-jump probability always depends on the full evolution of the correlation matrix.

In the general case, the long time limit of the no-jump probability reads

$$P_{\mathrm{no}}(t)\sim\exp\left(-\,\mathrm{tr}\left[\mathbf{\Phi}(\mathrm{i}\mathbf{\Omega}+\mathbf{\Theta}_{\mathrm{no}}^{\infty})\right]t\right)\,,\qquad t\sim\infty \tag{7.205}$$

where $\mathbf{\Theta}_{\mathrm{no}}^{\infty}$ is the stationary solution of the Riccati equation (7.199).

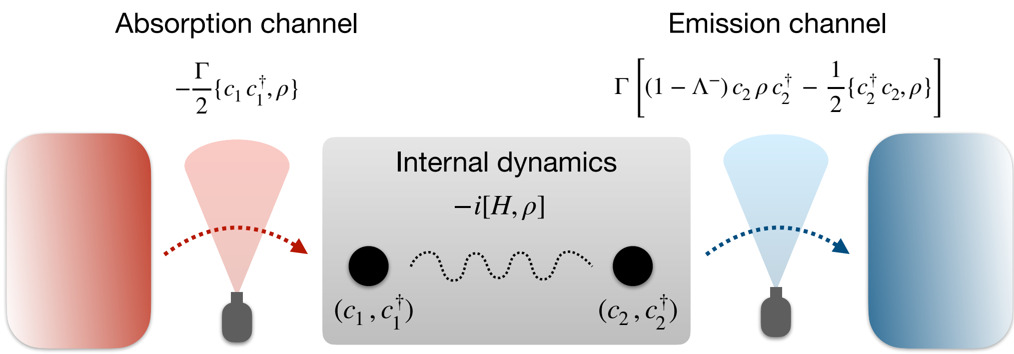

Figure 7.9: Sketch of the boundary-driven system: we study the no-jump dynamics (7.206) which undergoes a non-ideal measurement process on the emission channel, with monitory efficiency Λ^-. The internal dynamics is generated by the Hamiltonian H, which takes the form (7.207) for fermions and (7.208) for bosons.

7.8 Example: boundary driven system

As an application of the no-jump dynamics with pairing terms (see Sec. 7.6 and Sec. 7.7), we study a simple boundary driven system of bosons (B) and fermions (F). More specifically, we couple a 2-site system to two reservoirs, with an absorption channel on site 1 and an emission channel on site 2 (see Fig. 7.9). We assume jump rates $\Gamma_1^+ = \Gamma_2^- = \Gamma$ and two local detectors monitoring the particle exchange. In particular, we suppose that the detector on the hot bath works with perfect efficiency $\Lambda^+ = 1$ and the other one on the cold reservoir with efficiency $\Lambda^- \in (0, 1)$. We prepare the system in the vacuum state $|00\rangle$, which is a Gaussian state, and then we apply the theoretical results of Sec. 7.6 and Sec. 7.7 to study the no-jump dynamics

$$\mathcal{L}_0(\rho) = -\mathrm{i}[H, \rho] - \frac{\Gamma}{2}\{c_1 c_1^\dagger, \rho\} + \Gamma\left[(1-\Lambda^-)\, c_2 \rho c_2^\dagger - \frac{1}{2}\{c_2^\dagger c_2, \rho\}\right], \tag{7.206}$$

where H is the prototypical Hamiltonian

$$H = c_1^\dagger c_2 + c_2^\dagger c_1 + g(c_1 c_2 - c_1^\dagger c_2^\dagger), \qquad \text{(F)} \tag{7.207}$$

$$H = c_1^\dagger c_2 + c_2^\dagger c_1 + g(c_1 c_2 + c_1^\dagger c_2^\dagger), \qquad \text{(B)} \tag{7.208}$$

and g is the amplitude of the pairing terms. The full experimental setup is schematically represented in Fig. 7.9.

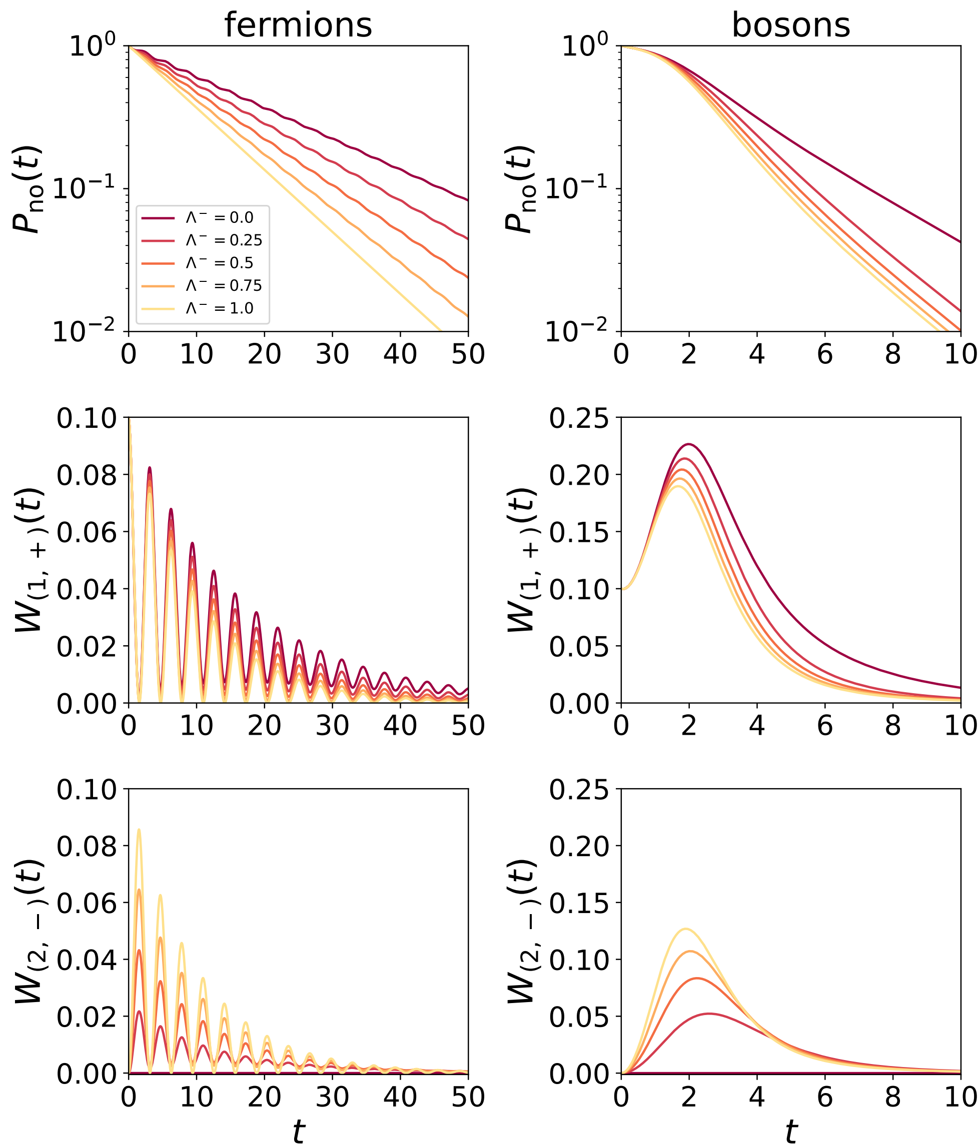

Figure 7.10: Conditional dynamics (7.206) for $\Gamma = 0.1$, $g = 1$ and monitoring efficiency $\Lambda^- = \{0, 0.25, 0.5, 0.75, 1\}$. As expected, the no-jump probability and the WTDs always show an exponential decay.

As usual, we aim to compute the no-jump probability

$$P_{\text{no}}(t) = \begin{cases} \exp\left(-\int_0^t ds\ \text{tr}\left[\mathbf{\Phi}\left(\mathbb{1} + \mathbf{\Theta}_{\text{no}}(s)\right)\right]\right), & \text{(F)} \\ \exp\left(-\int_0^t ds\ \text{tr}\left[\mathbf{\Phi}\left(\text{i}\mathbf{\Omega} + \mathbf{\Theta}_{\text{no}}(s)\right)\right]\right), & \text{(B)} \end{cases} \tag{7.209}$$

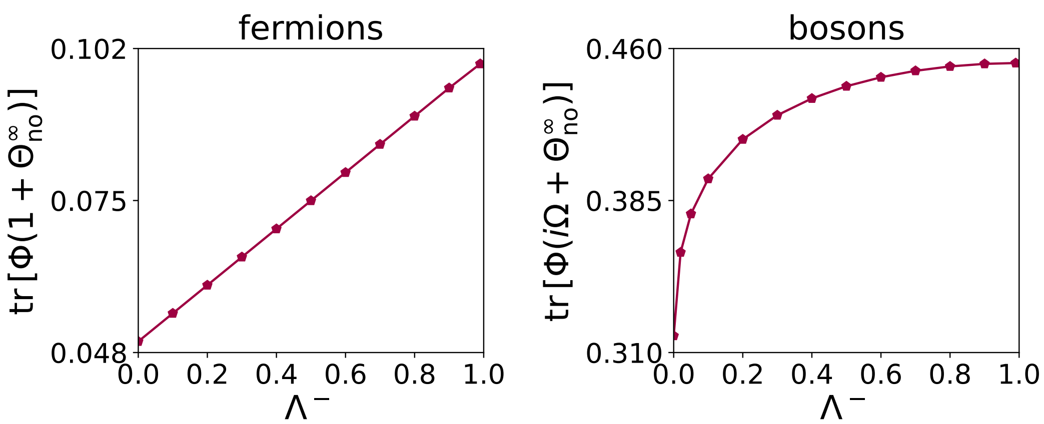

Figure 7.11: We show the decay coefficients of the no-jump probability (7.209) and the WTDs (7.210,7.211), as a function of the monitoring efficiency Λ^- (bosonic and fermionic case).

and the WTDs

$$W_{(2,-)}(t) = \Gamma\Lambda^- P_{\mathrm{no}}(t)\,\langle c_2^\dagger c_2\rangle_{\mathrm{no}}(t)$$
$$= \Gamma\Lambda^- P_{\mathrm{no}}(t) \times \begin{cases} \frac{1}{2}\left(1 + \mathrm{i}\boldsymbol{\Theta}_{\mathrm{no}}(t)_{24}\right)\,, & \text{(F)} \\ \\ \frac{1}{4}\left(\boldsymbol{\Theta}_{\mathrm{no}}(t)_{22} + \boldsymbol{\Theta}_{\mathrm{no}}(t)_{44} - 2\right)\,, & \text{(B)} \end{cases} \tag{7.210}$$

$$W_{(1,+)}(t) = \Gamma P_{\mathrm{no}}(t)\,\langle c_1 c_1^\dagger\rangle_{\mathrm{no}}(t)$$
$$= \Gamma P_{\mathrm{no}}(t) \times \begin{cases} \frac{1}{2}\left(1 - \mathrm{i}\boldsymbol{\Theta}_{\mathrm{no}}(t)_{13}\right)\,, & \text{(F)} \\ \\ \frac{1}{4}\left(\boldsymbol{\Theta}_{\mathrm{no}}(t)_{11} + \boldsymbol{\Theta}_{\mathrm{no}}(t)_{33} + 2\right)\,, & \text{(B)} \end{cases} \tag{7.211}$$

which are formulated in terms of the 4×4 correlation matrix $\boldsymbol{\Theta}$. The definition and the dynamics of $\boldsymbol{\Theta}$ are different for the bosonic and fermionic case; see Eqs. (7.129,7.146) for fermions and Eqs. (7.180,7.199) for bosons. We remember that $P_{\mathrm{no}}(t)$ is the probability of not detecting any jump in $[0,t]$, while $W_{(2,-)}(t)$ and $W_{(1,+)}(t)$ are the probability distributions to observe the first jump in the channel $(2,-)$ and $(1,+)$, respectively. Due to the normalization condition, the WTDs satisfy

$$\int_0^\infty dt\, \left(W_{(1,+)}(t) + W_{(2,-)}(t)\right) = 1\,. \tag{7.212}$$

In Fig. 7.10, we show the no-jump probability (7.209) and the WTDs (7.210,7.211) for $\Gamma = 0.1$, $g = 1$ and different values of the monitoring efficiency Λ^-. The two columns refer to the fermionic and bosonic dynamics, respectively. The no-jump probability is a decreasing function of Λ^-, since particles escaping through the right channel are likely monitored before being ejected. If the bosonic WTDs show a fast decay, revealing that the system quickly reaches an asymptotic regime where the pair creation-annihlation processes are balanced by the missed detection, the fermionic WTDs follow a damped oscillatory behaviour with the same periodicity of the particle occupation, with maxima and minima reflecting the back and forth motion of the fermions. The exponential decay of $P_{\mathrm{no}}(t)$, $W_{(1,+)}(t)$ and $W_{(2,-)}(t)$ is determined by the stationary state, characterised by $\mathbf{\Theta}_{\mathrm{no}}^{\infty}$, which always exists except for the fermionic case under perfect monitoring ($\Lambda^- = 1$). In addition, for the sake of completeness, Fig. 7.11 shows $\mathrm{tr}\left[\mathbf{\Phi}\left(\mathbb{1}+\mathbf{\Theta}_{\mathrm{no}}^{\infty}\right)\right]$ and $\mathrm{tr}\left[\mathbf{\Phi}\left(\mathrm{i}\mathbf{\Omega}+\mathbf{\Theta}_{\mathrm{no}}^{\infty}\right)\right]$ as a function of the parameter Λ^-, which are the decay coefficients of the fermionic and bosonic no-jump probabilities; since data in Fig. 7.11 come from the numerical solutions of highly nonlinear equations, the functions $\mathrm{tr}\left[\mathbf{\Phi}\left(\mathbb{1}+\mathbf{\Theta}_{\mathrm{no}}^{\infty}\right)\right]$ and $\mathrm{tr}\left[\mathbf{\Phi}\left(\mathrm{i}\mathbf{\Omega}+\mathbf{\Theta}_{\mathrm{no}}^{\infty}\right)\right]$ are very involved. However, Fig. 7.11 apparently shows a linear growth for $\mathrm{tr}\left[\mathbf{\Phi}\left(\mathbb{1}+\mathbf{\Theta}_{\mathrm{no}}^{\infty}\right)\right]$ as a function of Λ^-. The decay coefficient is a monotonically increasing function of Λ^-, for both bosons and fermions, as we expect if approaching the ideal monitoring regime.

7.9 Discussion and conclusion

In this chapter, we analysed the conditional no-jump dynamics under partial monitoring. After providing some general theoretical results, we focused on single qubits with simple emission and absorption profiles, whose conditional and unconditional dynamics show a rich behaviour. Afterwards, we studied open non-interacting chains with single particle gain-loss processes, whose conditional dynamics is solved by a Gaussian ansatz. We successfully generalised the results of Ref. [167], for both fermionic and bosonic systems. We analysed the no-jump probabilities and the WTDs, which come from the solution of a Riccati-type differential equation for the correlation matrix. Finally, we applied the theoretical results to hopping chains with specific emission/absorption profiles and simple boundary-driven systems. Especially, the results for non-interacting bosons with non-vanishing pairing terms offer natural applications in quantum optics.

Conclusions

In this thesis, we have investigated some aspects of one-dimensional open quantum systems driven out-of-equilibrium. We have addressed the problem from many different perspectives, exhibiting very rich behaviours which have been assessed both analytically and numerically.

In Chapter 4 [A1], we presented a numerical work, based on the entanglement dynamics for a quantum chain of hopping fermions perturbed by local projective measurements. The most relevant results concern the scaling of the dynamical and asymptotic entanglement entropy: the linear growth is replaced by a logarithmic one, while the stationary entanglement entropy undergoes a sharp transition from volume to area-law. We further supported our results by using the collapsed quasi-particle ansatz. Finally we analysed the fluctuations of the stationary entanglement entropy and its scaling behaviour.
In Chapter 4, we have often pointed out the limitations of the entangled-pair quasi-particle ansatz, which is an incomplete picture to capture the dynamical behaviour and the higher moments of the entanglement. A possible working direction could be to unravel and control the multiplets structure behind quantum correlations.

In Chapter 5 [A2], we generalised the hydrodynamic approach for open systems under inhomogeneous gain and loss processes with dephasing. Following a semiclassical approach, we derived the equation of motion of the Wigner function which, for weakly-entangled and highly excited initial states, can be pictorially viewed as a distribution of classical non-interacting particles moving in the phase space. We applied our results to different physical scenarios, comparing the hydrodynamic picture, which applies in mesoscopic scales, with the exact microscopic dynamics.
The theoretical results of Chapter 5 even hold for inhomogeneous dephasing rates, but those scenarios are not explored in this work. The constant dephasing introduces a crossover-time between the ballistic and the diffusive regimes. A possible working direction could be the study of space-dependent dephasing rates, with an expected crossover point in space-time.

Chapter 6 [A3] is maybe the most ambitious part of this thesis, since we really

tried to answer fundamental questions about open markovian quantum dynamics. We compared two of the most famous models of damped harmonic oscillator, namely the friction and cavity models. Apparently, it passed unnoticed that these two models do not reproduce the same time evolution and this gave us the motivation to go deeply into their dynamical behaviour.
More specifically, the friction and cavity models are based on two sets of Langevin equations, involving different deterministic damping terms and stochastic markovian noises with correlators depending on the two times t, t' only through delta functions $\delta(t-t')$. By itself, this means that such a form can only hold true after a microscopic transient time τ_{micro} such that any peaked 'initial' noise correlator will converge to a delta-correlated form for $|t-t'| \gg \tau_{\text{micro}}$. The noise correlators are obtained by four physically reasonable requirements. This gives access to the two-point functions and then the master equations for the reduced density matrix. Surprisingly, the master equation of the friction model turns out to be a non-completely positive map, which, microscopically, may arise from initially correlated states. We mapped the master equations into Fokker-Plank differential equations for the Wigner function, and then we studied the relaxation to equilibrium. For the friction model we distinguished between over-damped and under-damped regimes, while the cavity model only exhibits an under-damped regime. The asymptotic Wigner function reveals that the friction model always guarantees relaxation to equilibrium, while for the cavity model this is true only for vanishing magnetic fields. Finally, we recast the friction and cavity models as mean-field approximations of a many-body interacting magnet and we analyse the nature of the phase diagrams at zero temperature.
Given these results, it is natural to extend the study to other physical models, such as the quantum spherical model. What would the spherical constraint imply for the friction and cavity models? What about the many-body generalisation?

In Chapter 7 [A4], we analysed the conditional no-jump dynamics for non-interacting particles coupled to Lindblad baths. More formally, any quantum jump may be pictorially viewed as the action of some detectors monitoring the system-baths exchange of particles. The non-deal detection is realised by assigning to each dissipative channel a finite efficiency $\Lambda \in [0,1]$, with $\Lambda = 1$ for perfect efficiency and $\Lambda = 0$ when the channel is not monitored at all. In this chapter, we computed the time-evolved no-jump state, whose dynamics is conditioned on no jumps being detected in $[0,t]$. For many-body systems and linear jump operators, the Gaussian ansatz solves the no-jump evolution. We got a Riccati-type differential equation for the correlation matrix, which gives access to the no-jump probability and the waiting-time distributions. These quantities have been computed for specific quantum systems, such as tight-binding chains with particular emission/absorption profiles and simple boundary driven systems.

In Chapter 7, we generalised the results in Ref. [167], where the author derived the waiting-time distributions for boundary driven chains of hopping fermions. In Chapter 7, we provided analytical results for any quadratic model and more general emission/absorption profiles, including the bosonic case. The application of our results covers a huge spectrum, especially for bosonic systems, where pair creation terms play a fundamental role in quantum optics.

References

Articles covering the presented results

A1 M. Coppola, E. Tirrito, D. Karevski and M. Collura:
'Growth of entanglement entropy under local projective measurements',
Physical Review B **105**, 094303 (2022), arXiv:2109.10837v2.

A2 M. Coppola, G. T. Landi and D. Karevski:
'Wigner dynamics for quantum gases under inhomogeneous gain and loss processes with dephasing',
Physical Review A **107**, 052213 (2023), arXiv:2212.11029v2.

A3 M. Coppola, Z. Daouma and M. Henkel:
'From lindblad master equations to langevin dynamics and back',
arXiv:2305.06312v1, Submitted on Physical Review A.

A4 M. Coppola, D. Karevski and G. T. Landi:
'Conditional no-jump dynamics of non-interacting quantum chains',
arXiv:2311.05515v1, Submitted on Physical Review B.

Related articles

B1 M. Coppola and D. Karevski:
'Some speculations about local thermalization of nonequilibrium extended quantum systems',
Condensed Matter Physics **26**, 13502 (2023), arXiv:2303.01881v1.

Books

C1 J. B. Anderson:
Quantum monte carlo: origins, development, applications,
(Oxford University Press, 2007).

C2 M. M. Wilde:
Quantum information theory,
(Cambridge university press, 2013).

C3 J. S. Bell:
Speakable and unspeakable in quantum mechanics: collected papers on quantum philosophy,
(Cambridge university press, 2004).

C4 M. Henkel:
Conformal invariance and critical phenomena,
(Springer Science & Business Media, 1999).

C5 H. Nishimori and G. Ortiz:
Elements of phase transitions and critical phenomena,
(Oxford University Press, 2010).

C6 H.-P. Breuer and F. Petruccione:
The theory of open quantum systems,
(Oxford University Press on Demand, 2002).

C7 C. Cohen-Tannoudji, J. Dupont-Roc and G. Grynberg:
Atom-photon interactions: basic processes and applications,
(John Wiley & Sons, 1998).

C8 H. Carmichael:
Statistical methods in quantum optics 1: master equations and fokker-planck equations,
Vol. 1 (Springer Science & Business Media, 1999).

C9 R. Becker:
Theorie der wärme,
2nd (Springer, Heidelberg, 1978).

C10 G. W. Collins:
The virial theorem in stellar astrophysics,
(Pachart Publishing House, Tucson, 1978).

C11 M. Harwit:
Astrophysical concepts,
4th (Springer, Heidelberg, 2006).

C12 W. P. Schleich:
Quantum optics in phase space,
(John Wiley & Sons, 2011).

C13 K. Huang:
Statistical Mechanics, 2nd Edition,
(Wiley, 1987).

C14 C. Gardiner and P. Zoller:
Quantum noise,
(Springer, Heidelberg, 2004).

C15 G. Schaller:
Open quantum systems far from equilibrium,
Vol. LNP 881 (Springer, Heidelberg, 2014).

C16 U. C. Täuber:
Critical dynamics,
(Cambridge University Press, 2014).

C17 U. Weiss:
Quantum dissipative systems,
5th (World Scientific, Singapour, 2022).

C18 R. Zwanzig:
Non-equilibrium statistical mechanics,
(Oxford University Press, 2001).

C19 R. Alicki and K. Lendi:
Quantum dynamical semigroups and applications,
Vol. LNP 717 (Springer, Heidelberg, 2007).

C20 R. Livi and P. Politi:
Nonequilibrium statistical physics: a modern perspective,
(Cambridge University Press, 2017).

C21 A. Householder:
Principles of Numerical Analysis,
(McGraw-Hill, New York, 1953).

C22 G. Fischer:
Lineare Algebra,
17^{th} ed. (Vieweg-Teubner, Wiesbaden, 2010).

C23 Y. Meyer:
Wavelets and operators: volume 1,
(Cambridge University Press, 1992).

C24 V. Mazya and G. Schmidt:
Approximate approximations,
(American Mathematical Society, Providence, 2007).

C25 S. Sachdev:
Quantum Phase Transitions,
2nd ed. (Cambridge University Press, 2011).

Articles

1 U. Schollwöck:
'The density-matrix renormalization group in the age of matrix product states',
Annals of physics **326**, 96–192 (2011).

2 A. Georges, G. Kotliar, W. Krauth and M. J. Rozenberg:
'Dynamical mean-field theory of strongly correlated fermion systems and the limit of infinite dimensions',
Reviews of Modern Physics **68**, 13 (1996).

3 J. I. Cirac and F. Verstraete:
'Renormalization and tensor product states in spin chains and lattices',
Journal of physics a: mathematical and theoretical **42**, 504004 (2009).

4 G. Vidal:
'Classical simulation of infinite-size quantum lattice systems in one spatial dimension',
Physical review letters **98**, 070201 (2007).

5 A. J. Daley, C. Kollath, U. Schollwöck and G. Vidal:
'Time-dependent density-matrix renormalization-group using adaptive effective hilbert spaces',
Journal of Statistical Mechanics: Theory and Experiment **2004**, P04005 (2004).

6 S. R. White and A. E. Feiguin:
'Real-time evolution using the density matrix renormalization group',
Physical review letters **93**, 076401 (2004).

7 M. Rigol, V. Dunjko, V. Yurovsky and M. Olshanii:
'Relaxation in a completely integrable many-body quantum system: an ab initio study of the dynamics of the highly excited states of 1d lattice hard-core bosons',
Physical review letters **98**, 050405 (2007).

8 F. Lange, Z. Lenarčič and A. Rosch:
'Time-dependent generalized gibbs ensembles in open quantum systems',
Physical Review B **97**, 165138 (2018).

9 O. A. Castro-Alvaredo, B. Doyon and T. Yoshimura:
'Emergent hydrodynamics in integrable quantum systems out of equilibrium',
Physical Review X **6**, 041065 (2016).

10 P. Ruggiero, P. Calabrese, B. Doyon and J. Dubail:
'Quantum generalized hydrodynamics',
Physical review letters **124**, 140603 (2020).

11 S. Vinjanampathy and J. Anders:
'Quantum thermodynamics',
Contemporary Physics **57**, 545–579 (2016).

12 J.-M. Raimond, M. Brune and S. Haroche:
'Manipulating quantum entanglement with atoms and photons in a cavity',
Reviews of Modern Physics **73**, 565 (2001).

13 D. Leibfried, R. Blatt, C. Monroe and D. Wineland:
'Quantum dynamics of single trapped ions',
Reviews of Modern Physics **75**, 281 (2003).

14 R. Araújo, S. Wald and M. Henkel:
'Axiomatic construction of quantum langevin equations',
Journal of Statistical Mechanics: Theory and Experiment, 053101 (2019).

15 A. Einstein, B. Podolsky and N. Rosen:
'Can quantum-mechanical description of physical reality be considered complete?',
Physical review **47**, 777 (1935).

16 J. S. Bell:
'On the einstein podolsky rosen paradox',
Physics Physique Fizika **1**, 195 (1964).

17 J. S. Bell:
'On the problem of hidden variables in quantum mechanics',
Reviews of Modern physics **38**, 447 (1966).

18 A. Aspect, J. Dalibard and G. Roger:
'Experimental test of bell's inequalities using time-varying analyzers',
Physical review letters **49**, 1804 (1982).

19 A. Aspect, P. Grangier and G. Roger:
'Experimental realization of einstein-podolsky-rosen-bohm gedankenexperiment: a new violation of bell's inequalities',
Physical review letters **49**, 91 (1982).

20 A. Aspect, P. Grangier and G. Roger:
'Experimental tests of realistic local theories via bell's theorem',
Physical review letters **47**, 460 (1981).

21 J. F. Clauser, M. A. Horne, A. Shimony and R. A. Holt:
'Proposed experiment to test local hidden-variable theories',
Physical review letters **23**, 880 (1969).

22 S. J. Freedman and J. F. Clauser:
'Experimental test of local hidden-variable theories',
Physical Review Letters **28**, 938 (1972).

23 J. F. Clauser and A. Shimony:
'Bell's theorem. experimental tests and implications',
Reports on Progress in Physics **41**, 1881 (1978).

24 P. G. Kwiat, K. Mattle, H. Weinfurter, A. Zeilinger, A. V. Sergienko and Y. Shih:
'New high-intensity source of polarization-entangled photon pairs',
Physical Review Letters **75**, 4337 (1995).

25 D. M. Greenberger, M. A. Horne, A. Shimony and A. Zeilinger:
'Bell's theorem without inequalities',
American Journal of Physics **58**, 1131–1143 (1990).

26 E. Wigner:
'On the quantum correction for thermodynamic equilibrium',
Physical Review **40**, 749 (1932).

27 B. Skinner, J. Ruhman and A. Nahum:
'Measurement-induced phase transitions in the dynamics of entanglement',
Physical Review X **9**, 031009 (2019).

28 B. N. Datta:
'Numerical linear algebra and applications. brooks',
Cole, New York (1995).

29 M. B. Plenio and S. Virmani:
'An introduction to entanglement measures.',
Quantum Inf. Comput. **7**, 1–51 (2007).

30 E. Chitambar, D. Leung, L. Mančinska, M. Ozols and A. Winter:
'Everything you always wanted to know about locc (but were afraid to ask)',
Communications in Mathematical Physics **328**, 303–326 (2014).

31 M. A. Nielsen:
'Conditions for a class of entanglement transformations',
Physical Review Letters **83**, 436 (1999).

32 E. H. Lieb and M. B. Ruskai:
'A fundamental property of quantum-mechanical entropy',
Physical Review Letters **30**, 434 (1973).

33 E. H. Lieb and M. B. Ruskai:
'Proof of the strong subadditivity of quantum-mechanical entropy',
Les rencontres physiciens-mathématiciens de Strasbourg-RCP25 **19**, 36–55 (1973).

34 S. Morelli, C. Klöckl, C. Eltschka, J. Siewert and M. Huber:
'Dimensionally sharp inequalities for the linear entropy',
Linear Algebra and its Applications **584**, 294–325 (2020).

35 R. Ursin, T. Jennewein, M. Aspelmeyer, R. Kaltenbaek, M. Lindenthal, P. Walther and A. Zeilinger:
'Quantum teleportation across the danube',
Nature **430**, 849–849 (2004).

36 C. H. Bennett, G. Brassard, C. Crépeau, R. Jozsa, A. Peres and W. K. Wootters:
'Teleporting an unknown quantum state via dual classical and einstein-podolsky-rosen channels',
Physical review letters **70**, 1895 (1993).

37 D. Bouwmeester, J.-W. Pan, K. Mattle, M. Eibl, H. Weinfurter and A. Zeilinger:
'Experimental quantum teleportation',
Nature **390**, 575–579 (1997).

38 I. Marcikic, H. De Riedmatten, W. Tittel, H. Zbinden and N. Gisin:
'Long-distance teleportation of qubits at telecommunication wavelengths',
Nature **421**, 509–513 (2003).

39 X.-S. Ma, T. Herbst, T. Scheidl, D. Wang, S. Kropatschek, W. Naylor, B. Wittmann, A. Mech, J. Kofler, E. Anisimova et al.:
'Quantum teleportation over 143 kilometres using active feed-forward',
Nature **489**, 269–273 (2012).

40 S. Sachdev:
'Quantum phase transitions',
Physics world **12**, 33 (1999).

41 A. Pires:
'Quantum-phase transition in a xy model',
Physica A: Statistical Mechanics and its Applications **373**, 387–391 (2007).

42 D. Karevski:
'Surface and bulk critical behaviour of the xy chain in a transverse field',
Journal of Physics A: Mathematical and General **33**, L313 (2000).

43 P. Calabrese and J. Cardy:
'Entanglement entropy and conformal field theory',
Journal of physics a: mathematical and theoretical **42**, 504005 (2009).

44 G. Vidal, J. I. Latorre, E. Rico and A. Kitaev:
'Entanglement in quantum critical phenomena',
Physical review letters **90**, 227902 (2003).

45 C. Holzhey, F. Larsen and F. Wilczek:
'Geometric and renormalized entropy in conformal field theory',
Nuclear physics b **424**, 443–467 (1994).

46 M. Goldstein and E. Sela:
'Symmetry-resolved entanglement in many-body systems',
Physical review letters **120**, 200602 (2018).

47 I. Peschel:
'Entanglement in solvable many-particle models',
Brazilian Journal of Physics **42**, 267–291 (2012).

48 I. Peschel and V. Eisler:
'Reduced density matrices and entanglement entropy in free lattice models',
Journal of physics a: mathematical and theoretical **42**, 504003 (2009).

49 I. Peschel:
'Calculation of reduced density matrices from correlation functions',
Journal of Physics A: Mathematical and General **36**, L205 (2003).

50 M.-C. Chung and I. Peschel:
'Density-matrix spectra of solvable fermionic systems',
Physical Review B **64**, 064412 (2001).

51 S. Bravyi:
'Lagrangian representation for fermionic linear optics',
arXiv preprint quant-ph/0404180 (2004).

52 V. Eisler and Z. Zimborás:
'On the partial transpose of fermionic gaussian states',
New Journal of Physics **17**, 053048 (2015).

53 B. Bertini, M. Fagotti, L. Piroli and P. Calabrese:
'Entanglement evolution and generalised hydrodynamics: noninteracting systems',
Journal of Physics A: Mathematical and Theoretical **51**, 39LT01 (2018).

54 P. Calabrese and J. Cardy:
'Quantum quenches in extended systems',
Journal of Statistical Mechanics: Theory and Experiment **2007**, P06008 (2007).

55 V. Alba and P. Calabrese:
'Entanglement dynamics after quantum quenches in generic integrable systems',
SciPost Physics **4**, 017 (2018).

56 P. Calabrese and J. Cardy:
'Evolution of entanglement entropy in one-dimensional systems',
Journal of Statistical Mechanics: Theory and Experiment **2005**, P04010 (2005).

57 M. Collura, M. Kormos and P. Calabrese:
'Stationary entanglement entropies following an interaction quench in 1d bose gas',
Journal of Statistical Mechanics: Theory and Experiment **2014**, P01009 (2014).

58 M. Fagotti:
'Finite-size corrections versus relaxation after a sudden quench',
Physical Review B **87**, 165106 (2013).

59 X. Cao, A. Tilloy and A. De Luca:
'Entanglement in a fermion chain under continuous monitoring',
SciPost Physics **7**, 024 (2019).

60 P. Pechukas:
'Reduced dynamics need not be completely positive',
Physical Review Letters **73**, 1060 (1994).

61 G. Lindblad:
'On the generators of quantum dynamical semigroups',
Communications in Mathematical Physics **48**, 119 (1976).

62 A. J. Daley:
'Quantum trajectories and open many-body quantum systems',
Advances in Physics **63**, 77–149 (2014).

63 H. M. Wiseman:
'Quantum trajectories and quantum measurement theory',
Quantum and Semiclassical Optics: Journal of the European Optical Society Part B **8**, 205 (1996).

64 J. Dalibard, Y. Castin and K. Mølmer:
'Wave-function approach to dissipative processes in quantum optics',
Physical review letters **68**, 580 (1992).

65 C. W. Gardiner, A. S. Parkins and P. Zoller:
'Wave-function quantum stochastic differential equations and quantum-jump simulation methods',
Physical Review A **46**, 4363 (1992).

66 F. Carollo, R. L. Jack and J. P. Garrahan:
'Unraveling the large deviation statistics of markovian open quantum systems',
Physical review letters **122**, 130605 (2019).

67 D. Bedeaux and P. Mazur:
'Mesoscopic non-equilibrium thermodynamics for quantum systems',
Physica A **298**, 81 (2001).

68 D. Bedeaux:
'Non-equilibrium thermodynamics for quantum systems',
Technische Mechanik **22**, 89 (2002).

69 R. Sarpeshkar, T. Delbruck and C. A. Mead:
'White noise in mos transistors and resistors',
IEEE Circuits and Devices Magazine **9**, 23–29 (1993).

70 J. Gabelli, G. Fève, J.-M. Berroir and B. Plaçais:
'A coherent rc circuit',
Reports on progress in physics **75**, 126504 (2012).

71 U. Vool and M. Devoret:
'Introduction to quantum electromagnetic circuits',
International Journal of Circuit Theory and Applications **45**, 897–934 (2017).

72 G. Ford, M. Kac and P. Mazur:
'Statistical mechanics of assemblies of coupled oscillators',
J. Math. Phys. **6**, 504 (1965).

73 V. Fock:
'Bemerkung zum virialsatz',
Zeitschrift für Physik **63**, 855 (1930).

74 G. Ford, J. Lewis and R. O'Connell:
'Quantum Langevin equation',
Phys. Rev. A **37**, 4419 (1988).

75 J. E. Moyal:
'Quantum mechanics as a statistical theory',
in Mathematical proceedings of the cambridge philosophical society, Vol. 45, 1 (Cambridge University Press, 1949), pp. 99–124.

76 M. Hillery, R. O'Connell, M. Scully and E. Wigner:
'Distribution functions in physics: fundamentals',
Phys. Rep. **106**, 121 (1984).

77 H.-W. Lee:
'Theory and application of the quantum phase-space distribution functions',
Phys. Rep. **259**, 150 (1995).

78 W. Case:
'Wigner functions and Weyl transforms for pedestrians',
Am. J. Phys. **76**, 937 (2008).

79 T. Prosen:
'Third quantization: a general method to solve master equations for quadratic open fermi systems',
New Journal of Physics **10**, 043026 (2008).

80 A. Polkovnikov:
'Phase space representation of quantum dynamics',
Annals of Physics **325**, 1790–1852 (2010).

81 M. Hillery, R. F. O'Connell, M. O. Scully and E. P. Wigner:
'Distribution functions in physics: fundamentals',
Physics reports **106**, 121–167 (1984).

82 L. Wang and R. O'Connell:
'Quantum mechanics without wave functions',
Foundations of physics **18**, 1023–1033 (1988).

83 D. Karevski:
'Physique quantique des champs et des transitions de phase: avec exercices corrigés',
Édition Marketing Ellipses, 1–684 (2022).

84 M. Fagotti:
'Locally quasi-stationary states in noninteracting spin chains',
SciPost Physics **8**, 048 (2020).

85 L. Amico, R. Fazio, A. Osterloh and V. Vedral:
'Entanglement in many-body systems',
Reviews of modern physics **80**, 517 (2008).

86 J. Eisert, M. Cramer and M. B. Plenio:
'Colloquium: area laws for the entanglement entropy',
Reviews of Modern Physics **82**, 277 (2010).

87 N. Laflorencie:
'Quantum entanglement in condensed matter systems',
Physics Reports **646**, 1–59 (2016).

88 E. H. Lieb and D. W. Robinson:
'The finite group velocity of quantum spin systems',
in *Statistical mechanics* (Springer, 1972), pp. 425–431.

89 V. Alba and P. Calabrese:
'Entanglement and thermodynamics after a quantum quench in integrable systems',
Proceedings of the National Academy of Sciences **114**, 7947–7951 (2017).

90 V. Alba:
'Entanglement and quantum transport in integrable systems',
Physical Review B **97**, 245135 (2018).

91 C. Von Keyserlingk, T. Rakovszky, F. Pollmann and S. L. Sondhi:
'Operator hydrodynamics, otocs, and entanglement growth in systems without conservation laws',
Physical Review X **8**, 021013 (2018).

92 T. Rakovszky, F. Pollmann and C. Von Keyserlingk:
'Sub-ballistic growth of rényi entropies due to diffusion',
Physical review letters **122**, 250602 (2019).

93 V. Alba and P. Calabrese:
'Quantum information scrambling after a quantum quench',
Physical Review B **100**, 115150 (2019).

94 D. Basko, I. Aleiner and B. Altshuler:
'On the problem of many-body localization',
Problems of Condensed Matter Physics, 50–70 (2006).

95 M. Žnidarič, T. Prosen and P. Prelovšek:
'Many-body localization in the heisenberg x x z magnet in a random field',
Physical Review B **77**, 064426 (2008).

96 J. H. Bardarson, F. Pollmann and J. E. Moore:
'Unbounded growth of entanglement in models of many-body localization',
Physical review letters **109**, 017202 (2012).

97 S. Iyer, V. Oganesyan, G. Refael and D. A. Huse:
'Many-body localization in a quasiperiodic system',
Physical Review B **87**, 134202 (2013).

98 H. Kim and D. A. Huse:
'Ballistic spreading of entanglement in a diffusive nonintegrable system',
Physical review letters **111**, 127205 (2013).

99 D. A. Huse, R. Nandkishore and V. Oganesyan:
'Phenomenology of fully many-body-localized systems',
Physical Review B **90**, 174202 (2014).

100 B. Bauer and C. Nayak:
'Area laws in a many-body localized state and its implications for topological order',
Journal of Statistical Mechanics: Theory and Experiment **2013**, P09005 (2013).

101 J. A. Kjäll, J. H. Bardarson and F. Pollmann:
'Many-body localization in a disordered quantum ising chain',
Physical review letters **113**, 107204 (2014).

102 Y. Li, X. Chen and M. P. Fisher:
'Quantum zeno effect and the many-body entanglement transition',
Physical Review B **98**, 205136 (2018).

103 Y. Li, X. Chen and M. P. Fisher:
'Measurement-driven entanglement transition in hybrid quantum circuits',
Physical Review B **100**, 134306 (2019).

104 Y. Li, X. Chen, A. W. Ludwig and M. Fisher:
'Conformal invariance and quantum non-locality in hybrid quantum circuits',
Physical Review B **104** (2021).

105 M. Szyniszewski, A. Romito and H. Schomerus:
'Universality of entanglement transitions from stroboscopic to continuous measurements',
Physical review letters **125**, 210602 (2020).

106 L. Zhang, J. A. Reyes, S. Kourtis, C. Chamon, E. R. Mucciolo and A. E. Ruckenstein:
'Nonuniversal entanglement level statistics in projection-driven quantum circuits',
Physical Review B **101**, 235104 (2020).

107 A. Zabalo, M. J. Gullans, J. H. Wilson, S. Gopalakrishnan, D. A. Huse and J. Pixley:
'Critical properties of the measurement-induced transition in random quantum circuits',
Physical Review B **101**, 060301 (2020).

108 O. Shtanko, Y. A. Kharkov, L. P. García-Pintos and A. V. Gorshkov:
'Classical models of entanglement in monitored random circuits',
arXiv preprint arXiv:2004.06736 (2020).

109 C.-M. Jian, B. Bauer, A. Keselman and A. W. Ludwig:
'Criticality and entanglement in non-unitary quantum circuits and tensor networks of non-interacting fermions',
arXiv preprint arXiv:2012.04666 (2020).

110 A. Nahum, J. Ruhman, S. Vijay and J. Haah:
'Quantum entanglement growth under random unitary dynamics',
Physical Review X **7**, 031016 (2017).

111 A. Chan, R. M. Nandkishore, M. Pretko and G. Smith:
'Unitary-projective entanglement dynamics',
Phys. Rev. B **99**, 224307 (2019).

112 M. Szyniszewski, A. Romito and H. Schomerus:
'Entanglement transition from variable-strength weak measurements',
Physical Review B **100**, 064204 (2019).

113 A. Chan, R. M. Nandkishore, M. Pretko and G. Smith:
'Unitary-projective entanglement dynamics',
Physical Review B **99**, 224307 (2019).

114 A. Lavasani, Y. Alavirad and M. Barkeshli:
'Topological order and criticality in (2+ 1) d monitored random quantum circuits',
arXiv preprint arXiv:2011.06595 (2020).

115 A. Lavasani, Y. Alavirad and M. Barkeshli:
'Measurement-induced topological entanglement transitions in symmetric random quantum circuits',
Nature Physics **17**, 342–347 (2021).

116 M. Block, Y. Bao, S. Choi, E. Altman and N. Yao:
'The measurement-induced transition in long-range interacting quantum circuits',
arXiv preprint arXiv:2104.13372 (2021).

117 S. Sang and T. H. Hsieh:
'Measurement-protected quantum phases',
Physical Review Research **3**, 023200 (2021).

118 B. Shi, X. Dai and Y.-M. Lu:
'Entanglement negativity at the critical point of measurement-driven transition',
arXiv preprint arXiv:2012.00040 (2020).

119 O. Lunt and A. Pal:
'Measurement-induced entanglement transitions in many-body localized systems',
Physical Review Research **2**, 043072 (2020).

120 P. Sierant and X. Turkeshi:
Universal behavior beyond multifractality of wave-functions at measurement–induced phase transitions,
2021.

121 S. Dhar and S. Dasgupta:
'Measurement-induced phase transition in a quantum spin system',
Physical Review A **93**, 050103 (2016).

122 X. Turkeshi, R. Fazio and M. Dalmonte:
'Measurement-induced criticality in (2+ 1)-dimensional hybrid quantum circuits',
Physical Review B **102**, 014315 (2020).

123 N. Lang and H. P. Büchler:
'Entanglement transition in the projective transverse field ising model',
Physical Review B **102**, 094204 (2020).

124 D. Rossini and E. Vicari:
'Measurement-induced dynamics of many-body systems at quantum criticality',
Physical Review B **102**, 035119 (2020).

125 X. Turkeshi, A. Biella, R. Fazio, M. Dalmonte and M. Schiró:
'Measurement-induced entanglement transitions in the quantum ising chain: from infinite to zero clicks',
Physical Review B **103**, 224210 (2021).

126 T. Botzung, S. Diehl and M. Müller:
'Engineered dissipation induced entanglement transition in quantum spin chains: from logarithmic growth to area law',
arXiv preprint arXiv:2106.10092 (2021).

127 T. Boorman, M. Szyniszewski, H. Schomerus and A. Romito:
'Diagnosing entanglement dynamics in noisy and disordered spin chains via the measurement-induced steady-state entanglement transition',
arXiv preprint arXiv:2107.11354 (2021).

128 Y. Fuji and Y. Ashida:
'Measurement-induced quantum criticality under continuous monitoring',
Physical Review B **102**, 054302 (2020).

129 M. Ippoliti and V. Khemani:
'Postselection-free entanglement dynamics via spacetime duality',
Physical Review Letters **126**, 060501 (2021).

130 X. Turkeshi:
'Measurement-induced criticality as a data-structure transition',
arXiv preprint arXiv:2101.06245 (2021).

131 T. J. Elliott, W. Kozlowski, S. Caballero-Benitez and I. B. Mekhov:
'Multipartite entangled spatial modes of ultracold atoms generated and controlled by quantum measurement',
Physical review letters **114**, 113604 (2015).

132 S. Czischek, G. Torlai, S. Ray, R. Islam and R. G. Melko:
'Simulating a measurement-induced phase transition for trapped ion circuits',
arXiv preprint arXiv:2106.03769 (2021).

133 C. Noel, P. Niroula, A. Risinger, L. Egan, D. Biswas, M. Cetina, A. V. Gorshkov, M. Gullans, D. A. Huse and C. Monroe:
'Observation of measurement-induced quantum phases in a trapped-ion quantum computer',
arXiv preprint arXiv:2106.05881 (2021).

134 P. Sierant, G. Chiriacò, F. M. Surace, S. Sharma, X. Turkeshi, M. Dalmonte, R. Fazio and G. Pagano:
'Dissipative floquet dynamics: from steady state to measurement induced criticality in trapped-ion chains',
arXiv preprint arXiv:2107.05669 (2021).

135 A. Degasperis, L. Fonda and G. Ghirardi:
'Does the lifetime of an unstable system depend on the measuring apparatus?',
Il Nuovo Cimento A (1965-1970) **21**, 471–484 (1974).

136 B. Misra and E. G. Sudarshan:
'The zeno's paradox in quantum theory',
Journal of Mathematical Physics **18**, 756–763 (1977).

137 A. Peres:
'Zeno paradox in quantum theory',
American Journal of Physics **48**, 931–932 (1980).

138 K. Snizhko, P. Kumar and A. Romito:
'Quantum zeno effect appears in stages',
Physical Review Research **2**, 033512 (2020).

139 A. Biella and M. Schiró:
'Many-body quantum zeno effect and measurement-induced subradiance transition',
Quantum **5**, 528 (2021).

140 O. Alberton, M. Buchhold and S. Diehl:
'Entanglement transition in a monitored free-fermion chain: from extended criticality to area law',
Physical Review Letters **126**, 170602 (2021).

141 T. Müller, S. Diehl and M. Buchhold:
'Measurement-induced dark state phase transitions in long-ranged fermion systems',
arXiv preprint arXiv:2105.08076 (2021).

142 S. Goto and I. Danshita:
'Measurement-induced transitions of the entanglement scaling law in ultracold gases with controllable dissipation',
Physical Review A **102**, 033316 (2020).

143 M. Buchhold, Y. Minoguchi, A. Altland and S. Diehl:
'Effective theory for the measurement-induced phase transition of dirac fermions',
arXiv preprint arXiv:2102.08381 (2021).

144 T. Minato, K. Sugimoto, T. Kuwahara and K. Saito:
'Fate of measurement-induced phase transition in long-range interactions',
arXiv preprint arXiv:2104.09118 (2021).

145 T. Maimbourg, D. M. Basko, M. Holzmann and A. Rosso:
'Bath-induced zeno localization in driven many-body quantum systems',
Phys. Rev. Lett. **126**, 120603 (2021).

146 M. Žnidarič:
'Large-deviation statistics of a diffusive quantum spin chain and the additivity principle',
Physical Review E **89**, 042140 (2014).

147 F. Carollo, J. P. Garrahan, I. Lesanovsky and C. Pérez-Espigares:
'Fluctuating hydrodynamics, current fluctuations, and hyperuniformity in boundary-driven open quantum chains',
Physical Review E **96**, 052118 (2017).

148 I. Poboiko, P. Pöpperl, I. V. Gornyi and A. D. Mirlin:
'Theory of free fermions under random projective measurements',
arXiv preprint arXiv:2304.03138 (2023).

149 M. Coppola and D. Karevski:
'Some speculations about local thermalization of nonequilibrium extended quantum systems',
Condensed Matter Physics **26**, 13502 (2023), arXiv:2303.01881v1.

150 L. Lumia, E. Tirrito, R. Fazio and M. Collura:
'Measurement-induced transitions beyond gaussianity: a single particle description',
arXiv preprint arXiv:2311.09043 (2023).

151 F. Carollo and V. Alba:
'Entangled multiplets and spreading of quantum correlations in a continuously monitored tight-binding chain',
Phys. Rev. B **106**, L220304 (2022).

152 L. Boltzmann:
'Weitere studien über das wärmegleichgewicht unter gas-molekülen',
Wissenschaftliche Abhandlungen, 316–402 (1872).

153 S. Stoimenov and M. Henkel:
'Conformal invariance of the 1 d collisionless boltzmann equation',
in Lie theory and its applications in physics: varna, bulgaria, june 2015 11 (Springer, 2016), pp. 453–463.

154 M. Hinarejos, A. Pérez and M.-C. Bañuls:
'Wigner function for a particle in an infinite lattice',
New Journal of Physics **14**, 103009 (2012).

155 D. S. Dean, P. Le Doussal, S. N. Majumdar and G. Schehr:
'Wigner function of noninteracting trapped fermions',
Physical Review A **97**, 063614 (2018).

156 B. De Bruyne, D. S. Dean, P. Le Doussal, S. N. Majumdar and G. Schehr:
'Wigner function for noninteracting fermions in hard-wall potentials',
Physical Review A **104**, 013314 (2021).

157 I. Bouchoule, B. Doyon and J. Dubail:
'The effect of atom losses on the distribution of rapidities in the one-dimensional bose gas',
SciPost Physics **9**, 044 (2020).

158 D. Dast, D. Haag, H. Cartarius and G. Wunner:
'Quantum master equation with balanced gain and loss',
Physical Review A **90**, 052120 (2014).

159 V. Alba and F. Carollo:
'Noninteracting fermionic systems with localized losses: exact results in the hydrodynamic limit',
Physical Review B **105**, 054303 (2022).

160 V. Alba and F. Carollo:
'Hydrodynamics of quantum entropies in ising chains with linear dissipation',
Journal of Physics A: Mathematical and Theoretical **55**, 074002 (2022).

161 F. Carollo and V. Alba:
'Dissipative quasiparticle picture for quadratic markovian open quantum systems',
Physical Review B **105**, 144305 (2022).

162 F. Riggio, L. Rosso, D. Karevski and J. Dubail:
'Effects of atom losses on a one-dimensional lattice gas of hardcore bosons',
(2023).

163 J. P. Santos, G. T. Landi and M. Paternostro:
'Wigner entropy production rate',
Physical review letters **118**, 220601 (2017).

164 W. T. Malouf, J. P. Santos, L. A. Correa, M. Paternostro and G. T. Landi:
'Wigner entropy production and heat transport in linear quantum lattices',
Physical Review A **99**, 052104 (2019).

165 Q.-W. Wang:
'Exact dynamical correlations of nonlocal operators in quadratic open fermion systems: a characteristic function approach',
SciPost Physics Core **5**, 027 (2022).

166 V. Alba and F. Carollo:
'Spreading of correlations in markovian open quantum systems',
Physical Review B **103**, L020302 (2021).

167 G. T. Landi:
'Waiting time statistics in boundary-driven free fermion chains',
Physical Review B **104**, 195408 (2021).

168 S. H. Silva, G. T. Landi and E. Pereira:
'Non-trivial effect of dephasing: enhancement of rectification of spin current in graded xx chains',
arXiv preprint arXiv:2207.02693 (2022).

169 D. KAREVSKI and T. PLATINI:
'Quantum nonequilibrium steady states induced by repeated interactions',
Physical review letters **102**, 207207 (2009).

170 T. PROSEN:
'Exact nonequilibrium steady state of a strongly driven open x x z chain',
Physical review letters **107**, 137201 (2011).

171 D. KAREVSKI, V. POPKOV and G. SCHÜTZ:
'Exact matrix product solution for the boundary-driven lindblad x x z chain',
Physical review letters **110**, 047201 (2013).

172 V. POPKOV, D. KAREVSKI and G. M. SCHÜTZ:
'Driven isotropic heisenberg spin chain with arbitrary boundary twisting angle: exact results',
Physical Review E **88**, 062118 (2013).

173 G. T. LANDI, E. NOVAIS, M. J. DE OLIVEIRA and D. KAREVSKI:
'Flux rectification in the quantum x x z chain',
Physical Review E **90**, 042142 (2014).

174 G. T. LANDI and D. KAREVSKI:
'Open heisenberg chain under boundary fields: a magnonic logic gate',
Physical Review B **91**, 174422 (2015).

175 B. DOYON:
'Lecture notes on Generalised Hydrodynamics',
SciPost Phys. Lect. Notes, 18 (2020).

176 A. BASTIANELLO, V. ALBA and J.-S. CAUX:
'Generalized hydrodynamics with space-time inhomogeneous interactions',
Physical Review Letters **123**, 130602 (2019).

177 L. CAPIZZI, S. SCOPA, F. ROTTOLI and P. CALABRESE:
'Domain wall melting across a defect',
Europhysics Letters **141**, 31002 (2023).

178 S. SCOPA, P. CALABRESE and J. DUBAIL:
'Exact hydrodynamic solution of a double domain wall melting in the spin-1/2 XXZ model',
SciPost Phys. **12**, 207 (2022).

179 M. FAGOTTI:
'Higher-order generalized hydrodynamics in one dimension: the noninteracting test',
Physical Review B **96**, 220302 (2017).

180 S. SCOPA, A. KRAJENBRINK, P. CALABRESE and J. DUBAIL:
'Exact entanglement growth of a one-dimensional hard-core quantum gas during a free expansion',
Journal of Physics A: Mathematical and Theoretical **54**, 404002 (2021).

181 J. DUBAIL, J.-M. STÉPHAN, J. VITI and P. CALABRESE:
'Conformal field theory for inhomogeneous one-dimensional quantum systems: the example of non-interacting fermi gases',
SciPost Physics **2**, 002 (2017).

182 M. Collura, A. De Luca and J. Viti:
'Analytic solution of the domain-wall nonequilibrium stationary state',
Physical Review B **97**, 081111 (2018).

183 M. Collura, A. De Luca, P. Calabrese and J. Dubail:
'Domain wall melting in the spin-1 2 xxz spin chain: emergent luttinger liquid with a fractal quasiparticle charge',
Physical Review B **102**, 180409 (2020).

184 V. Alba, B. Bertini, M. Fagotti, L. Piroli and P. Ruggiero:
'Generalized-hydrodynamic approach to inhomogeneous quenches: correlations, entanglement and quantum effects',
Journal of Statistical Mechanics: Theory and Experiment **2021**, 114004 (2021).

185 I. Bouchoule and J. Dubail:
'Generalized hydrodynamics in the one-dimensional bose gas: theory and experiments',
Journal of Statistical Mechanics: Theory and Experiment **2022**, 014003 (2022).

186 V. B. Bulchandani, R. Vasseur, C. Karrasch and J. E. Moore:
'Solvable hydrodynamics of quantum integrable systems',
Physical review letters **119**, 220604 (2017).

187 V. B. Bulchandani, R. Vasseur, C. Karrasch and J. E. Moore:
'Bethe-boltzmann hydrodynamics and spin transport in the xxz chain',
Physical Review B **97**, 045407 (2018).

188 B. Doyon, T. Yoshimura and J.-S. Caux:
'Soliton gases and generalized hydrodynamics',
Physical review letters **120**, 045301 (2018).

189 M. Schemmer, I. Bouchoule, B. Doyon and J. Dubail:
'Generalized hydrodynamics on an atom chip',
Physical review letters **122**, 090601 (2019).

190 N. Malvania, Y. Zhang, Y. Le, J. Dubail, M. Rigol and D. S. Weiss:
'Generalized hydrodynamics in strongly interacting 1d bose gases',
Science **373**, 1129–1133 (2021).

191 M. Collura, H. Aufderheide, G. Roux and D. Karevski:
'Entangling many-body bound states with propagative modes in bose-hubbard systems',
Physical Review A **86**, 013615 (2012).

192 P. Wendenbaum, M. Collura and D. Karevski:
'Hydrodynamic description of hard-core bosons on a galileo ramp',
Physical Review A **87**, 023624 (2013).

193 T. Jin, T. Gautié, A. Krajenbrink, P. Ruggiero and T. Yoshimura:
'Interplay between transport and quantum coherences in free fermionic systems',
Journal of Physics A: Mathematical and Theoretical **54**, 404001 (2021).

194 P. Würtz, T. Langen, T. Gericke, A. Koglbauer and H. Ott:
'Experimental demonstration of single-site addressability in a two-dimensional optical lattice',
Physical review letters **103**, 080404 (2009).

195 D. Schneble, G. K. Campbell, E. W. Streed, M. Boyd, D. E. Pritchard and W. Ketterle:
'Raman amplification of matter waves',
Physical Review A **69**, 041601 (2004).

196 G. Piccitto, A. Russomanno and D. Rossini:
'Entanglement transitions in the quantum ising chain: a comparison between different unravelings of the same lindbladian',
Physical Review B **105**, 064305 (2022).

197 T. Müller, S. Diehl and M. Buchhold:
'Measurement-induced dark state phase transitions in long-ranged fermion systems',
Physical Review Letters **128**, 010605 (2022).

198 D. Bernard, T. Jin and O. Shpielberg:
'Transport in quantum chains under strong monitoring',
Europhysics Letters **121**, 60006 (2018).

199 Z. Cai and T. Barthel:
'Algebraic versus exponential decoherence in dissipative many-particle systems',
Physical review letters **111**, 150403 (2013).

200 E. Tirrito, A. Santini, R. Fazio and M. Collura:
'Full counting statistics as probe of measurement-induced transitions in the quantum ising chain',
arXiv preprint arXiv:2212.09405 (2022).

201 V. Eisler:
'Crossover between ballistic and diffusive transport: the quantum exclusion process',
Journal of Statistical Mechanics: Theory and Experiment **2011**, P06007 (2011).

202 X. Turkeshi and M. Schiró:
'Diffusion and thermalization in a boundary-driven dephasing model',
Physical Review B **104**, 144301 (2021).

203 D. S. Dean, P. Le Doussal, S. N. Majumdar and G. Schehr:
'Nonequilibrium dynamics of noninteracting fermions in a trap',
Europhysics Letters **126**, 20006 (2019).

204 L. Cugliandolo:
'Dynamics of glassy systems',
in Slow relaxations and non-equilibrium dynamics in condensed matter, edited by J.-L. Barrat, M. Feigelman, J. Kurchan and J. Dalibard (2003), p. 367.

205 H.-P. Breuer, E.-M. Laine, J. Piilo and B. Vacchini:
'Non-markovian dynamics in open quantum systems',
Reviews of Modern Physics **88**, 021002 (2016).

206 I. De Vega and D. Alonso:
'Dynamics of non-markovian open quantum systems',
Reviews of Modern Physics **89**, 015001 (2017).

207 P. Hänggi and G.-L. Ingold:
'Fundamental aspects of quantum brownian motion',
Chaos **15**, 026105 (2005).

208 L. Sieberer, A. Chiocchetta, A. Gambassi, U. C. Täuber and S. Diehl:
'Thermodynamic equilibrium as a symmetry of the Schwinger-Keldysh action',
Physical Review B **92**, 134307 (2015).

209 G. Ford:
'The fluctuation–dissipation theorem',
Contemporary Physics **58**, 244 (2017).

210 M. de Oliveira:
'Quantum Langevin equation',
Journal of Statistical Mechanics: Theory and Experiment, 023106 (2020).

211 A. L. F. Benatti R. Floreanini:
'Open quantum systems and complete positivity',
Cybernetics and Systems **32**, 343 (2001).

212 R. Alicki:
'Comment on "Reduced dynamics need not be completely positive"',
Physical Review Letters **75**, 3020 (1995).

213 P. Pechukas:
'Pechukas replies',
Physical Review Letters **75**, 3021 (1995).

214 I. Sargolzahi:
'Linearity conditions leading to complete positivity',
Physical Review A **106**, 032205 (2022).

215 K. M. F. Romero, P. Talkner and P. Hänggi:
'Is the dynamics of open quantum systems always linear?',
Physical Review A **69**, 052109 (2004).

216 A. Shaji and E. C. G. Sudarshan:
'Who's afraid of not completely positive maps ?',
Physics Letters A **341**, 48 (2005).

217 H. A. Carteret, D. R. Terno and K. Zyczkowski:
'Dynamics beyond completely positive maps: some properties and applications',
Physical Review A **77**, 042113 (2008).

218 C. A. Rodríguez-Rosario, K. Modi, A.-m. Kuah, A. Shaji and E. C. G. Sudarshan:
'Completely positive maps and classical correlations',
Journal of Physics A: Mathematical and Theoretical **41**, 205301 (2008).

219 J. M. Dominy and D. A. Lidar:
'Beyond complete positivity',
Quantum Information Processing **15**, 1349 (2016).

220 T. Becker, A. Schnell and J. Thingna:
'Canonically consistent quantum master equation',
Physical Review Letters **129**, 200403 (2022).

221 P. S. Correia, P. C. Obando, R. O. Vallejos and F. de Melo:
'Macro-to-micro quantum mapping and the emergence of nonlinearity',
Physical Review A **103**, 052210 (2021).

222 R. O. Vallejos, P. S. Correia, P. C. Obando, N. M. O'Neill, A. B. Tacla and F. de Melo: 'Quantum state inference from coarse-grained descriptions: analysis and an application to quantum thermodynamics',
Physical Review A **106**, 012219 (2022).

223 A. Colla, N. Neubrand and H.-P. Breuer:
'Initial correlations in open quantum systems: constructing linear dynamical maps and master equations',
New J. Phys. **24**, 123005 (2022).

224 D. Schmid, K. Ried and R. Spekkens:
'Why initial-system-environment correlations do not imply the failure of complete positivity: a causal perspective',
Phys. Rev. A **100**, 022112 (2019).

225 G. Lindblad:
'Brownian motion of a quantum harmonic oscillator',
Reports on Mathematical Physics **10**, 393 (1976).

226 P. Talkner:
'The failure of the quantum regression hypothesis',
Annals of Physics **167**, 390–436 (1986).

227 A. Isar, A. Sandulescu, H. Scutaru, E. Stefanescu and W. Scheid:
'Open quantum systems',
International Journal of Modern Physics E **3**, 635 (1994).

228 A. Isar and A. Sandulescu:
'Damped quantum harmonic oscillator',
(2006).

229 A. Isar, A. Sandulescu and W. Scheid:
'Lindblad master equation for the damped harmonic oscillator with deformed dissipation',
Physica **A322**, 233 (2003).

230 D. Kohen, C. C. Marston and D. J. Tannor:
'Phase space approach to theories of quantum dissipation',
The Journal of chemical physics **107**, 5236–5253 (1997).

231 J. Weinbub and D. Ferry:
'Recent advances in wigner function approaches',
Applied Physics Reviews **5**, 041104 (2018).

232 P. Vatiwutipong and N. Phewchean:
'Alternative way to derive the distribution of the multivariate Ornstein–Uhlenbeck process',
Advances in Difference Equations **2019**, 1 (2019).

233 A. Polkovnikov:
'Phase space representation of quantum dynamics. lecture notes at boulder summer school', in Disorder and dynamics in quantum systems - boulder summer school lecture notes, edited by A. Gurarie, J. Meyer, G. Refael, A. Jacoby and L. Radzhihovsky (2013).

234 C. Calcaterra and A. Boldt:
'Approximating with gaussians',
(2008).

235 M. Henkel:
'Quantum dynamics far from equilibrium: A case study in the spherical model',
in Lie theory and its applications in physics xiv, edited by V. Dobrev (2023), p. 111.

236 T. H. Berlin and M. Kac:
'The spherical model of a ferromagnet',
Physical Review **86**, 821 (1952).

237 H. Lewis and G. Wannier:
'Spherical model of a ferromagnet',
Physical Review **88**, 682 (1952).

238 M. Henkel and C. Hoeger:
'Hamiltonian formulation of the spherical model in $d = r + 1$ dimensions',
Zeitschrift für Physik B **55**, 67 (1984).

239 T. M. Nieuwenhuizen:
'Quantum description of spherical spins',
Physical Review Letters **74**, 4293 (1995).

240 T. Vojta:
'Quantum version of a spherical model: crossover from quantum to classical critical behaviour',
Physical Review B **53**, 710 (1996).

241 C. Godrèche and J.-M. Luck:
'Response of non-equilibrium systems at criticality: ferromagnetic models in dimension two and above',
Journal of Physics A: Mathematical and General **33**, 9141 (2000).

242 M. Rokni and P. Chandra:
'Dynamical study of the disordered quantum $p = 2$ spherical model',
Phys. Rev. **69**, 094403 (2004).

243 M. Oliveira, E. Raposo and M. Coutinho-Filho:
'Quantum spherical spin model on hypercubic lattices',
Physical Review B **74**, 184101 (2006).

244 A. Chandran, A. Nanduri, S. Gubser and S. Sondhi:
'Equilibration and coarsening in the quantum O(N) model at infinite N',
Phys. Rev. **B88**, 024306 (2013).

245 R. Bienzobaz and S. Salinas:
'Modelo esférico quântico elementar',
Revista Brasileira de Ensino de Física **35**, 3311 (2013).

246 A. Maraga, A. Chiocchetta, A. Mitra and A. Gambassi:
'Aging and coarsening in isolated quantum systems after a quench: Exact results for the quantum O(N) model with $N \to \infty$',
Physical Review E **92**, 042151 (2015).

247 P. Gagel, P. P. Orth and J. Schmalian:
'Universal postquench coarsening and ageing at a quantum critical point',
Phys. Rev. **B92**, 115121 (2015).

248 M. Pérez-Maldonado, G. Monsivais and R. Mulet:
'Redfield dynamics of a quantum spherical spin',
Revista Cubana de Física **34**, 158 (2017).

249 D. Barbier, L. F. Cugliandolo, G. S. Lozano, N. Nessi, M. Picco and A. Tartaglia:
'Pre-asymptotic dynamics of the infinite size neumann (p= 2 spherical) model',
Journal of Physics A: Mathematical and Theoretical **52**, 454002 (2019).

250 S. Wald and M. Henkel:
'Quantum phase transition in the spin-anisotropic quantum spherical model',
Journal of Statistical Mechanics: Theory and Experiment, P07006 (2015).

251 S. Wald, G. T. Landi and M. Henkel:
'Lindblad dynamics of the quantum spherical model',
Journal of Statistical Mechanics: Theory and Experiment, 013103 (2018).

252 S. Wald, M. Henkel and A. Gambassi:
'Non-equilibrium dynamics of the open quantum O(n)-model with non-Markovian noise: exact results',
Journal of Statistical Mechanics: Theory and Experiment, 103105 (2021).

253 S. Wald and M. Henkel:
'Lindblad dynamics of a quantum spherical spin',
Journal of Physics A: Mathematical and Theoretical **49**, 125001 (2016).

254 G. T. Landi, D. Poletti and G. Schaller:
'Nonequilibrium boundary-driven quantum systems: models, methods, and properties',
Reviews of Modern Physics **94**, 045006 (2022).

255 L. S. Levitov and G. B. Lesovik:
'Charge distribution in quantum shot noise',
JETP LETTERS C/C OF PIS'MA V ZHURNAL EKSPERIMENTAL'NOI TEORETICHESKOI FIZIKI **58**, 230–230 (1993).

256 M. Esposito, U. Harbola and S. Mukamel:
'Fluctuation theorem for counting statistics in electron transport through quantum junctions',
Physical Review B **75**, 155316 (2007).

257 M. Esposito, U. Harbola and S. Mukamel:
'Nonequilibrium fluctuations, fluctuation theorems, and counting statistics in quantum systems',
Reviews of modern physics **81**, 1665 (2009).

258 G. T. Landi, M. J. Kewming, M. T. Mitchison and P. P. Potts:
'Current fluctuations in open quantum systems: bridging the gap between quantum continuous measurements and full counting statistics',
(2023).

259 T. Brandes:
'Waiting times and noise in single particle transport',
Annalen der Physik **520**, 477–496 (2008).

260 M. Aspelmeyer, T. J. Kippenberg and F. Marquardt:
'Cavity optomechanics',
Reviews of Modern Physics **86**, 1391 (2014).

261 M. B. Plenio and P. L. Knight:
'The quantum-jump approach to dissipative dynamics in quantum optics',
Reviews of Modern Physics **70**, 101 (1998).

262 A. Purkayastha:
'Lyapunov equation in open quantum systems and non-hermitian physics',
Physical Review A **105** (2022).

263 M. G. Genoni, L. Lami and A. Serafini:
'Conditional and unconditional gaussian quantum dynamics',
Contemporary Physics **57**, 331–349 (2016).

264 A. Belenchia, M. Paternostro and G. T. Landi:
'Informational steady states and conditional entropy production in continuously monitored systems: the case of gaussian systems',
Physical Review A **105** (2022).

Résumé détaillé en français

Cette thèse analyse certains aspects de systèmes quantiques à plusieurs corps, chassés de l'équilibre par l'interaction avec un environnement externe, comme les bains de Lindblad ou les appareils de mesure. Cette étude de recherche s'inscrit dans le vaste sujet des systèmes quantiques ouverts, dont la dynamique et la relaxation à l'équilibre sont toujours un problème ouvert. La complexité des interactions système-bain(s) et les difficultés liées à l'extrapolation de la dynamique réduite ont conduit à la formulation de plusieurs approches théoriques, selon la perspective dans laquelle le problème est cadré. En fait, parallèlement à l'approche standard qui dérive la dynamique des premiers principes, de nombreuses approches phénoménologiques ont été proposées, qui ont le privilège de contourner certains problèmes mathématiques, mais en préservant les exigences physiques nécessaires.

Notre analyse porte sur les chaînes quantiques de particules libres (non interagissantes), même si une partie des résultats obtenus dans ce travail de thèse pourraient être généralisés à des dimensions supérieures. Ces dernières années, il y a eu un regain d'intérêt pour la physique des systèmes unidimensionnels, en raison du boom technologique, de la manipulation expérimentale de plates-formes quantiques, telles que les chaînes de spin quantiques, les atomes froids et de la réalisation ultérieure de géométries unidimensionnelles avec l'aide de potentiels de confinement. De plus, les modèles de particules libres jouent toujours un rôle clé dans la compréhension de la physique à plusieurs corps, où les connaissances acquises sur la dynamique des systèmes fermés sont un tremplin pour généraliser les mêmes images physiques pour les homologues ouverts, tels que les points quantiques ou systèmes mesurés en continu.

La première partie du manuscrit (Chapitres 1, 2, 3) introduit le lecteur au contexte général et aux outils théoriques qui seront utilisés dans ce travail. A savoir, le but est de guider tout lecteur, même non expert, vers la pleine compréhension de la physique, mais en évitant la superficialité d'un exposé simpliste et approximatif des concepts.

En particulier, au Chapitre 1, nous traitons de l'entropie d'intrication, qui est une grandeur à la base de la théorie de l'information. Ici, nous présentons

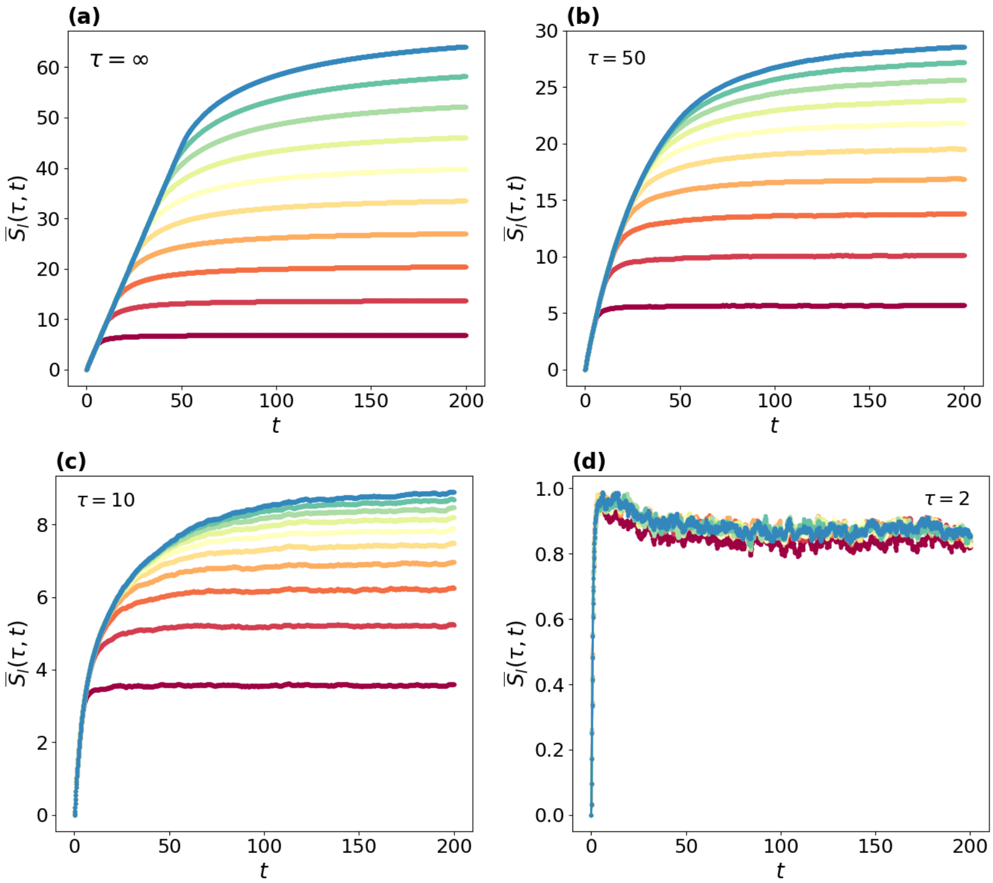

Figure 7.12: Évolution de l'intrication pour un état initial de Néel et $L = 500$. Les lignes, de bas en haut, représentent les tailles croissantes des sous-systèmes $l \in \{10n : n \in \mathbb{N} \wedge n \leq 10\}$. Les résultats pour chaque taux $\tau \in \{2, 10, 50, \infty\}$ ont été calculés en faisant la moyenne de plus de 1000 trajectoires quantiques différentes.

également l'hydrodynamique généralisée et le calcul de l'entropie d'intrication pour les états gaussiens. Dans le Chapitre 2, nous introduisons le lecteur au formalisme des systèmes ouverts, avec un accent particulier sur la dynamique de Lindblad et Langevin. Dans le Chapitre 3, nous présentons l'approche de Wigner, basée sur la représentation des opérateurs de Hilbert comme des fonctions avec domaine dans l'espace des phases.

Dans la deuxième partie du manuscrit (Chapitres 4, 5, 6, 7), nous exposons les résultats originaux obtenus au cours de ce travail de thèse. L'exposition fait suite à la publication des travaux de recherche des trois dernières années de thèse.

Dans le Chapitre 4, nous considérons une chaîne de fermions libres décrite

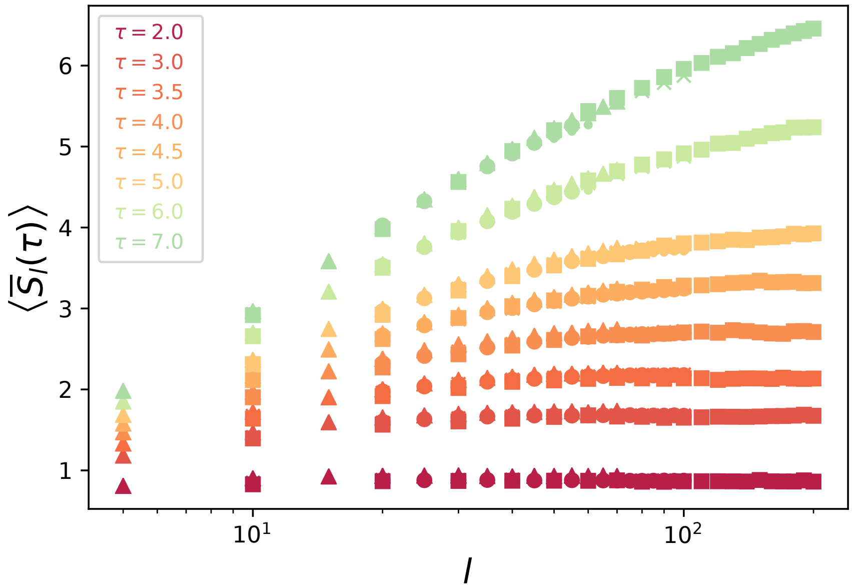

Figure 7.13: Intrication stationnaire pour $L \in \{200, 300, 400, 500, 800\}$ (différents symboles) et différents taux de mesure τ^{-1} (différentes couleurs), en fonction de la taille du sous-système $l \in [1, 200]$, tracée en échelle log-linéaire.

par l'hamiltonien

$$H = -\frac{1}{2} \sum_{i=0}^{L-1} c_i^\dagger c_{i+1} + c_{i+1}^\dagger c_i \,,$$

où les $(c_i^\dagger, c_i)$ sont les opérateurs fermioniques de création et de destruction au site i et L est la longueur de la chaîne quantique. Pour les systèmes fermés, la dynamique est décrite par la transformation unitaire

$$\rho(t) = e^{-\mathrm{i}Ht} \rho(0)\, e^{\mathrm{i}Ht} \,,$$

où $\rho(t)$ est l'état au temps t (avec $\hbar = 1$). Supposons que la dynamique unitaire soit perturbée par des mesures projectives aléatoires des opérateurs $n_i = c_i^\dagger c_i$, dont la fréquence est modulée par le paramètre τ^{-1}. Suite à chaque mesure, l'état est projeté sur la variété propre correspondante de valeur propre 0 ou 1, selon la règle de Born. Suite à ce protocole dynamique, dans ce chapitre, nous nous concentrons sur le comportement de l'entropie d'intrication. En préparant le système dans l'état initial de Néel, on trouve comme premier résultat que la croissance linéaire de l'intrication d'entropie est remplacée par une croissance logarithmique. En ce qui concerne l'intrication stationnaire, nous trouvons une transition nette de la loi de volume à la loi de surface. Les figures 7.12 et 7.13

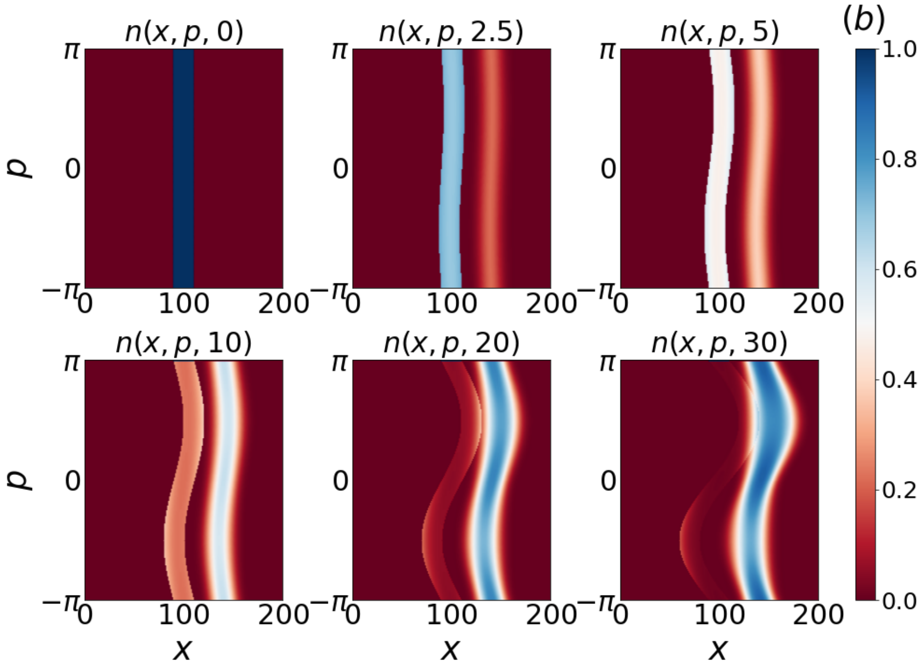

Figure 7.14: Évolution temporelle de la fonction de Wigner pour les profils d'émission/absorption gaussiens à une seule particule (configuration initiale de *double-domain wall*).

montrent l'évolution temporelle de l'intrication et de l'intrication stationnaire pour différentes valeurs de la cadence de mesure τ. A noter que pour des cadences de mesure élevées, l'état converge rapidement vers le régime de Zénon. De plus, la mise à l'échelle de l'intrication stationnaire a été réalisée à l'aide de le *collapsed quasi-particle ansatz*.

Dans le Chapitre 5, nous généralisons l'approche hydrodynamique pour les systèmes de particules libres en contact avec les bains Lindblad. Pour les processus de gain / perte d'une seule particule et le déphasage, la dynamique des fonctions à deux points est effectivement décrite par la fonction de Wigner qui, pour les états excités à faible intrication, peut être interprétée comme une distribution de particules sans interaction en mouvement dans l'espace des phases. Ensuite, nous appliquons les résultats théoriques à quelques systèmes fermioniques, où nous comparons la dynamique microscopique avec l'hydrodynamique généralisée. Dans la figure 7.14, nous présentons l'évolution de la fonction de Wigner sous des processus dissipatifs décrits par des taux d'émission/absorption gaussiens.

Dans le Chapitre 6, nous essayons de répondre à des questions fondamentales sur la dynamique quantique markovienne ouverte. Nous avons comparé deux

des modèles les plus célèbres d'oscillateur harmonique amorti, à savoir les modèles de frottement et de cavité. Apparemment, il est passé inaperçu que ces deux modèles ne reproduisent pas la même dynamique. Cela nous a donné la motivation pour approfondir le comportement dynamique.
Plus précisément, les modèles de frottement et de cavité sont basés sur deux ensembles d'équations de Langevin, impliquant différents termes d'amortissement et bruits markoviens. Les corrélateurs de bruit sont obtenus par quatre exigences physiquement raisonnables, ce qui donne accès aux fonctions à deux points puis aux équations de la matrice de densité réduite. De manière surprenante, l'équation du modèle de frottement s'avère ne pas être une carte complètement positive, qui peut provenir d'états initialement corrélés. Nous avons également étudié la relaxation par l'approche de la fonction de Wigner, l'évolution étant régie par une équation différentielle de Fokker-Plank. Nous avons distingué les régimes sur-amortis et sous-amortis, montrant la dynamique de certains états initiaux notables. La fonction asymptotique de Wigner révèle que seulement pour des champs magnétiques nuls, les deux modèles assurent l'existence d'états d'équilibre appropriés. Enfin, nous refondons les modèles de frottement et de cavité comme des approximations de champ moyen d'un aimant interagissant à plusieurs corps et analysons la nature de leurs diagrammes de phase respectifs à température nulle.

Dans le Chapitre 7, nous avons analysé la dynamique conditionnelle sans saut pour des particules libres couplées à des bains de Lindblad. Plus formellement, tout saut quantique peut être vu comme l'action de certains détecteurs mesurant l'échange de particules système-bains. La détection partielle est réalisée en affectant à chaque canal dissipatif une efficacité finie $\Lambda \in [0,1]$, avec $\Lambda = 1$ pour une efficacité parfaite et $\Lambda = 0$ lorsque le canal n'a pas été mesuré du tout. Dans ce chapitre, nous avons calculé l'état sans saut évolué dans le temps, qui est l'état quantique conditionné par l'absence de sauts détectés dans $[0,t]$. Pour les systèmes à plusieurs corps et les opérateurs de sauts linéaires, l'hypothèse de gaussianité sur les états initiaux permet d'écrire l'évolution sans saut en termes d'une équation différentielle de Riccati. La résolution de l'équation de Riccati donne accès à la probabilité sans saut et aux distributions de temps d'attente.